Novel Roles for Ribonucleic Acids in Programmed Cell Death

Novel Roles for Ribonucleic Acids in Programmed Cell Death

A dissertation presented

by

Marshall Peter Thomas

to

The Division of Medical Sciences

in partial fulfillment of the requirements

for the degree of

Doctor of Philosophy

in the subject of

Biological and Biomedical Sciences

Harvard University

Cambridge, Massachusetts

August 2014

Dissertation Advisor: Professor Judy Lieberman Marshall Peter Thomas

Novel Roles for Ribonucleic Acids in Programmed Cell Death

Abstract

Apoptosis is a tightly coordinated program to shut down and dismantle a cell, characterized by mitochondrial outer membrane permeabilization (MOMP), caspase activation to cleave hundreds of proteins, DNA fragmentation, and blocked translation. Little is known about the fate of RNA as cells die, even though apoptosis has been intensively studied for decades. Here I show that mRNAs, but not noncoding RNAs (ncRNAs), are rapidly and globally degraded during apoptosis. The decay occurs in many cell types responding to diverse apoptotic stimuli. mRNA decay is triggered early in apoptosis, preceding membrane lipid scrambling, genomic DNA fragmentation and modifications to translation initiation factors that might cause translational arrest. mRNA decay depends on MOMP and is amplified by effector caspase activity. 3′ truncated mRNA decay intermediates with nontemplated uridylate-rich tails are generated during apoptosis and degraded by the 3′ to 5′ exonuclease DIS3L2. Knockdown of *DIS3L2* reduces apoptotic mRNA decay and partially rescues cell death. I propose that global mRNA decay is a new hallmark of apoptosis caused by the concerted action of several nucleases.

I also report a new role for RNA and DNA in directing cytotoxic leukocyte proteases to their substrates. When cytotoxic lymphocytes recognize and attack infected or cancerous cells, they deliver the granzyme (Gzm) serine proteases into the target cell. The Gzms cleave diverse protein substrates to orchestrate cell death. RNA binding proteins are highly enriched in

unbiased proteomic screens of Gzm protein substrates. I hypothesized that the Gzms are guided to nucleic acid binding protein targets via direct binding to RNA or DNA. Using fluorescence polarization, I show that the Gzms and related leukocyte proteases bind to RNA and DNA with low nanomolar affinity. Nucleic acid binding by the Gzms facilitates their cleavage of RNA and DNA binding proteins, and guides them into target cell nuclei and onto neutrophil extracellular traps. Nucleic acid binding provides an elegant mechanism to confer protease substrate specificity for cleavage of nucleic acid-binding proteins that play essential roles in cellular gene expression and cell proliferation.

Acknowledgements

I am extremely grateful to **Dr. Judy Lieberman** for her superb mentorship and support over the past six years. She nurtured my scientific growth and diverse interests and cared deeply about my professional development and betterment. She always suggested the right experiments and asked the right questions to bring this work to a higher plane of scientific rigor.

I want to thank several other mentor figures. **Dr. Michael Walch** and **Dr. Ashish Lal** were indispensable for their scientific advice, friendship and mentorship. Equally important were my collaborators **Dr. Jennifer Whangbo, Geoffrey McCrossan** and **Dr. Nancy Kedersha**.

I am grateful to all of the members of the Lieberman lab for years of advice, support and friendship. I am deeply thankful for our wonderful lab manager, **Zhan Xu**, who took such good care of me and the rest of the lab.

My dissertation advisory committee and defense committee took time out of their busy schedules to advise me and evaluate my work. I am indebted to **Dr. Paul Anderson** and **Dr. Karen Cichowski** for their service on my dissertation advisory committee, and **Dr. Melissa Moore**, **Dr. Richard Gregory** and **Dr. Nika Danial** for their service on my defense committee. **Dr. Steve Buratowski** deserves special thanks for his service as chair of both committees and his caring scientific and career mentorship.

Most importantly, I want to thank my family: **Heather, Will, Elizabeth, Jason, George and Patty** for three decades of love, inspiration and support. I would never have made it to this day without you.

Table of Contents

Chapter 1: Introduction **1**

Effectors of programmed cell death *2*

Hallmarks of apoptosis *6*

Immune-mediated cell death *7*

Pathways of mRNA decay *10*

Translation in cell stress and cell death *13*

Unexplored connections between RNA and cell death *16*

Chapter 2: Rapid and global mRNA decay during apoptosis with 3´ uridylated intermediates degraded by DIS3L2 ..... **17**

Contributions *18*

Abbreviations used in this study *19*

Global mRNA decay during apoptosis *20*

Decay is specific to mRNAs *23*

Apoptotic mRNA decay occurs in diverse cell types *24*

mRNA decay begins early in apoptosis and requires MOMP *25*

mRNA decay intermediates contain nontemplated 3´ uridylates *28*

DIS3L2 knockdown inhibits mRNA decay and cell death *31*

Methods *39*

Chapter 3: Conclusions for rapid and global mRNA decay during apoptosis with 3´ uridylated intermediates degraded by DIS3L2 48

Summary 49

Broader implications and future directions 51

Why is mRNA eliminated in apoptosis? 54

Chapter 4: Cytotoxic leukocyte protease binding to nucleic acids promotes nuclear localization and cleavage of nucleic acid binding proteins 57

Contributions 58

Abbreviations used in this study 59

Introduction 60

Gzm targets are enriched for nucleic acid binding proteins 61

RNA promotes GzmA and GzmB cleavage of RNA-binding proteins 62

Gzms bind RNA with nanomolar affinity 64

Gzms bind DNA with nanomolar affinity 65

Myeloid granule serine proteases bind nucleic acids 68

DNA binding mediates localization of Gzms to the nucleus 70

Localization of NE and CATG to NETs is mediated by DNA binding 71

Methods 74

Chapter 5: Conclusions for cytotoxic leukocyte protease binding to nucleic acids promotes nuclear localization and cleavage of nucleic acid binding proteins 80

Summary 81

Is nucleic acid binding specific? 81

Broader implications and functional significance 82

Future directions 83

References 85

Appendix 1: Supplemental materials related to chapter 4 97

Appendix 2: Publications 102

Chapter 1:

Introduction

Effectors of programmed cell death

Apoptosis is a highly conserved and tightly controlled cell death program used to eliminate unwanted cells during development, infection or malignant transformation and to remove cells experiencing irreparable stress-related damage [1]. Cell death is crucial for preventing carcinogenesis and genes that participate in apoptosis are frequently mutated in human cancers [2,3]. Apoptotic cells are rapidly recognized and cleared by professional phagocytes without provoking inflammation or harming bystander cells [1]. The best-studied cell death program (classical apoptosis) is mediated by the caspase proteases. There are alternate, caspase-independent programs of cell death triggered *in vivo* (for example, in response to injury) and by killer immune cells [4,5]. In apoptosis, dying cells undergo membrane blebbing, mitochondrial damage, DNA degradation, chromatin condensation and nuclear fragmentation. Apoptotic cells also secrete soluble signals and display surface lipids to attract phagocytes and stimulate immune clearance. Apoptosis is generally triggered in two distinct modes, either by stress stimuli (the intrinsic pathway) or death receptor signaling (the extrinsic pathway). The major effectors of classical apoptosis are the BCL2 family proteins and the caspases, which form intertwined cell death pathways [1].

Mitochondrial effectors of cell death

Mitochondria are the site of action of the BCL2 family proteins and a key control center of apoptosis. The BCL2 family is divided into three classes: multi-domain anti-apoptotic proteins (BCL2, BCL-xL, MCL-1), pro-apoptotic BH3-only proteins (such as BID, NOXA and BIM), and pro-apoptotic multi-domain proteins (BAX and BAK) [6–8]. BAX and BAK multimerize to form pores in the mitochondrial outer membrane. The pores cause mitochondrial outer membrane permeabilization (MOMP), which leads to the release of apoptogenic factors such as cytochrome c and SMAC/DIABLO from the intermembrane space to the cytosol. The BH3-only

proteins promote, while the anti-apoptotic proteins inhibit, the multimerization of BAX and BAK by a variety of mechanisms [7,8]. In the cytosol, cytochrome c orchestrates the formation of the apoptosome which activates the initiator caspase 9, while SMAC/DIABLO promotes cell death by inactivating caspase inhibitors (the IAP proteins) [9]. Early studies suggested that the intermembrane space proteins AIF and ENDOG are also released by MOMP and participate in the execution of apoptosis, but this has not been supported by subsequent work [10]. When a cell experiences sustained or irreparable stress, MOMP is triggered, setting off the instrinsic apoptosis pathway. Stressors generally enhance the activity or expression of BH3-only proteins or block the activity of anti-apoptotic BCL2 family proteins [6]. For example, after genotoxic stress, TP53 transactivates the expression of the BH3-only proteins NOXA and PUMA to promote MOMP [6,11].

The caspases are major cell death effectors

The caspases are cysteine proteases that cleave after aspartates. Caspases were originally identified as mediators of cell death, but they are now recognized to have non-apoptotic functions in inflammation and cell activation [12,13]. To prevent unwanted cell damage or death, but enable their rapid activation, the caspases are present in living cells as inactive zymogens. The apoptotic caspases are arranged in a pathway with initiator caspases triggering effector caspase activation. The initiator caspases are activated by dimerization and recruitment into multiprotein complexes, whereupon they activate the effector caspases by cleavage.

Both the intrinsic and extrinsic death pathways activate initiator and effector caspases, but the intrinsic pathway generally begins with MOMP (Figure 1.1). Mitochondrial release of cytochrome c triggers formation of the apoptosome – a scaffold that binds to and activates caspase 9 [14]. Once activated, caspase 9 cleaves and activates the downstream effector caspase zymogens (caspases 3, 6 and 7), which then cleave hundreds of cellular substrates in an accelerating

cascade to complete the cell death program [1,15]. Although the caspases have some degree of substrate specificity, they cleave hundreds of proteins and not every target is essential for the execution of cell death [16,17]. A handful of well-characterized substrates, such as PARP-1, ICAD and ROCK1, are likely to be important in apoptosis. Although most stresses are thought to first act on the mitochondrial death pathway, some can directly promote caspase activity. For example, endoplasmic reticulum (ER) stress promotes the expression and activity of caspase 2, another initiator caspase [12,18,19].

In the extrinsic pathway of cell death, death receptor ligands (such as FASL and TRAIL) engage cell surface death receptors to trigger the aggregation of the death induced signaling complex (Figure 1.1). This is a platform that activates the initiator caspases 8 and/or 10. Like caspase 9, these caspases can cleave and activate the effector caspases, but they also cleave the BH3-only protein BID to generate truncated BID (tBID). tBID activates BAX and BAK to trigger MOMP, thus linking the mitochondrial and extrinsic cell death pathways. Cells differ in their requirement for MOMP to initiate death receptor-dependent apoptosis. In type I cells, the effector caspases are directly activated by death receptor signaling, whereas type II cells require MOMP to amplify the death signal and execute apoptosis downstream of death receptors [20]. A balance in expression of proteins that promote and inhibit effector caspase activity determines whether cells are type I or type II [21]. Caspase inhibitors can completely block apoptosis triggered by death receptors because initiator caspase activity is one of the earliest signaling events in the extrinsic pathway and lies upstream of MOMP.

The prevailing view is that MOMP – as measured by cytochrome c release – is *the* trigger that irreversibly initiates caspase-mediated apoptosis. In single-cell studies of apoptosis triggered by death receptor ligands, initiator caspase activity builds slowly before MOMP and switch-like effector caspase activation [21,22]. This model posits that the effector caspases are positioned downstream of MOMP. However the effector caspases also promote MOMP. For example, the

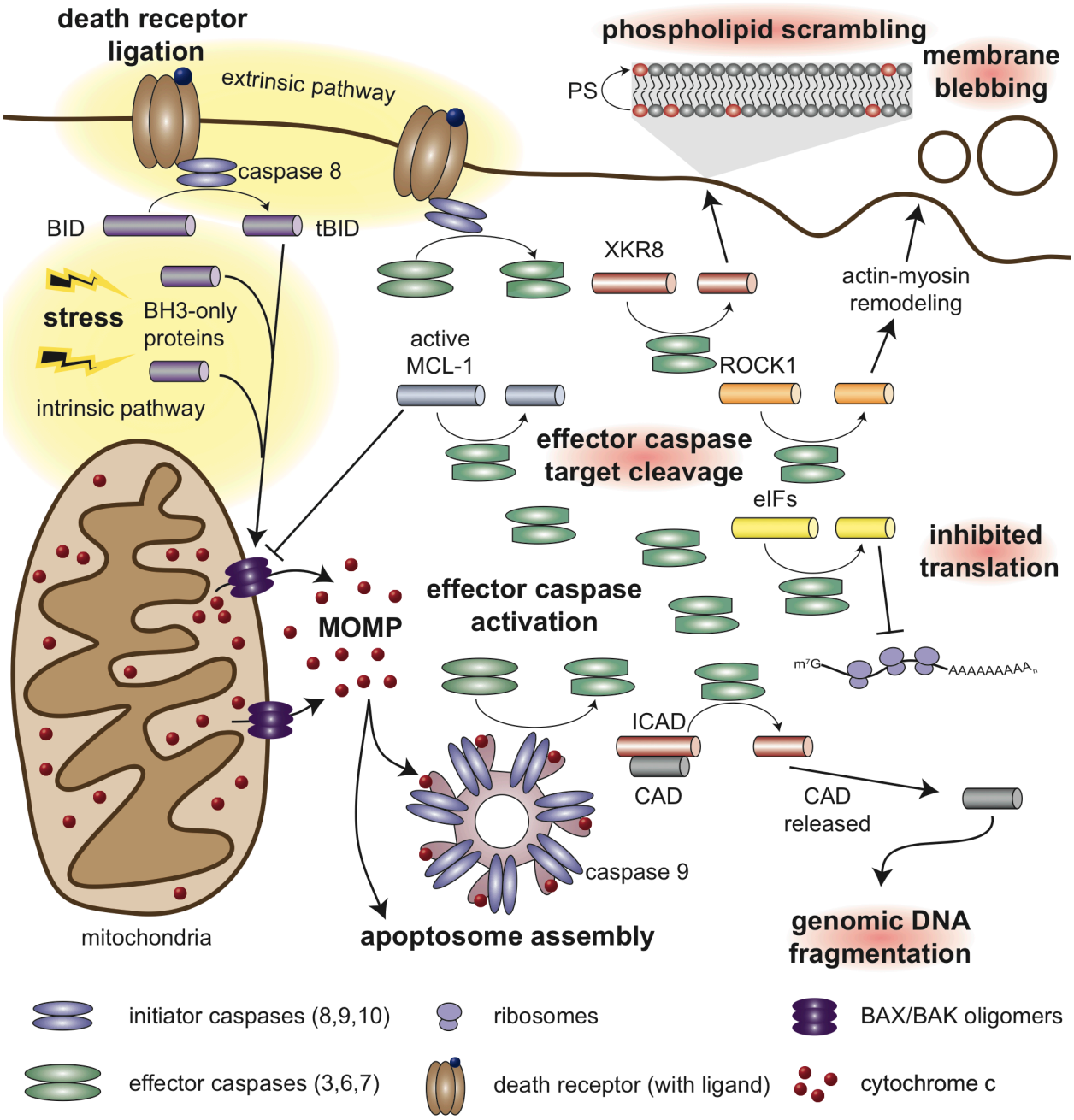

Figure 1.1: Major events in classical apoptosis

The signaling cascades that trigger apoptosis are shown on the left; hallmarks of cell death are shown on the right. Cell death is triggered by stress (the intrinsic pathway) or by death receptor signaling (the extrinsic pathway). Both pathways lead to MOMP by promoting the expression or activity of BH3-only proteins. Caspase 8 cleaves BID to generate tBID, while BH3-only proteins are induced by stress. Caspase 8 can also directly cleave and activate the effector caspases (caspase 3,6 and 7). Cytosolic cytochrome c triggers apoptosome assembly, which activates caspase 9, which in turn cleaves and activates the effector caspases. Effector caspases enhance MOMP, notably by cleaving and inactivating MCL-1. Most of the hallmarks of apoptosis are attributed to effector caspase activity. Phospholipid scrambling may be due to the cleavage of XKR8 and blebbing is due to ROCK1 cleavage. DNA fragmentation is caused by the release and nuclear translocation of caspase-activated DNase (CAD) after its inhibitor, ICAD, is cleaved by caspase 3. Translation inhibition might be caused by the cleavage of translation initiation factors, but there are also caspase-independent alterations to translation that occur during apoptosis.

mitochondrial death pathway is severely impaired in mouse cells lacking the effector caspases 3 and 7 [23]. In apoptosis induced by genotoxic stress, the initial release of a small amount of cytochrome c is caspase-independent, but the later release of a much greater amount of cytochrome c is blocked by caspase inhibitors [24]. This suggests that cytochrome c release may be biphasic. Cells experimentally loaded with exogenous cytochrome c undergo cell death, but death is dependent on MOMP (the release of endogenous cytochrome c) and caspase activity [25]. The effector caspases promote further MOMP by cleaving and inactivating mitochondrial death effectors, including MCL-1. Caspase-uncleavable MCL-1 mutants rescue cells from death induced by TRAIL [26]. This feed-forward loop involving MOMP and caspase activation may be crucial for the proper execution of apoptosis.

Hallmarks of apoptosis

The term apoptosis was coined to describe the characteristic morphology of certain types of dying cells *in vivo* [27]. Cells shrink and break off small membrane-bound bodies (called blebs or apoptotic bodies), their chromatin condenses and nuclei fragment, and they are rapidly taken up by phagocytic cells. These morphological features have been joined by a few new hallmarks of apoptosis over the decades (Figure 1.1). During classical apoptosis, most morphological changes are caspase-dependent. Membrane blebbing is caused by caspase 3 cleavage of the ROCK1 kinase, which becomes constitutively active and phosphorylates substrates in the actin-myosin cytoskeletal network to drive membrane contraction [28–30]. Nuclear DNA is cleaved by CAD (caspase-activated DNase), which is released from its inhibitor ICAD when ICAD is cleaved by caspase 3 [31]. Apoptotic cells signal to professional phagocytes by exposing phosphatidylserine (PS) on the outer leaflet of their cell membrane. Because PS is recognized by macrophages that phagocytose the apoptotic cell, it is called an “eat me” signal. It was hypothesized that a protein that drives bidirectional scrambling of membrane lipids causes PS exposure. This putative apoptotic “scramblase” has been sought for some time. A recent report

suggests that caspase 3 cleavage of XKR8 is responsible for PS exposure on the outer leaflet [32]. However, it is unclear how XKR8 causes phospholipid scrambling, and other studies report that PS exposure can occur in a caspase-independent manner [33]. Protein translation also ceases during cell death. Although caspase cleavage of translation initiation factors, or proteins that modify translation initiation factors, is often cited as responsible for translation arrest [1], these alterations may not be necessary or sufficient to block translation [34]. The factors that might collude to arrest translation during apoptosis are discussed in more detail below.

Immune-mediated cell death

In addition to the intrinsic and extrinsic pathways of apoptosis, cell death can be triggered by immune killer cells. Cytotoxic T lymphocytes (CTLs) and natural killer (NK) cells recognize infected or transformed cells and eliminate them through cytotoxic attack [5]. In cytotoxic attack, the killer cell delivers a lethal dose of proteins into its target cell through an immune synapse. The proteins are stored in cytotoxic granules, specialized secretory vesicles stored in the cytosol of killer cells [5,35]. The primary cytotoxic effector molecules in these granules are the pore forming molecule perforin (Pfn) and the granzyme (Gzm) serine proteases. The granules are released into the immune synapse, where Pfn causes a calcium influx in the target cell to activate a membrane repair response that culminates in the endocytosis of the granule contents. After endocytosis, Pfn forms pores in the endosomal membrane to allow the release of the Gzms into the cytosol [36]. The Gzms orchestrate independent programs of cell death by cleaving substrates in the cytosol, mitochondria, and nucleus. A single cytotoxic lymphocyte can serially recognize and kill several target cells before its supply of cytotoxic granules is exhausted [37].

The Gzms (five enzymes in humans, ten in mice) activate diverse and redundant pathways of programmed cell death by cleaving many cellular proteins to guarantee that infected or

transformed cells can't readily evade immune attack [5]. GzmA and GzmB are the most abundant Gzms. GzmB acts like an initiator caspase and triggers mitochondrial and caspase-dependent death by directly cleaving BID and caspase 3 [38]. GzmA initiates a distinct pathway of caspase-independent apoptosis with mostly non-overlapping substrates that damages mitochondria without causing MOMP and causes single-stranded, rather than double-stranded, DNA damage [5,39]. The death mechanisms activated by the other Gzms are distinct, but not well characterized. During cytotoxic attack, the Gzms enter the target cell nucleus and concentrate there by an unknown mechanism [40–42]. Once in the nucleus, the Gzms cleave many RNA and DNA binding proteins to contribute to cell death [43]. The Gzms can cause death across diverse taxa (from human cells to bacteria) by cleaving key components of the electron transport chain and generating a lethal oxidative burst, while simultaneously blocking the oxidative stress response [44–46].

Alterations to pre-mRNA processing during cell death

Pre-mRNA splicing (hereafter, splicing) occurs co-transcriptionally to remove introns and join exon ends to generate a mature mRNA. Splicing is controlled by hundreds of constitutive and regulated splicing factors [47]. The splicing reaction is catalyzed by the spliceosome, a complex RNA-protein machine [47,48]. Through an ordered assembly process, the spliceosome joins the 5′ and 3′ splice sites of adjacent exons and excises the intervening intron. Cell stresses can alter the splicing of pro- and anti-apopototic mRNAs. Many BCL2 family genes encode multiple splice isoforms with opposing effects on cell death. For example, the *BCL2L1* locus encodes for a pro-apoptotic splice isoform (*BCL-xS*), and an anti-apoptotic mRNA (*BCL-xL*) [49,50]. Cell stresses alter splicing by a variety of mechanisms, including post-translational modifications to splicing factors, alterations to the rate of transcription driven by polymerase II, and transactivation of splicing factor expression [34]. Although stresses do alter the expression of apoptotic mRNA splice isoforms, the change in the ratio of pro- and anti- apoptotic isoforms

occurs slowly. In many cases, it is unclear whether stress-induced changes in alternative splicing has a significant effect on apoptosis [34].

In contrast to the subtle effects of alternative splicing, we recently found that pre-mRNA splicing is profoundly disrupted during apoptosis and GzmA-dependent, caspase-independent cell death [43]. We uncovered this connection between the Gzms and splicing with an unbiased proteomic screen. Because the Gzm serine proteases accumulate in the nuclei of their target cells, we wished to identify their nuclear substrates. The proteomes of intact nuclei that were treated or not with GzmA were analyzed for proteins degraded by GzmA. Of 44 nuclear GzmA substrates, 33 were RNA-binding proteins, including 14 heterogeneous nuclear ribonucleoproteins (hnRNPs) [43]. Many hnRNPs were also degraded following caspase activation. Since hnRNPs assemble on newly synthesized transcripts to orchestrate post-transcriptional processing, this prompted us to look at the fate of newly synthesized RNA in cells undergoing Gzm-mediated cell death. Newly synthesized RNA was retained in the nucleus and pre-mRNA splicing was severely compromised as measured by intron retention. hnRNP A1 was a robust GzmA target. A noncleavable mutant of hnRNP A1 restored splicing and partially rescued cells from death, suggesting that the inhibition of pre-mRNA processing was an important component of the cell death program. Of note, alterations in mRNA splicing and nuclear export were absent in cells experiencing oxidative stress, suggesting that global inhibition of splicing is not a general feature of non-apoptotic stress. The splicing defect is likely the reason for nuclear retention of newly synthesized mRNAs. Intronless transcripts of immediate early genes (such as Jun) transcriptionally activated in response to stress were rapidly exported and translated into protein, while stress-activated transcripts that contain introns (such as Fos) were not translated into new protein. Based on these findings we hypothesize that disrupted splicing during apoptosis blunts an adaptive stress response and tips cells towards death. The profound link

between splicing and cell death led us to further explore whether apoptosis also affects the stability of pre-existing mRNAs.

Pathways of mRNA decay

Human mRNAs have a mean half-life of approximately seven hours [51]. There is a large variation in decay rates amongst mRNAs. Much of the variability in half-life is determined by *cis* regulatory elements in the mRNAs, particularly in their 3´ untranslated regions (UTRs) [52]. These *cis* regulatory elements are recognized by RNA binding proteins (RBPs) and other RNAs. microRNA (miRNA) recognition elements and AU rich elements are two well-studied examples of *cis* regulatory elements frequently found in 3´UTRs that can alter mRNA translation and stability [52,53]. The complex code that underpins the stability and translation of each mRNA is only understood at a descriptive level.

Although decay rates vary widely amongst mRNAs, most mRNAs are thought to be degraded by one major decay pathway. In metazoan cells, mRNA degradation initiates with deadenylation followed by decapping and exonucleolytic decay from the 5´ and 3´ ends by XRN1 and the exosome, respectively (Figure 1.2) [54,55]. There are two major cytosolic deadenylase complexes, the CCR4-NOT (CNOT) complex and the PAN complex [55]. CNOT is a multiprotein complex that contains two distinct nuclease activities attributable to two pairs of functionally redundant paralogs, CNOT7/CNOT8 and CNOT6/CNOT6L. The PAN complex is a heterodimer of PAN2 (the nuclease) and PAN3. In human cells, it is thought that PAN2 initiates deadenylation and the CNOT complex completes it, but this model is based on limited studies using inducible reporter constructs [56], and has not been broadly tested. The triggers of deadenylation, and the roles of each cytosolic deadenylase complex in mRNA decay, merit further investigation. A deadenylated mRNA can be decapped by DCP2 and degraded by the 5´ to 3´ exonuclease XRN1 or degraded from the 3´ end by the exosome. The exosome is a

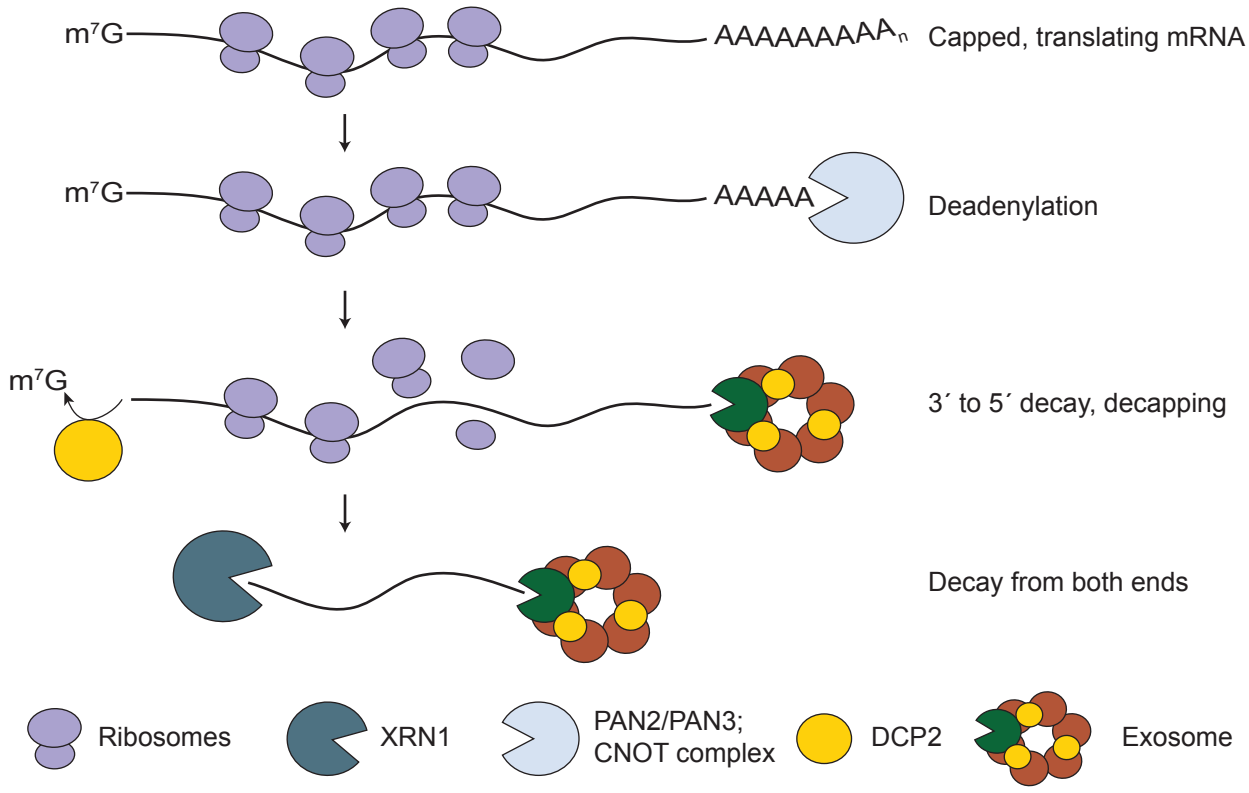

Figure 1.2: Canonical mRNA decay in human cells
mRNA decay typically initiates with deadenylation followed by decapping and decay from both ends of the molecule. In some cases, decay products are still found on polyribosomes, while in others an exit from translation is required for decay to occur.

complex consisting of a nine-protein ring plus two subunits with distinct ribonuclease activities: DIS3 (RRP44) or its homolog DIS3L1, and EXOSC10 (PM/Scl-100; RRP6). DIS3 and DIS3L1 possess independent endoribonuclease and 3´ to 5´ exoribonuclease activities, while EXOSC10 is a 3´ to 5´ exoribonuclease [57].

Although this canonical mRNA decay pathway is driven by exonucleases, endonucleases also contribute to mRNA decay. Endonuclease cleavage can initiate nonsense-mediated decay, a pathway that eliminates transcripts with premature termination codons that encode for non-functional proteins. Another recently-discovered mRNA decay pathway is triggered by ER stress [58]. During ER stress, many mRNAs that encode membrane or secreted proteins that are localized to the ER are cleaved by the ER-resident endonuclease IRE1 [59–61]. The cleaved

mRNAs are presumably degraded by the exosome and XRN1. Decay of ER-localized mRNAs might reduce the load of proteins translated in the ER to alleviate ER stress.

3′ uridylation acts as a signal for decay of some RNA species [62]. Nontemplated uridylate residues, added by terminal uridylyl transferases (TUTases), have been found on histone mRNAs [63–66], pre-miRNAs [67], and in mRNAs at miRNA cleavage sites [68]. Human cells express a 3′ to 5′ exoribonuclease, DIS3L2, which is homologous to the exosome subunits DIS3 and DIS3L1. Unlike its homologs, DIS3L2 does not associate with the exosome, probably because it lacks the N-terminal PIN domain responsible for DIS3 and DIS3L1 association with the exosome [69]. DIS3L2 preferentially degrades RNAs with 3′ uridylate residues and has been implicated in degradation of uridylated pre-miRNAs [70,71] in human cells and mRNAs in fission yeast [72]. Knockdown of human *DIS3L2* prolongs the half-life of some polyadenylated mRNAs [69], suggesting that it contributes to basal mRNA decay.

In addition to these intrinsic pathways of mRNA decay, some viruses can also instigate global mRNA decay. The gammaherpesvirus SOX proteins trigger the decay of host mRNAs while sparing viral transcripts [73–75]. This is known as host shutoff. Polymerase I and Polymerase III transcripts are not degraded in host shutoff, suggesting that decay is directed toward translation-competent mRNAs. Since the discovery of the SOX proteins, unrelated proteins encoded by other viruses have been shown to trigger host shutoff, suggesting that this could be a common mechanism used by viruses to hijack a host cell [76]. It has been proposed that 3′ hyperadenylation of mRNAs is a trigger for SOX-mediated host mRNA decay. The host exonuclease XRN1 appears to participate in all of these viral decay pathways [74,76]. However, the complete mechanism of host shutoff is not fully understood and likely varies from one virus to the next [76].

There is an intricate relationship between the translation status of an mRNA and its degradation. In some cases, translation promotes mRNA decay, while in others, an exit from translation is a

prerequisite for mRNA decay [77]. Numerous studies have explored the relationship between translation and decay in the context of miRNA target suppression [78]. The most recent studies of the miRNA pathway suggest that translation inhibition precedes mRNA decay [79,80]. However these findings may not be generalizable to all mRNA decay pathways. Notably, recent studies have identified mRNA decay products and enzymes involved in mRNA decay on polyribosomes [66,81,82], suggesting that at least some modes of decay can initiate before translation ceases (Figure 1.2).

Translation in cell stress and cell death

Many non-apoptotic stresses cause a rapid and nearly global shutoff of protein synthesis through one of two mechanisms that interfere with translation initiation – phosphorylation of eukaryotic translation initiation factor 2α (eIF2α) and inhibition of the eIF4F complex. Translation initiation requires a ternary complex composed of eIF2, GTP and the methionine initiator tRNA (Met-tRNA$_i^{Met}$). During translation initiation, the GTP is hydrolyzed to GDP, which must be recycled by eIF2B to form a new initiation-competent eIF2-GTP-Met-tRNA$_i^{Met}$ ternary complex. Stresses activate one of four kinases that phosphorylate the eIF2 regulatory subunit (eIF2α) on serine 51 [83]. eIF2α phosphorylation leads to a stable, inhibitory association of the eIF2-GDP complex with eIF2B, blocking ternary complex recycling. This results in a fast, potent and reversible block of translation initiation. eIF2α phosphorylation is the main feature of the "integrated stress response," a common protective program activated by most cellular stresses [84]. Although inhibition is nearly global, some transcripts are able to escape this translation arrest.

Stresses also block translation by inhibiting the formation of the eIF4F complex, which is composed of the cap binding protein eIF4E, the RNA helicase eIF4A, and the adaptor protein eIF4G [85]. eIF4F is required for initiating cap-dependent translation; most mRNAs are

translated in this manner and thus dependent on eIF4F. The best-studied regulators of eIF4F are the eIF4E binding proteins (4E-BPs), which bind to eIF4E and block its interaction with eIF4G. 4E-BP binding to eIF4E is regulated by phosphorylation – hypophosphorylated 4E-BP binds eIF4E with high affinity, but phosphorylated 4E-BP doesn't bind [86]. The 4E-BPs are phosphorylated by mTORC1, a kinase complex that integrates signaling from multiple mitogenic pathways [86]. In the absence of eIF4F, selected mRNAs can be translated through structured elements in their 5´UTRs termed internal ribosomal entry sites (IRES). Numerous apoptosis-associated transcripts (with both pro- and anti-apoptotic functions) contain IRESs that sustain their translation during cell stress.

Pre-apoptotic alterations of translation complexes

Many stimuli that trigger cell death cause concomitant cellular stress that arrests translation through the aforementioned pathways. MCF-7 cells treated with etoposide have reduced translation even when caspase activity is inhibited. Wild-type mouse embryonic fibroblasts (MEFs) treated with etoposide have increased eIF2α phosphorylation and association of 4E-BP1 with eIF4E concurrent with translation inhibition. However MEFs deficient in the eIF2α kinase PKR have a comparable block to translation in response to etoposide without any increase of eIF2α phosphorylation or 4E-BP1–eIF4E interaction [87]. These results suggest that other unknown events besides eIF2α phosphorylation and disruption of eIF4E binding to eIF4G may be important for inhibiting translation in cell death triggered by DNA damage. Similarly, global translation is reduced by ~50% in MCF-7 cells treated with the death receptor ligand TRAIL for a short period, even though there is very little caspase activity or PS externalization on the cell membrane. However, at this early time 4E-BP1 hypophosphorylation and reduced binding of eIF4G to eIF4E inhibits the eIF4F complex to block cap-dependent translation [88]. These alterations to 4E-BP1 are independent of caspase 3, but sensitive to the pan-caspase inhibitor zVAD-FMK, suggesting a role for the initiator caspases triggered by death receptor

signaling [87]. These pre-apoptotic and caspase-independent signaling events confound any straightforward analysis of the steps that cause apoptotic translation arrest.

Caspase-dependent alterations of translation complexes

In addition to caspase-independent translation inhibition, the effector caspases directly cleave many translation factors. Notably, caspase 3 cleaves eIF4G [89–91]. However it is unclear whether eIF4G cleavage products still support translation [92], or to what extent eIF4G cleavage contributes to translation inhibition, which is often already well underway by the time eIF4G is cleaved. In some studies, eIF4G cleavage correlates well with translation inhibition [89,91], while in others, translation inhibition precedes eIF4G cleavage [93,94]. The relative impact of eIF4G cleavage on translation may depend on the cell type and death-inducing stimulus. eIF4G is not cleaved in caspase 3 deficient MCF-7 cells treated with TRAIL, but translation is still effectively inhibited [87]. The eIF2α kinase PKR is cleaved by the caspases during death receptor-mediated apoptosis in Jurkat cells, but PKR cleavage and eIF2α phosphorylation are late events that occur well after translation inhibition and are probably not major contributors to blocked translation in cell death [34,94].

Although large alterations in translation factors have been cataloged during the initiation and execution of apoptosis, it is still unclear whether these modifications are responsible for blocking translation. Alterations to translation factors have only been studied in bulk cell populations undergoing asynchronous cell death. Even genetically identical sister cells die asynchronously in response to apoptotic stimuli [95], making it difficult to dissect which alterations occur in the pre-apoptotic phase. For example, it has been argued that many IRES-containing mRNAs are up-regulated in apoptotic cells [88], but markers of caspase activity remained low at the time IRES-dependent translation was analyzed, raising the possibility that these translation

alterations are actually pre-apoptotic. At an even more fundamental level, although widely assumed, it has never been proven that translation inhibition contributes to apoptosis.

Unexplored connections between RNA and cell death

Given the profound alterations of mRNA splicing in apoptotic cells, I hypothesized that mRNA stability might also change during cell death. In contrast to the well-known changes that occur to proteins, lipids and DNA during cell death, the fate of RNA in apoptotic cells has not been well studied. In some cells, the *28S* ribosomal RNA (rRNA) is cleaved during apoptosis by an unknown endonuclease to generate distinct fragments [96]. Because this occurs late in the death program and is not universally seen, it is unlikely to be essential for apoptosis. In a few intriguing studies, individual mRNAs were assayed by Northern blotting and found to decline in apoptotic cells [93,97]. However, the kinetics and mechanisms of mRNA decay were not investigated in detail in these studies.

Here I show that global decay of mRNAs, but not noncoding RNAs (ncRNAs), occurs early in apoptosis induced by diverse classical apoptotic stimuli. Decay is triggered by MOMP and begins around the same time as caspase activation and before DNA degradation. I found that apoptotic mRNA decay intermediates are truncated and uridylated at their 3´ ends. The uridylated intermediates are further degraded by the 3´ to 5´ exonuclease DIS3L2. Knockdown of *DIS3L2* or the *CNOT7/CNOT8* deadenylases partially rescues apoptotic mRNA decay and cell death, suggesting that they participate in apoptotic mRNA decay and that mRNA decay promotes the execution of apoptosis. I propose that global mRNA decay is a novel hallmark of apoptosis.

Chapter 2:

Rapid and global mRNA decay during apoptosis with 3´ uridylated intermediates degraded by DIS3L2

Contributions

I am grateful for the contributions of several individuals to this work. **Dr. Jennifer Whangbo** and **Geoffrey McCrossan** assisted with the experiments shown in Figure 2.6. **Dr. Keri Sanborn** assisted with the experiments shown in Figure 2.5, panels C and D. **Dr. Emre Basar** assisted with the quantitative analysis shown in Figure 2.1, panel E. **Dr. Michael Walch** assisted with the experiments shown in Figure 2.5, panels C and D, and provided invaluable advice on this project. All experiments were designed and analyzed by me, with mentorship from **Dr. Judy Lieberman**, who directed the research and supported me every step of the way.

Abbreviations used in this study

ActD	Actinomycin D
CFSE	Carboxyfluorescein succinimidyl ester
cRACE	Circular rapid amplification of cDNA ends
ER	Endoplasmic reticulum
FISH	Fluorescence in situ hybridization
Gzm	Granzyme
hnRNP	heterogeneous nuclear ribonucleoprotein
HR	Hammerhead ribozyme
MOMP	Mitochondrial outer membrane permeabilization
NK cell	Natural killer cell
ORF	Open reading frame
PAS	Polyadenylation signal sequence
Pol	Polymerase
PS	Phosphatidylserine
RBP	RNA binding protein
STS	Staurosporine
TAP	Tobacco acid pyrophosphatase
TSS	Transcription start site
UTR	Untranslated region
zVAD	carbobenzoxy-valyl-alanyl-aspartyl-[O-methyl]-fluoromethylketone

Global mRNA decay during apoptosis

To investigate what happens to mRNAs during apoptosis, we measured housekeeping mRNAs and ncRNAs by qRT-PCR and northern blot of total RNA in Jurkat cells treated with a Fas receptor-activating antibody (αFas) for 4 hours with or without the pan-caspase inhibitor z-VAD-fmk (zVAD) (Figure 2.1A-C). We confirmed cell death with Annexin V staining. 85% of αFas-treated cells stained with annexin V, and death was completely rescued by zVAD (Figure 2.1C). qRT-PCR experiments were normalized to *U6* snRNA, which remained relatively stable during apoptosis. Six normally stable mRNAs, including *GAPDH* and *ACTB* (both with reported half-lives >12 hours [51,98]), declined approximately ten-fold. In contrast, some ncRNAs increased (*miR-16*, *miR-21* and *5S* rRNA), while others (*U2*, *7SL*, *28S*) declined, but much less than the mRNAs (Figure 2.1B). When the same cells were treated with Actinomycin D (ActD) for 4 hours to block transcription, mRNAs only declined slightly (Figure 2.1C), indicating that mRNA half-life was drastically reduced in apoptosis. To test whether mRNA levels change globally during apoptosis, we used fluorescence in situ hybridization (FISH) to probe for *18S* rRNA and poly(A) mRNA (with a dT_{50} oligonucleotide) in Jurkat cells treated with αFas±zVAD or ActD for 3 hours (Figure 2.1D,E). Living cells had strong poly(A) and *18S* staining, while apoptotic cells retained rRNA staining but lost poly(A) staining, which was rescued by zVAD. ActD had no significant effect on the relative strength of the poly(A) and *18S* signals. This strongly suggests that mRNA is globally degraded, because the poly(A) tail stabilizes mRNA and deadenylated mRNAs are rapidly degraded. Controls showed that the FISH assay specifically detected RNA (Figure 2.2). The reduction in qPCR and Northern blot signals for several mRNAs, coupled with the global loss of poly(A) staining, strongly suggest that global mRNA decay occurs during Fas receptor-mediated apoptosis.

To determine whether the reduction in mRNA might be caused by mRNA release into apoptotic blebs, αFas was added to Jurkat cells in the presence of blebbistatin, a myosin II inhibitor that

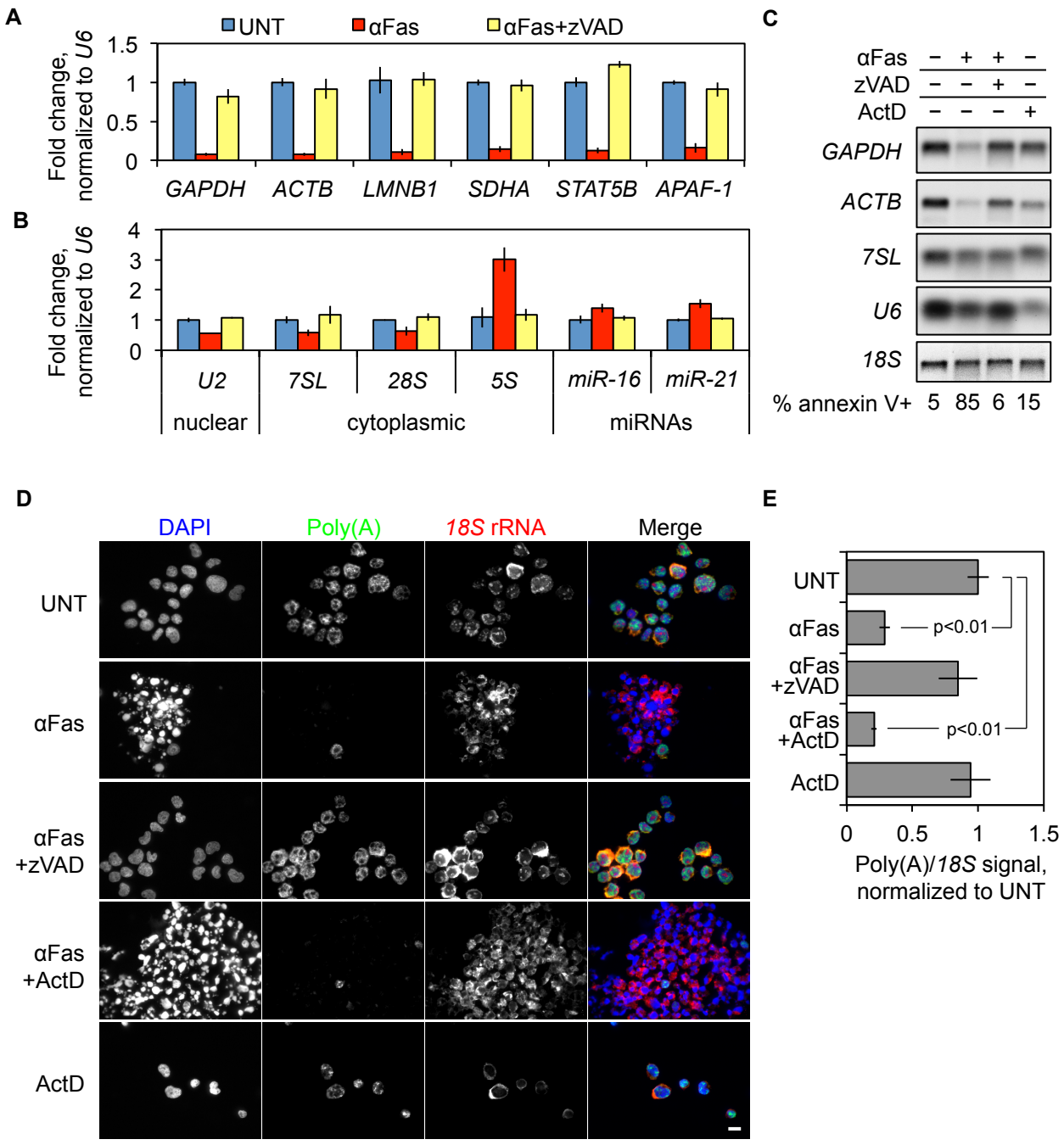

Figure 2.1: Rapid and global mRNA decay in apoptosis of Jurkat T cells initiated by αFas
(A-C) Jurkat cells were treated for 4 hr with αFas±zVAD and ActD. The indicated mRNAs **(A)** and ncRNAs **(B)** were analyzed by qRT-PCR (UNT – untreated), or northern blot **(C)**. All of the mRNAs measured declined drastically, while ncRNAs were more stable. **(D,E)** Jurkat cells were treated for 3 hr with αFas±zVAD and ActD and cytospun onto coverslips. The cells were stained for poly(A) mRNA with an oligo(dT) probe or *18S* rRNA with a complementary probe, and visualized by bright field fluorescence microscopy at 63X **(D)**. The results of 4 independent experiments were automatically quantified and normalized to UNT **(E)**. Poly(A) mRNA declined drastically in apoptotic cells, identified by their pyknotic nuclei. Scale bar represents 10 μm. Error bars represent SEM of at least 3 independent experiments.

blocks blebbing [30]. Blebbistatin did not inhibit mRNA disappearance (Figure 2.3), suggesting that mRNA is not exported selectively in apoptotic blebs during cell death. Thus, we hypothesized that mRNA decays *in situ* as cells die.

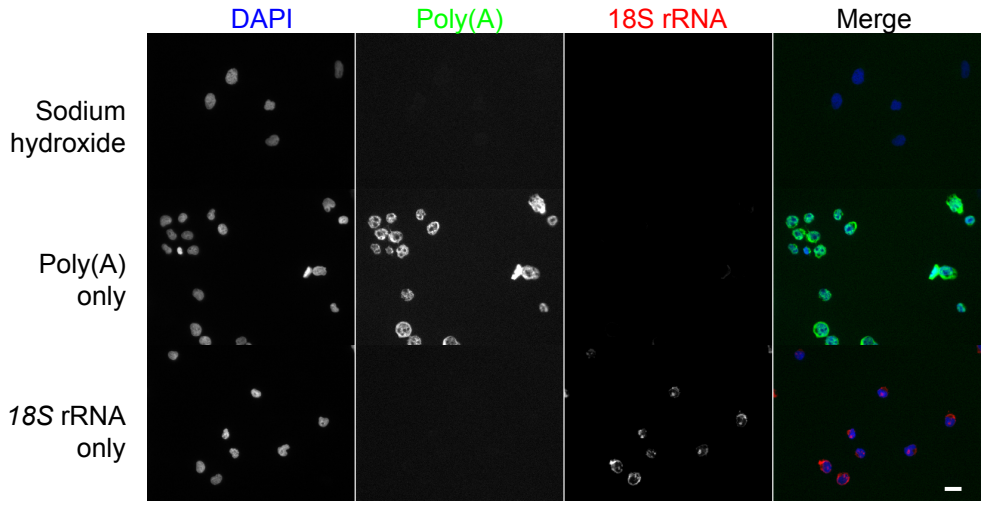

Figure 2.2: **Controls for RNA FISH**
FISH performed on untreated Jurkat cells confirmed the specificity of poly(A) and *18S* FISH. Sodium hydroxide treatment, which hydrolyzes RNA but not DNA, abolished mRNA and rRNA staining, but not DAPI staining. Scale bar represents 10 μm.

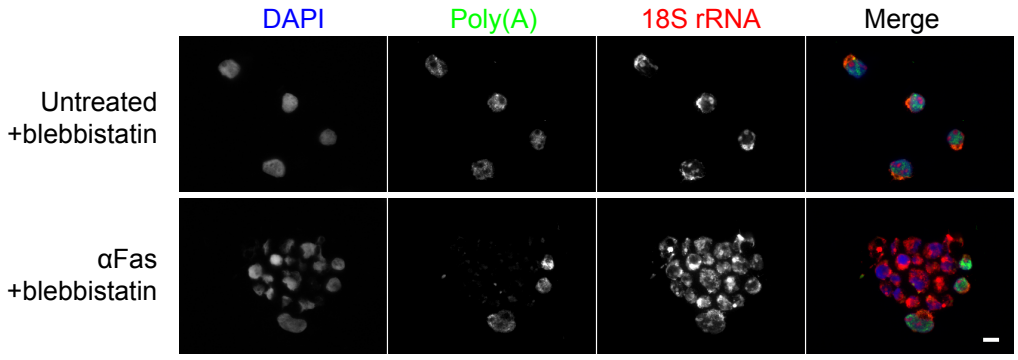

Figure 2.3: Reduced cellular mRNA is not due to RNA release in apoptotic blebs
Jurkat cells were treated with αFas for 3 hr in the presence of blebbistatin, an inhibitor of blebbing, then stained by FISH for mRNA and *18S* rRNA. Apoptosis was confirmed by annexin V staining (data not shown). mRNA still disappeared in non-blebbing αFas-treated cells undergoing apoptosis. The minority of cells with persistent poly(A) signal had DAPI staining of non-apoptotic nuclei.

Decay is specific to mRNAs

We tested a series of GFP reporter variants [74,76] to characterize the RNA species targeted for decay in cell death. The parental reporter carries GFP driven by a polymerase II (Pol II) promoter and terminated by a standard polyadenylation signal sequence (PAS). To terminate transcription without polyadenylation, the PAS was replaced with a self-cleaving hammerhead ribozyme (HR) sequence. Additionally, 60 adenine or uridine nucleotides were placed before the HR sequence to rescue translation (Figure 2.4A). Two additional variants were driven by Pol I

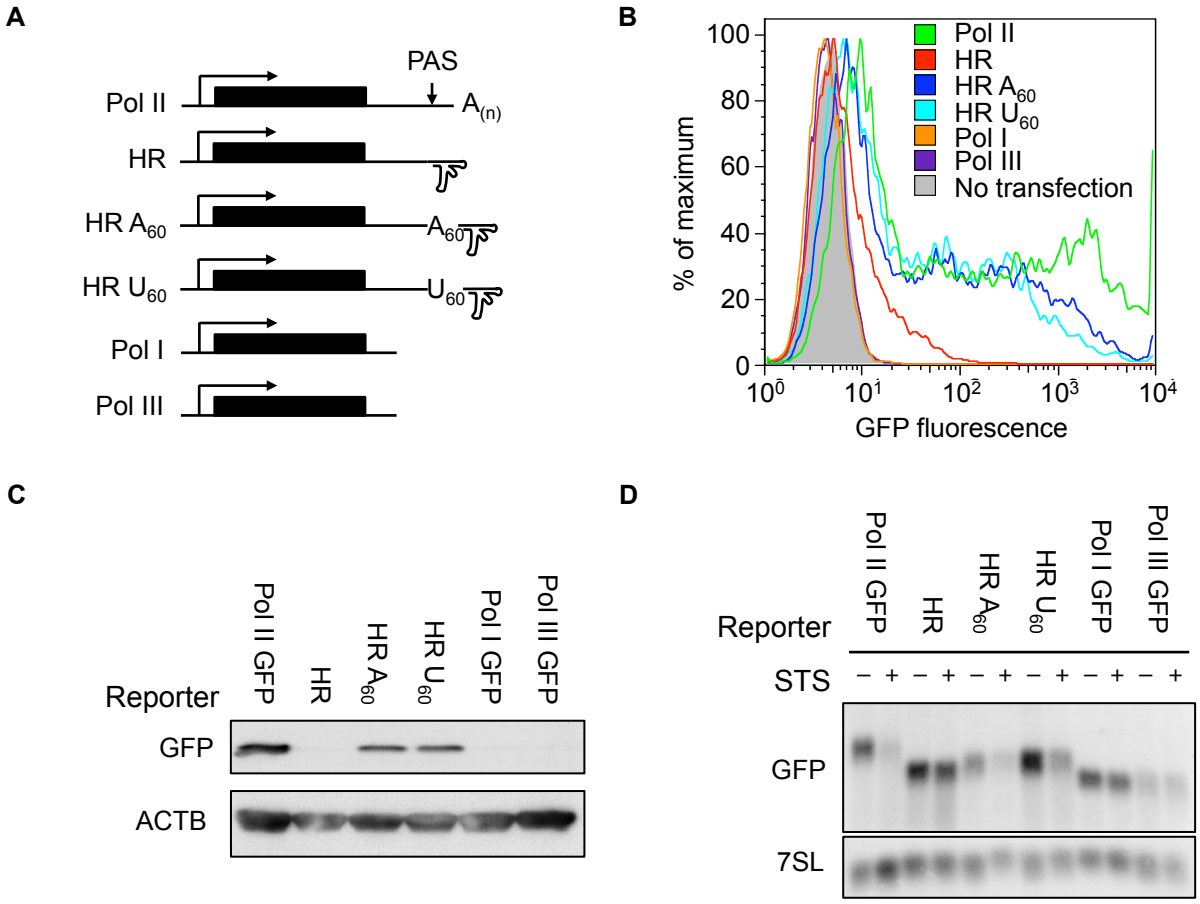

Figure 2.4: mRNAs are specifically degraded during apoptosis
(A-D) The indicated reporters **(A)** were transfected into HeLa cells and GFP protein expression was assayed by flow cytometry **(B)** and immunoblot **(C)**. There was high protein expression from transcripts driven by a polymerase II (Pol II) promoter. When the polyadenylation signal sequence (PAS) was replaced by a self-cleaving hammerhead ribozyme (HR), protein expression was lost, but rescued by the addition of 60 adenine or 60 uridine nucleotides before the HR sequence. Pol I and Pol III transcripts expressed no protein. GFP RNA levels were assayed by northern blot of total RNA from HeLa cells transfected with the indicated reporter, then treated with STS or left untreated. The northern blot probe targeted the GFP coding region. Only the translated RNAs were decayed in cell death.

and Pol III promoters. When transfected into HeLa cells, GFP-Pol II, HR-A_{60} and, surprisingly, HR-U_{60} all drove high levels of protein expression (Figure 2.4B,C), while the other reporters drove negligible GFP expression. All of the translated mRNAs were decayed in HeLa cells treated with STS, while untranslated RNAs were not degraded (Figure 2.4D). This suggests that ncRNAs are spared from apoptotic RNA decay.

Apoptotic mRNA decay occurs in diverse cell types

We hypothesized that global mRNA decay is a universal feature of cell death that occurs in many different cell types responding to diverse cytotoxic stimuli. To test this, we performed FISH on HCT116 cells that were treated with TRAIL or ActD for 2.5 hours, and on HeLa cells treated with a cytotoxic concentration of ActD for 6 hours (Figure 2.5A,B). In both cases, apoptotic cells were almost devoid of poly(A) mRNA signal, but retained strong rRNA staining.

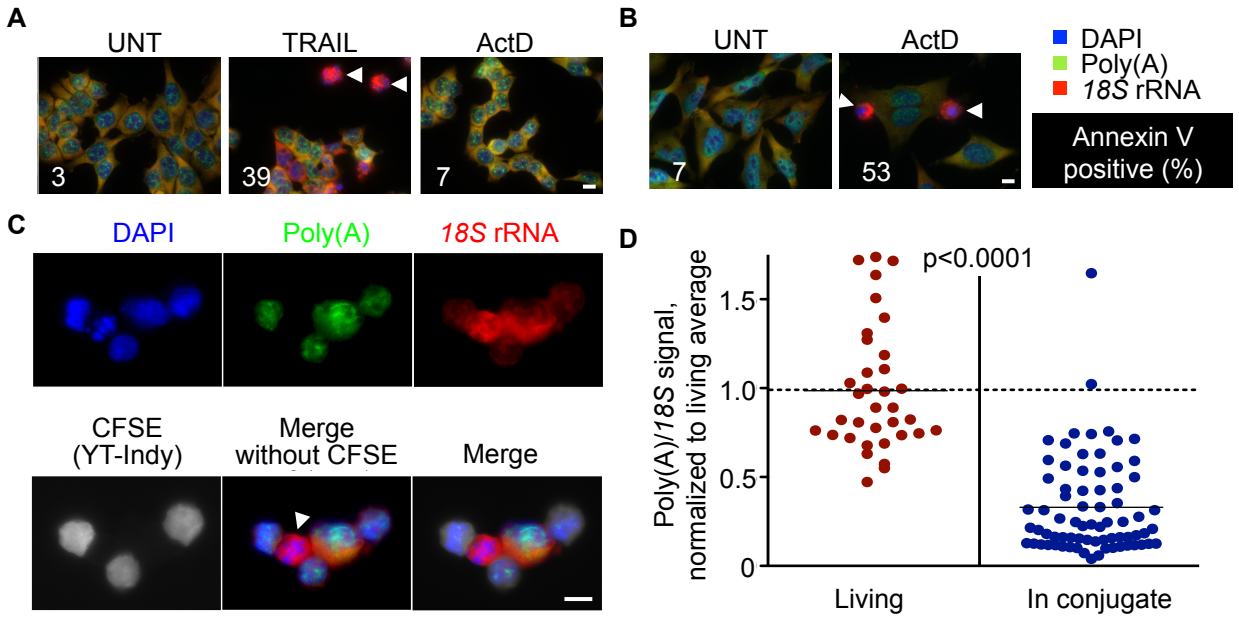

Figure 2.5: Global mRNA decay is a shared feature of apoptosis in diverse cell types
(A) HCT116 cells, treated for 2.5 hr with TRAIL or a nontoxic concentration of ActD, and **(B)** HeLa cells, treated for 6 hr with a cytotoxic concentration of ActD, were analyzed by FISH. The percentage of annexin V+ cells is shown for each condition. **(C)** A representative image of CFSE-labeled YT-Indy cells mixed with 721.221 cells for 3 hr and stained by FISH. **(D)** Quantification of the poly(A)/*18S* ratio in nonapoptotic 721.221 cells compared to target cells in conjugates with killer cells in 3 independent experiments. Poly(A) mRNA declined drastically, while rRNA was constant in apoptotic cells. Apoptotic cells are indicated by arrowheads (A-C). Scale bar represents 10 μm.

These experiments were internally controlled, because living cells lacking apoptotic DNA changes by DAPI staining in the same fields retained a strong poly(A) signal, even with complete transcription inhibition with ActD. mRNA staining also disappeared in target cells undergoing cytotoxic attack. YT-Indy NK cells were labeled with carboxyfluorescein succinimidyl ester (CFSE) then incubated with 721.221 B cells for 3 hours at a ratio of 3:1 and stained by

FISH (Figure 2.5C,D). 60% of 721.221 cells underwent apoptosis as assessed by ^{51}Cr release (data not shown). Apoptotic 721.221 cells, identified by their condensed nuclei, but not living target cells, lost mRNA signal. The ratio of poly(A) signal to *18S* signal declined significantly in 721.221 cells when they were coincubated with YT-Indy cells (Figure 2.5D). Thus, mRNAs, but not ncRNAs, declined drastically during apoptosis in multiple cell types responding to different apoptotic stimuli.

mRNA decay begins early in apoptosis and requires MOMP

We next determined the kinetics of mRNA decay relative to other hallmarks of apoptosis. Jurkat cells treated with ActD±αFas were harvested hourly over a 4 hour time course and analyzed for housekeeping gene mRNA stability by qRT-PCR, cleavage of PARP-1 and eiF4G and phosphorylation of eiF2α by immunoblot, caspase activation by a luminescent assay, annexin V binding, and DNA fragmentation (Figure 2.6A-E). The time course was performed in the presence of ActD to assess mRNA stability normalized to *U6* in apoptotic cells relative to healthy cells. *ACTB* and *GAPDH* mRNAs began to decline within 1 hour of adding αFas and leveled off by 3 hours, while *7SL* ncRNA was stable (Figure 2.6A). Non-apoptotic oxidative stress caused by arsenite (+ActD) and caspase-independent programmed cell death induced by the killer protease GzmA did not affect mRNA levels (Figure 2.6A and data not shown). Thus, the reduction in mRNA was specific for classical apoptosis. Caspase activation and cleavage of the caspase substrate PARP-1 began at 1 hour and were complete after 3 hours (Figure

2.6B,D). eIF2α phosphorylation and eIF4G cleavage, two alterations associated with translation arrest, were first detected after 2 hours of αFas treatment (Figure 2.6D). PS externalization, as quantified by annexin V binding, was not detected until 2 hours after αFas was added (Figure

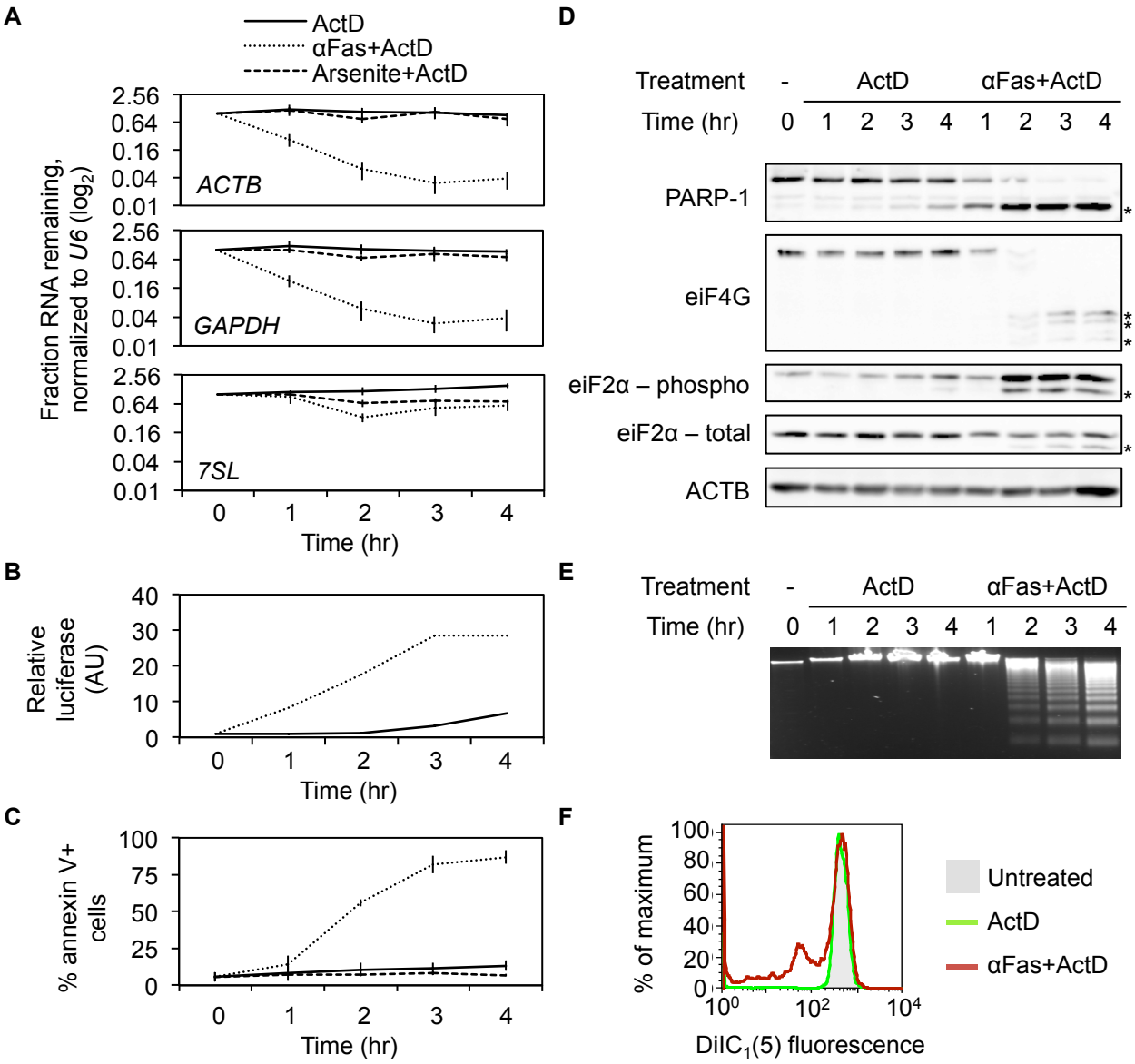

Figure 2.6: mRNA decay is a very early event in apoptosis
(A-E) Jurkat cells were treated with ActD±αFas or arsenite for 4 hr and harvested hourly for **(A)** qRT-PCR, **(B)** caspase activity by luminescent assay (AU – arbitrary units), **(C)** annexin V staining by flow cytometry, **(D)** immunoblot for caspase targets and translation initiation factors and **(E)** DNA fragmentation by electrophoresis. Asterisks indicate caspase cleavage products in panel D. mRNA decay was concurrent with caspase activation, but preceded DNA cleavage and phosphatidylserine externalization. Notably, mRNA decay initiated before the cleavage of eIF4G or the phosphorylation of eIF2α. **(F)** Jurkat cells were treated for 1 hr with ActD±αFas and stained with $DiIC_1(5)$ to measure mitochondrial depolarization. Transmembrane potential began dissipating within 1 hr of αFas treatment.

2.6C). Similarly, genomic DNA fragmentation was only detectable after 2 hours of αFas treatment (Figure 2.6E). We stained the cells with $DiIC_1(5)$, which only binds to mitochondria with an active transmembrane potential. Mitochondrial depolarization began within 1 hour of αFas treatment (Figure 2.6F). Thus mRNA decay occurred early in cell death, coincident with caspase activation and mitochondrial disruption.

We next wanted to investigate which effectors of cell death are necessary for apoptotic mRNA decay. Because mRNA decay began very early in cell death and MOMP marks an early committed step in apoptosis [21], we hypothesized that MOMP is required for mRNA decay. Stressors such as STS activate cell death by initiating MOMP upstream of caspase activity, whereas αFas activates caspase 8 to trigger MOMP. Thus zVAD blocks MOMP induced by αFas but not STS [10,99]. We compared HeLa cells stably expressing BCL2 (HeLa-BCL2) or an empty vector (HeLa-puro). In agreement with previous studies [10], BCL2 blocked release of cytochrome c and effector caspase activation caused by STS (Figure 2.7A). In contrast, zVAD blocked STS-triggered caspase activation, but did not completely block cytochrome c release or cell death. mRNA decay was completely rescued by BCL2 expression, but only partially by zVAD (Figure 2.7B). BAX and BAK are the BCL2 family proteins that form pores in the mitochondrial outer membrane to drive MOMP. Previous work has shown that MOMP is severely impaired in *BAX/BAK* knockout cells [100]. We tested the effect of *BAX/BAK* knockdown on mRNA levels after treatment with STS±zVAD (Figure 2.7C,D). Combined *BAX/BAK* knockdown rescued mRNA levels after treatment with STS to a greater extent than effector caspase inhibition by zVAD (Figure 2.7D). Collectively, these results suggest that mRNA decay is dependent on MOMP triggered by *BAX* and *BAK*.

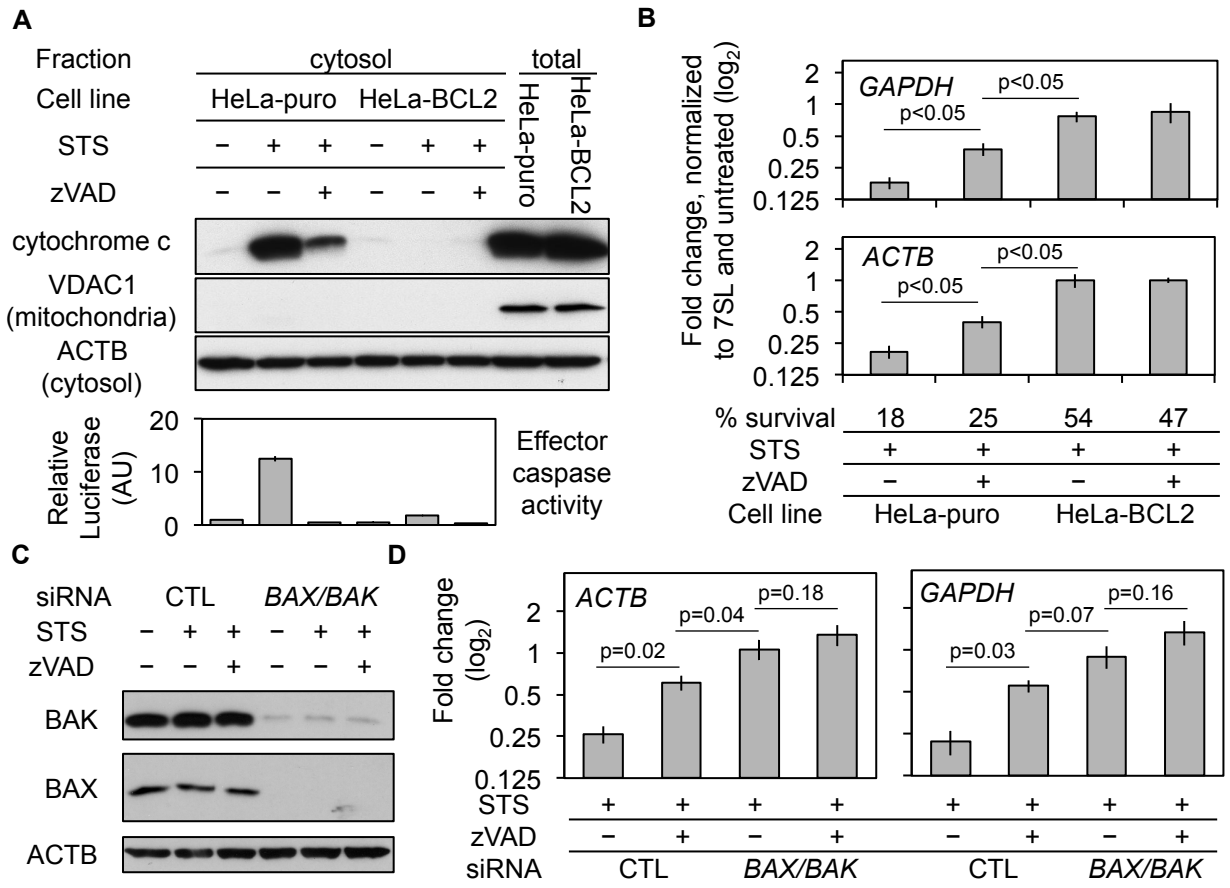

Figure 2.7: mRNA decay requires MOMP

(A,B) HeLa-BCL2 and HeLa-puro were treated for 6 hr with STS±zVAD. **(A)** Fractionated cells were analyzed by immunoblot (top) for cytochrome c release. STS-dependent cytochrome c release was partially inhibited by zVAD, but fully blocked by forced BCL2 expression. Effector caspase activity was measured by luminescent reporter assay (bottom). **(B)** RNAs were assayed by qRT-PCR. Results were normalized to untreated cells. BCL2 over-expression inhibited mRNA decay to a greater extent than zVAD. Survival, assayed by CytoTox-Glo assay performed after 6 hr STS treatment followed by a 24 hr recovery period, was normalized to untreated cells. mRNA decay correlated better with cytochrome c release than with effector caspase activation. **(C,D)** HeLa cells were transfected with control (CTL) siRNAs or siRNAs against *BAX* and *BAK*, then treated for 4 hr with STS±zVAD. Protein levels were quantified by immunoblot **(C)** and mRNA levels were quantified by qRT-PCR **(D)**. Results were normalized to untreated cells and 7SL ncRNA. Error bars represent SEM of at least 3 independent experiments.

mRNA decay intermediates contain nontemplated 3´ uridylates

To begin to understand the mechanism of mRNA decay during cell death, we searched for decay intermediates using circular RACE (cRACE) [64]. In cRACE, T4 RNA ligase circularizes RNA molecules by ligating their 3´ and 5´ ends. The circular mRNA is reverse transcribed with a

primer targeting the 5′ end of the molecule; this is a template for PCR with primers spanning the ligated junction (Figure 2.8A). We treated HeLa cells with STS±zVAD for 6 hours and performed cRACE on total RNA with and without tobacco acid pyrophosphatase (TAP) pre-treatment to distinguish between capped and decapped decay intermediates (only decapped mRNAs can be self-ligated without TAP pre-treatment). We amplified *ACTB* junctions using a forward primer directed to the *ACTB* 3′UTR near its polyadenylation site and a reverse primer in the *ACTB* 5′UTR. Full-length *ACTB* mRNAs were amplified from both untreated and STS-treated apoptotic cells, but only using TAP-treated RNA (Figure 2.8A,B). There were no visible decapped decay intermediates (−TAP). When these cRACE products were cloned and sequenced, they contained poly(A) tails of similar lengths, independently of treatment (Figure 2.8C). This suggests that if deadenylation is a component of apoptotic mRNA decay, it is a rapid step in the decay pathway.

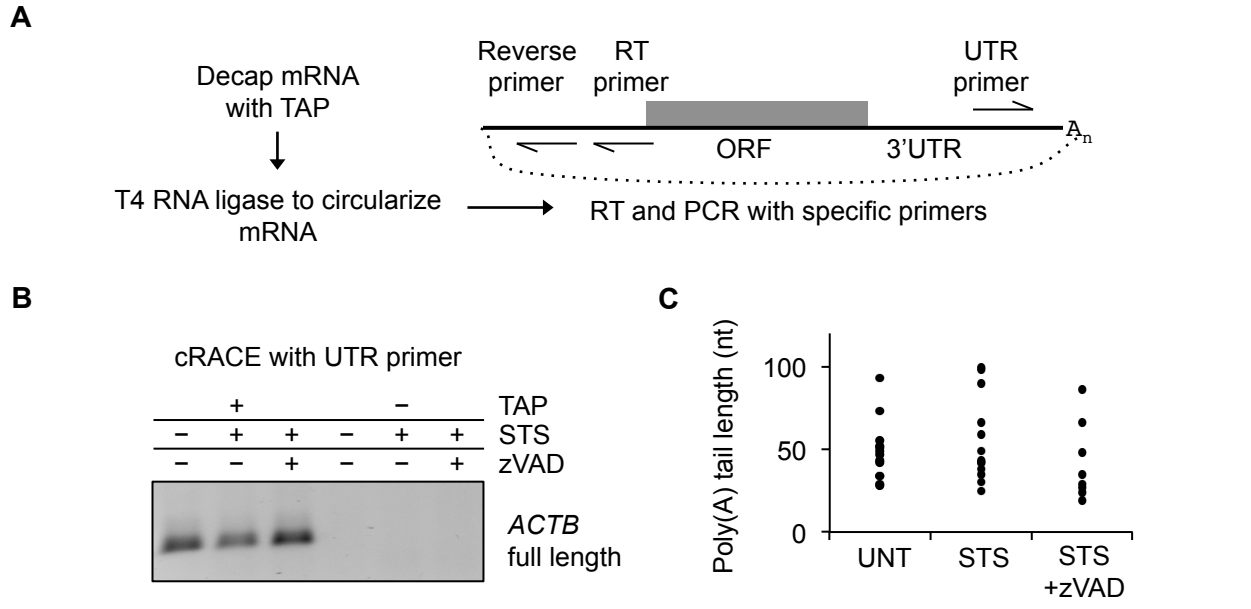

Figure 2.8: Full-length mRNAs in apoptotic cells
(A) Schematic of circularized RACE (cRACE) method used to identify *ACTB* mRNA decay intermediates in HeLa cells treated for 6 hr with STS±zVAD. *ACTB* decay products were amplified by PCR with a forward primer targeting the *ACTB* 3′UTR, and a reverse primer on the *ACTB* 5′UTR. **(B)** Gel electrophoresis of amplified *ACTB* junctions indicates that the full-length *ACTB* mRNA remained mostly capped, even in apoptosis. **(C)** cRACE clones were sequenced and poly(A) tail lengths of capped, polyadenylated *ACTB* mRNA termini amplified with a primer targeting the ACTB 3′UTR are shown. Poly(A) lengths did not change significantly with treatment.

When the ligated *ACTB* junctions were amplified using a forward PCR primer located near the stop codon in the *ACTB* open reading frame (ORF) and a reverse primer in the 5′UTR (Figure 2.9A), novel mRNA decay intermediates were detected in apoptotic cell RNA even in cells treated with zVAD (Figure 2.9B). This agrees with our finding that apoptotic mRNA decay is partially caspase independent (Figure 2.7). The novel decay intermediates were also amplified without TAP pre-treatment, indicating that at least some of the decay intermediates were decapped. We cloned and sequenced cRACE products from STS-treated cells to map the mRNA termini. The junctions that mapped exactly to the *ACTB* mRNA had two notable features (Figure 2.9C,D). First, their 3′ termini were mostly within 50 nt 3′ of the *ACTB* stop codon, suggesting stalled decay near the ORF. Second, most junctions captured from TAP-treated RNA had 5′ termini mapping exactly to the *ACTB* transcription start site (TSS), while all of the 5′ termini captured from TAP-untreated RNA began after the TSS. These results suggest that decay proceeds 3′ to 5′ on deadenylated mRNAs before decapping. Surprisingly, some clones had non-templated residues between the 3′ and 5′ termini. These added bases were rich in uridylates (Figure 2.9E). To confirm that 3′ uridylated *ACTB* decay intermediates were produced during apoptosis, we performed RT-PCR on RNA isolated from cells treated or not with STS using an A_{12}-adapter for RT to prime poly(U) sequences and nested primers targeting the *ACTB* ORF and the adapter primer (Figure 2.9F). Novel decay products reproducibly appeared only in STS-treated cells (Figure 2.9G). Cloning and sequencing confirmed that these were similar to the cRACE products (data not shown). The decay products captured during apoptosis are consistent with two possible modes of mRNA decay. Either decay in apoptosis involves deadenylation, followed by 3′ directed decay and decapping, or these uridylated decay intermediates are generated after internal cleavage by an unknown endonuclease.

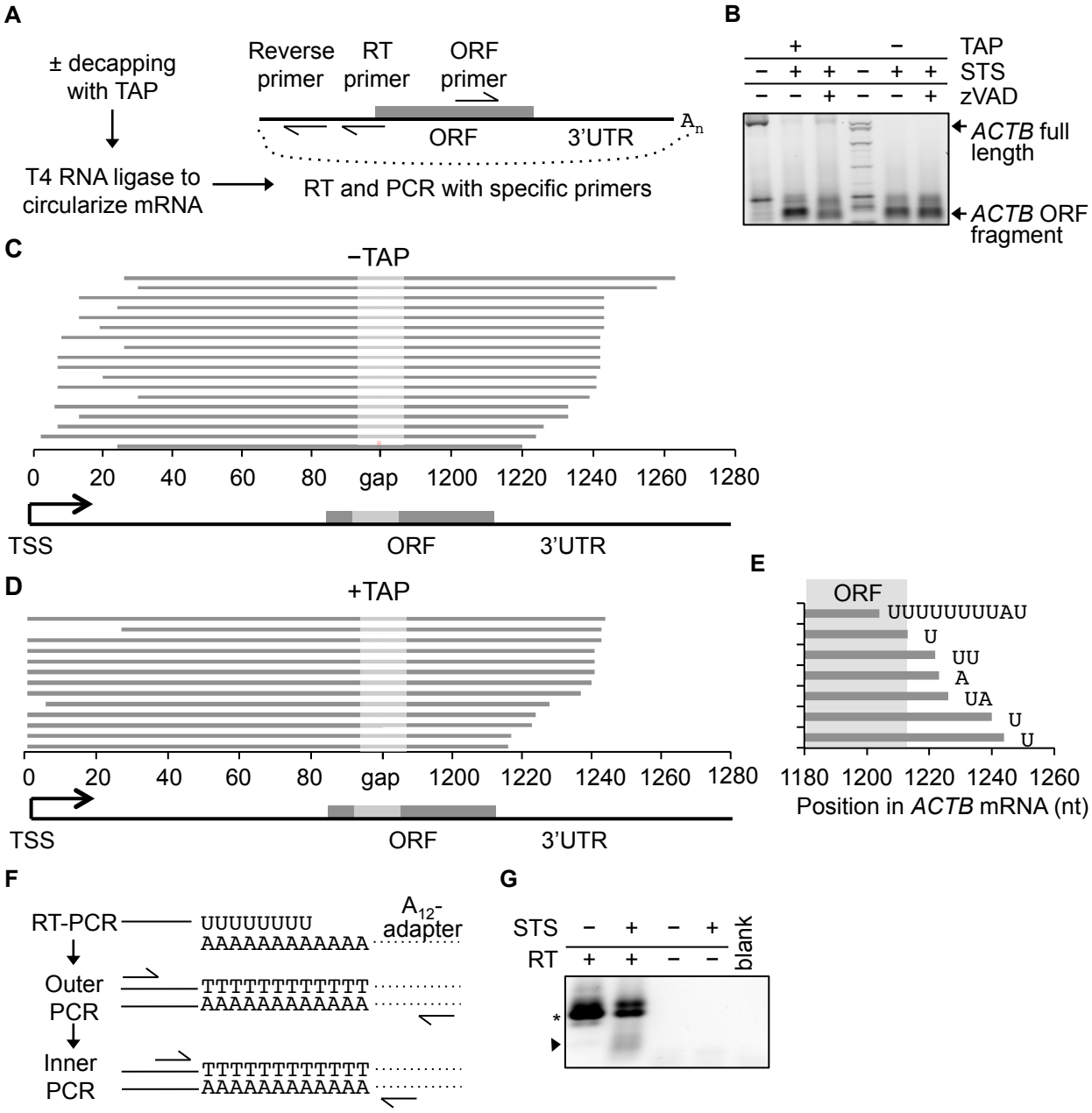

Figure 2.9: 3′ uridylation of apoptotic decay intermediates

(A) Schematic of cRACE method used to identify *ACTB* mRNA decay intermediates in HeLa cells treated for 6 hr with STS±zVAD. **(B-E)** *ACTB* decay products were amplified using an ORF-targeted primer and analyzed by gel electrophoresis **(B)** and cloning and sequencing of RNA that was treated **(C)** or not treated **(D)** with tobacco acid pyrophosphatase (TAP) prior to cRACE. Decay intermediates were truncated just 3′ of the stop codon. Line diagrams (C, D) depict all ORF-primer amplified cRACE clones, excluding clones with nontemplated 3′ extensions. Decapped decay intermediates (−TAP) had shortened 5′ ends, whereas most clones derived from TAP-treated RNA had a complete 5′ sequence. **(E)** Some apoptotic *ACTB* mRNA fragments had nontemplated 3′ tails. Shown are nontemplated RNAs obtained for TAP-treated RNA. Templated residues matching the *ACTB* sequence are depicted as a line; uridylate-rich nontemplated tails are indicated. **(F)** Schematic of the RT-PCR method used to amplify 3′ uridylated RNAs. **(G)** Gel electrophoresis of RT-PCR products. Arrow indicates new uridylated *ACTB* mRNA decay fragments in apoptotic cells. Asterisk denotes products primed from oligouridylate tracts elsewhere in the *ACTB* 3′UTR.

DIS3L2 knockdown inhibits mRNA decay and cell death

Because DIS3L2 preferentially targets 3´ uridylated pre-miRNAs [70,71], we hypothesized that DIS3L2 digests the uridylated mRNA decay products we observed in cell death. To test this hypothesis, we knocked down *DIS3L1* (as a control) and *DIS3L2* in HeLa cells (Figure 2.10A) and used RT-PCR with an A_{12}-adapter to amplify 3´ uridylated *ACTB* mRNA intermediates (Figure 2.10B). Novel uridylated *ACTB* products were detected in nonapoptotic cells transfected with *DIS3L2* siRNA, but not those transfected with *DIS3L1* or control siRNA. The appearance of uridylated mRNA decay intermediates in living cells after *DIS3L2* knockdown suggests that DIS3L2 plays a role in basal mRNA decay. After STS treatment, the uridylated *ACTB* mRNA intermediates greatly increased with *DIS3L2* knockdown, and increased somewhat with *DIS3L1* knockdown. *DIS3L2*, but not *DIS3L1*, knockdown also significantly reduced STS-mediated mRNA decay of three housekeeping genes (*ACTB*, *GAPDH*, *SDHA*) (Figure 2.10C). Thus DIS3L2 is a mediator of mRNA decay in apoptosis and may also play a role in basal mRNA decay.

To examine whether mRNA decay contributes to executing apoptosis, we compared caspase activation, annexin V staining and cell survival of STS-treated HeLa cells knocked down for *DIS3L2*, *DIS3L1* or transfected with a control siRNA. Although caspase 3 cleavage was readily apparent by immunoblot after 4 hours of STS treatment in cells treated with *DIS3L1* or control siRNA, *DIS3L2* knockdown rescued caspase 3 cleavage (Figure 2.10D). *DIS3L2* knockdown also specifically and significantly reduced annexin V staining (Figure 2.10E) and enhanced cell viability (Figure 2.10F) in response to both STS and TRAIL.

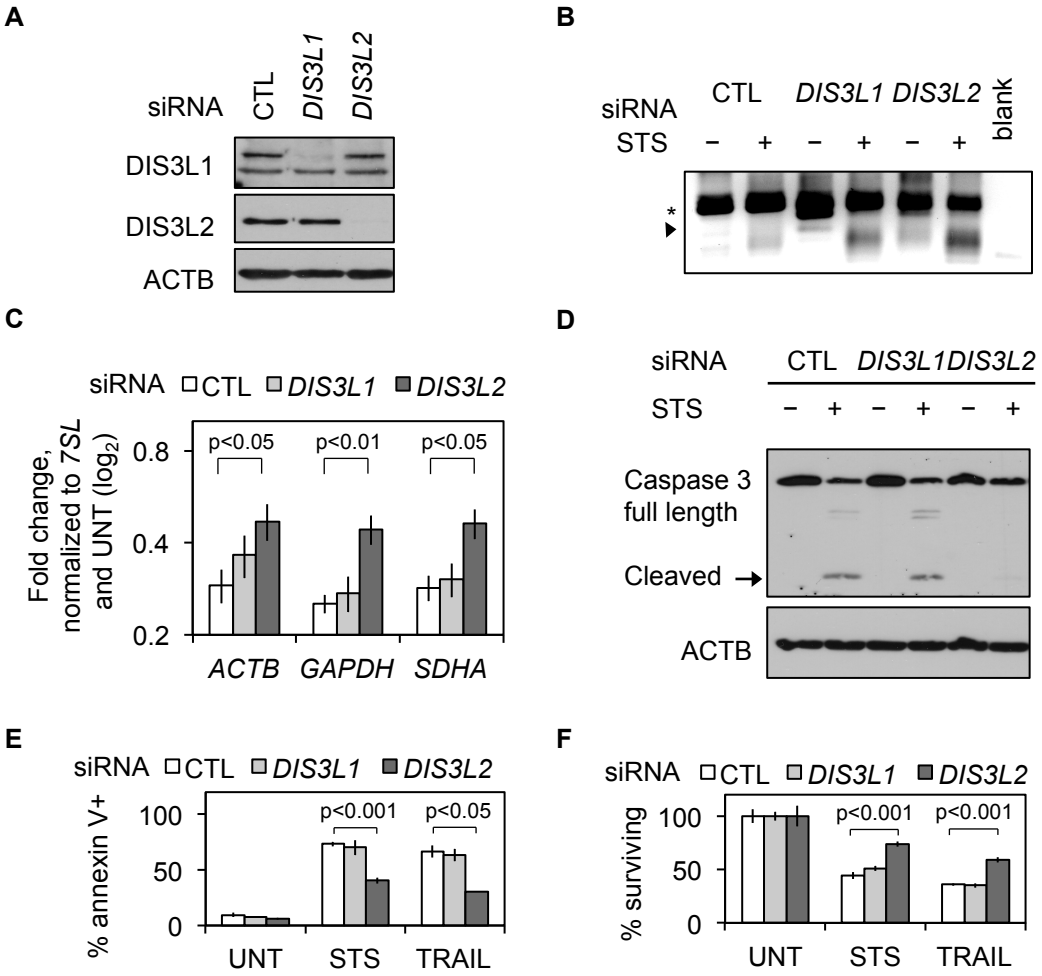

Figure 2.10: *DIS3L2* knockdown inhibits cell death and mRNA decay in HeLa cells
(A) HeLa cells transfected with control (CTL), *DIS3L1* or *DIS3L2* siRNAs, were harvested 72 hr later for immunoblot. **(B)** Accumulation of uridylated decay intermediates was assessed by RT-PCR with an A_{12}-adapter primer (as in Fig. 2.9F,G). Uridylated intermediates accumulated in STS-treated cells regardless of the siRNA, but accumulated to a greater extent after DIS3L2 knockdown. Arrowhead denotes new products; an asterisk denotes products primed from oligouridylate tracts in the *ACTB* 3´UTR. **(C,D)** After knockdown and STS treatment, mRNA levels were assayed by qRT-PCR **(C)** and caspase activation was assessed by immunoblot for caspase 3 **(D)**. *DIS3L2* knockdown partially restored mRNA levels and reduced caspase 3 cleavage. **(E,F)** Cells, treated for 3 hr with STS or TRAIL, were analyzed for cell death by annexin V staining and flow cytometry **(E)**, and for survival assessed after a 24 hr recovery by CytoTox-Glo assay **(F)**. *DIS3L2* knockdown partially rescued PS externalization and cell survival. Error bars represent SEM of at least 3 independent experiments.

To establish whether these results were broadly applicable and not due to off-target effects of a single siRNA, we tested the effect of knocking down *DIS3L2* with a different siRNA (Figure 2.11). We confirmed robust knockdown at the mRNA and protein level (Figure 2.11A,B). As before, *DIS3L2* knockdown led to the accumulation of 3´ uridylated decay products and partially

rescued mRNA decay after treatment with STS (Figure 2.11C-E). To validate the change in 3′ uridylation with a more quantitative assay, we performed cRACE on total RNA from cells transfected with *DIS3L2* or control siRNAs, and treated with STS. Tails with two or more uridylates increased significantly in apoptosis after *DIS3L2* knockdown as compared to control knockdown (p=0.035, Fisher's exact test) (Figure 2.11D). We also observed an increase in *ACTB* decay intermediates with nontemplated 3′ uridylate tails in living cells after *DIS3L2* knockdown (Figure 2.11C), in agreement with our earlier findings (Figure 2.10B). We confirmed that *DIS3L2* knockdown reduced effector caspase activation upon STS treatment with a luminescent assay (Figure 2.11F) and by immunoblot for caspase 3 (Figure 2.11G). Collectively, these results suggest that DIS3L2 targets 3′ uridylated mRNAs in living and dying cells, and that DIS3L2 promotes caspase activation and cell death.

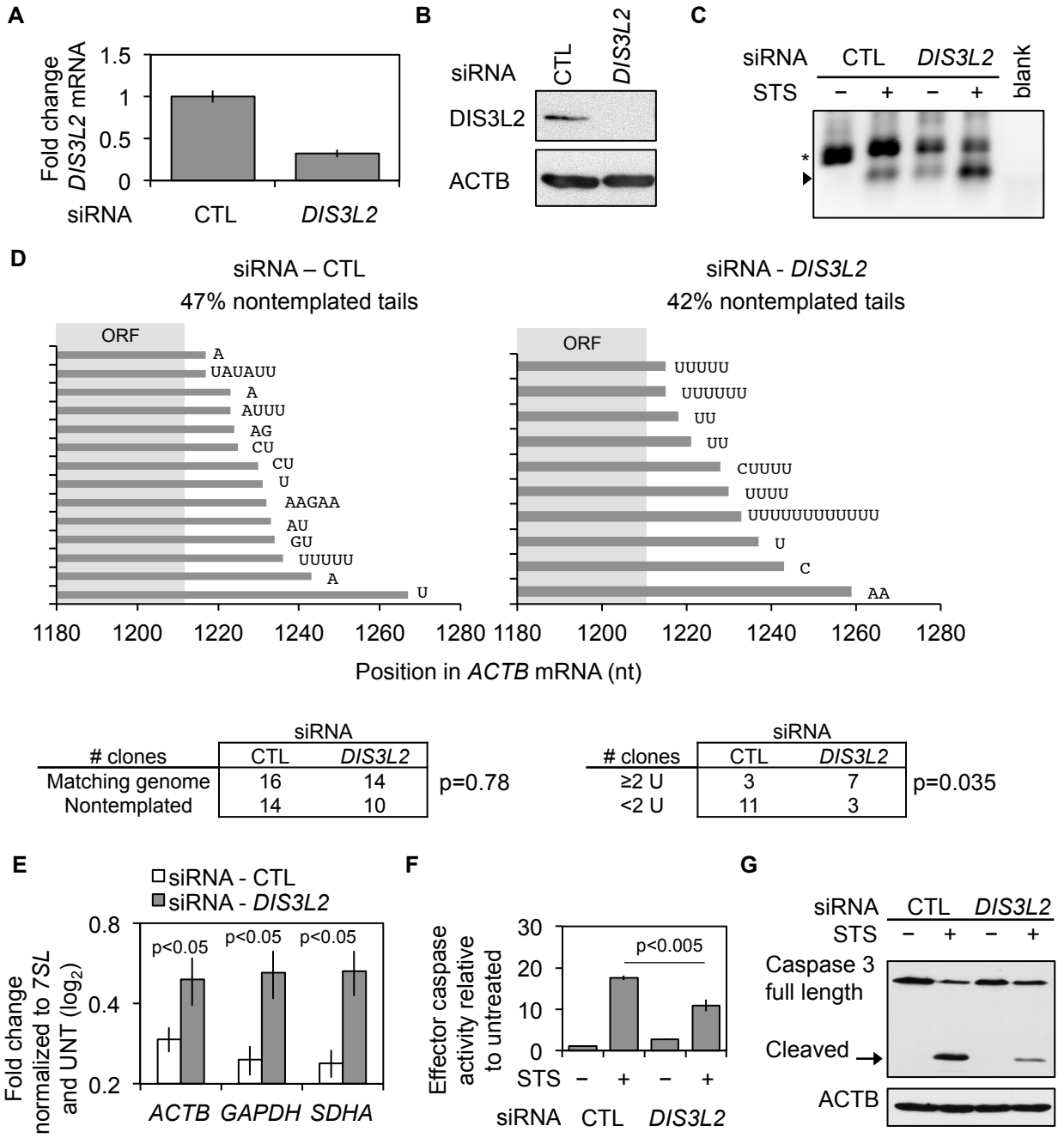

Figure 2.11: DIS3L2 degrades 3´ uridylated decay intermediates during cell death
(A,B) qRT-PCR and immunoblot confirmed siRNA knockdown of *DIS3L2* in HeLa cells. A different siRNA sequence was used in these experiments than in Figure 2.10. **(C,D)** U-tailed *ACTB* decay intermediates (arrow) accumulated in STS-treated HeLa cells after *DIS3L2* knockdown as measured by RT-PCR **(C)** and cRACE **(D)**. Asterisk in (C) denotes products amplified from oligouridylate tracts in the *ACTB* 3´UTR. U-tailed intermediates also accumulated in untreated living cells after *DIS3L2* knockdown (C). The number of clones exactly matching the genome and with nontemplated 3´ ends is shown **(D)**. There was a significant increase in clones with two or more nontemplated uridylates on the 3´ end after DIS3L2 knockdown (Fisher's exact test). **(E-G)** *DIS3L2* knockdown partially restored mRNA levels **(G)** and reduced effector caspase activation **(F)** and caspase 3 cleavage (**G)** caused by STS. Error bars represent SEM of at least 3 independent experiments.

DIS3L2 is a caspase substrate

Immunoblots of STS and TRAIL treated HeLa cells showed that DIS3L2 protein was cleaved inefficiently during apoptosis, generating a persistent fragment (Figure 2.12B). DIS3L2 cleavage was blocked by zVAD. We hypothesized that this persistent fragment might retain nuclease activity or be more active than the full-length protein. Using N- and C-terminally GFP tagged DIS3L2 (NT-GFP DIS3L2 and CT-GFP DIS3L2, respectively), we found that DIS3L2 was cleaved near its N-terminus (Figure 2.12C). Using the Cascleave software [101], we identified likely caspase cleavage sites in DIS3L2 and mutated the aspartate at the highest-scoring predicted site to glutamate (D188E) in NT-GFP DIS3L2. We found that the mutant protein was no longer cleaved (Figure 2.12D), suggesting that DIS3L2 is cleaved after this aspartate. We generated expression constructs of catalytically inactive DIS3L2 (DIS3L2-D391N) and truncated DIS3L2 lacking amino acids 1-188 (DIS3L2-ΔN), which was the same size as cleaved DIS3L2 (Figure 2.12A,E). We expressed these proteins and wild-type CT-GFP DIS3L2 in HeLa cells and performed immunoprecipitation (IP) of the proteins from cytosolic lysates using anti-GFP agarose beads. Finally, we incubated a 5´-end-labeled, 3´-uridylated oligoribonucleotide with the immunoprecipitated protein and analyzed degradation products by gel electrophoresis and autoradiography (Figure 2.12G). Although there was background nuclease activity in all of the IPs, there were distinct decay products (arrowhead) generated by DIS3L2 and DIS3L2-ΔN, but not DIS3L2-D391N. We tested other substrate RNAs and found that DIS3L2-ΔN was an active RNase, but did not differ from DIS3L2 in its substrate specificity (data not shown). These experiments indicated that the cleaved DIS3L2 was still an active nuclease. Because only a small fraction of the total protein pool was cleaved and caspase cleavage did not alter target specificity, we suspect that DIS3L2 cleavage is an epiphenomenon unrelated to the execution of apoptosis.

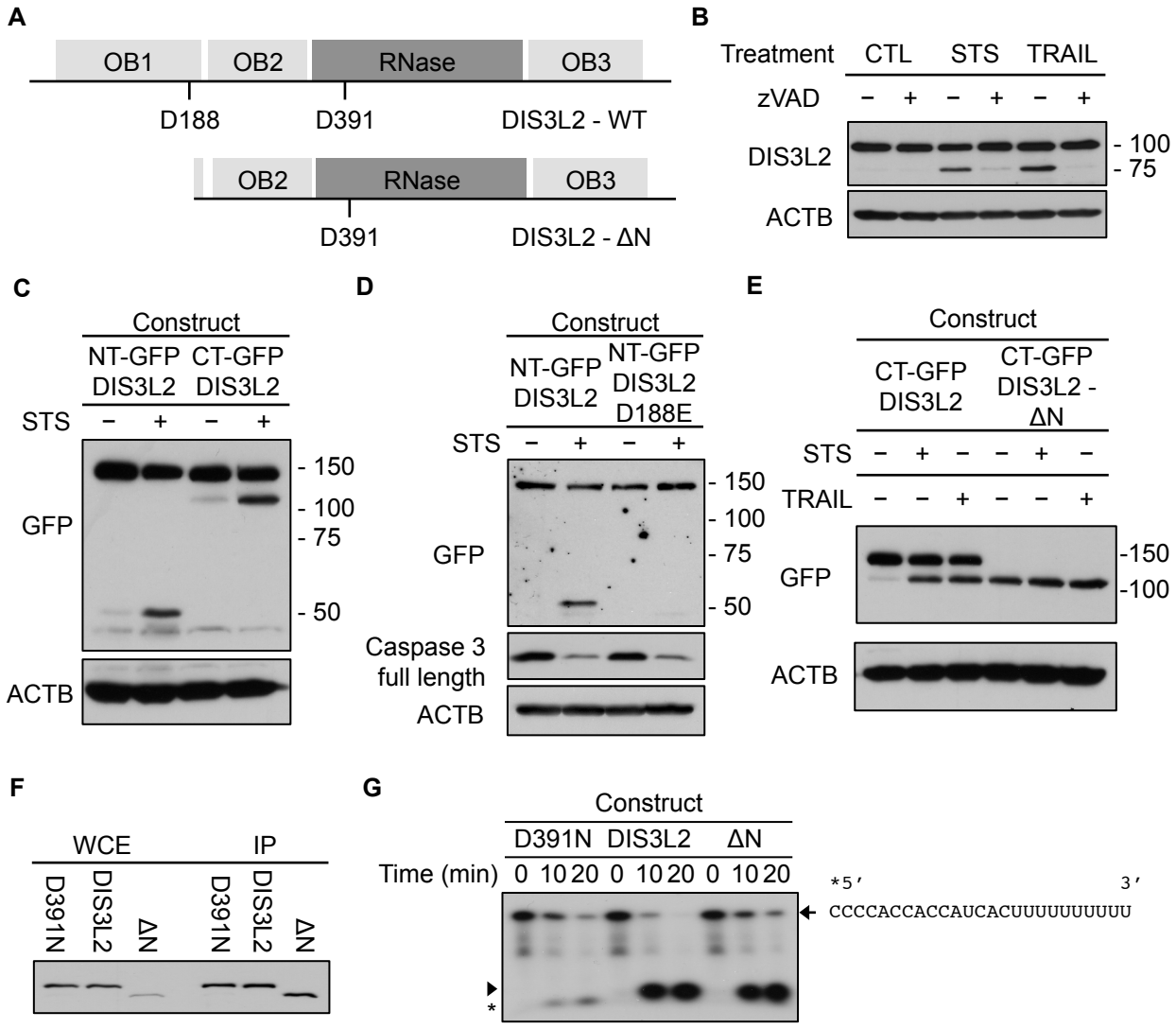

Figure 2.12: DIS3L2 is cleaved by caspases during cell death

(A) DIS3L2 protein is composed of three oligonucleotide binding (OB) domains and an RNase domain. The caspase cleavage site (D188) and truncated DIS3L2 (DIS3L2-ΔN) are indicated. **(B)** HeLa cells were treated with STS or TRAIL ±zVAD for 4 hr and lysates were harvested and immunoblotted for endogenous DIS3L2 and ACTB. DIS3L2 cleavage was rescued by zVAD. **(C)** HeLa cells were transfected with plasmids encoding DIS3L2 tagged at its N-terminus or C-terminus with GFP (NT-GFP DIS3L2 and CT-GFP DIS3L2, respectively). Cells were treated with STS for 4 hr and lysates were blotted for GFP. DIS3L2 is cleaved near its N-terminus. **(D)** A predicted aspartate caspase cleavage residue (D188) was mutated in NT-GFP DIS3L2. Mutation of D188 to glutamate (D188E) abolished NT-GFP DIS3L2 cleavage. **(E)** Ectopically expressed CT-GFP DIS3L2-ΔN is the same size as the apoptotic fragment of CT-GFP DIS3L2. **(F,G)** Plasmids encoding CT-GFP catalytically inactive DIS3L2 (D391N), DIS3L2 or DIS3L2-ΔN were transfected into HeLa cells. Tagged DIS3L2 was purified by GFP IP. Protein loading was equalized **(F)** (WCE − whole cell extract). Beads containing comparable amounts of bound enzyme were incubated with a 5′-end labeled oligonucleotide for the indicated times, and reaction products were analyzed by gel electrophoresis and autoradiography **(G)**. DIS3L2 activity, as measured by the appearance of a specific decay product (arrowhead), was abolished by active site mutation (D391N), but not by N-terminal truncation (DIS3L2-ΔN). Background RNase activity reduced the full-length RNA signal and generated distinct decay products (asterisk).

Nucleases other than DIS3L2 likely participate in apoptotic mRNA degradation. Paired knockdown of the cytosolic deadenylases *CNOT7* and *CNOT8*, but not *CNOT6* and *CNOT6L*, also reduced mRNA decay (Figure 2.13A,B). Like *DIS3L2* knockdown, *CNOT7/CNOT8* knockdown partially rescued cell death in response to STS and TRAIL (Figure 2.13C,D). (The other cytosolic deadenylases (*PAN2*/*PAN3*) were not well expressed in HeLa cells.) Collectively, these results suggest that multiple exonucleases participate in apoptotic mRNA decay, as in basal mRNA decay.

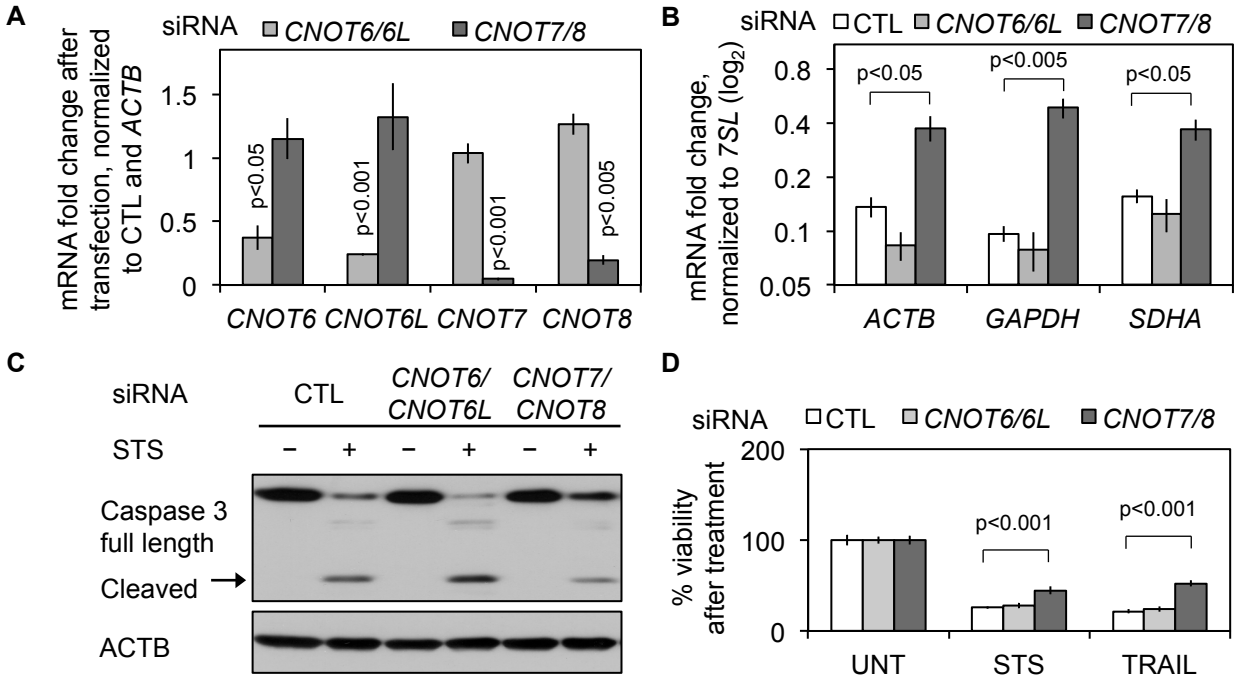

Figure 2.13: *CNOT7* and *CNOT8* knockdown inhibits mRNA decay and cell death
(A) Knockdown was verified by qRT-PCR of total RNA harvested 72 hr after HeLa cells were transfected with control (CTL), *CNOT6* and *CNOT6L,* or *CNOT7* and *CNOT8* siRNAs. (p-values are relative to CTL siRNA transfection). **(B,C)** Cells were treated with STS for 4 hr or left untreated, and the indicated mRNAs were measured by qRT-PCR **(B)**, and caspase 3 cleavage was assessed by immunoblot **(C)**. Knockdown of *CNOT7* and *CNOT8*, but not *CNOT6* and *CNOT6L*, partially rescued apoptotic mRNA decay and caspase 3 cleavage in response to STS. **(D)** Cell survival was measured by a luminescent assay after 3 hr treatment with STS or TRAIL followed by a 24 hr recovery period and normalized to non-apoptotic transfected cells (untreated, UNT). Only knockdown of *CNOT7* and *CNOT8* partially rescued cell death after treatment with both apoptotic stimuli. Error bars represent SEM of at least 3 independent experiments.

Methods

Cells

HeLa, Jurkat, HCT116, 721.221 and YT-Indy were obtained from ATCC. Jurkat, YT-Indy and 721.221 cells were grown in RPMI with 10% heat-inactivated fetal bovine serum, 100 U/mL penicillin G, 100 µg/mL streptomycin sulfate, 6 mM HEPES, 1.6 mM L-glutamine and 50 µM β-mercaptoethanol. Adherent cells were grown in DMEM with the same supplement. Stable HeLa-Puro and HeLa-BCL2 cells were generated by retroviral infection and selection with puromycin using the pBABE-puro vector as described previously [43].

Cell treatments

Jurkat cells were treated with 1:1000 αFas antibody (Millipore, clone CH11). All cells except HeLa were treated with 2 µg/mL ActD (Sigma A9415) to inhibit transcription. HeLa cells were treated with 10 µg/mL ActD (Figure 2.5B) or 500 nM STS (Cell signaling #9953) for the indicated times. HCT116 cells were treated with 100 ng/mL superkiller TRAIL (Enzo Life Sciences ALX-201-115-C010). To inhibit caspase activity, cells were treated with 100 µM zVAD (BD 550377). STS, ActD and zVAD were dissolved in DMSO; an equivalent amount of DMSO (Sigma D2650) was added to all control treatments to equalize the final DMSO concentration. For cytotoxic attack experiments, YT-Indy cells were mixed with 721.221 cells at an effector:target ratio of 3:1.

Assessment of apoptosis

For cytotoxic attack experiments, death was assessed by ^{51}Cr release assays as previously described [43]. In other experiments, cells were stained with annexin V-APC (Life Technologies A35110) or $DiIC_1(5)$ (Life Technologies M34151) according to the manufacturer's instructions. Both dyes were measured on a FACSCalibur flow cytometer. For measurements of effector

caspase activity and cell survival, cells, plated on 96 well tissue culture plates (Corning 3610) one day before treatment, were treated for the indicated time, and activity was assessed with the Caspase-Glo (Promega G8090) or CytoTox-Glo (Promega G9290) kits, respectively, according to the manufacturer's instructions. Luminescence was measured on a BioTek Synergy 2 plate reader. For cell fractionation, cells were washed with PBS and harvested by scraping in PBS on ice. Cells were washed once in PBS and resuspended in 5 cell volumes of mitochondrial isolation buffer (250 mM sucrose, 10 mM Tris-HCl (pH 7.0), 100 mM KCl, 1 mM EDTA, 1X protease inhibitors (Roche 04 693 159 001)). Cells were incubated for 30 min in this buffer on ice, then lysed by passage through a 27 gauge needle 30 times. Lysates were spun at 800 x g for 10 min to remove cell debris. The supernatant was spun again at maximum speed for 25 min and this supernatant (cytosolic fraction) was suspended in RIPA buffer for immunoblotting. Total protein was harvested in RIPA buffer to control for non-cytosolic proteins. For DNA extraction, cells were resuspended and vortexed in lysis buffer (10 mM Tris-HCl, pH 8.0, 10 mM EDTA pH 8.0, 100 mM NaCl, 0.5% SDS with 40 mg/mL proteinase K (Sigma) and incubated for 3 hr at 56^{o}C. Lysate was mixed with an equal volume of TE-buffered phenol, pH 8.0 (Sigma P4557) and vortexed well before centrifugation for 10 min at 13,000 rpm. The aqueous phase was extracted once with an equal volume of chloroform, ethanol precipitated, and dissolved in TE. DNA laddering was analyzed by agarose gel electrophoresis.

qRT-PCR

RNA was harvested and extracted with TRIzol reagent (Life Technologies 15596018) according to the manufacturer's instructions. 500-1000 ng of total RNA was first treated with the DNA-free kit (Life Technologies AM1906) according to the manufacturer's instructions, and half was reverse transcribed in a 20 µl volume with iScript RT reagent (BioRad 1708841) according to the manufacturer's instructions. The other half was used as an RT− control. qRT-PCR was performed with SsoFast reagent (BioRad 172-5204) in 20 µl reaction volumes with 1 µl of cDNA

and 500 nM primers, using a BioRad CFX96 PCR machine with the recommended cycling parameters for the Ssofast reagent. Primers are given in Table 2.1. Taqman miRNA qRT-PCR was performed according to the manufacturer's instructions (Life Technologies N808-0234). The following kits from Life Technologies were used for reverse transcription and qPCR. miR-16: #000391, miR-21: #000397, U6: #001093.

Immunoblotting

Immunoblotting was performed as described previously [43]. All primary antibodies were used at 1:1000 and secondary antibodies at 1:2500. The following antibodies were used: ACTB (DSHB, #JLA20-c); PARP-1 (Santa Cruz, H-250); eIF4G (Cell Signaling, 2498); phospho-eiF2α (Cell Signaling, 9721); total eiF2α (Cell Signaling, 9722); VDAC1 (Santa Cruz, sc-8828); cytochrome c (Biolegend, 612504); Caspase 3 (Cell Signaling, 9662); DIS3L1 (Abcam, ab89042); DIS3L2 (Novus, NBP1-84740); GFP (ABM, G160); Anti-Mouse HRP (GE Healthcare, NA931V); Anti-Rabbit HRP (GE Healthcare, NA934V); Anti-Chicken HRP (Abcam, ab6753-1500); Anti-Goat HRP (Santa Cruz, sc-2020).

Northern blotting

2 µg of total RNA was ethanol-precipitated, washed, and dissolved in gel loading buffer (Life Technologies AM8547). RNA was denatured and run on a 1.5% denaturing agarose gel in MOPS buffer (Life Technologies AM8671). rRNA was visualized with ethidium bromide staining, and the RNA was transferred to a Nytran (GE Healthcare 10416296) membrane in SSC (Life Technologies AM9763). Probes were prepared by in vitro transcription (AM1314) of PCR templates. Samples were hybridized in Ultrahyb buffer (Life Technologies AM8670) and washed twice at 65^{o}C for 5 min in 2X SSC, 0.1% SDS, then twice at 65^{o}C for 15 min in 0.1X SSC, 0.1% SDS before autoradiography.

Table 2.1: Primers used in this study

qRT-PCR primers

Target	Forward	Reverse
28S rRNA	TCATCAGACCCCAGAAAAGG	GATTCGGCAGGTGAGTTGTT
5S rRNA	GGCCATACCACCCTGAACGC	CAGCACCCGGTATTCCCAGG
7SL	ATCGGGTGTCCGCACTAAGTT	CAGCACGGGAGTTTTGACCT
U6	CGCTTCGGCAGCACATATAC	CGAATTTGCGTGTCATCCTT
U2	TGGAGCAGGGAGATGGAATA	CGTTCCTGGAGGTACTGCAA
ACTB	AAGGCCAACCGCGAGAAGAT	ACAGCCTGGATAGCAACGTACA
GAPDH	AAGGTGAAGGTCGGAGTCAAC	GGGGTCATTGATGGCAACAATA
SDHA	TGGGAACAAGAGGGCATCTG	CCACCACTGCATCAAATTCATG
LMNB1	TGCTACTGCACTTGGTGACA	AGGCTCTGACAACGATTCTCCA
STAT5B	AAATTCAAGGCCGAAGTGCAGAGC	CATCACACCGTCAAACCATTGCCA
APAF1	GTCACCATACATGGAATGGCA	CTGATCCAACCGTGTGCAAA
CNOT6L	AGAAATCTCGGGTAGAGTGCG	CAATATCAGGTGGAATGCGACT
CNOT6	CCTGACCCTCGGAGGATGTAT	GCTTGGCAATGTCTGAAGGAA
CNOT7	TGGTTGTCATTTCATAGCGGTT	CAGGCAAGTTAGAGTTGGTTAGG
CNOT8	CTGCGGTGCAATGTTGACC	GATTCCAGAAGGATACTCTCCCT

Cloning primers

Plasmid name	Forward Primer	Reverse Primer
D188E mutant	GAAGGTGTTAAGAAACTCTCAGTTTGTG	AACCAGCACATTTTGTGTGATGC
DIS3L2- ΔN	GGTGTTAAGAAACTCTCAGTTTGTG	CATAGATCTGAGTCCGGTAGC
D391N mutant	AATGATGCCCTCTCCTGCAAGC	GAGGTCTCGGGCGGTTGA
pBABE-BCL2	ATCGAATTCGGAAGGATGGCGCACGCTGGGAGA	ATCGTCGACTCACTTGTGGCCCAGATAGG

cRACE primers

Name	Sequence
RT primer	GCTGGCGGCGGGTGTG
Universal Reverse primer	GCAAAGGCGAGGCTCTGTG
UTR Forward primer	CCAGTTGAATAAAAGTGCACACC
ORF Forward primer	TCCATCGTCCACCGCAAATG

RT for uridylated products primers

RT Adapter	GCGAGCACAGAATTAATACGACTCACTATAGGAAAAAAAAAAAA
OUTER_REV	GCGAGCACAGAATTAATACGACT
OUTER_ACTB_FWD	AAGCAGGAGTATGACGAGTCC
INNER_REV	CGCGGATCCGAATTAATACGACTCACTATAGG
INNER_ACTB_FWD	TCCATCGTCCACCGCAAATG

FISH

Adherent cells were grown in 24 well plates (Corning 3524) on 12 mm glass coverslips (VWR 89015-724) pre-treated with poly-L-lysine (Sigma P8920) for 5 min. Jurkat cells were washed, resuspended in PBS (Life Technologies 14190-144) with 0.5% BSA (Sigma A9647) and 2 mM EDTA (Life Technologies AM9260G), then cytospun (Shandon Cytospin 3) for 4 min onto coverslips at 400 rpm before fixation, whereas YT-Indy:721.221 immune conjugates were fixed first, then cytospun as above. Cells were fixed for 10 min in 2% formaldehyde (Polysciences 18814) in 1X PBS, and permeabilized in pure methanol (Fisher BP1105-4) on dry ice for 10 min. Slides were washed 3 times for 5 min in 2X SSC. A control for each experiment was treated for 30 min in 0.1 M NaOH (Fisher SS255-1) in 2X SSC to hydrolyze all RNA. All coverslips were inverted onto a drop of hybridization buffer (10% Dextran Sulfate, 35% Formamide, 0.3 M NaCl, 30 mM sodium citrate, 20 mM DTT) containing 1 µM *18S* rRNA probe (Cy5-ACCAGACTTGCCCTCC) and 333 nM poly(A) (Cy3-dT_{50}) probe. Samples were placed in a humidified chamber, and denatured for 5 min at 65^{o}C, followed by 30 min at 45^{o}C and at least 90 min at 42^{o}C. The samples were washed 3 times for 5 min in 2X SSC at 37^{o}C, and stained with DAPI (Sigma D9542) in 2X SSC. Finally, the slides were mounted using polyvinyl alcohol (Sigma P-8136) aqueous mounting medium. Cells were imaged using an Axiovert 200M microscope (Pan Apochromat, 1.4 NA; Carl Zeiss) at 63X. Images were analyzed with SlideBook 4.2 (Intelligent Imaging Innovations). For quantification, cells were automatically identified based on rRNA signal, and background intensity was subtracted. All images shown are representative of at least 3 independent experiments.

cRACE

20 µg of total RNA was treated with the DNA-free kit (Life Technologies) as per the manufacturer's instructions. RNA was ethanol precipitated overnight and washed twice with

70% ethanol. RNA was resuspended in 11 µl of 1X TAP buffer (Epicentre T19050). 5 µl was treated with 2 units of TAP for 1 hr at 37°C, the other half was treated the same but TAP was not added. The reactions were then treated overnight at RT in a 100 µl volume with 10 units of T4 RNA ligase (NEB M0204S) with 1 mM ATP in 1X RNA ligase buffer. RNA was ethanol precipitated and washed, then resuspended in 20 µl dH_2O. 3 µl of this RNA was mixed with 1 µl of 10 mM dNTPs, 2 µl of the *ACTB* RT primer and 7 µl of dH_2O. This was heated to 65°C for 5 min and cooled to 25°C. 7 µl of a master mix containing 4 µl 5X SuperScript III buffer, 1 µl 100 mM DTT, 1 µl SuperScript III (Life Technologies 18080-093) and 1 µl RNaseOUT (Life Technologies 10777-019) was added. The reaction was incubated at 55°C for 60 min and 70°C for 15 min before storage at 4°C. 2 µl of this reaction was mixed with 1 µl of each PCR primer (at 10 µM), 6 µl dH_2O, and 10 µl 2X Phusion polymerase mix (NEB M0531L) and cycled as follows: 98°C for 30 s; 35 cycles of 98°C for 10 s, 60°C for 10 s, 72°C for 10 s; and 72°C for 3 min. PCR products were gel extracted and cloned using the Zero-Blunt PCR kit (Life Technologies K2750) according to the manufacturer's instructions. Primers are given in Table 2.1. In the figures, line diagrams depict the mapped 5´ and 3´ ends; the sequence between the primers is inferred to be full-length *ACTB* mRNA.

RT-PCR with adenylated adapter primer to detect uridylated decay products

1 µg of total RNA was mixed with 3 µl of a 100 µM adapter primer and 1 µl 10 mM dNTPs in a final volume of 13 µl. This was heated to 65°C for 5 min and cooled to 25°C. 7 µl of a master mix containing 4 µl 5X SuperScript III buffer, 1 µl 100 mM DTT, 1 µl SuperScript III and 1 µl RNaseOUT was added. The reaction was incubated at 25°C for 10 min, 50°C for 30 min, and 70°C for 15 min before storage at 4°C. 2 µl of this reaction was mixed with 1 µl of each outer primer, 6 µl dH_2O, and 10 µl 2X Phusion polymerase mix and cycled as follows: 98°C for 30 s; 30 cycles of 98°C for 10 s, 60°C for 10 s, 72°C for 10 s; and 72°C for 3 min. PCR was repeated

using identical parameters with the inner primers. Products were cloned as above. Primers are given in Table 2.1.

siRNA knockdown of target genes

HeLa cells were plated on 6 well plates at a density of $8x10^4$ cells per well 1 day before transfection. For transfection, cells were washed twice with PBS and 867 µl of OptiMEM (Life Technologies 51985-091) was added to each well. 5 µl OligoFectamine (Life Technologies 12252-011) was mixed with 24 µl OptiMEM and allowed to rest for 5 min at RT. 100 µl OptiMEM pre-mixed with 2.5 µl of a 20 µM siRNA (or siRNA pool) was added to the OligoFectamine complexes, mixed well, and incubated for 20 min at RT. The entire reaction mixture was added to 1 well of cells. After 6 hr, the cells were washed in PBS and returned to growth medium. Unless otherwise indicated, all assays were performed 72 hr after transfection. The following siRNAs were from Dharmacon: CTL (D-001210-05-05); CNOT7 (M-012897-02-0005); CNOT8 (M-018791-00-0005); CNOT6 (M-019101-01-0005); CNOT6L (M-016411-01-0005); DIS3L1 (M-015333-00-0005); DIS3L2 (M-018715-01-0005). In Figure 2.11, the following siRNAs were used (from Ambion): CTL (4390843); DIS3L2 (4392420).

Cloning

The GFP reporter constructs shown in Figure 2.4 were kindly provided by Dr. Britt Glaunsinger [74,76]. GFP-DIS3L2 constructs were kindly provided by Dr. Andrzej Dziembowski [69] and used as a template for PCR mutagenesis. Briefly, primer pairs were mixed with 100 ng of plasmid at a final concentration of 500 nM in 1X Phusion PCR mix, and subjected to 24 cycles of PCR. Products were cleaned up with a column kit (Qiagen 28106) and brought to a 18.5 µl volume in 1X T4 DNA ligase buffer (NEB). This was treated with 0.5 µl T4 PNK (NEB M0201S) for 30 min at 37^{o}C, 0.5 µl T4 DNA ligase (NEB M0202S) for 1 hr at RT and 0.5 µl DpnI (NEB R0176S) for 30 min at 37^{o}C, followed by chemical transformation into high efficiency *E. coli*. The

BCL2 expression vector was generated by PCR amplification of BCL2 and subcloning into the EcoRI and SalI sites of pBABE-puro. In all cases, multiple clones were picked and correct insertions/mutations were verified by sequencing. Primer sequences are provided in Table 2.1.

GFP immunoprecipitation (IP) and *in vitro* activity of DIS3L2

One day before transfection, $1.1x10^6$ HeLa cells were plated on 10 cm dishes in antibiotic-free medium. The following day, each plate was transfected by mixing 600 µl of OptiMEM and 6 µl Lipofectamine 2000 (Life Technologies 11668-027) with 600 µl of OptiMEM and 3 µg of plasmid. After 20 min incubation, lipoplexes were added to cells in 4.8 ml of antibiotic-free medium. The medium was changed after 6 hrs of transfection. The following day, cells were washed in cold PBS, scraped and washed again in a 15 mL conical tube in PBS. The cells were then resuspended in lysis buffer (50 mM Tris-HCl, pH 8.0, 200 mM NaCl, 2.5 mM $MgCl_2$, 0.5% v/v Triton-X with 1X protease inhibitors (Roche)), mixed well by pipetting and tumbled for 30 min at 4^oC. Lysates were centrifuged for 10 min at 10,000 rpm and supernatants were transferred to a new tube. GFP-Trap agarose beads (ChromoTek gta-20) were washed three times in lysis buffer without Triton-X, the lysates were added directly to the beads and tumbled for 2 hr at 4^oC. The beads were washed once in lysis buffer and then three times in lysis buffer without Triton-X, and finally resuspended in RNase activity buffer (10 mM Tris-HCl, pH 8.0, 75 mM NaCl, 1 mM DTT, 0.2 mM $MgCl_2$). A small fraction of each IP was used for immunoblot to equalize protein loading. For end labeling, 5 µl of RNA oligo (1 µM) was mixed with 1 µl T4 PNK and 4 µl γ^{32}P-ATP (3000 µCi/mmol) in a 25 µl volume in 1X T4 PNK buffer, and incubated for 30 min at 37^oC, then cleaned up with a G-25 column (GE Healthcare 27-5325-01). Equal amounts of protein were incubated with the end-labeled oligomer (sequence shown in Figure 2.12) for the indicated times at 37^oC, the reactions were stopped by adding 2 volumes of 2X gel loading buffer (Life Technologies AM8547) and analyzed by denaturing PAGE and autoradiography.

Statistical analysis

Pooled data from 3 independent cytotoxic attack FISH experiments were compared using a Mann-Whitney test. cRACE results after *DIS3L2* knockdown were compared by Fisher's exact test. All other p-values were computed with a two-tailed student's t-test.

Chapter 3: Conclusions

Rapid and global mRNA decay during apoptosis with 3´ uridylated intermediates degraded by DIS3L2

Summary

Although much is known about the changes to genomic DNA, proteins and lipid membranes that occur during cell death, little is known about what happens to RNA. Here we show that early, global mRNA decay is a new hallmark of classical apoptotic cell death. Global mRNA degradation, which did not occur in ncRNAs, was instigated by a variety of proapoptotic signals (death receptor ligation, STS, high dose ActD and NK cell attack) in several different cell types. It was specific to classical apoptosis and did not occur during non-apoptotic oxidative stress or caspase-independent programmed cell death triggered by GzmA. We are unaware of any other physiological setting in which mRNA is degraded so rapidly and globally. Global mRNA decay was completely inhibited by blocking MOMP using BCL2 over-expression and *BAX/BAK* knockdown, but only partially attenuated by caspase inhibition. In this study we began to define the mRNA decay pathway activated during apoptosis. mRNA decay products appear during cell death that are absent in living cells. *ACTB* mRNA decay intermediates were truncated at their 3´ ends just downstream of the stop codon. Some of the 3´ truncated decay products had nontemplated, uridylate-rich tails. The 3´ uridylated intermediates increased after *DIS3L2* knockdown, which also inhibited global mRNA decay. These findings suggest that DIS3L2 is one of the RNases responsible for apoptotic mRNA decay. *DIS3L2* knockdown also led to similar decay intermediates in non-apoptotic cells, adding to growing evidence suggesting that DIS3L2 is also involved in normal mRNA turnover [69]. Knockdown of *CNOT7* and *CNOT8* also implicates these deadenylases in apoptotic mRNA digestion.

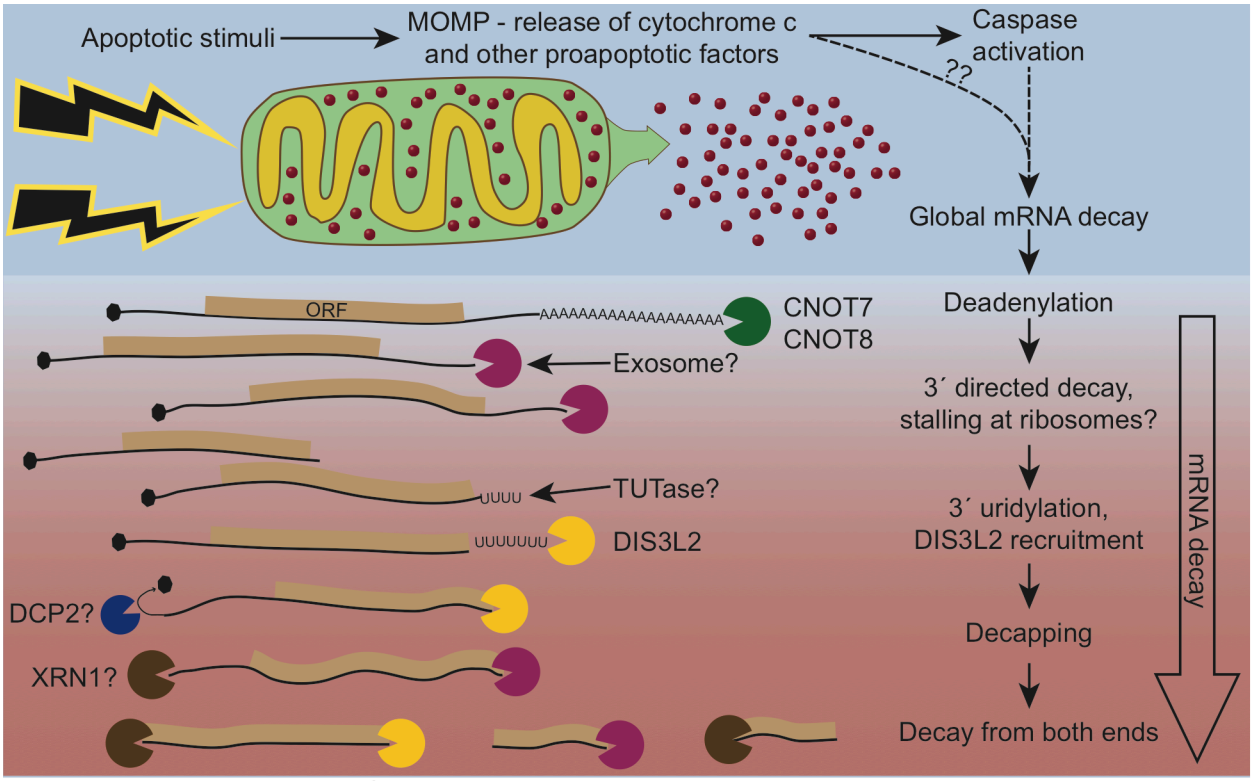

Figure 3.1: A working model for global apoptotic mRNA decay
Global mRNA decay during classical apoptosis is triggered by MOMP. The presumed mitochondrial factor(s) that trigger decay are, as yet, unknown. We hypothesize that apoptotic mRNA decay is similar to decay in living cells, with multiple nucleases collaborating to degrade the mRNA. Knockdown of *CNOT7* and *CNOT8* partially rescues mRNA decay, suggesting that deadenylation might be an early event. The exosome may participate by targeting decay products lacking a poly(A) tail. Decay is stalled, possibly at structured elements or at translating ribosomes. Decayed intermediates are uridylated on their 3´ end, and the uridylated products are degraded by DIS3L2. Decapping and 5´ to 3´ decay could occur before or after stalled decay, but it is depicted in sequence after uridylation here. Question marks indicate hypothetical steps in need of further experimental support.

Our data are consistent with a model (Figure 3.1) in which apoptotic mRNA decay mimics normal mRNA decay and begins at the 3´ end with (1) deadenylation by CNOT7 and/or CNOT8; (2) 3´ to 5´ digestion by the exosome or other 3´ to 5´ exonucleases, which might stall at ribosomes or secondary structure; (3) oligouridylation of the 3´ ends of stalled decay products by an unidentified TUTase; (4) digestion of oligouridylated decay intermediates by DIS3L2; (5) decapping followed by complete decay from both ends of the mRNA. It is unlikely that this sequence proceeds in a strictly linear manner. For example, decapping likely follows deadenylation, but could precede 3´ to 5´ exonucleolytic decay. Detailed kinetic and mechanistic

studies will be necessary to fully characterize the sequence of events. Even in living cells it can be unclear what signal marks mRNAs for destruction. Because decay during apoptosis is rapid and synchronous, it may be a useful system to probe general mechanisms of mRNA decay.

Broader implications and future directions

Although this study identified some components of the apoptotic mRNA decay pathway, there are still many open questions (Figure 3.1). Our results suggest that a mitochondrial product released during MOMP initiates global mRNA decay. Future studies will be needed to define the mechanism that instigates mRNA destabilization. The mechanism of caspase activation downstream of MOMP was discovered through careful biochemical characterization of cytosolic extracts that could recapitulate caspase 3 cleavage and activation [14]. This approach identified the release of cytochrome c from the mitochondrial intermembrane space as the trigger for apoptosome formation and caspase 9 activation. It is possible to recapitulate some aspects of mRNA decay *in vitro*. Similar biochemical systems combining fractionation of mitochondrial extracts with an mRNA decay assay could be used to identify the factor(s) that trigger apoptotic mRNA decay. Type I cells, which do not require MOMP to execute apoptosis triggered by death receptors, have delayed cytochrome c release relative to type II cells [21]. It would be informative to determine whether there is a difference in the rate of mRNA decay between type I and type II cells. Based on our observation that decay is dependent on MOMP, we hypothesize that mRNA decay is slightly delayed in type I cells.

Biochemical studies should be complemented by further genetic studies of the nucleases that participate in apoptotic mRNA decay. Systematic knockdown or knockout of known ribonucleases and their cofactors in human cells, paired with functional phenotyping, such as deep sequencing, uridylation assays, and quantification of mRNA decay rates and poly(A) tail lengths could be a powerful approach to better understand mRNA decay in dying cells. Studies

that have characterized the nucleases that participate in human cell mRNA decay usually focused on reporter mRNAs and used siRNAs for loss-of-function [56,102]. mRNA decay has been well-characterized in yeast with detailed genetic, functional and biochemical studies [103]. A systematic study of human cells with loss-of-function of specific decay factors could provide valuable insight into the role of these enzymes in living and dying cells.

Although *CNOT7* and *CNOT8* knockdown rescued mRNA decay and cell death, we did not observe an increase in partially deadenylated decay intermediates in apoptotic cell RNA, probably because deadenylated mRNAs are rapidly eliminated. We suspect that another 3´ to 5´ exoribonuclease digests the deadenylated mRNA. The most likely candidate is the exosome, which is responsible for basal digestion of deadenylated mRNAs [54]. DIS3L2 or the cytosolic 3´ to 5´ exonuclease ERI1 [104] could also participate in these early stages of decay. Exosomes in the cytosol can contain three different exoribonucleases, DIS3, DIS3L1 and EXOSC10. Knockdown of *DIS3L1* had little impact on mRNA decay or apoptosis. In our preliminary experiments, knockdown of *EXOSC10* appears to reduce mRNA decay and cell death triggered by STS (data not shown). We intend to investigate this promising lead in more detail. If the exosome is involved, it would further support our current working model (Figure 3.1).

It remains to be determined what role *DIS3L2* might play in regulating the stability of different classes of RNAs. Here we found that DIS3L2 targets 3´ uridylated mRNA decay products in a manner analogous to the degradation of uridylated pre-miRNAs [70]. However DIS3L2 might not target all 3´ uridylated RNAs in every setting. Although uridylation is thought to be an important signal in histone mRNA degradation, in a recent study knockdown of *EXOSC10* extended histone mRNA half-life, but *DIS3L2* knockdown had no effect on histone mRNA levels [66]. mRNA decay can occur on translating polyribosomes [66,69,81,82]. Uridylation of stalled transcripts and DIS3L2 digestion of uridylated mRNAs may serve to reinitiate degradation caused by stalling at ribosomes. Future studies using 3´ end-directed deep sequencing

protocols [105], paired with knockdown or knockout of DIS3L2, could lead to powerful insights into its substrates and sequence specificity.

Next generation sequencing will also be a powerful approach to uncover more about the biology of RNA decay during cell death. Future studies should include deep sequencing of ribosomal RNA-depleted total RNA from apoptotic cells, which might provide new information about the patterns and kinetics of mRNA decay. For example, it may be that mRNAs with a large amount of secondary structure are resistant to decay, or that ribosomes protect RNA from decay. This could be tested by comparing the regions of mRNAs that are resistant to apoptotic decay to the profile of ribosome protected sequence fragments [106]. It may be that certain *cis* regulatory elements in mRNAs (primary sequence, secondary structure, or both) protect them from apoptotic mRNA decay. Such a *cis* regulatory element was found to protect the *IL6* mRNA from decay driven by the viral SOX proteins [107].

Newer sequencing approaches might also be revealing. Notably, 3´ end sequencing should reveal whether the global distribution of mRNA poly(A) tail lengths changes during cell death and whether many decay products have nontemplated 3´ uridylation or if this is a more isolated phenomenon. Apoptotic mRNA decay may have been overlooked for decades in part because apoptosis has been studied in bulk populations of asynchronously dying cells. It is challenging to assess the disappearance of mRNA when only a fraction of cells in a bulk population are apoptotic at any given time point. Indeed, the FISH approach taken in this study was critical for showing that mRNA decay was truly global. An approach was recently developed to perform RNA deep sequencing *in situ* on fixed cells [108]. If paired with immunofluorescence staining for markers of cell death, this method could provide greater insight into the kinetics of mRNA decay.

We have not yet identified the putative TUTase that is responsible for adding uridylate-rich tails to the 3´ end of *ACTB* decay intermediates. Our preliminary studies have identified a candidate TUTase, but this work requires further validation (data not shown). It will be interesting to see whether knocking down TUTases reduces apoptotic mRNA decay or cell death.

Although our data are consistent with 3´ to 5´ exonucleolytic decay of mRNAs, we cannot rule out the possibility that an endonuclease is involved. Endonuclease cleavage occurs in some mRNA decay pathways, such as nonsense-mediated decay [58]. During ER stress, many mRNAs that encode membrane or secreted proteins that are localized to the ER are endonucleolytically cleaved by the the ER-resident endonuclease IRE1 [59–61]. Decay of ER-localized mRNAs is thought to reduce the translation of ER proteins to alleviate ER stress. In our experiments, *IRE1* knockdown, unlike knockdown of *CNOT7*, *CNOT8* and *DIS3L2*, promoted cell death, even in untreated cells (data not shown), probably because cells lacking IRE1 have a blunted stress response. It thus seems unlikely that this ER-specific exonuclease, which probably protects against cell death, is responsible for global mRNA decay during apoptosis, which enhances cell death

Why is mRNA eliminated in apoptosis?

It is unclear how mRNA decay contributes to the execution of programmed cell death. We previously found that mRNA splicing and RNA export were disabled during both classical apoptosis and caspase-independent programmed cell death [43]. This prevented the expression of mRNAs that were transcribed in response to the death-inducing stimuli and thus promoted apoptosis by blocking new protein synthesis needed for cellular repair. Now we find that preexisting mRNAs are rapidly degraded during classical apoptosis, which should interfere with the expression of repair proteins as well as housekeeping and other cellular proteins.

Global mRNA decay seems important to cell death execution, since interfering with it by knocking down enzymes responsible for apoptotic mRNA degradation reduced apoptosis and promoted cell survival. Unexpectedly, knockdown of *DIS3L2* also reduced caspase 3 cleavage during apoptosis. How this happens remains to be defined. It may be that mRNA decay blocks the translation of antiapoptotic proteins. For example, the BCL2 family member MCL-1 has a very short protein half-life [109]. It could be that mRNA decay prevents new MCL-1 protein from being translated. The pool of pre-existing MCL-1 declines rapidly when it is not replenished by translation, thus activating a feed-forward loop that promotes further release of mitochondrial effectors. If this is true, it may be that the release of a small amount of cytochrome c is only the prelude to commitment to apoptosis and a second wave of cytochrome c release is required for cell death.

Global mRNA decay during cell death could also be useful for eliminating viral mRNAs to contain the spread of infection. However, some viruses encode proteins that trigger host cell mRNA degradation [73,74,76]. It might be informative to compare and contrast the modes of RNA decay induced by viral infection and cell death. Apoptotic cells are also recognized and cleared by professional phagocytes. It has been speculated that genomic DNA is fragmented during apoptosis to expedite immune clearance of dead cells. It could be that mRNA decay plays a similar role.

We favor a simple hypothesis that, by degrading all of their mRNA, apoptotic cells block new protein synthesis. Cells that cannot synthesize new proteins are unable to survive. However, it is challenging to tease apart the relationship between translation and mRNA decay. It is well known that most cellular stresses arrest protein translation [34]. The stimuli that trigger apoptosis also induce stress and stress-associated alterations to translation initiation factors [34]. We found that changes to translation initiation factors during apoptosis occur after most of the cellular mRNA has already been degraded. Thus inhibiting translation initiation could

contribute to blocking *de novo* protein synthesis during apoptosis, but likely has less of an impact than global mRNA decay. In stress-induced translation arrest, mRNAs remain stable. In contrast, the translation arrest in cell death is coupled with global RNA decay. Future studies should assess, in parallel, the translation status of cells treated with apoptotic stimuli and the rate of decay of their mRNAs. Careful kinetic analyses, similar to those used to study miRNA-induced translation arrest and RNA decay [80], might reveal the order of events in cell death.

Chapter 4:

Cytotoxic leukocyte protease binding to nucleic acids promotes nuclear localization and cleavage of nucleic acid binding proteins

Contributions

This project was a collaboration with **Dr. Jennifer Whangbo**, and she deserves equal credit for the work. **Geoffrey McCrossan** performed many of the experiments and made thoughtful intellectual contributions. I initially conceived the study with **Dr. Michael Walch**. I performed all of the bioinformatics analyses. I also designed and performed the preliminary studies showing that RNA promoted Gzm cleavage of RNA binding proteins and that the Gzms bound directly to single-stranded RNA. Jennifer and Geoffrey joined the project and replicated and expanded the experimental results. Almost all of the experiments were designed and analyzed in collaboration with Jennifer and Michael. We also received invaluable advice from **Kimberly Martinod** on neutrophil extracellular traps, and **Aaron Deutsch** showed that G3BP1 is a target of GzmB and caspase 3. Last, but not least, **Dr. Judy Lieberman** supervised and directed the project.

This work was published on June 1, 2014 in *The Journal of Immunology* (Appendix 2) [110].

Abbreviations used in this study

AF488	AlexaFluor 488
CATG	Cathepsin G
CTL	Cytotoxic T lymphocyte
dsDNA	Double-stranded DNA
FAM	Fluorescein amidite
FP	Fluorescence polarization
GO	Gene ontology
Gzm	Granzyme
H1	Histone H1
hnRNP	Heterogeneous nuclear ribonucleoprotein
MOMP	Mitochondrial outer membrane permeabilization
NE	Neutrophil elastase
NET	Neutrophil extracellular trap
NK cell	Natural killer cell
PE	Pancreatic elastase
Pfn	Perforin
PMA	Phorbol 12-myristate 13-acetate
RBP	RNA binding protein
ssDNA	Single-stranded DNA
ssRNA	Single-stranded RNA

Introduction

CTLs and NK cells eliminate virus-infected cells and tumor cells by releasing the Gzm serine proteases and Pfn from cytotoxic granules into the immune synapse formed with the cell destined for elimination [5]. GzmA and GzmB, the most abundant and best studied Gzms, are delivered to the target cell cytosol by Pfn and rapidly concentrate in the target cell nucleus by an unknown mechanism and induce independent programs of cell death [41,42]. To orchestrate cell death in diverse types of target cells, the Gzms cleave multiple substrates, likely numbering in the hundreds, within the cytosol, nucleus, and mitochondria [5,43].

Although all of the Gzms can cause target cell death, the killing mechanisms of GzmA and GzmB are best understood. GzmB acts like an initiator caspase – it triggers MOMP and effector caspase activity in parallel. GzmB cleaves BID to generate tBID, which triggers MOMP through the formation of BAX/BAK oligomers [111]. GzmB also directly cleaves and activates caspase 3. GzmA triggers a distinct cell death pathway. It cleaves numerous substrates in the nucleus, cytosol and mitochondria [40,43–45,112,113] to initiate a unique program of cell death characterized by mitochondrial damage and single-stranded DNA nicks without MOMP or caspase activation [5,39]. The multiple death programs initiated by the different Gzms make it very difficult for a cell to resist cytotoxic attack.

DNA and RNA binding proteins are highly represented in the set of Gzm substrates. A recent proteomics study that profiled GzmA substrates in isolated nuclei identified 44 candidate substrates, of which 33 were RBPs, including 12 hnRNPs [43]. The remaining 11 candidate substrates were mostly DNA binding proteins. In some cases, the nucleic acid appears to play an important role in the Gzm/target interaction. GzmA cleavage of histone H1 and binding to PARP-1 depends on the presence of DNA [112,113]. All five human Gzms cleave hnRNP K in an RNA-dependent manner [114]. Gzm cleavage of viral and host nucleic acid binding proteins

also plays an important role in controlling viral infection [115,116]. Thus many of the substrates of GzmA and GzmB are nucleic acid binding proteins that are physiologically important for cytotoxicity or the control of viral infections.

Although serine proteases have a high degree of sequence similarity, the Gzms are most closely related to a group of myeloid cell granule proteases involved in microbial defense. These immune proteases include the neutrophil proteases neutrophil elastase (NE) and cathepsin G (CATG) [117]. When neutrophils are activated, they can ensnare and kill microbes in neutrophil extracellular traps (NETs), which are formed by nuclear DNA in a unique non-apoptotic cell death mechanism called NETosis [118]. NE participates in NETosis by translocating to the neutrophil nucleus where it cleaves histones [119]. Histone cleavage promotes chromatin decondensation, which precipitates the extrusion of nuclear DNA through the cell membrane. The extruded DNA is coated with histones, antimicrobial peptides, NE and CATG [120].

The aim of this study was to explore further the role of nucleic acids in mediating Gzm/substrate interactions and trafficking. We find that RNA enhances *in vitro* cleavage of RBP substrates, but not non-RBP substrates. We show that Gzms directly bind RNA and DNA with nanomolar affinity. NE and CATG also bind nucleic acids with high affinity, while digestive serine proteases do not. In the presence of competitor DNA, the leukocyte serine proteases do not localize to nuclei and NETs. Together, our findings indicate that nucleic acid binding is a conserved and functionally important property of leukocyte serine proteases that directs them to and enhances their cleavage of nucleic acid binding protein targets.

Gzm targets are enriched for nucleic acid binding proteins

Because the Gzms concentrate in the nucleus of target cells, we hypothesized that proteins that function in the nucleus might be over-represented amongst Gzm substrates. Two proteomics studies identified candidate GzmA and GzmB substrates without bias by analyzing Gzm-

incubated cell lysates for novel cleavage products [121,122]. We analyzed these target lists using the FuncAssociate gene ontology (GO) tool [123] for over-represented GO terms in both GzmA and GzmB datasets (Figure 4.1A and Appendix 1 – Supplemental Table 1). Proteins with nucleic acid-related GO terms were the most highly enriched categories, when analyzed for each Gzm individually or together. The top 7 GO terms for both Gzms (mRNA metabolic process, nucleic acid metabolic process, gene expression, RNA metabolic process, nuclear part, nucleotide metabolic process, RNA binding) were highly significantly over-represented (P-values of ~10^{-50} for each Gzm). This analysis suggested that Gzms might have a special preference for nucleic acid binding, especially RBP, substrates.

RNA promotes GzmA and GzmB cleavage of RNA-binding proteins

We first asked whether RNA enhances Gzm RBP cleavage by comparing Gzm cleavage of RBPs in whole cell lysates depleted of RNA. HeLa cell lysates were pretreated or not with a mixture of RNase A and T1 before a 15 minute incubation with varying concentrations of recombinant human GzmA or GzmB. The samples were then immunoblotted for known GzmA and GzmB targets. All three GzmA RBP targets analyzed (hnRNP U, DDX5, hnRNP A1) were cleaved less efficiently in RNase-treated samples (Figure 4.1B). Similarly, cleavage of RBP targets of GzmB (hnRNP U, G3BP1, hnRNP C1/C2) was reduced by removing RNA (Figure 4.1C). In contrast, non-RBP targets (LMNB1, HMGB2, TUBA, ICAD) were cleaved equally or more efficiently in RNase-treated lysates, suggesting that Gzm target preference is altered to favor non-RBPs in the absence of RNA (Figure 4.1B,C). This effect is not universal to cytotoxic proteases as RNase treatment did not affect caspase 3 cleavage of its RBP substrates hnRNP C1/C2 and G3BP1 (Figure 4.1D). We next tested whether adding HeLa cell total RNA would alter *in vitro* GzmB cleavage of recombinant hnRNP C1 and LNMB1. The RBP hnRNP C1 was more efficiently cleaved in the presence of added RNA, while cleavage of the non-RBP LMNB1

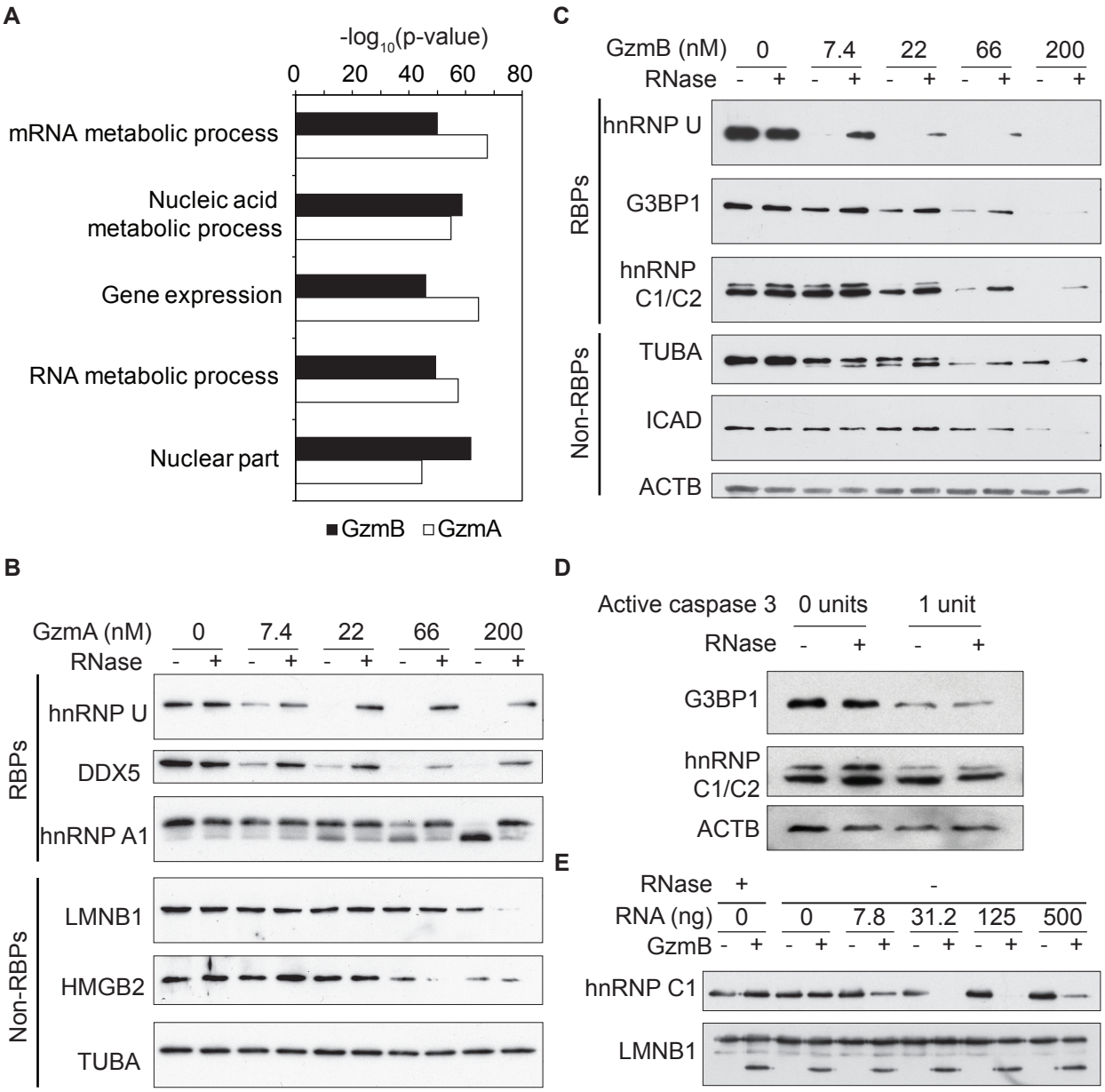

Figure 4.1: RBP target cleavage by Gzms is enhanced by RNA
(A) GO analysis of GzmA and GzmB targets. Nucleic acid binding proteins were highly enriched. **(B,C)** Cell lysates were incubated with RNase or left untreated, then incubated with the indicated concentration of GzmA **(B)** or GzmB **(C)**. The reactions were analyzed by immunoblot. RNase treatment of HeLa cell lysates reduced GzmA and GzmB cleavage of RBP targets, but not non-RBP targets. Results in (B) and (C) are representative of at least three independent experiments. **(D)** HeLa cell lysates were treated with RNase or left untreated, then treated with recombinant caspase 3. RNase treatment of HeLa cell lysates did not affect cleavage of RBP targets by active caspase 3. **(E)** GST-tagged recombinant proteins were pre-incubated with RNase or the indicated concentration of HeLa cell total RNA, then incubated with GzmB. Cleavage of recombinant hnRNP C1, but not recombinant LMNB1, was enhanced by exogenous RNA. Results in (D) and (E) are representative of at least two independent experiments.

was unaffected (Figure 4.1E). These results indicate that RNA enhances Gzm cleavage of RBP targets. Of note, although the highest concentration of RNA still enhanced cleavage, GzmB cleavage of hnRNP C1 was more efficient when less RNA was added.

Gzms bind RNA with nanomolar affinity

Because RNA enhanced Gzm activity against RBPs, we hypothesized that the Gzms are directed to RBP targets by binding to RNA. We tested RNA binding by fluorescence polarization (FP), a technique widely used to measure protein-nucleic acid interactions [124], using a 3′ fluorescein amidite (FAM)-labeled oligouridylate homopolymer (rU_{30}). As a positive control, we measured RNA binding of human antigen R (HuR), a GzmB substrate that binds to AU-rich RNA sequences [125]. GzmA, GzmB and HuR all bound to rU_{30} with high affinity, while the negative control protein BSA did not bind (Figure 4.2A). The apparent equilibrium dissociation constants (K_d) between all three purified proteins and the rU_{30} oligo determined by FP were in the nanomolar range (Table 4.1).

GzmB cleavage of HuR is enhanced by HuR binding to RNA

Because HuR preferentially binds AU-rich sequences, we used its specificity to assess the effect of substrate binding to RNA on GzmB cleavage. We compared GzmB cleavage of HuR in the presence of an AU-rich target sequence (AU RNA) [126] that both HuR and GzmB bound with similar affinity (Figure 4.2B and Table 4.1) and in the presence of a control sequence (BB94) that bound well only to GzmB (Figure 4.2C and Table 4.1). Formation of the cleavage product was enhanced by AU RNA, but only minimally increased by BB94 RNA (Figure 4.2D). These results suggest that RBP targets are optimally cleaved by Gzms when both the target and Gzm interact with RNA.

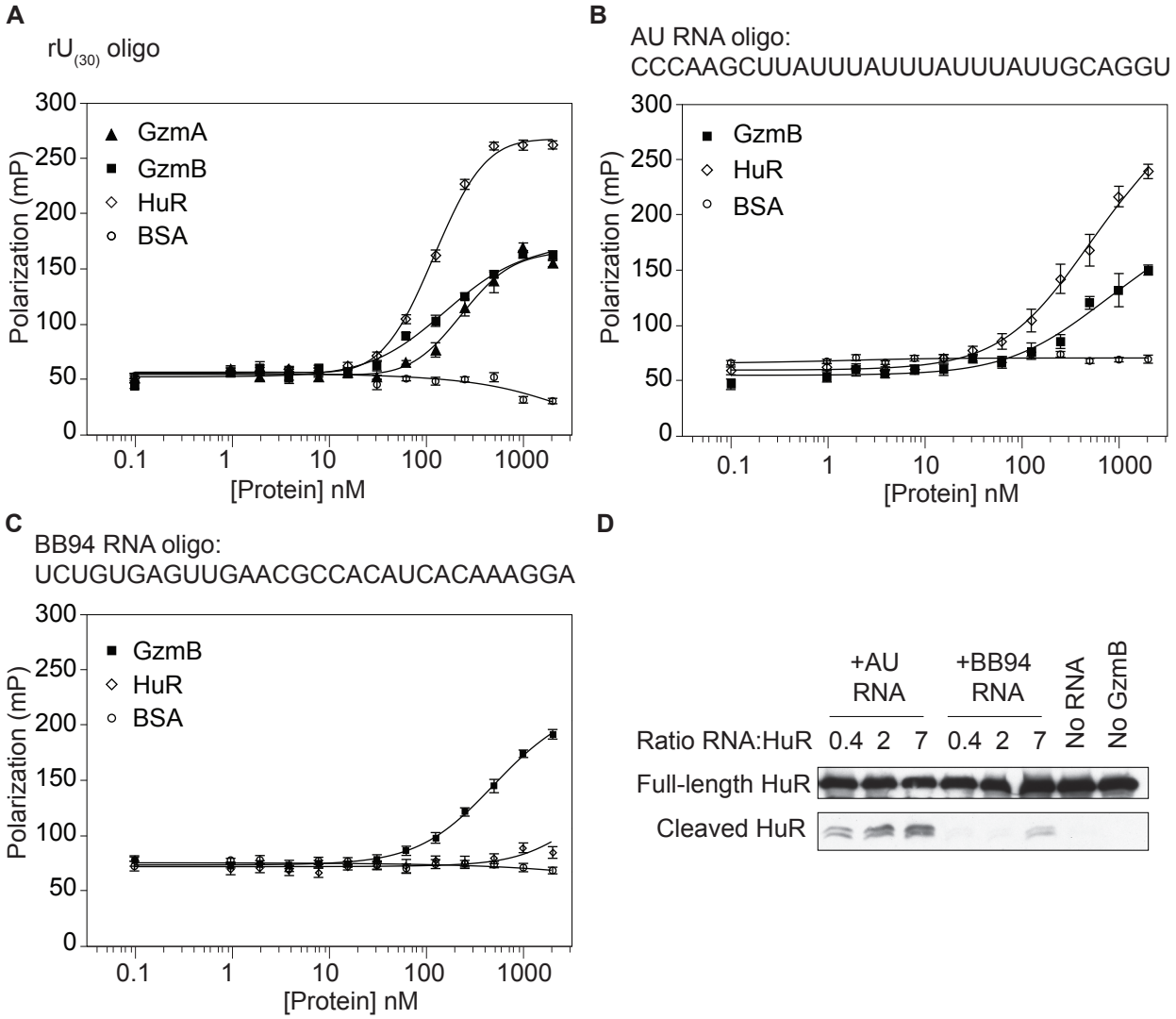

Figure 4.2: Gzms directly bind RNA
(A-C) FP assays were peformed with Gzms and the indicated RNAs. **(A)** GzmA, GzmB and the positive control HuR all bound to a FAM-labeled 30-nt uridylate homopolymer, but BSA did not bind. **(B)** GzmB and HuR bound a 30-nt RNA containing an AU-rich sequence (AU RNA). **(C)** GzmB, but not HuR, bound a length-matched control RNA (BB94 RNA). The mean polarization values and SEM are plotted. The apparent *Kd* is shown in Table 4.1. Results are representative of at least 3 independent experiments. **(D)** The GzmB target HuR was most efficiently cleaved when it was bound to RNA. GST-tagged HuR protein was incubated with the indicated molar ratio of AU RNA or BB94 RNA, and GzmB was then added for 30 min. HuR cleavage was detected by immunoblot for GST.

Gzms bind DNA with nanomolar affinity

Because the Gzms bind to RNA and cleave many DNA binding proteins, we asked whether they could also bind DNA. We used FP to measure the binding of GzmA and GzmB to a single-

Table 4.1: Protein – nucleic acid interactions measured by FP in this study
The apparent dissociation constant (K_d) with 95% confidence interval (CI) in brackets is given for each binding interaction.

Oligo	Protein	K_d (nM) [95% CI]
$rU_{(30)}$	GzmA	232 [194-277]
	GzmB	159 [125-202]
	HuR	121 [113-129]
AU RNA	GzmA	401 [35 nM-4.5 mM]
	GzmB	651 [157 nM-2.7 mM]
	NE	602 [304 nM-1.2 mM]
	CATG	165 [139-197]
	HuR	492 [255-952]
BB94 ssRNA	GzmA	1.6 mM [188 nM-15.2 mM]
	GzmB	480 [337-685]
	HuR	4.8 mM [16 nM-1465.9 mM]
BB94 ssDNA	GzmA	122 [95-158]
	GzmB	35 [31-40]
	NE	272 [219-339]
	CATG	22 [17-29]
	Histone H1	10 [8-12]
BB94 dsDNA	GzmA	120 [106-136]
	GzmB	161 [112-231]
	NE	607 [516-712]
	CATG	35 [24-52]
	Histone H1	9 [7-13]
$dC_{(30)}$	GzmA	91 [65-127]
	GzmB	175 [140-219]
$dT_{(30)}$	GzmA	48 [42-55]
	GzmB	45 [26-78]

stranded DNA (ssDNA) oligonucleotide of the same sequence as BB94 RNA (Figure 4.3A). Both GzmA and GzmB bound ssDNA with nanomolar apparent K_d (Table 4.1). GzmB (K_d = 35 nM, 95% CI [31,40]) bound ssDNA almost as strongly as histone H1 (H1) (K_d = 10 nM, 95% CI [8, 12]), similar to reported values [127]). GzmA binding was somewhat weaker (K_d = 122 nM, 95% CI [95, 158]). Both Gzms also bound to a double-stranded DNA (dsDNA) oligonucleotide containing the same BB94 sequence with nanomolar affinities (Figure 4.3B and Table 4.1). To determine if Gzm binding might have a sequence preference, we performed FP assays with ssDNA homopolymers (dA_{30}, dT_{30} and dC_{30}). Oligo(dG) was not tested because it tends to form

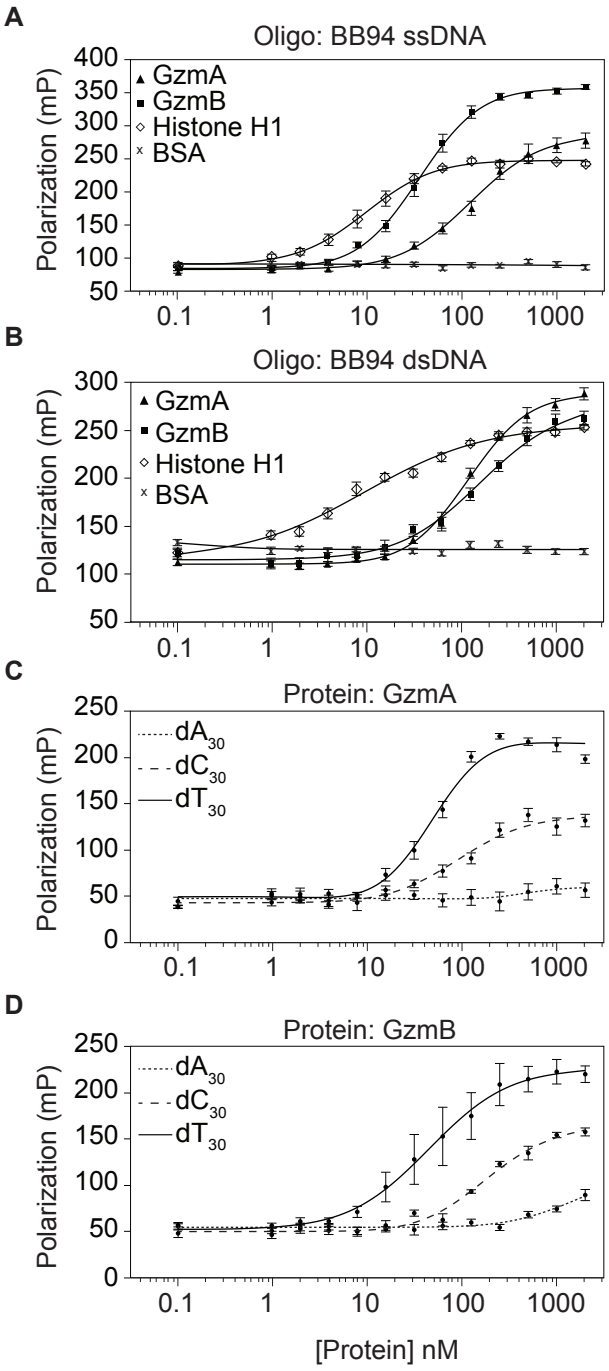

Figure 4.3: GzmA and GzmB bind DNA with nanomolar affinity
(A,B) The binding of a FAM-labelled ssDNA **(A)** or dsDNA **(B)** oligonucleotide to GzmA, GzmB, H1, and BSA was measured by FP. **(C,D)** To determine whether binding was sequence-dependent, interactions of GzmA **(C)** and GzmB **(D)** with FAM-labeled homo-oligomers was measured by FP. Both Gzms bound to pyrimidine tracts (dT_{30} and dC_{30}) more strongly than the purine tract dA_{30}. The mean polarization values are plotted with SEM. Results are representative of at least 3 independent experiments. The apparent K_d for each interaction is given in Table 4.1.

higher order structures and aggregate. Both Gzms bound dT_{30} > dC_{30} with nanomolar affinity, but only weakly bound to dA_{30} (Figure 4.3C,D). This suggests that the Gzms bind preferentially to pyrimidines. These assays were performed in buffer containing 100 mM NaCl. Since many protein-DNA complexes are sensitive to salt concentration, we performed FP assays over a range of NaCl and KCl concentrations, while holding the GzmB and nucleic acid concentration constant. Although binding decreased at higher salt concentrations, binding of GzmB to DNA and RNA remained strong at physiological concentrations (150 mM NaCl or KCl) (Appendix 1 - Supplemental Figure 1).

Myeloid granule serine proteases bind nucleic acids

Next we asked whether nucleic acid binding is a general property of serine proteases or limited to a subset. To visualize the evolutionary relationships between the Gzms and other serine proteases, we performed a phylogenetic analysis of all annotated human serine proteases. The Gzms form a monophyletic group with other leukocyte serine proteases (Figure 4.4A). This group includes five neutrophil proteases (NE, CATG, NSP4, PRTN3, AZU1) [128] and the mast cell protease CMA1. The Gzms are more distantly related to digestive enzymes, such as pancreatic elastase (PE) and trypsin. We used FP to assess the affinity of native human CATG and NE, porcine PE, and bovine trypsinogen (the proenzyme of trypsin) for RNA, ssDNA and dsDNA (Figure 4.4B and Table 4.1). Both neutrophil proteases bound these nucleic acids with nanomolar affinity like the Gzms, but neither digestive protease bound. This agrees with an earlier study showing that NE binds to DNA [129]. To validate DNA binding with an independent assay, we used oligo(dT)-conjugated beads to pull down the Gzms, neutrophil proteases and PE (Figure 4.4C). Consistent with the FP results, the leukocyte proteases (GzmA, GzmB, NE and CATG), but not the digestive protease, bound to oligo(dT) beads. Binding was specific to DNA since it was decreased by pretreating the beads with DNase. The proteases also did not bind to protein G-conjugated beads. We hypothesized that DNA binding would enhance

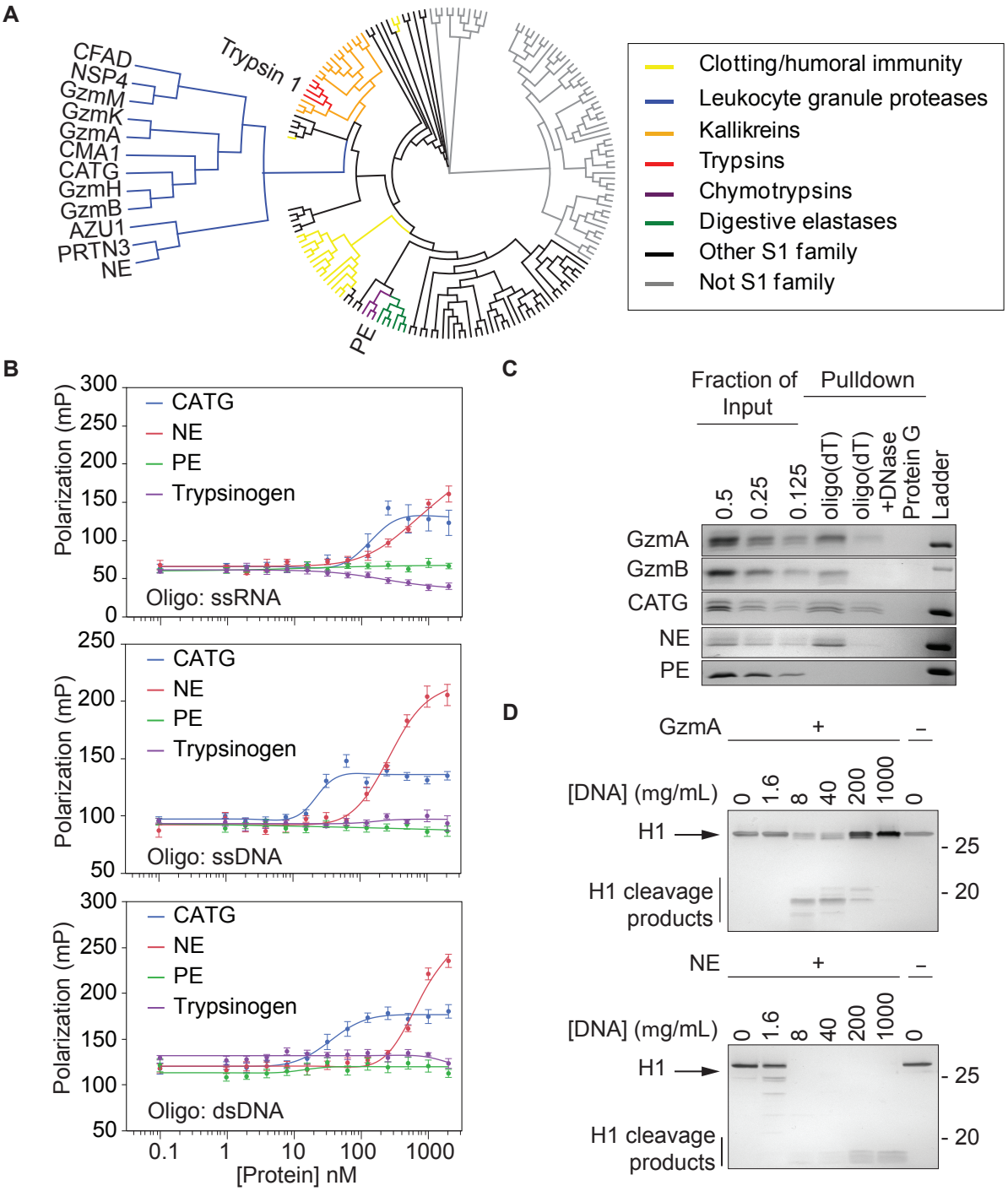

Figure 4.4: Leukocyte serine proteases bind to DNA and RNA with nanomolar affinity

(A) Phylogenetic analysis of all human serine proteases. The leukocyte proteases form a monophyletic group. **(B)** Binding of CATG and NE (neutrophil proteases) and PE and Trypsinogen (digestive proteases) to ssRNA, ssDNA and dsDNA was measured by FP. The leukocyte proteases bound and digestive proteases did not. **(C)** Binding was assayed by affinity pulldown with oligo(dT)-conjugated beads. The leukocyte proteases bound oligo(dT) beads while the digestive protease PE did not. DNase pre-treatment reduced binding, and none of the proteases bound the same beads conjugated to protein G instead of oligo(dT). **(D)** H1 was pre-incubated with the indicated amount of salmon sperm DNA, then treated with GzmA or NE. The proteins were separated by SDS-PAGE and visualized by silver staining. DNA enhanced H1 cleavage by GzmA and NE.

leukocyte protease cleavage of DNA binding protein substrates, as shown above for RNA and previously shown for GzmA cleavage of histone H1 [113]. We treated purified histone H1, a target of both GzmA and NE with each protease in the presence of increasing concentrations of salmon sperm DNA. H1 cleavage by NE was greatly increased by adding even a small amount of DNA (Figure 4.4D). H1 cleavage by GzmA was first promoted, then inhibited, by increasing amounts of salmon sperm DNA. Inhibition by high concentrations of exogenous RNA was also seen when we analyzed GzmB cleavage of hnRNP C1 (Figure 4.1E). These results suggest that an excess of nucleic acids interferes with formation of a substrate-nucleic acid-protease complex. Collectively, these results demonstrate that nucleic acid binding is a conserved and functionally important property of leukocyte serine proteases.

DNA binding mediates localization of Gzms to the nucleus

During killer cell attack, the Gzms rapidly concentrate in the nucleus of target cells by an unknown mechanism. A previous study suggested that nuclear localization is mediated by affinity of the Gzms for insoluble nuclear factors [42]. We hypothesized that the nuclear accumulation of Gzms is driven by direct binding to nuclear DNA. To test this idea, we incubated fixed and permeabilized HeLa cells with AlexaFluor488 (AF488) labeled serine proteases and visualized their localization with fluorescence microscopy (Figure 4.5). As expected, the Gzms stained the cytosol and nucleus, but concentrated in the nucleus. To test whether nuclear accumulation was mediated by DNA binding, we co-incubated the Gzms with salmon sperm DNA before adding them to the fixed cells. Incubation with exogenous DNA abolished both cytosolic and nuclear staining of the Gzms (Figure 4.5). We treated fixed cells with DNase and RNase, which modestly reduced nuclear and cytosolic GzmB staining, respectively (Appendix 1 – Supplemental Figure 2). DNase treatment did not remove all nuclear DNA, so it may be that GzmB binds to residual nucleic acids after nuclease treatment. Labeled NE also accumulated in the nuclei of fixed cells, in agreement with the known nuclear

translocation of this enzyme during NETosis [119]. PE did not localize to fixed cell nuclei and its staining intensity and pattern were not impacted by pre-incubation with salmon sperm DNA (Figure 4.5). Thus, DNA binding by the Gzms and NE likely mediates their nuclear trafficking during cytotoxic attack and NETosis, respectively.

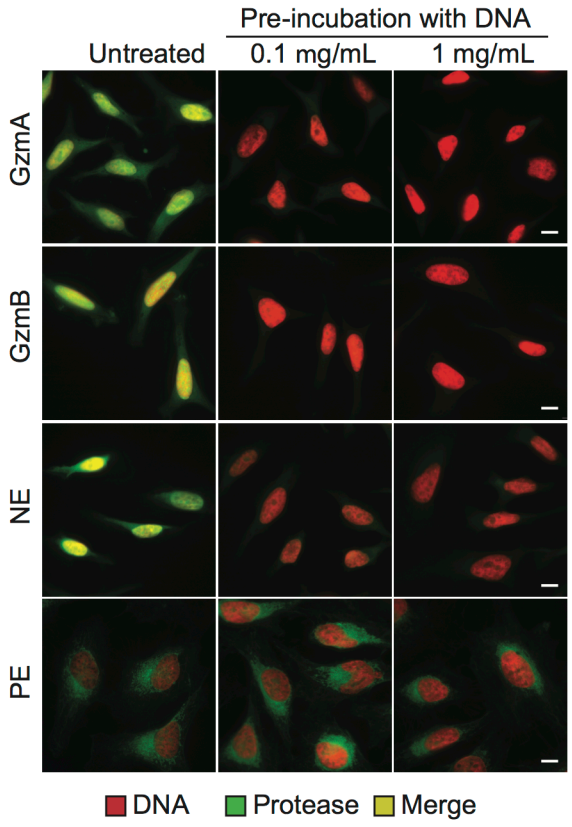

Figure 4.5: DNA binding mediates nuclear localization of leukocyte serine proteases
HeLa cells were fixed and permeabilized, pre-incubated with the indicated concentration of salmon sperm DNA, incubated with the indicated AF488-labeled serine protease, then stained with DAPI for DNA. All of the proteases (green) stained the nuclei (red) and cytopasm, but the leukocyte proteases GzmA, GzmB and NE were strongly enriched in the nucleus. Addition of salmon sperm DNA reduced leukocyte protease staining in the nucleus and cytoplasm, but had no effect on the staining intensity or pattern of the digestive protease PE. Results are representative of at least three independent experiments. Scale bar is 10 μm.

Localization of NE and CATG to NETs is mediated by DNA binding

CATG and NE both concentrate on NETs [120]. We asked whether DNA binding facilitates localization of these enzymes to NETs. Neutrophils isolated from human peripheral blood were

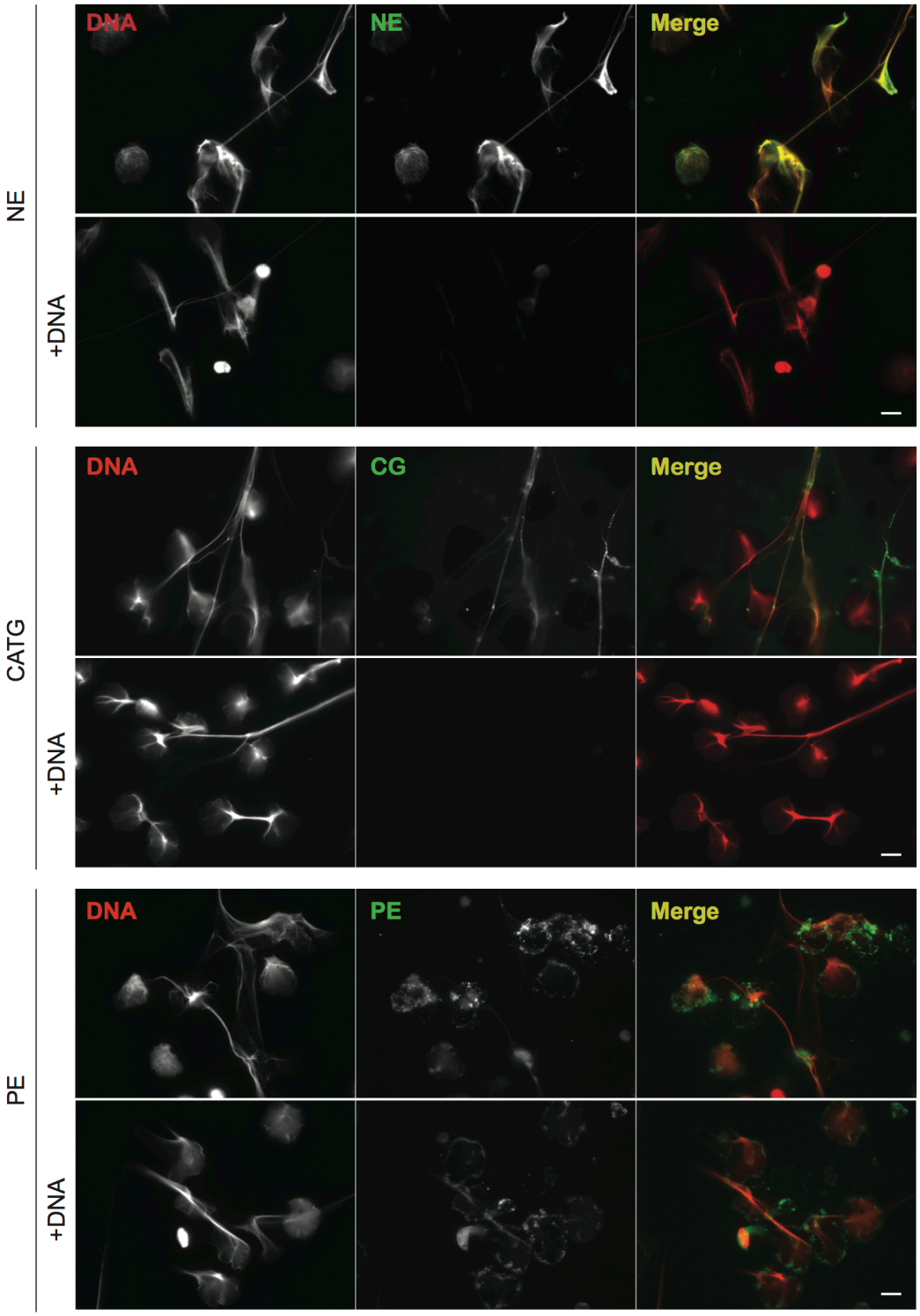

Figure 4.6: DNA binding regulates NE and CATG binding to NETs
Primary neutrophils were treated with PMA to induce NETs and coincubated with AF488-labeled NE, CATG or PE (green) ± salmon sperm DNA. The NETs were fixed and stained with DAPI (red). NE and CATG localized strongly to NETs, but NET localization was competed off by exogenous DNA. PE bound mostly to non-DNA structures and exogenous DNA did not impact its staining intensity or localization. Scale bar is 10 μm.

treated with phorbol 12-myristate 13-acetate (PMA) for 3 hours to induce NET formation in the presence of AF488-labeled NE, CATG or PE. Competitor DNA was added to some samples during NET formation. Both neutrophil enzymes, but not PE, spontaneously concentrated on the NETs, and binding to the NETs was inhibited by adding salmon sperm DNA (Figure 4.6). Exogenous DNA added during NETosis also reduced the association of endogenous NE to NETs (Appendix 1 - Supplemental Figure 3). Thus, CATG and NE specifically localize to NETs by binding to DNA.

Methods

Antibodies

The following antibodies were used at the indicated final concentration or dilution: mouse monoclonal antibodies to hnRNP U (Santa Cruz; 3G6; 0.2 mg/ml), hnRNP A1 (Sigma; 4B10; 2 mg/ml), lamin B1 (Calbiochem; 101-B7; 1/1,000), α-tubulin (Sigma; B-5-1-2; 1/1,000), G3BP1 (BD; 23/G3BP; 0.25 mg/ml), hnRNP C1/C2 (Sigma; 4F4; 0.4 mg/ml), β-actin (Developmental Studies Hybridoma Bank; 1/1,000), HuR (Santa Cruz; 3A2; 0.2 mg/ml); rabbit antisera to HMGB2 (Abcam; 1/1,000), ICAD (Abcam; 0.5 mg/ml), NE (Abcam; 1 mg/ml); DDX5 (Abcam; 0.5 mg/ml). Secondary antibodies were sheep anti-mouse-HRP (GE; 1/2,500), donkey anti-rabbit-HRP (GE; 1/2,500), donkey anti-goat-HRP (GE, 1/2,500), goat anti-rabbit AF488 (Invitrogen; 1/200), donkey anti-mouse Cy3 (Jackson ImmunoResearch 715-165-150; 1:200). Normal rabbit IgG (Cell Signaling 2729; 1 mg/ml) was used as an isotype control for immunofluorescence.

Proteins

Human GzmA and GzmB expression plasmids [43] were transfected into HEK 293T cells by calcium phosphate precipitation. The transfected cells were grown in serum-free ExCell 293 medium (Sigma) for 4 days. Recombinant granzymes were purified from the culture supernatants by immobilized metal affinity chromatography using Nickel-NTA (Qiagen) following the manufacturer's instructions. Eluted granzymes were treated with enterokinase (0.05 IU/mL supernatant; Sigma) for 16 hours at room temperature. Active Gzms were finally purified on an S column, concentrated, and quality tested as previously described [130]. GST-tagged HuR, hnRNPC1, and LMNB1 were expressed and purified as described [43]. H1 (NEB M2501S) and caspase 3 (Enzo – ALX-201-059-U025) were purchased. Other serine proteases were NE (Athens Research and Technology, Athens, GA 16-14-051200), PE (Millipore 324682), CATG (Athens Research and Technology 16-14-030107) and trypsinogen (Sigma T1143). Proteins

were fluorescently labeled with AF488 according to the manufacturer's instructions (Invitrogen A30006).

In vitro cleavage in cell lysates

Whole cell lysates were made from 10^6 HeLa cells suspended in 1 mL of lysis buffer (50 mM Tris-HCl, pH 8.0, 100 mM NaCl) by alternating freezing in an ethanol/dry ice bath and thawing at 37°C three times. Cell debris was pelleted by centrifugation (16,000 x g for 10 min at 4°C). The supernatant was divided, and half was treated with RNase A/T1 (Thermo) at a concentration of 325 U/mL for 30 min at 37°C. RNaseOUT (Invitrogen) was added at a concentration of 1000 U/mL to the remaining half. The lysates were then treated with the indicated amounts of Gzms in a volume of 60 µL for 15 min at 37°C. In some cases, GzmB was incubated with varying amounts of salmon sperm DNA on ice for 30 min before addition to lysates. The cleavage reaction was stopped by adding 5x SDS loading buffer and boiling at 95°C for 5 min. For caspase 3 experiments, lysates were incubated with or without 1 unit of recombinant capsase 3 for 1 hour before stopping the reaction. Samples were analyzed by SDS-PAGE and immunoblot.

In vitro cleavage of recombinant proteins

In vitro cleavage was performed in 100 mM NaCl, 50 mM Tris-HCl (pH 7.5). Each protein was first incubated in the indicated concentration of HeLa cell total RNA or salmon sperm DNA for 20 min and then incubated with 50 nM GzmB for 15 min (hnRNP C), 50 nM GzmB for 30 min (LMNB1), 200 nM GzmA for 20 min (H1) or 5 nM NE for 10 min (H1). Total HeLa cell RNA was purified with Trizol (Invitrogen) according to the manufacturer's instructions. The final concentrations of hnRNP C, LMNB1 and H1 were 333 nM, 1 nM and 400 nM respectively. For HuR cleavage, RNA oligos were diluted to 10 µM, heated at 70°C for 10 min and cooled on ice. 400 nM recombinant GST-tagged HuR was incubated with or without 200 nM recombinant

GzmB. The cleavage reactions were performed in the presence of 3 ng/μL total HeLa RNA, AU RNA or BB94 RNA at the indicated molar ratios and incubated in a total volume of 40 μL at 37°C for 30 min. Cleavage reactions were stopped by adding 5X SDS loading buffer and boiling for 5 min. Cleavage was assayed by immunoblot or silver staining (Invitrogen SilverQuest kit).

Protease localization in permeabilized HeLa cells

HeLa cells were obtained from ATCC and maintained in DMEM supplemented with 10% heat-inactivated fetal bovine serum, 100 U/mL penicillin G, 100 μg/mL streptomycin sulfate, 6 mM HEPES, 1.6 mM L-glutamine and 50 μM β-mercaptoethanol. HeLa cells were grown overnight on 12 mm coverslips, then fixed for 10 min at RT in 2% formaldehyde, then permeabilized for 10 min in methanol on dry ice. In some experiments the cells were treated with DNase I (NEB) or RNase A/T1 (Thermo) at a 1:50 dilution for 4 hours at RT before blocking. The cells were blocked with 1% bovine serum albumin (BSA) in PBS for 1 hour at RT, coverslips were incubated with blocking buffer containing salmon sperm DNA or no DNA for 30 min on ice and then incubated at RT for 1 hour with 100 nM AF488-labeled serine proteases. The cover slips were then washed and stained with 4 μg/mL DAPI in PBS and mounted on slides (VWR 48311-703) using polyvinyl alcohol (Sigma P-8136) aqueous mounting medium. Cells were imaged using an Axiovert 200M microscope (Pan Apochromat, 1.4 NA; Carl Zeiss). Images were analyzed with SlideBook 4.2 (Intelligent Imaging Innovations Inc.).

Neutrophil isolation and activation

Human studies were reviewed and approved by the Harvard Committee on the Use of Human Subjects (IRB-P00005698). Neutrophils were isolated from the blood of de-identified healthy donors by density gradient centrifugation as described [131]. The neutrophil layer was washed with HBSS and resuspended at 10^6 cells/mL in RPMI. Neutrophils ($2.5x10^5$) were incubated at 37°C for 15 min on 12 mm coverslips in 24-well flat-bottom cell culture plates and then treated in

500 ml RPMI for 3 hours with 100 nM PMA (phorbol 12-myristate 13-acetate, Sigma P1585). In some experiments, 100 nM AlexaFluor-488 (AF488)-labeled protease and/or salmon sperm DNA (Sigma D7656) were added just prior to adding PMA. Treated cells were fixed in PBS containing 4% formaldehyde. For immunofluorescence staining of endogenous NE, the fixed cells were incubated with primary antibody or rabbit antiserum control for 1 hour at RT, washed three times in PBS, and then incubated in secondary antibody (AF488-labeled goat α-rabbit IgG) for 1 hour at RT. The cells were washed, stained with DAPI, and mounted as above.

Gene Ontology and phylogenetic analysis of serine proteases

We analyzed the candidate targets of human GzmA [122] and GzmB [121] identified by proteomics using the FuncAssociate tool [123] on default settings. Top gene ontology (GO) terms were ranked by the sum of the $-\log_{10}(p)$ values for enrichment of targets of each enzyme. All human proteins having the GO term "serine-type peptidase activity" (GO:0008236) were identified with AmiGO [132]. Of these proteins, the manually annotated and reviewed Swiss-Prot sequences were downloaded using the UniProt retrieve tool [133]. The sequences were trimmed to focus on their protease domains and exclude spurious alignment of other protein domains in multidomain proteins. The ClustalW2 [134] multiple sequence alignment and phylogeny tools were used with default parameters to construct a phylogenetic tree. Phylogeny was visualized with the EvolView web tool [135].

Fluorescence polarization oligonucleotides

The following FAM-labeled oligonucleotides were used for FP, all from Integrated DNA Technologies:

BB94 DNA: 5'TCTGTGAGTTGAACGCACACATCACAAAGGAG-FAM-3'

dA(30): 5'AAAAAAAAAAAAAAAAAAAAAAAAAAAAAA-FAM-3'

dC(30): 5'CCCCCCCCCCCCCCCCCCCCCCCCCCCCCC-FAM-3'

dT(30): 5'TTTTTTTTTTTTTTTTTTTTTTTTTTTTTT-FAM-3'

rU(30): 5'UUUUUUUUUUUUUUUUUUUUUUUUUUUUUU-FAM-3'

BB94 RNA: 5'UCUGUGAGUUGAACGCACACAUCACAAAGGA-FAM-3'

AU RNA: 5'CCCAAGCUUAUUUAUUUAUUUAUUGCAGGUC-FAM-3'

Fluorescence polarization assays

FAM-labeled oligonucleotides were used at 10 nM, and binding reactions were performed in a total volume of 20 µL. Proteins and oligos were diluted in 10 mM Tris-HCl, pH 7.5, 100 mM NaCl and 2.5 mM $MgCl_2$. For RNA oligos, RNAseOUT was added to a final concentration of 1 U/µL. Diluted RNA oligos were heated to 70°C for 10 min prior to use. In the salt concentration assay, protein concentration was fixed (100 nM) and either NaCl or KCl was added to the assay buffer at the indicated final concentrations. Samples were equilibrated in 384-well black polystyrene assay plates (Corning 3575) for 20 min at room temperature, and polarization was determined using a Synergy 2 Microplate Reader and Gen5 Data Analysis Software (BioTek).

Fluorescence polarization data analysis

The apparent equilibrium K_d was determined from fitting the data to a sigmoidal dose-response function using JMP Pro 10 (JMP Statistical Discovery Software from SAS). The apparent K_d was determined for each protein/nucleic acid interaction using the equation f=c+{(d-c)/(1+10^(-a($\log_{10}$([P]-b))))}, where f is the fraction bound or the polarization value, [P] is the protein concentration, b is the equilibrium K_d, a is the Hill coefficient, d is the maximum polarization and c is the minimum polarization [136]. Each experiment was performed at least in duplicate. The

average and standard error of the polarization value for each protein concentration was calculated from at least 10 independent samples.

Oligo(dT) pulldown

120 µl Oligo$(dT)_{25}$ Dynabeads (Invitrogen 61002) and 10 µl Protein G Dynabeads (Invitrogen 10004D) were washed three times in 50 mM Tris-HCl, pH 7.5, 100 nM NaCl. The beads were blocked for 30 min at RT in the same buffer containing 0.5% bovine serum albumin (BSA) (Sigma A9647). Following blocking, half of the Oligo$(dT)_{25}$ Dynabeads were treated at RT for 30 min with 25 U Benzonase® Nuclease (Sigma E1014), the other half was left untreated. After this incubation, the beads were incubated with 120 µl of protein (final concentration 1 µM) in blocking buffer for 30 min at room temperature. The beads were washed three times and protein was eluted by boiling samples for 3 min in 30 µl SDS loading buffer. Samples were electrophoresed through a 12% polyacrylamide denaturing gel and visualized by Coomassie staining.

Chapter 5: Conclusions

Cytotoxic leukocyte protease binding to nucleic acids promotes nuclear localization and cleavage of nucleic acid binding proteins

Summary

This work demonstrates that the Gzms and related leukocyte proteases are *bona fide* nucleic acid binding proteins with nanomolar affinities. The basis for substrate specificity of the Gzms, which are highly specific proteases, remains largely unknown. Although each Gzm has a strong preference for specific P1 residues in its substrates, primary amino acid sequence around the cleavage site does not predict Gzm cleavage. Structural features likely play a key role in Gzm substrate recognition. We find that the high affinity of the Gzms for nucleic acids may be an important determinant of substrate specificity. Nucleic acid binding is a simple and elegant mechanism to direct leukocyte serine proteases to DNA and RNA binding protein targets and probably explains why nucleic acid binding proteins are highly over-represented amongst Gzm substrates. Gzms and their substrates may be brought together by binding to nearby sites on the same nucleic acid strand. The Gzms form a monophyletic group with other leukocyte serine proteases, which also bind nucleic acids with high affinity. Importantly, nucleic acid binding regulates the sub-cellular localization of Gzms and neutrophil proteases. Leukocyte protease concentration in cell nuclei was prevented by exogenous DNA. Our results support the “affinity” model for Gzm nuclear concentration posited over a decade ago and identify DNA as the unknown factor mediating this phenomenon [42]. Similarly, the localization of NE and CATG to NETs and the antimicrobial activity of NETs likely depend in part upon the affinity of these proteases for DNA.

Is nucleic acid binding specific?

The leukocyte serine proteases rank amongst the most cationic proteins in the cell, with very high predicted isoelectric points (pIs): GzmA – 9.22, GzmB – 9.69, CATG – 11.37, NE – 9.89 [133]. The empirical pIs of NE and CATG are ~11 and >11, respectively [137]. This raises the question of whether nucleic acid binding is specific or simply a consequence of charge-

balancing electrostatic interactions. For several reasons, we believe binding is specific and physiologically relevant. First, the digestive serine proteases, which do not bind nucleic acids, are also cationic with similar pIs as the Gzms. Porcine PE has a reported pI of 9.5 to >11, while the pI of trypsinogen is ~9.3, but neither binds nucleic acids [138–140]. Second, Gzm binding to DNA is sequence-specific, favoring pyrimidine-rich sequences. Third, these proteases directly bind DNA under physiologic conditions. Finally, charge alone does not preclude specificity; RNA and DNA binding proteins are characterized by cationic patches that mediate binding to nucleic acids by electrostatic interactions [141]. In fact, many nucleic acid binding proteins (such as the histones) have a highly cationic net charge. The crystal structures of the Gzms show that they have positively charged surfaces that could be nucleic acid binding sites [142,143].

Broader implications and functional significance

Negatively charged sugars play a significant role in granule packaging and target cell uptake of cationic Gzms. In cytotoxic granules, the Gzms bind serglycin, a small negatively charged proteoglycan containing chondroitin 4-sulfate [144]. Serglycin-null T cells are defective in packaging GzmB into granules. Upon degranulation, GzmB is released from serglycin and binds to cell membrane proteoglycans, notably heparan sulfate. Purified GzmB has higher affinity for heparan sulfate than serglycin [145]. Our results suggest that when Gzms enter target cells they bind to another class of negatively charged molecule, nucleic acids. Gzm binding to different anionic biomolecules as they move from the granules to the target cell nucleus may form a physical ‘chain of custody’ to ensure proper Gzm trafficking and targeting.

Nucleic acid binding enhances the activity and function of leukocyte serine proteases, which may be critical to Gzm induction of cell death and neutrophil protease-mediated NET formation and function. Exogenous DNA transformed purified H1 from a very weak substrate to a robust target. However excess DNA and RNA inhibited cleavage of H1 and hnRNP C1, respectively. A

previous study also found that DNA inhibited NE and CATG proteolysis of the non-nucleic acid binding protein elastin [146]. An excess of nucleic acid, which has high affinity for both the protease and its substrate, likely interferes with formation of the ternary protease-nucleic acid-substrate complex.

Preferential targeting of DNA and RNA binding proteins by Gzms is an underappreciated property critical for executing cell death. Nucleic acid binding is a simple mechanism to guide Gzms to targets that are essential for survival. Cleavage of nucleic acid binding substrates should enhance Gzm execution of death, independently of caspase activation. During Gzm-mediated cell death, targeting of RBPs disrupts pre-mRNA processing and nuclear export [43]. In the extracellular environment, DNA binding may sequester leukocyte serine proteases to focus their activity on pathogens, which get caught in NETs, and minimize tissue injury.

Future directions

Many important questions raised by this work could be answered with further biochemical and structural characterization of the interaction between the Gzms and nucleic acids. The leukocyte serine proteases share a common structural fold with digestive proteases such as trypsin [147], but only the leukocyte proteases bind nucleic acids. Computational modeling, comparing the leukocyte serine proteases with digestive serine proteases, might generate some predictions about the critical residues that interact with RNA and DNA. A more direct approach would be to obtain a crystal structure of a Gzm in complex with DNA or RNA. There are numerous crystal structures of the Gzms and other serine proteases [142,143]. It might be relatively straightforward to use similar experimental conditions to crystallize a Gzm in complex with RNA or DNA. Such a structure would probably aid in identifying the key residues that interact with nucleic acid, and might provide hints about the sequence specificity of Gzm-nucleic acid

interaction. Targeted mutagenesis, or domain-swapping with other serine proteases, could be used to test the contribution of specific residues to nucleic acid binding.

Structural insights into Gzm-target interactions would permit further characterization of the biological significance of nucleic acid binding. It might be possible to identify Gzm mutations that abolish nucleic acid binding, but not protease activity. These mutant Gzms could be tested *in vitro* for their substrate specificity and their cytotoxicity towards human cells and pathogens. They should no longer concentrate in the nucleus of target cells or fixed and permeabilized cells, as we showed in this study. It might even be possible to generate mutant mice expressing Gzms deficient in nucleic acid binding and test their ability to control infections and tumors. GzmA/GzmB double knockout mice are relatively healthy, but are highly susceptible to poxvirus infections [148]. Furthermore, GzmB cleaves nucleic acid binding proteins to control latent HSV infections and block poxvirus replication in cell culture [115,116]. We hypothesize that nucleic acid binding directs the Gzms towards proteins that are essential for viral replication and host cell survival, thus suppressing viral infection. If this hypothesis is correct, these mutant mice should be immunodeficient (but perhaps less immunodeficient than knockout mice). However, the mutations might cause immunodeficiency for reasons other than nucleic acid binding, for example if the residues that bind nucleic acids are also important for the interaction of Gzms with serglycins or the surface of their target cells. It would therefore be important to test whether the CTLs and NK cells of these mice have normal cytotoxic granules, and whether Gzm delivery into target cells is impaired.

This study reports a novel mechanism for proteases to target their substrates. It explains the localization of the Gzms during cytotoxic attack and their preference for targeting DNA and RNA binding proteins, and will stimulate new research into the cytotoxic functions of leukocyte proteases.

References

1. Taylor RC, Cullen SP, Martin SJ (2008) Apoptosis: controlled demolition at the cellular level. Nat Rev Mol Cell Biol 9: 231–241. doi:10.1038/nrm2312.

2. Johnstone RW, Ruefli AA, Lowe SW (2002) Apoptosis: A Link between Cancer Genetics and Chemotherapy. Cell 108: 153–164. doi:10.1016/S0092-8674(02)00625-6.

3. Hanahan D, Weinberg RA (2011) Hallmarks of Cancer: The Next Generation. Cell 144: 646–674. doi:10.1016/j.cell.2011.02.013.

4. Vandenabeele P, Galluzzi L, Berghe TV, Kroemer G (2010) Molecular mechanisms of necroptosis: an ordered cellular explosion. Nat Rev Mol Cell Biol 11: 700–714. doi:10.1038/nrm2970.

5. Chowdhury D, Lieberman J (2008) Death by a Thousand Cuts: Granzyme Pathways of Programmed Cell Death. Annu Rev Immunol 26: 389–420. doi:10.1146/annurev.immunol.26.021607.090404.

6. Danial NN, Korsmeyer SJ (2004) Cell Death: Critical Control Points. Cell 116: 205–219. doi:10.1016/S0092-8674(04)00046-7.

7. Llambi F, Moldoveanu T, Tait SWG, Bouchier-Hayes L, Temirov J, et al. (2011) A Unified Model of Mammalian BCL-2 Protein Family Interactions at the Mitochondria. Mol Cell 44: 517–531. doi:10.1016/j.molcel.2011.10.001.

8. Danial NN (2007) BCL-2 Family Proteins: Critical Checkpoints of Apoptotic Cell Death. Clin Cancer Res 13: 7254–7263. doi:10.1158/1078-0432.CCR-07-1598.

9. Verhagen AM, Ekert PG, Pakusch M, Silke J, Connolly LM, et al. (2000) Identification of DIABLO, a Mammalian Protein that Promotes Apoptosis by Binding to and Antagonizing IAP Proteins. Cell 102: 43–53. doi:10.1016/S0092-8674(00)00009-X.

10. Arnoult D, Gaume B, Karbowski M, Sharpe JC, Cecconi F, et al. (2003) Mitochondrial release of AIF and EndoG requires caspase activation downstream of Bax/Bak-mediated permeabilization. EMBO J 22: 4385–4399. doi:10.1093/emboj/cdg423.

11. Green DR, Kroemer G (2009) Cytoplasmic functions of the tumour suppressor p53. Nature 458: 1127–1130. doi:10.1038/nature07986.

12. Bouchier-Hayes L, Green DR (2012) Caspase-2: the orphan caspase. Cell Death Differ 19: 51–57. doi:10.1038/cdd.2011.157.

13. Creagh EM, Conroy H, Martin SJ (2003) Caspase-activation pathways in apoptosis and immunity. Immunol Rev 193: 10–21. doi:10.1034/j.1600-065X.2003.00048.x.

14. Li P, Nijhawan D, Budihardjo I, Srinivasula SM, Ahmad M, et al. (1997) Cytochrome c and dATP-Dependent Formation of Apaf-1/Caspase-9 Complex Initiates an Apoptotic Protease Cascade. Cell 91: 479–489. doi:10.1016/S0092-8674(00)80434-1.

15. Riedl SJ, Shi Y (2004) Molecular mechanisms of caspase regulation during apoptosis. Nat Rev Mol Cell Biol 5: 897–907. doi:10.1038/nrm1496.

16. Mahrus S, Trinidad JC, Barkan DT, Sali A, Burlingame AL, et al. (2008) Global Sequencing of Proteolytic Cleavage Sites in Apoptosis by Specific Labeling of Protein N Termini. Cell 134: 866–876. doi:10.1016/j.cell.2008.08.012.

17. Dix MM, Simon GM, Cravatt BF (2008) Global Mapping of the Topography and Magnitude of Proteolytic Events in Apoptosis. Cell 134: 679–691. doi:10.1016/j.cell.2008.06.038.

18. Upton J-P, Wang L, Han D, Wang ES, Huskey NE, et al. (2012) IRE1α cleaves select microRNAs during ER stress to derepress translation of proapoptotic Caspase-2. Science 338: 818–822. doi:10.1126/science.1226191.

19. Upton J-P, Austgen K, Nishino M, Coakley KM, Hagen A, et al. (2008) Caspase-2 Cleavage of BID Is a Critical Apoptotic Signal Downstream of Endoplasmic Reticulum Stress. Mol Cell Biol 28: 3943–3951. doi:10.1128/MCB.00013-08.

20. Scaffidi C, Fulda S, Srinivasan A, Friesen C, Li F, et al. (1998) Two CD95 (APO-1/Fas) signaling pathways. EMBO J 17: 1675–1687. doi:10.1093/emboj/17.6.1675.

21. Aldridge BB, Gaudet S, Lauffenburger DA, Sorger PK (2011) Lyapunov exponents and phase diagrams reveal multi-factorial control over TRAIL-induced apoptosis. Mol Syst Biol 7: 553. doi:10.1038/msb.2011.85.

22. Albeck JG, Burke JM, Aldridge BB, Zhang M, Lauffenburger DA, et al. (2008) Quantitative Analysis of Pathways Controlling Extrinsic Apoptosis in Single Cells. Mol Cell 30: 11–25. doi:16/j.molcel.2008.02.012.

23. Lakhani SA, Masud A, Kuida K, Porter GA, Booth CJ, et al. (2006) Caspases 3 and 7: Key Mediators of Mitochondrial Events of Apoptosis. Science 311: 847–851. doi:10.1126/science.1115035.

24. Chen Q, Gong B, Almasan A (2000) Distinct stages of cytochrome c release from mitochondria: evidence for a feedback amplification loop linking caspase activation to mitochondrial dysfunction in genotoxic stress induced apoptosis. Cell Death Differ 7: 227–233. doi:10.1038/sj.cdd.4400629.

25. Gabriel B, Sureau F, Casselyn M, Teissié J, Petit PX (2003) Retroactive pathway involving mitochondria in electroloaded cytochrome c-induced apoptosis: Protective properties of Bcl-2 and Bcl-XL. Exp Cell Res 289: 195–210. doi:10.1016/S0014-4827(03)00255-6.

26. Weng C, Li Y, Xu D, Shi Y, Tang H (2005) Specific Cleavage of Mcl-1 by Caspase-3 in Tumor Necrosis Factor-related Apoptosis-inducing Ligand (TRAIL)-induced Apoptosis in Jurkat Leukemia T Cells. J Biol Chem 280: 10491–10500. doi:10.1074/jbc.M412819200.

27. Kerr JF, Wyllie AH, Currie AR (1972) Apoptosis: a basic biological phenomenon with wide-ranging implications in tissue kinetics. Br J Cancer 26: 239–257.

28. Sebbagh M, Renvoizé C, Hamelin J, Riché N, Bertoglio J, et al. (2001) Caspase-3-mediated cleavage of ROCK I induces MLC phosphorylation and apoptotic membrane blebbing. Nat Cell Biol 3: 346–352. doi:10.1038/35070019.

29. Coleman ML, Sahai EA, Yeo M, Bosch M, Dewar A, et al. (2001) Membrane blebbing during apoptosis results from caspase-mediated activation of ROCK I. Nat Cell Biol 3: 339–345. doi:10.1038/35070009.

30. Orlando KA, Stone NL, Pittman RN (2006) Rho kinase regulates fragmentation and phagocytosis of apoptotic cells. Exp Cell Res 312: 5–15. doi:10.1016/j.yexcr.2005.09.012.

31. Nagata S, Nagase H, Kawane K, Mukae N, Fukuyama H (2003) Degradation of chromosomal DNA during apoptosis. Cell Death Differ 10: 108–116. doi:10.1038/sj.cdd.4401161.

32. Suzuki J, Denning DP, Imanishi E, Horvitz HR, Nagata S (2013) Xk-Related Protein 8 and CED-8 Promote Phosphatidylserine Exposure in Apoptotic Cells. Science 341: 403–406. doi:10.1126/science.1236758.

33. Ferraro-Peyret C, Quemeneur L, Flacher M, Revillard J-P, Genestier L (2002) Caspase-Independent Phosphatidylserine Exposure During Apoptosis of Primary T Lymphocytes. J Immunol 169: 4805–4810.

34. Thomas MP, Lieberman J (2013) Live or let die: posttranscriptional gene regulation in cell stress and cell death. Immunol Rev 253: 237–252. doi:10.1111/imr.12052.

35. Peters PJ, Borst J, Oorschot V, Fukuda M, Krähenbühl O, et al. (1991) Cytotoxic T lymphocyte granules are secretory lysosomes, containing both perforin and granzymes. J Exp Med 173: 1099–1109.

36. Thiery J, Keefe D, Boulant S, Boucrot E, Walch M, et al. (2011) Perforin pores in the endosomal membrane trigger the release of endocytosed granzyme B into the cytosol of target cells. Nat Immunol 12: 770–777. doi:10.1038/ni.2050.

37. Choi PJ, Mitchison TJ (2013) Imaging burst kinetics and spatial coordination during serial killing by single natural killer cells. Proc Natl Acad Sci 110: 6488–6493. doi:10.1073/pnas.1221312110.

38. Bots M, Medema JP (2006) Granzymes at a glance. J Cell Sci 119: 5011 –5014. doi:10.1242/jcs.03239.

39. Susanto O, Stewart SE, Voskoboinik I, Brasacchio D, Hagn M, et al. (2013) Mouse granzyme A induces a novel death with writhing morphology that is mechanistically distinct from granzyme B-induced apoptosis. Cell Death Differ 20: 1183–1193. doi:10.1038/cdd.2013.59.

40. Fan Z, Beresford PJ, Zhang D, Xu Z, Novina CD, et al. (2003) Cleaving the oxidative repair protein Ape1 enhances cell death mediated by granzyme A. Nat Immunol 4: 145–153. doi:10.1038/ni885.

41. Jans DA, Jans P, Briggs LJ, Sutton V, Trapani JA (1996) Nuclear Transport of Granzyme B (Fragmentin-2). J Biol Chem 271: 30781 –30789. doi:10.1074/jbc.271.48.30781.

42. Jans DA, Briggs LJ, Jans P, Froelich CJ, Parasivam G, et al. (1998) Nuclear targeting of the serine protease granzyme A (fragmentin-1). J Cell Sci 111: 2645 –2654.

43. Rajani DK, Walch M, Martinvalet D, Thomas MP, Lieberman J (2012) Alterations in RNA processing during immune-mediated programmed cell death. Proc Natl Acad Sci 109: 8688–8693. doi:10.1073/pnas.1201327109.

44. Martinvalet D, Zhu P, Lieberman J (2005) Granzyme A Induces Caspase-Independent Mitochondrial Damage, a Required First Step for Apoptosis. Immunity 22: 355–370. doi:10.1016/j.immuni.2005.02.004.

45. Martinvalet D, Dykxhoorn DM, Ferrini R, Lieberman J (2008) Granzyme A Cleaves a Mitochondrial Complex I Protein to Initiate Caspase-Independent Cell Death. Cell 133: 681–692. doi:10.1016/j.cell.2008.03.032.

46. Walch M, Dotiwala F, Mulik S, Thiery J, Kirchhausen T, et al. (2014) Cytotoxic Cells Kill Intracellular Bacteria through Granulysin-Mediated Delivery of Granzymes. Cell 157: 1309–1323. doi:10.1016/j.cell.2014.03.062.

47. Jurica MS, Moore MJ (2003) Pre-mRNA Splicing: Awash in a Sea of Proteins. Mol Cell 12: 5–14. doi:10.1016/S1097-2765(03)00270-3.

48. Hoskins AA, Moore MJ (2012) The spliceosome: a flexible, reversible macromolecular machine. Trends Biochem Sci 37: 179–188. doi:10.1016/j.tibs.2012.02.009.

49. Boise LH, González-García M, Postema CE, Ding L, Lindsten T, et al. (1993) bcl-x, a bcl-2-related gene that functions as a dominant regulator of apoptotic cell death. Cell 74: 597–608. doi:10.1016/0092-8674(93)90508-N.

50. Shkreta L, Michelle L, Toutant J, Tremblay ML, Chabot B (2011) The DNA Damage Response Pathway Regulates the Alternative Splicing of the Apoptotic Mediator Bcl-x. J Biol Chem 286: 331–340. doi:10.1074/jbc.M110.162644.

51. Tani H, Mizutani R, Salam KA, Tano K, Ijiri K, et al. (2012) Genome-wide determination of RNA stability reveals hundreds of short-lived noncoding transcripts in mammals. Genome Res 22: 947–956. doi:10.1101/gr.130559.111.

52. Alonso CR (2012) A complex “mRNA degradation code” controls gene expression during animal development. Trends Genet 28: 78–88. doi:10.1016/j.tig.2011.10.005.

53. Fabian MR, Sonenberg N, Filipowicz W (2010) Regulation of mRNA translation and stability by microRNAs. Annu Rev Biochem 79: 351–379. doi:10.1146/annurev-biochem-060308-103103.

54. Schoenberg DR, Maquat LE (2012) Regulation of cytoplasmic mRNA decay. Nat Rev Genet 13: 246. doi:10.1038/nrg3160.

55. Wahle E, Winkler GS (2013) RNA decay machines: Deadenylation by the Ccr4–Not and Pan2–Pan3 complexes. Biochim Biophys Acta BBA - Gene Regul Mech 1829: 561–570. doi:10.1016/j.bbagrm.2013.01.003.

56. Akio Yamashita, Chang T-C, Yamashita Y, Zhu W, Zhong Z, et al. (2005) Concerted action of poly(A) nucleases and decapping enzyme in mammalian mRNA turnover. Nat Struct Mol Biol 12: 1054–1063. doi:10.1038/nsmb1016.

57. Januszyk K, Lima CD (2014) The eukaryotic RNA exosome. Curr Opin Struct Biol 24: 132–140. doi:10.1016/j.sbi.2014.01.011.

58. Schoenberg DR (2011) Mechanisms of endonuclease-mediated mRNA decay. Wiley Interdiscip Rev RNA 2: 582–600. doi:10.1002/wrna.78.

59. Han D, Lerner AG, Vande Walle L, Upton J-P, Xu W, et al. (2009) IRE1α Kinase Activation Modes Control Alternate Endoribonuclease Outputs to Determine Divergent Cell Fates. Cell 138: 562–575. doi:10.1016/j.cell.2009.07.017.

60. Hollien J, Weissman JS (2006) Decay of Endoplasmic Reticulum-Localized mRNAs During the Unfolded Protein Response. Science 313: 104–107. doi:10.1126/science.1129631.

61. Hollien J, Lin JH, Li H, Stevens N, Walter P, et al. (2009) Regulated Ire1-dependent decay of messenger RNAs in mammalian cells. J Cell Biol 186: 323–331. doi:10.1083/jcb.200903014.

62. Norbury CJ (2013) Cytoplasmic RNA: a case of the tail wagging the dog. Nat Rev Mol Cell Biol 14: 643–653. doi:10.1038/nrm3645.

63. Mullen TE, Marzluff WF (2008) Degradation of histone mRNA requires oligouridylation followed by decapping and simultaneous degradation of the mRNA both 5′ to 3′ and 3′ to 5′. Genes Dev 22: 50–65. doi:10.1101/gad.1622708.

64. Rissland OS, Norbury CJ (2009) Decapping is preceded by 3|[prime]| uridylation in a novel pathway of bulk mRNA turnover. Nat Struct Mol Biol 16: 616–623. doi:10.1038/nsmb.1601.

65. Schmidt M-J, West S, Norbury CJ (2011) The human cytoplasmic RNA terminal U-transferase ZCCHC11 targets histone mRNAs for degradation. RNA N Y N 17: 39–44. doi:10.1261/rna.2252511.

66. Slevin MK, Meaux S, Welch JD, Bigler R, Miliani de Marval PL, et al. (2014) Deep Sequencing Shows Multiple Oligouridylations Are Required for 3′ to 5′ Degradation of Histone mRNAs on Polyribosomes. Mol Cell 53: 1020–1030. doi:10.1016/j.molcel.2014.02.027.

67. Thornton JE, Chang H-M, Piskounova E, Gregory RI (2012) Lin28-mediated control of let-7 microRNA expression by alternative TUTases Zcchc11 (TUT4) and Zcchc6 (TUT7). RNA 18: 1875–1885. doi:10.1261/rna.034538.112.

68. Shen B, Goodman HM (2004) Uridine Addition After MicroRNA-Directed Cleavage. Science 306: 997–997. doi:10.1126/science.1103521.

69. Lubas M, Damgaard CK, Tomecki R, Cysewski D, Jensen TH, et al. (2013) Exonuclease hDIS3L2 specifies an exosome-independent 3′-5′ degradation pathway of human cytoplasmic mRNA. EMBO J 32: 1855–1868. doi:10.1038/emboj.2013.135.

70. Chang H-M, Triboulet R, Thornton JE, Gregory RI (2013) A role for the Perlman syndrome exonuclease Dis3l2 in the Lin28-let-7 pathway. Nature 497: 244–248. doi:10.1038/nature12119.

71. Ustianenko D, Hrossova D, Potesil D, Chalupnikova K, Hrazdilova K, et al. (2013) Mammalian DIS3L2 exoribonuclease targets the uridylated precursors of let-7 miRNAs. RNA N Y N 19: 1632–1638. doi:10.1261/rna.040055.113.

72. Malecki M, Viegas SC, Carneiro T, Golik P, Dressaire C, et al. (2013) The exoribonuclease Dis3L2 defines a novel eukaryotic RNA degradation pathway. EMBO J 32: 1842–1854. doi:10.1038/emboj.2013.63.

73. Abernathy E, Clyde K, Yeasmin R, Krug LT, Burlingame A, et al. (2014) Gammaherpesviral Gene Expression and Virion Composition Are Broadly Controlled by Accelerated mRNA Degradation. PLoS Pathog 10: e1003882. doi:10.1371/journal.ppat.1003882.

74. Lee YJ, Glaunsinger BA (2009) Aberrant Herpesvirus-Induced Polyadenylation Correlates With Cellular Messenger RNA Destruction. PLoS Biol 7: e1000107. doi:10.1371/journal.pbio.1000107.

75. Glaunsinger B, Chavez L, Ganem D (2005) The Exonuclease and Host Shutoff Functions of the SOX Protein of Kaposi's Sarcoma-Associated Herpesvirus Are Genetically Separable. J Virol 79: 7396–7401. doi:10.1128/JVI.79.12.7396-7401.2005.

76. Gaglia MM, Covarrubias S, Wong W, Glaunsinger BA (2012) A Common Strategy for Host RNA Degradation by Divergent Viruses. J Virol 86: 9527–9530. doi:10.1128/JVI.01230-12.

77. Roy B, Jacobson A (2013) The intimate relationships of mRNA decay and translation. Trends Genet 29: 691–699. doi:10.1016/j.tig.2013.09.002.

78. Omer AD, Janas MM, Novina CD (2009) The Chicken or the Egg: MicroRNA-Mediated Regulation of mRNA Translation or mRNA Stability. Mol Cell 35: 739–740. doi:10.1016/j.molcel.2009.09.003.

79. Fabian MR, Mathonnet G, Sundermeier T, Mathys H, Zipprich JT, et al. (2009) Mammalian miRNA RISC Recruits CAF1 and PABP to Affect PABP-Dependent Deadenylation. Mol Cell 35: 868–880. doi:10.1016/j.molcel.2009.08.004.

80. Bazzini AA, Lee MT, Giraldez AJ (2012) Ribosome Profiling Shows That miR-430 Reduces Translation Before Causing mRNA Decay in Zebrafish. Science 336: 233–237. doi:10.1126/science.1215704.

81. Hu W, Sweet TJ, Chamnongpol S, Baker KE, Coller J (2009) Co-translational mRNA decay in Saccharomyces cerevisiae. Nature 461: 225–229. doi:10.1038/nature08265.

82. Hu W, Petzold C, Coller J, Baker KE (2010) Nonsense-mediated mRNA decapping occurs on polyribosomes in Saccharomyces cerevisiae. Nat Struct Mol Biol 17: 244–247. doi:10.1038/nsmb.1734.

83. Wek RC, Jiang H-Y, Anthony TG (2006) Coping with stress: eIF2 kinases and translational control. Biochem Soc Trans 34: 7. doi:10.1042/BST20060007.

84. Harding HP, Zhang Y, Zeng H, Novoa I, Lu PD, et al. (2003) An Integrated Stress Response Regulates Amino Acid Metabolism and Resistance to Oxidative Stress. Mol Cell 11: 619–633. doi:10.1016/S1097-2765(03)00105-9.

85. Gingras A-C, Raught B, Sonenberg N (2001) Regulation of translation initiation by FRAP/mTOR. Genes Dev 15: 807–826. doi:10.1101/gad.887201.

86. Silvera D, Formenti SC, Schneider RJ (2010) Translational control in cancer. Nat Rev Cancer 10: 254–266. doi:10.1038/nrc2824.

87. Jeffrey IW, Bushell M, Tilleray VJ, Morley S, Clemens MJ (2002) Inhibition of Protein Synthesis in Apoptosis Differential Requirements by the Tumor Necrosis Factor α Family and a DNA-damaging Agent for Caspases and the Double-stranded RNA-dependent Protein Kinase. Cancer Res 62: 2272–2280.

88. Bushell M, Stoneley M, Kong YW, Hamilton TL, Spriggs KA, et al. (2006) Polypyrimidine Tract Binding Protein Regulates IRES-Mediated Gene Expression during Apoptosis. Mol Cell 23: 401–412. doi:16/j.molcel.2006.06.012.

89. Clemens MJ, Bushell M, Morley SJ (1998) Degradation of eukaryotic polypeptide chain initiation factor (eIF) 4G in response to induction of apoptosis in human lymphoma cell lines. Oncogene 17: 2921–2931. doi:10.1038/sj.onc.1202227.

90. Clemens MJ, Bushell M, Jeffrey IW, Pain VM, Morley SJ (2000) Translation initiation factor modifications and the regulation of protein synthesis in apoptotic cells. Cell Death Differ 7: 603–615. doi:10.1038/sj.cdd.4400695.

91. Marissen WE, Lloyd RE (1998) Eukaryotic Translation Initiation Factor 4G Is Targeted for Proteolytic Cleavage by Caspase 3 during Inhibition of Translation in Apoptotic Cells. Mol Cell Biol 18: 7565–7574.

92. Morley SJ, Coldwell MJ, Clemens MJ (2005) Initiation factor modifications in the preapoptotic phase. Cell Death Differ 12: 571–584. doi:10.1038/sj.cdd.4401591.

93. Bushell M, Stoneley M, Sarnow P, Willis AE (2004) Translation inhibition during the induction of apoptosis: RNA or protein degradation? Biochem Soc Trans 32: 606–610. doi:10.1042/BST0320606.

94. Saelens X, Kalai M, Vandenabeele P (2001) Translation Inhibition in Apoptosis. J Biol Chem 276: 41620 –41628. doi:10.1074/jbc.M103674200.

95. Spencer SL, Gaudet S, Albeck JG, Burke JM, Sorger PK (2009) Non-genetic origins of cell-to-cell variability in TRAIL-induced apoptosis. Nature 459: 428–432. doi:10.1038/nature08012.

96. Degen WG, Pruijn GJ, Raats JM, van Venrooij WJ (2000) Caspase-dependent cleavage of nucleic acids. Cell Death Differ 7: 616–627. doi:10.1038/sj.cdd.4400672.

97. Del Prete MJ, Robles MS, Guáo A, Martínez-A C, Izquierdo M, et al. (2002) Degradation of cellular mRNA is a general early apoptosis-induced event. FASEB J Off Publ Fed Am Soc Exp Biol 16: 2003–2005. doi:10.1096/fj.02-0392fje.

98. Fan J, Yang X, Wang W, Wood WH, Becker KG, et al. (2002) Global analysis of stress-regulated mRNA turnover by using cDNA arrays. Proc Natl Acad Sci 99: 10611–10616. doi:10.1073/pnas.162212399.

99. Holler N, Zaru R, Micheau O, Thome M, Attinger A, et al. (2000) Fas triggers an alternative, caspase-8–independent cell death pathway using the kinase RIP as effector molecule. Nat Immunol 1: 489–495. doi:10.1038/82732.

100. Wei MC, Zong W-X, Cheng EH-Y, Lindsten T, Panoutsakopoulou V, et al. (2001) Proapoptotic BAX and BAK: A Requisite Gateway to Mitochondrial Dysfunction and Death. Science 292: 727–730. doi:10.1126/science.1059108.

101. Wang M, Zhao X-M, Tan H, Akutsu T, Whisstock JC, et al. (2014) Cascleave 2.0, a new approach for predicting caspase and granzyme cleavage targets. Bioinforma Oxf Engl 30: 71–80. doi:10.1093/bioinformatics/btt603.

102. Zheng D, Ezzeddine N, Chen C-YA, Zhu W, He X, et al. (2008) Deadenylation Is Prerequisite for P-Body Formation and mRNA Decay in Mammalian Cells. J Cell Biol 182: 89–101.

103. Parker R, Song H (2004) The enzymes and control of eukaryotic mRNA turnover. Nat Struct Mol Biol 11: 121–127. doi:10.1038/nsmb724.

104. Hoefig KP, Rath N, Heinz GA, Wolf C, Dameris J, et al. (2013) Eri1 degrades the stem-loop of oligouridylated histone mRNAs to induce replication-dependent decay. Nat Struct Mol Biol 20: 73–81. doi:10.1038/nsmb.2450.

105. Chang H, Lim J, Ha M, Kim VN (2014) TAIL-seq: Genome-wide Determination of Poly(A) Tail Length and 3′ End Modifications. Mol Cell 53: 1044–1052. doi:10.1016/j.molcel.2014.02.007.

106. Ingolia NT, Ghaemmaghami S, Newman JRS, Weissman JS (2009) Genome-Wide Analysis in Vivo of Translation with Nucleotide Resolution Using Ribosome Profiling. Science 324: 218–223. doi:10.1126/science.1168978.

107. Hutin S, Lee Y, Glaunsinger BA (2013) An RNA element in human interleukin 6 confers escape from degradation by the gammaherpesvirus SOX protein. J Virol 87: 4672–4682. doi:10.1128/JVI.00159-13.

108. Lee JH, Daugharthy ER, Scheiman J, Kalhor R, Yang JL, et al. (2014) Highly multiplexed subcellular RNA sequencing in situ. Science 343: 1360–1363. doi:10.1126/science.1250212.

109. Stewart DP, Koss B, Bathina M, Perciavalle RM, Bisanz K, et al. (2010) Ubiquitin-Independent Degradation of Antiapoptotic MCL-1. Mol Cell Biol 30: 3099–3110. doi:10.1128/MCB.01266-09.

110. Thomas MP, Whangbo J, McCrossan G, Deutsch AJ, Martinod K, et al. (2014) Leukocyte Protease Binding to Nucleic Acids Promotes Nuclear Localization and Cleavage of Nucleic Acid Binding Proteins. J Immunol 192: 5390–5397. doi:10.4049/jimmunol.1303296.

111. Waterhouse NJ, Sedelies KA, Browne KA, Wowk ME, Newbold A, et al. (2005) A Central Role for Bid in Granzyme B-induced Apoptosis. J Biol Chem 280: 4476–4482. doi:10.1074/jbc.M410985200.

112. Zhu P, Martinvalet D, Chowdhury D, Zhang D, Schlesinger A, et al. (2009) The cytotoxic T lymphocyte protease granzyme A cleaves and inactivates poly(adenosine 5′-diphosphate-ribose) polymerase-1. Blood 114: 1205 –1216. doi:10.1182/blood-2008-12-195768.

113. Zhang D, Pasternack MS, Beresford PJ, Wagner L, Greenberg AH, et al. (2001) Induction of Rapid Histone Degradation by the Cytotoxic T Lymphocyte Protease Granzyme A. J Biol Chem 276: 3683 –3690. doi:10.1074/jbc.M005390200.

114. Van Domselaar R, Quadir R, van der Made AM, Broekhuizen R, Bovenschen N (2012) All human granzymes target hnRNP K that is essential for tumor cell viability. J Biol Chem 287: 22854–22864. doi:10.1074/jbc.M112.365692.

115. Knickelbein JE, Khanna KM, Yee MB, Baty CJ, Kinchington PR, et al. (2008) Noncytotoxic Lytic Granule–Mediated CD8+ T Cell Inhibition of HSV-1 Reactivation from Neuronal Latency. Science 322: 268 –271. doi:10.1126/science.1164164.

116. Marcet-Palacios M, Duggan BL, Shostak I, Barry M, Geskes T, et al. (2011) Granzyme B Inhibits Vaccinia Virus Production through Proteolytic Cleavage of Eukaryotic Initiation Factor 4 Gamma 3. PLoS Pathog 7: e1002447. doi:10.1371/journal.ppat.1002447.

117. Krem MM, Rose T, Di Cera E (2000) Sequence Determinants of Function and Evolution in Serine Proteases. Trends Cardiovasc Med 10: 171–176. doi:10.1016/S1050-1738(00)00068-2.

118. Brinkmann V, Zychlinsky A (2012) Neutrophil extracellular traps: Is immunity the second function of chromatin? J Cell Biol 198: 773–783. doi:10.1083/jcb.201203170.

119. Papayannopoulos V, Metzler KD, Hakkim A, Zychlinsky A (2010) Neutrophil elastase and myeloperoxidase regulate the formation of neutrophil extracellular traps. J Cell Biol 191: 677–691. doi:10.1083/jcb.201006052.

120. Urban CF, Ermert D, Schmid M, Abu-Abed U, Goosmann C, et al. (2009) Neutrophil Extracellular Traps Contain Calprotectin, a Cytosolic Protein Complex Involved in Host

Defense against Candida albicans. PLoS Pathog 5: e1000639. doi:10.1371/journal.ppat.1000639.

121. Van Damme P, Maurer-Stroh S, Plasman K, Van Durme J, Colaert N, et al. (2009) Analysis of Protein Processing by N-terminal Proteomics Reveals Novel Species-specific Substrate Determinants of Granzyme B Orthologs. Mol Cell Proteomics 8: 258 –272. doi:10.1074/mcp.M800060-MCP200.

122. Van Damme P, Maurer-Stroh S, Hao H, Colaert N, Timmerman E, et al. (2010) The substrate specificity profile of human granzyme A. Biol Chem 391: 983–997. doi:10.1515/BC.2010.096.

123. Berriz GF, Beaver JE, Cenik C, Tasan M, Roth FP (2009) Next generation software for functional trend analysis. Bioinformatics 25: 3043 –3044. doi:10.1093/bioinformatics/btp498.

124. Jantz D, Berg JM (2010) Probing the DNA-Binding Affinity and Specificity of Designed Zinc Finger Proteins. Biophys J 98: 852–860. doi:10.1016/j.bpj.2009.11.021.

125. Fialcowitz-White EJ, Brewer BY, Ballin JD, Willis CD, Toth EA, et al. (2007) Specific Protein Domains Mediate Cooperative Assembly of HuR Oligomers on AU-rich mRNA-destabilizing Sequences. J Biol Chem 282: 20948 –20959. doi:10.1074/jbc.M701751200.

126. Park S, Myszka DG, Yu M, Littler SJ, Laird-Offringa IA (2000) HuD RNA Recognition Motifs Play Distinct Roles in the Formation of a Stable Complex with AU-Rich RNA. Mol Cell Biol 20: 4765 –4772. doi:10.1128/MCB.20.13.4765-4772.2000.

127. Nightingale KP, Pruss D, Wolffe AP (1996) A Single High Affinity Binding Site for Histone H1 in a Nucleosome Containing the Xenopus borealis 5 S Ribosomal RNA Gene. J Biol Chem 271: 7090–7094. doi:10.1074/jbc.271.12.7090.

128. Perera NC, Schilling O, Kittel H, Back W, Kremmer E, et al. (2012) NSP4, an elastase-related protease in human neutrophils with arginine specificity. Proc Natl Acad Sci 109: 6229–6234. doi:10.1073/pnas.1200470109.

129. Belorgey D, Bieth JG (1995) DNA binds neutrophil elastase and mucus proteinase inhibitor and impairs their functional activity. FEBS Lett 361: 265–268. doi:10.1016/0014-5793(95)00173-7.

130. Thiery J, Walch M, Jensen DK, Martinvalet D, Lieberman J (2010) Isolation of cytotoxic T cell and NK granules and purification of their effector proteins. Curr Protoc Cell Biol Editor Board Juan Bonifacino Al Chapter 3: Unit3.37. doi:10.1002/0471143030.cb0337s47.

131. Brinkmann V, Laube B, Abu Abed U, Goosmann C, Zychlinsky A (2010) Neutrophil extracellular traps: how to generate and visualize them. J Vis Exp JoVE. doi:10.3791/1724.

132. Carbon S, Ireland A, Mungall CJ, Shu S, Marshall B, et al. (2008) AmiGO: online access to ontology and annotation data. Bioinformatics 25: 288–289. doi:10.1093/bioinformatics/btn615.

133. The UniProt Consortium (2011) Reorganizing the protein space at the Universal Protein Resource (UniProt). Nucleic Acids Res 40: D71–D75. doi:10.1093/nar/gkr981.

134. Goujon M, McWilliam H, Li W, Valentin F, Squizzato S, et al. (2010) A new bioinformatics analysis tools framework at EMBL–EBI. Nucleic Acids Res 38: W695–W699. doi:10.1093/nar/gkq313.

135. Zhang H, Gao S, Lercher MJ, Hu S, Chen W-H (2012) EvolView, an online tool for visualizing, annotating and managing phylogenetic trees. Nucleic Acids Res 40: W569–W572. doi:10.1093/nar/gks576.

136. Ryder SP, Williamson JR (2004) Specificity of the STAR/GSG domain protein Qk1: Implications for the regulation of myelination. RNA 10: 1449–1458. doi:10.1261/rna.7780504.

137. Travis J, Giles PJ, Porcelli L, Reilly CF, Baugh R, et al. (1979) Human leucocyte elastase and cathepsin G: structural and functional characteristics. Ciba Found Symp: 51–68.

138. Lewis UJ, Williams DE, Brink NG (1956) Pancreatic Elastase: Purification, Properties, and Function. J Biol Chem 222: 705–720.

139. Ardelt W (1975) Physical parameters and chemical composition of porcine pancreatic elastase II. Biochim Biophys Acta 393: 267–273.

140. Higaki JN, Light A (1985) The identification of neotrypsinogens in samples of bovine trypsinogen. Anal Biochem 148: 111–120. doi:10.1016/0003-2697(85)90635-9.

141. Shazman S, Mandel-Gutfreund Y (2008) Classifying RNA-Binding Proteins Based on Electrostatic Properties. PLoS Comput Biol 4: e1000146. doi:10.1371/journal.pcbi.1000146.

142. Estébanez-Perpiñá E, Fuentes-Prior P, Belorgey D, Braun M, Kiefersauer R, et al. (2000) Crystal Structure of the Caspase Activator Human Granzyme B, a Proteinase Highly Specific for an Asp-P1 Residue. Biol Chem 381: 1203–1214.

143. Hink-Schauer C, Estebanez-Perpina E, Kurschus FC, Bode W, Jenne DE (2003) Crystal structure of the apoptosis-inducing human granzyme A dimer. Nat Struct Mol Biol 10: 535–540. doi:10.1038/nsb945.

144. Kolset SO, Tveit H (2008) Serglycin – Structure and biology. Cell Mol Life Sci 65: 1073–1085. doi:10.1007/s00018-007-7455-6.

145. Raja SM, Metkar SS, Höning S, Wang B, Russin WA, et al. (2005) A novel mechanism for protein delivery: granzyme B undergoes electrostatic exchange from serglycin to target cells. J Biol Chem 280: 20752–20761. doi:10.1074/jbc.M501181200.

146. Duranton J, Belorgey D, Carrère J, Donato L, Moritz T, et al. (2000) Effect of DNase on the activity of neutrophil elastase, cathepsin G and proteinase 3 in the presence of DNA. FEBS Lett 473: 154–156. doi:10.1016/S0014-5793(00)01512-X.

147. Di Cera E (2009) Serine Proteases. IUBMB Life 61: 510–515. doi:10.1002/iub.186.

148. Müllbacher A, Waring P, Tha Hla R, Tran T, Chin S, et al. (1999) Granzymes are the essential downstream effector molecules for the control of primary virus infections by cytolytic leukocytes. Proc Natl Acad Sci 96: 13950 –13955. doi:10.1073/pnas.96.24.13950.

Appendix 1: Supplemental materials related to chapter 4

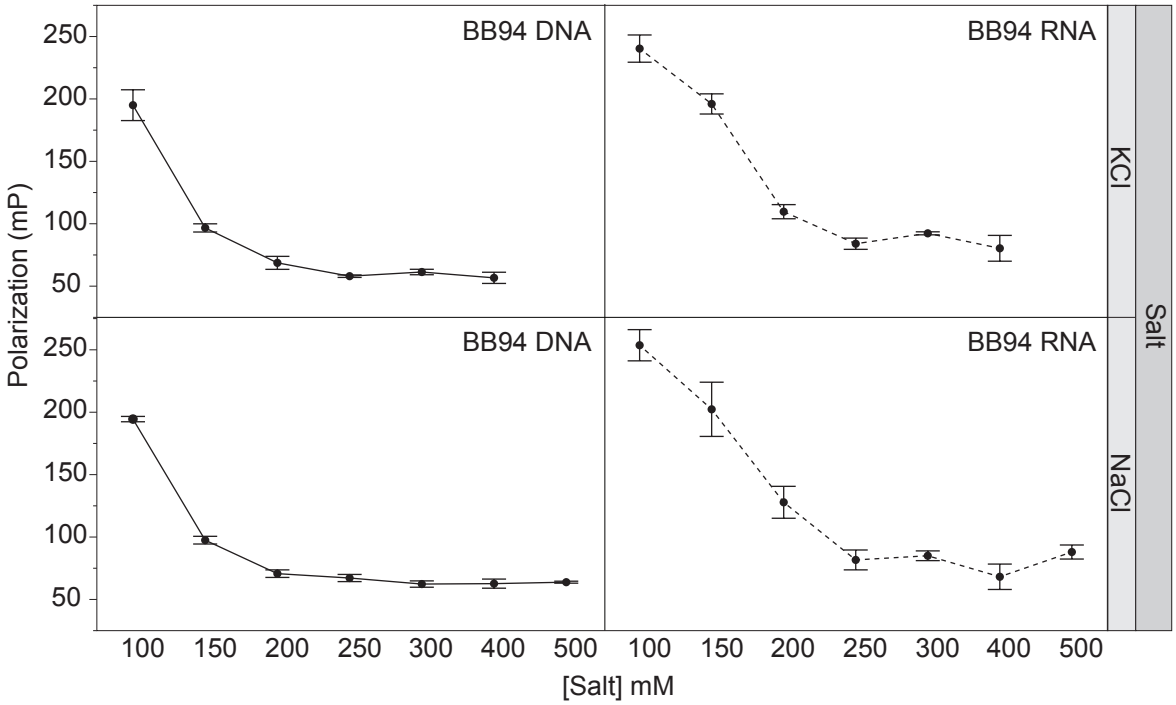

Supplemental Figure 1: Dependence on salt concentration of GzmB binding to nucleic acids
Binding of GzmB to BB94 RNA and BB94 ssDNA was assayed by FP in the presence of the indicated concentration of KCl or NaCl. Error bars represent SEM of at least 6 independent wells from 2 experiments.

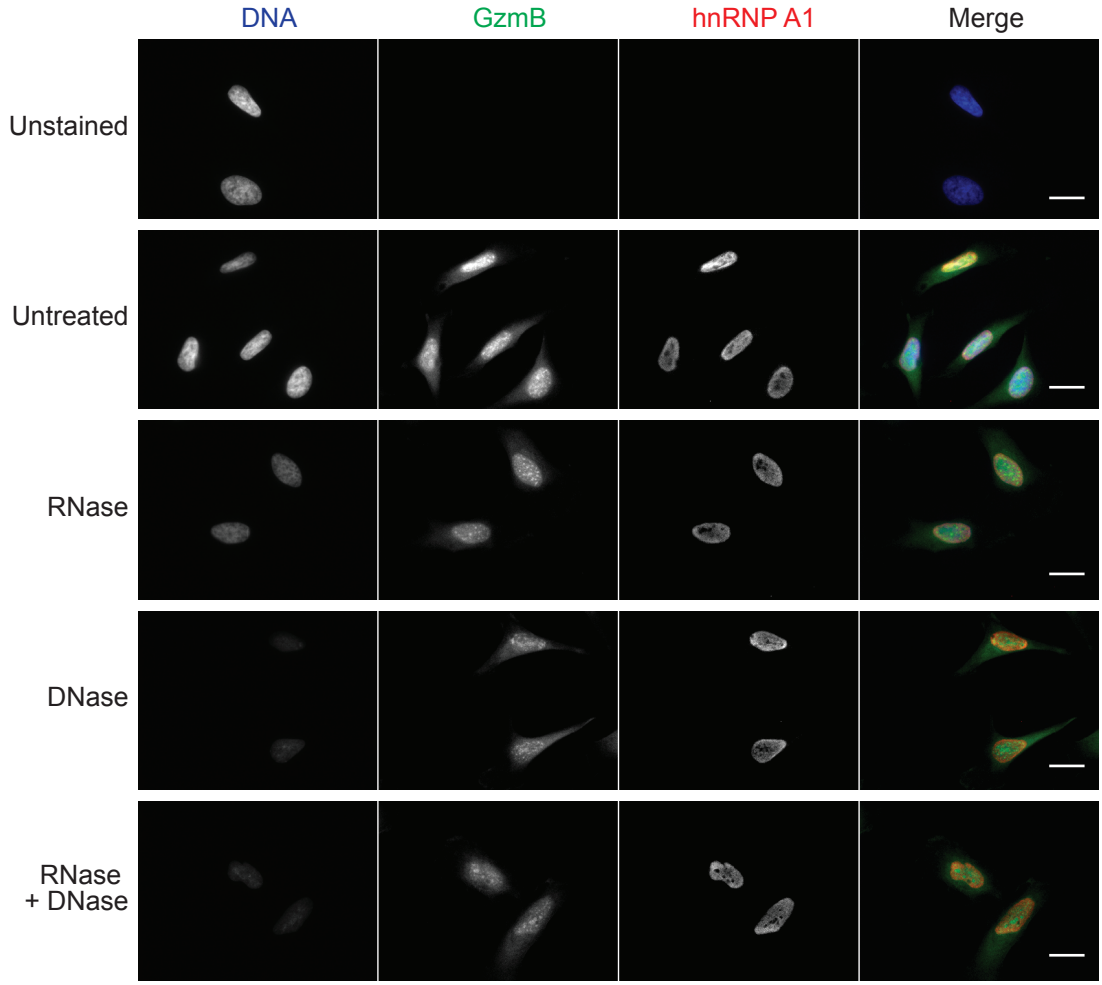

Supplemental Figure 2: RNase and DNase impact subcellular localization of GzmB in fixed cells
HeLa cells were fixed and permeabilized, then treated with RNase or DNase or both, then incubated with AF488-labeled GzmB and stained for DAPI. As an internal control for staining intensity and to visualize the nuclei, the cells were stained with an antibody against hnRNP A1. RNase modestly reduced cytosolic GzmB staining, while DNase modestly reduced nuclear GzmB staining. Scale bar is 10 μm.

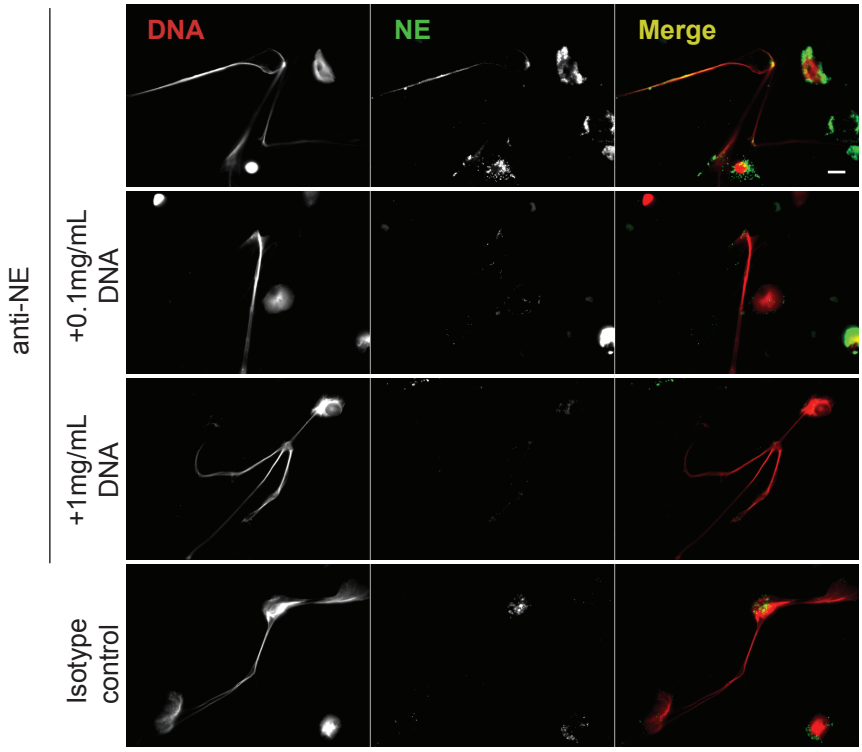

Supplemental Figure 3: DNA affinity mediates binding of endogenous NE to NETs
Primary neutrophils were treated with PMA to induce NETs and coincubated with the indicated concentration of salmon sperm DNA, then fixed and stained for endogenous NE (green) and for DNA with DAPI (red). Endogenous NE localized to NETs, and exogenous salmon sperm DNA reduced its localization to NETs. Scale bar is 10 μm.

Supplemental Table 1: GO analysis of GzmA and GzmB targets from proteomics studies
GO terms with a summed $-\log_{10}(P)$ of 50 or greater are presented. Many of the top terms relate to nucleic acid binding and metabolic functions.

	P-value (-log(10))		
GO term	GzmB	GzmA	Sum of –log(10) P-values
mRNA metabolic process	50.1	67.6	117.7
nucleic acid metabolic process	58.8	54.9	113.7
gene expression	46.1	64.5	110.7
RNA metabolic process	49.6	57.4	107.0
nuclear part	61.9	44.5	106.4
nucleobase, nucleoside, nucleotide and nucleic acid metabolic process	54.6	46.9	101.5
RNA binding	36.9	61.4	98.3
intracellular organelle part	48.6	47.0	95.7
organelle part	49.2	46.1	95.3
ribonucleoprotein complex	39.0	51.9	90.9
cellular nitrogen compound metabolic process	47.7	41.4	89.1
nitrogen compound metabolic process	45.9	40.8	86.7
intracellular part	48.1	37.6	85.8
cellular macromolecule metabolic process	50.2	35.5	85.7
nucleus	45.5	34.4	79.8
intracellular organelle	40.8	38.5	79.3
organelle	40.6	38.4	79.0
viral transcription	21.8	53.6	75.4
macromolecular complex	43.8	30.7	74.4
translational elongation	24.7	49.7	74.4
viral infectious cycle	21.0	52.0	73.0
non-membrane-bounded organelle	24.9	48.1	73.0
intracellular non-membrane-bounded organelle	24.9	48.1	73.0
translational termination	20.8	51.4	72.2
cellular component disassembly at cellular level	23.0	48.7	71.7
cellular component disassembly	23.0	48.6	71.5
cellular macromolecular complex disassembly	21.2	48.2	69.4
macromolecular complex disassembly	21.1	48.1	69.2
cellular protein complex disassembly	19.7	49.2	68.9
protein complex disassembly	19.6	49.1	68.7
macromolecule metabolic process	40.1	27.5	67.6
RNA processing	30.3	35.5	65.8
cellular macromolecular complex subunit organization	20.3	44.6	64.9
endocrine pancreas development	18.1	46.0	64.2
protein binding	44.2	18.1	62.2
viral reproductive process	16.4	44.4	60.9
cellular macromolecule biosynthetic process	27.2	31.8	59.0
nucleic acid binding	24.4	34.0	58.4
intracellular membrane-bounded organelle	35.3	22.6	57.9
cellular metabolic process	35.8	22.1	57.9
membrane-bounded organelle	35.3	22.5	57.8
RNA biosynthetic process	20.8	37.0	57.8
macromolecule biosynthetic process	26.6	31.1	57.7
nucleoplasm	35.1	22.4	57.5
cellular component organization or biogenesis at cellular level	26.7	30.5	57.2
macromolecular complex subunit organization	18.7	36.5	55.2
cellular component organization at cellular level	26.4	27.6	54.0
cellular component organization or biogenesis	25.4	28.6	53.9
cytosol	28.6	23.4	52.0
cytoplasm	39.4	12.6	52.0
viral reproduction	14.8	36.5	51.3
primary metabolic process	31.8	19.4	51.2
mRNA processing	25.0	26.0	51.1
cellular component organization	25.0	25.8	50.9

Appendix 2: Publications

Graduate school publications by Marshall Peter Thomas:

Thomas MP*, Whangbo J, McCrossan G, Deutsch AJ, Martinod K, et al. (2014) Leukocyte Protease Binding to Nucleic Acids Promotes Nuclear Localization and Cleavage of Nucleic Acid Binding Proteins. J Immunol 192: 5390–5397. doi:10.4049/jimmunol.1303296.

Thomas MP, Lieberman J (2013) Live or let die: posttranscriptional gene regulation in cell stress and cell death. Immunological Reviews 253: 237–252. doi:10.1111/imr.12052.

Rajani DK, Walch M, Martinvalet D, **Thomas MP**, Lieberman J (2012) Alterations in RNA processing during immune-mediated programmed cell death. PNAS 109: 8688–8693. doi:10.1073/pnas.1201327109.

Lal A, **Thomas MP***, Altschuler G, Navarro F, O'Day E, et al. (2011) Capture of MicroRNA–Bound mRNAs Identifies the Tumor Suppressor miR-34a as a Regulator of Growth Factor Signaling. PLoS Genet 7: e1002363. doi:10.1371/journal.pgen.1002363.

Thomas M, Lieberman J, Lal A (2010) Desperately seeking microRNA targets. Nat Struct Mol Biol 17: 1169–1174. doi:10.1038/nsmb.1921.

***co-first author**

THE JOURNAL OF IMMUNOLOGY

Leukocyte Protease Binding to Nucleic Acids Promotes Nuclear Localization and Cleavage of Nucleic Acid Binding Proteins

Marshall P. Thomas, Jennifer Whangbo, Geoffrey McCrossan, Aaron J. Deutsch, Kimberly Martinod, Michael Walch and Judy Lieberman

J Immunol 2014; 192:5390-5397; Prepublished online 25 April 2014;
doi: 10.4049/jimmunol.1303296
http://www.jimmunol.org/content/192/11/5390

The Journal of Immunology is published twice each month by
The American Association of Immunologists, Inc.,
9650 Rockville Pike, Bethesda, MD 20814-3994.

Print ISSN: 0022-1767 Online ISSN: 1550-6606.

Leukocyte Protease Binding to Nucleic Acids Promotes Nuclear Localization and Cleavage of Nucleic Acid Binding Proteins

Marshall P. Thomas,[1] Jennifer Whangbo,[1] Geoffrey McCrossan, Aaron J. Deutsch, Kimberly Martinod, Michael Walch,[2] and Judy Lieberman

Killer lymphocyte granzyme (Gzm) serine proteases induce apoptosis of pathogen-infected cells and tumor cells. Many known Gzm substrates are nucleic acid binding proteins, and the Gzms accumulate in the target cell nucleus by an unknown mechanism. In this study, we show that human Gzms bind to DNA and RNA with nanomolar affinity. Gzms cleave their substrates most efficiently when both are bound to nucleic acids. RNase treatment of cell lysates reduces Gzm cleavage of RNA binding protein targets, whereas adding RNA to recombinant RNA binding protein substrates increases in vitro cleavage. Binding to nucleic acids also influences Gzm trafficking within target cells. Preincubation with competitor DNA and DNase treatment both reduce Gzm nuclear localization. The Gzms are closely related to neutrophil proteases, including neutrophil elastase (NE) and cathepsin G. During neutrophil activation, NE translocates to the nucleus to initiate DNA extrusion into neutrophil extracellular traps, which bind NE and cathepsin G. These myeloid cell proteases, but not digestive serine proteases, also bind DNA strongly and localize to nuclei and neutrophil extracellular traps in a DNA-dependent manner. Thus, high-affinity nucleic acid binding is a conserved and functionally important property specific to leukocyte serine proteases. Furthermore, nucleic acid binding provides an elegant and simple mechanism to confer specificity of these proteases for cleavage of nucleic acid binding protein substrates that play essential roles in cellular gene expression and cell proliferation. ***The Journal of Immunology*****, 2014, 192: 5390–5397.**

Cytotoxic T lymphocytes and NK cells eliminate virus-infected cells and tumor cells by releasing the granzyme (Gzm) serine proteases and perforin from cytotoxic granules into the immunologic synapse formed with the cell destined for elimination (1). GzmA and GzmB, the most abundant and best-studied Gzms, are delivered to the target cell cytosol by perforin, rapidly concentrate in the target cell nucleus by an unknown mechanism, and induce independent programs of cell death (2, 3). To orchestrate cell death in diverse types of target cells, the Gzms cleave multiple substrates, likely numbering in the hundreds, within the cytosol, nucleus, and mitochondria (1, 4). DNA and RNA binding proteins are highly represented in the set of Gzm substrates. All but 1 of the 17 substrates of GzmA that have been carefully validated bind to DNA, RNA, or chromatin (1, 4). A recent proteomics study that profiled GzmA substrates in isolated nuclei identified 44 candidate substrates, of which 33 were RNA binding proteins (RBPs), including 12 heterogeneous nuclear ribonucleoproteins (hnRNP) (4). The remaining 11 candidate substrates were mostly DNA-binding proteins. In some cases, the nucleic acid appears to play an important role in the Gzm–target interaction. GzmA cleavage of histone H1 (H1) and binding to poly [ADP-ribose] polymerase 1 depends on the presence of DNA (5, 6). All five of the human Gzms cleave hnRNP K in an RNA-dependent manner (7). Gzm cleavage of viral and host nucleic acid binding proteins also plays an important role in controlling viral infection (8, 9). Thus many of the substrates of GzmA and GzmB are nucleic acid binding proteins that are physiologically important for cytotoxicity or the control of viral infections.

Although serine proteases have a high degree of sequence similarity, the Gzms are most closely related to a group of myeloid cell granule proteases involved in microbial defense. These immune proteases include the neutrophil proteases neutrophil elastase (NE) and cathepsin G (CATG) (10). When neutrophils are activated, they can ensnare and kill microbes in neutrophil extracellular traps (NETs), which are formed by nuclear DNA in a unique, non-apoptotic cell death mechanism called NETosis (11). NE participates in NETosis by translocating to the neutrophil nucleus, where it cleaves histones (12). Histone cleavage promotes chromatin decondensation, which precipitates the extrusion of nuclear DNA through the cell membrane. The extruded DNA is coated with histones, antimicrobial peptides, NE, and CATG (13).

The aim of this study was to explore further the role of nucleic acids in mediating Gzm–substrate interactions and trafficking. We

Program in Cellular and Molecular Medicine, Boston Children's Hospital, Boston, MA 02115; Division of Hematology-Oncology, Boston Children's Hospital, Boston, MA 02215; and Department of Pediatrics, Harvard Medical School, Boston, MA 02115

[1]M.P.T. and J.W. contributed equally to this work.

[2]Current address: Department of Medicine, Anatomy Unit, University of Fribourg, Fribourg, Switzerland.

Received for publication December 9, 2013. Accepted for publication March 24, 2014.

This work was supported by a National Science Foundation graduate research fellowship (to M.P.T.), National Institutes of Health K08 Grant HL094460 (to J.W.), a Boston Children's Hospital Career Development Fellowship (to J.W.), and National Institutes of Health Grant AI45587 (to J.L.).

Address correspondence and reprint requests to Dr. Judy Lieberman or Dr. Jennifer Whangbo, Harvard Medical School, WAB 255, 200 Longwood Avenue, Boston, MA 02115 (J.L.) or Boston Children's Hospital/Dana-Farber Cancer Institute, 450 Brookline Avenue, Boston, MA 02215 (J.W.). E-mail addresses: judy.lieberman@childrens.harvard.edu (J.L.) or jennifer.whangbo@childrens.harvard.edu (J.W.)

The online version of this article contains supplemental material.

Abbreviations used in this article: AF488, Alexa Fluor 488; CATG, cathepsin G; CI, confidence interval; FP, fluorescence polarization; GO, gene ontology; Gzm, granzyme; H1, histone H1; hnRNP, heterogeneous nuclear ribonucleoprotein; NE, neutrophil elastase; NET, neutrophil extracellular trap; pI, isoelectric point; RBP, RNA binding protein; RT, room temperature.

www.jimmunol.org/cgi/doi/10.4049/jimmunol.1303296

find that RNA enhances in vitro cleavage of RBP substrates, but not non-RBP substrates. We show that Gzms directly bind RNA and DNA with nanomolar affinity. NE and CATG also bind nucleic acids with high affinity, whereas digestive serine proteases do not. In the presence of competitor DNA, the leukocyte serine proteases do not localize to nuclei and NETs. Together, our findings indicate that nucleic acid binding is a conserved and functionally important property of leukocyte serine proteases that directs them to and enhances their cleavage of nucleic acid binding protein targets.

Materials and Methods

Abs

The following Abs were used at the indicated final concentration or dilution: mouse mAbs to hnRNP U (3G6; Santa Cruz Biotechnology; 0.2 μg/ml), hnRNP A1 (4B10; Sigma-Aldrich; 2 μg/ml), lamin B1 (101-B7; Calbiochem; 1/1,000), α-tubulin (B-5-1-2; Sigma-Aldrich; 1/1000), G3BP1 (23/G3BP; BD Biosciences; 0.25 μg/ml), hnRNP C1/C2 (4F4; Sigma-Aldrich; 0.4 μg/ml), β-actin (Developmental Studies Hybridoma Bank; 1/1000), HuR (3A2; Santa Cruz Biotechnology; 0.2 μg/ml); rabbit antisera to HMGB2 (Abcam; 1/1000), ICAD (Abcam; 0.5 μg/ml), and NE (Abcam; 1 μg/ml); and DDX5 (Abcam; 0.5 μg/ml). Secondary Abs were sheep anti-mouse HRP (GE Healthcare; 1/2500), donkey anti-rabbit HRP (GE; 1/2500), donkey anti-goat HRP (GE Healthcare; 1/2500), goat anti-rabbit Alexa Fluor 488 (AF488; Invitrogen; 1/200), and donkey anti-mouse Cy3 (715-165-150; Jackson ImmunoResearch Laboratories; 1:200). Normal rabbit IgG (2729; Cell Signaling Technology; 1 μg/ml) was used as an isotype control for immunofluorescence.

Proteins

Human GzmA and GzmB expression plasmids (4) were transfected into HEK 293T cells by calcium phosphate precipitation. The transfected cells were grown in serum-free ExCell 293 medium (Sigma-Aldrich) for 4 d. Recombinant Gzms were purified from the culture supernatants by immobilized metal affinity chromatography using Nickel-NTA (Qiagen) following the manufacturer's instructions. Eluted Gzms were treated with enterokinase (0.05 IU/ml supernatant; Sigma-Aldrich) for 16 h at room temperature (RT). Active Gzms were finally purified on an S column, concentrated, and quality tested as previously described (14). GST-tagged HuR, hnRNPC1, and LMNB1 were expressed and purified as described (4). H1 (M2501S; New England Biolabs) and caspase-3 (ALX-201-059-U025; Enzo Life Sciences) were purchased. Other serine proteases were NE (16-14-051200; Athens Research and Technology, Athens, GA), pancreatic elastase (324682; Millipore), CATG (16-14-030107; Athens Research and Technology), and trypsinogen (T1143; Sigma-Aldrich). Proteins were fluorescently labeled with AF488 according to the manufacturer's instructions (A30006; Invitrogen).

In vitro cleavage in cell lysates

Whole-cell lysates were made from 10^6 HeLa cells suspended in 1 ml lysis buffer (50 mM Tris-HCl [pH 8] and 100 mM NaCl) by alternating freezing in an ethanol/dry ice bath and thawing at 37°C three times. Cell debris was pelleted by centrifugation (16,000 × *g* for 10 min at 4°C). The supernatant was divided, and half was treated with RNase A/T1 (Thermo Scientific) at a concentration of 325 U/ml for 30 min at 37°C. RNaseOUT (Invitrogen) was added at a concentration of 1000 U/ml to the remaining half. The lysates were then treated with the indicated amounts of Gzms in a volume of 60 μl for 15 min at 37°C. In some cases, GzmB was incubated with varying amounts of salmon sperm DNA on ice for 30 min before addition to lysates. The cleavage reaction was stopped by adding 5× SDS loading buffer and boiling at 95°C for 5 min. For caspase-3 experiments, lysates were incubated with or without 1 U recombinant capsase-3 for 1 h before stopping the reaction. Samples were analyzed by SDS-PAGE and immunoblot.

In vitro cleavage of recombinant proteins

In vitro cleavage was performed in 100 mM NaCl and 50 mM Tris-HCl (pH 7.5). Each protein was first incubated in the indicated concentration of HeLa cell total RNA or salmon sperm DNA for 20 min and then incubated with 50 nM GzmB for 15 min (hnRNP C), 50 nM GzmB for 30 min (LMNB1), 200 nM GzmA for 20 min (H1), or 5 nM NE for 10 min (H1). Total HeLa cell RNA was purified with TRIzol (Invitrogen) according to the manufacturer's instructions. The final concentrations of hnRNP C, LMNB1, and H1 were 333, 1, and 400 nM, respectively. For HuR cleavage, RNA oligonucleotides were diluted to 10 μM, heated at 70°C for 10 min, and cooled on ice. A total of 400 nM recombinant GST-tagged HuR was incubated with or without 200 nM recombinant GzmB. The cleavage reactions were performed in the presence of 3 ng/μl total HeLa RNA, AU RNA, or BB94 RNA at the indicated molar ratios and incubated in a total volume of 40 μl at 37°C for 30 min. Cleavage reactions were stopped by adding 5× SDS loading buffer and boiling for 5 min. Cleavage was assayed by immunoblot or silver staining (Invitrogen SilverQuest kit; Invitrogen).

Protease localization in permeabilized HeLa cells

HeLa cells were obtained from American Type Culture Collection and maintained in DMEM supplemented with 10% heat-inactivated FBS, 100 U/ml penicillin G, 100 μg/ml streptomycin sulfate, 6 mM HEPES, 1.6 mM L-glutamine, and 50 μM 2-ME. HeLa cells were grown overnight on 12-mm coverslips, then fixed for 10 min at RT in 2% formaldehyde, and permeabilized for 10 min in methanol on dry ice. In some experiments, the cells were treated with DNase I (New England Biolabs) or RNase A/T1 (Thermo Scientific) at a 1:50 dilution for 4 h at RT before blocking. The cells were blocked with 1% BSA in PBS for 1 h at RT, and coverslips were incubated with blocking buffer containing salmon sperm DNA or no DNA for 30 min on ice and then incubated at RT for 1 h with 100 nM AF488-labeled serine proteases. The coverslips were then washed and stained with 4 μg/ml DAPI in PBS and mounted on slides (48311-703; VWR International) using polyvinyl alcohol (P-8136; Sigma-Aldrich) aqueous mounting medium. Cells were imaged using an Axiovert 200M microscope (Pan Apochromat, 1.4 numerical aperture; Carl Zeiss). Images were analyzed with SlideBook 4.2 (Intelligent Imaging Innovations).

Neutrophil isolation and activation

Human studies were reviewed and approved by the Harvard Committee on the Use of Human Subjects (IRB-P00005698). Neutrophils were isolated from the blood of deidentified healthy donors by density-gradient centrifugation as described (15). The neutrophil layer was washed with HBSS and resuspended at 10^6 cells/ml in RPMI 1640. Neutrophils (2.5×10^5) were incubated at 37°C for 15 min on 12-mm coverslips in 24-well flat-bottom cell-culture plates and then treated in 500 μl RPMI 1640 for 3 h with 100 nM PMA (P1585; Sigma-Aldrich). In some experiments, 100 nM AF488-labeled protease and/or salmon sperm DNA (D7656; Sigma-Aldrich) was added just prior to adding PMA. Treated cells were fixed in PBS containing 4% formaldehyde. For immunofluorescence staining of endogenous NE, the fixed cells were incubated with primary Ab or rabbit antiserum control for 1 h at RT, washed three times in PBS, and then incubated in secondary Ab (AF488-labeled goat anti-rabbit IgG) for 1 h at RT. The cells were washed, stained with DAPI, and mounted as above.

Gene ontology and phylogenetic analysis of serine proteases

We analyzed the candidate targets of human GzmA (16) and GzmB (17) identified by proteomics using the FuncAssociate tool (18) on default settings. Top gene ontology (GO) terms were ranked by the sum of the $-\log_{10}(p)$ values for enrichment of targets of each enzyme. All human proteins having the GO term "serine-type peptidase activity" (GO:0008236) were identified with AmiGO (19). Of these proteins, the manually annotated and reviewed Swiss-Prot sequences were downloaded using the UniProt retrieve tool (20). The sequences were trimmed to focus on their protease domains and exclude spurious alignment of other protein domains in multidomain proteins. The ClustalW2 (21) multiple sequence alignment and phylogeny tools were used with default parameters to construct a phylogenetic tree. Phylogeny was visualized with the EvolView Web tool (22).

Fluorescence polarization oligonucleotides

The following FAM-labeled oligonucleotides were used for fluorescence polarization (FP) (all from Integrated DNA Technologies): BB94 DNA, 5′-TCTGTGAGTTGAACGCACACATCACAAAGGAG-FAM-3′; $dA_{(30)}$, 5′-AAAAAAAAAAAAAAAAAAAAAAAAAAAAAA-FAM-3′; $dC_{(30)}$, 5′-CCCCCCCCCCCCCCCCCCCCCCCCCCCCCC-FAM-3′; $dT_{(30)}$, 5′-TTTTTTTTTTTTTTTTTTTTTTTTTTTTTT-FAM-3′; $rU_{(30)}$, 5′-UUUUUUUUUUUUUUUUUUUUUUUUUUUUUU-FAM-3′; BB94 RNA, 5′-UCUGUGAGUUGAACGCACACAUCACAAAGGA-FAM-3′; and AU RNA, 5′-CCCAAGCUUAUUUAUUUAUUUAUUGCAGGUC-FAM-3′.

FP assays

FAM-labeled oligonucleotides were used at 10 nM, and binding reactions were performed in a total volume of 20 μl. Proteins and oligonucleotides were diluted in 10 mM Tris-HCl (pH 7.5), 100 mM NaCl, and 2.5 mM $MgCl_2$. For RNA oligonucleotides, RNAseOUT was added to a final concentration of 1 U/μl. Diluted RNA oligonucleotides were heated to 70°C for 10 min prior to use. In the salt concentration assay, protein concentration was fixed (100 nM), and either NaCl or KCl was added to the

assay buffer at the indicated final concentrations. Samples were equilibrated in 384-well black polystyrene assay plates (3575; Corning) for 20 min at RT, and polarization was determined using a Synergy 2 Microplate Reader and Gen5 Data Analysis Software (BioTek).

FP data analysis

The apparent equilibrium K_d was determined from fitting the data to a sigmoidal dose-response function using JMP Pro 10 (JMP Statistical Discovery Software from SAS Institute). The apparent K_d was determined for each protein–nucleic acid interaction using the equation f = c + {[*d* − c]/[1 + 10^ (−a[$\log_{10}$([P] − b])]}, where f is the fraction bound or the polarization value, [P] is the protein concentration, b is the equilibrium K_d, a is the Hill coefficient, d is the maximum polarization, and c is the minimum polarization (23). Each experiment was performed at least in duplicate. The average and SE of the polarization value for each protein concentration was calculated from at least 10 independent samples.

Oligo(dT) pulldown

A total of 120 μl Oligo$(dT)_{25}$ Dynabeads (61002; Invitrogen) and 10 μl Protein G Dynabeads (10004D; Invitrogen) was washed three times in 50 mM Tris-HCl (pH 7.5) and 100 nM NaCl. The beads were blocked for 30 min at RT in the same buffer containing 0.5% BSA (A9647; Sigma-Aldrich). Following blocking, half of the Oligo$(dT)_{25}$ Dynabeads were treated at RT for 30 min with 25 U Benzonase Nuclease (E1014; Sigma-Aldrich), and the other half was left untreated. After this incubation, the beads were incubated with 120 μl protein (final concentration 1 μM) in blocking buffer for 30 min at RT. The beads were washed three times, and protein was eluted by boiling samples for 3 min in 30 μl SDS loading buffer. Samples were electrophoresed through a 12% polyacrylamide denaturing gel and visualized by Coomassie staining.

Results

Predicted targets of GzmA and GzmB are enriched for nucleic acid binding proteins

Because the Gzms concentrate in the nucleus of target cells, we hypothesized that proteins that function in the nucleus might be overrepresented among Gzm substrates. Two proteomics studies identified candidate GzmA and GzmB substrates without bias by analyzing Gzm-incubated cell lysates for novel cleavage products

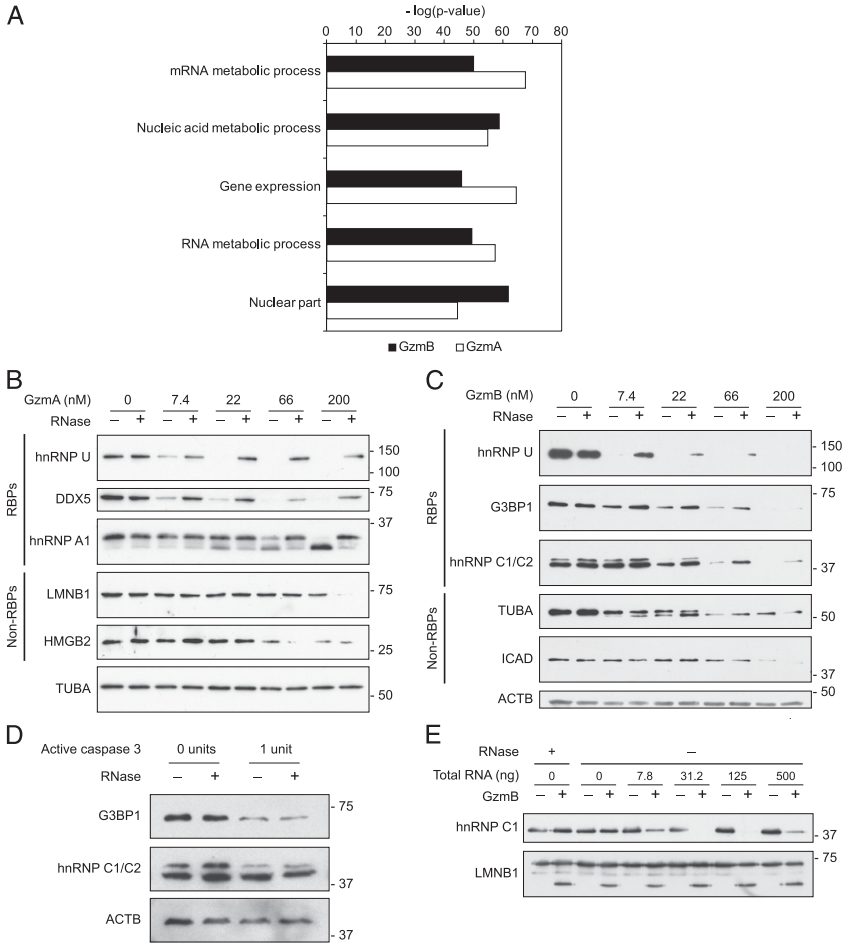

FIGURE 1. RBP target cleavage by Gzms is enhanced by RNA. (**A**) GO analysis of GzmA and GzmB targets. Nucleic acid binding proteins are highly enriched. (**B**–**E**) Cell lysates or recombinant proteins were incubated with RNase or the indicated concentration of total RNA followed by incubation with Gzms or caspase 3. The reactions were analyzed by immunoblot. RNase treatment of HeLa cell lysates reduced cleavage by GzmA (B) and GzmB (C) of RBP targets, but not non-RBP targets. Results in (B) and (C) are representative of at least three independent experiments. (D) RNase treatment of HeLa cell lysates did not affect cleavage of RBP targets by active caspase-3. (E) GzmB cleavage of recombinant hnRNP C1, but not recombinant LMNB1, was enhanced by exogenous total RNA. Results in (D) and (E) are representative of two independent experiments.

(16, 17). We analyzed these target lists using the FuncAssociate GO tool (18) for overrepresented GO terms in both GzmA and GzmB datasets (Fig. 1A, Supplemental Table I). Proteins with nucleic acid–related GO terms were the most highly enriched categories, when analyzed for each Gzm individually or together. The top seven GO terms for both Gzms (mRNA metabolic process, nucleic acid metabolic process, gene expression, RNA metabolic process, nuclear part, nucleotide metabolic process, and RNA binding) were highly significantly overrepresented (p values of $\sim 10^{-50}$ for each Gzm). This analysis suggested that Gzms might have a special preference for nucleic acid binding, especially RBP, substrates.

RNA promotes GzmA and GzmB cleavage of RNA-binding proteins

We first asked whether RNA enhances Gzm RBP cleavage by comparing Gzm cleavage of RBPs in whole-cell lysates depleted of RNA. HeLa cell lysates were pretreated or not with a mixture of RNase A and T1 before a 15-min incubation with varying concentrations of recombinant human GzmA or GzmB. The samples were then immunoblotted for known GzmA and GzmB targets. All three GzmA RBP targets analyzed (hnRNP U, DDX5, and hnRNP A1) were cleaved less efficiently in RNase-treated samples (Fig. 1B). Similarly, cleavage of RBP targets of GzmB (hnRNP U, G3BP1, and hnRNP C1/C2) was reduced by removing RNA (Fig. 1C). In contrast, non-RBP targets (LMNB1, HMGB2, TUBA, and ICAD) were cleaved equally or more efficiently in RNase-treated lysates, suggesting that Gzm target preference is altered to favor non-RBPs in the absence of RNA. This effect is not universal to cytotoxic proteases, as RNase treatment did not affect caspase-3 cleavage of hnRNP C1/C2 and G3BP1 RBP substrates (Fig. 1D). We next tested whether adding HeLa cell RNA would alter in vitro GzmB cleavage of recombinant hnRNP C1 and LNMB1. The RBP hnRNP C1 was more efficiently cleaved in the presence of added RNA, whereas cleavage of the non-RBP LMNB1 was unaffected (Fig. 1E). These results indicate that RNA enhances Gzm cleavage of RBP targets. Of note, although the highest concentration of RNA still enhanced cleavage, GzmB cleavage of hnRNP C1 was more efficient when less RNA was added.

The Gzms bind to RNA with nanomolar affinity

Because RNA enhanced Gzm activity against RBPs, we hypothesized that the Gzms might bind to RNA to direct them to RBP targets. We tested RNA binding by FP, a technique widely used to measure protein–nucleic acid interactions (24), using a 3′ FAM-labeled oligouridylate homopolymer (rU_{30}). As a positive control, we measured RNA binding of human Ag R (HuR), a GzmB substrate that binds to AU-rich RNA sequences (25). GzmA, GzmB, and HuR all bound to rU_{30} with high affinity, whereas the negative control protein BSA did not bind (Fig. 2A). The apparent equilibrium K_d of all three purified proteins with the rU_{30} oligonucleotide determined by FP was in the nanomolar range (Table I).

GzmB cleavage of HuR is enhanced by HuR binding to RNA

Because HuR preferentially binds AU-rich sequences, we used its specificity to assess the effect of substrate binding to RNA on GzmB cleavage. We compared GzmB cleavage of HuR in the presence of an AU-rich target sequence (AU RNA) (26) that both HuR and GzmB bind with similar affinity (Fig. 2B, Table I) and in the presence of a control sequence (BB94) that binds well only to GzmB (Fig. 2C, Table I). Formation of the cleavage product was enhanced by AU RNA, but only minimally increased by BB94 RNA (Fig. 2D). These results suggest that RBP targets are optimally cleaved by Gzms when both the target and Gzm interact with RNA.

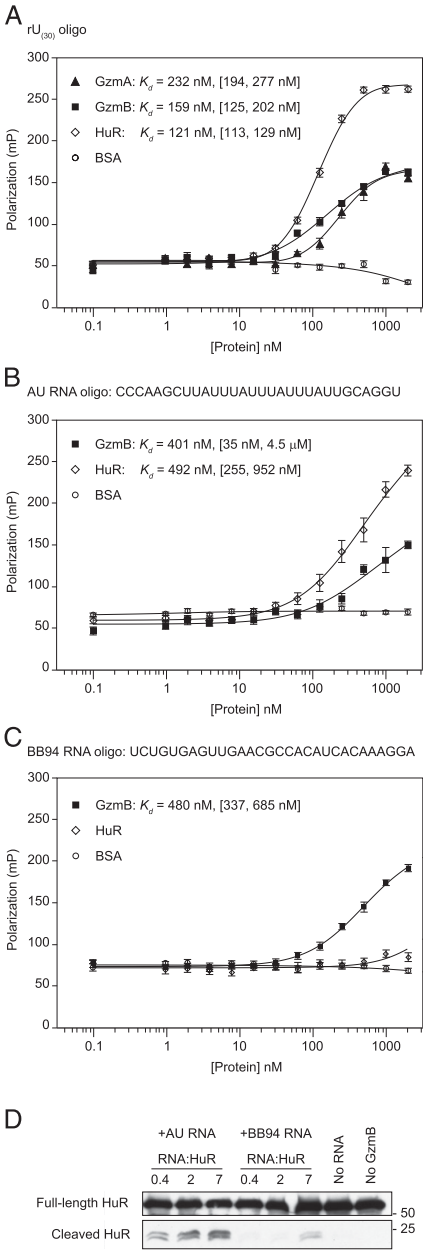

FIGURE 2. Gzms directly bind RNA. FP assays with purified Gzms and RNA. (**A**) GzmA and GzmB bound to a FAM-labeled 30-nt RNA [$rU_{(30)}$]. (**B**) GzmB and HuR bind a 30-nt RNA containing an AU-rich sequence (AU RNA). (**C**) GzmB, but not HuR, binds a length-matched control RNA (BB94 RNA). The mean polarization values ± SEM are plotted, and the apparent K_d with 95% CI in brackets is shown. Results are representative of at least three independent experiments. (**D**) GzmB cleaves HuR, an RBP target, most efficiently when it is bound to RNA. GST-tagged HuR protein was incubated with indicated molar ratios of AU RNA or BB94 RNA, and GzmB was then added for 30 min. HuR cleavage was detected by immunoblot probed for GST.

Table I. Protein–nucleic acid interactions measured by FP in this study

Oligonucleotide	Protein	K_d (nM)
$rU_{(30)}$	GzmA	232 (194–277)
	GzmB	159 (125–202)
	HuR	121 (113–129)
AU RNA	GzmA	401 (35 nM–4.5 μM)
	GzmB	651 (157 nM–2.7 μM)
	NE	602 (304 nM–1.2 μM)
	CATG	165 (139–197)
	HuR	492 (255–952)
BB94 ssRNA	GzmA	1.6 μM (188 nM–15.2 μM)
	GzmB	480 (337–685)
	HuR	4.8 μM (16 nM–1465.9 μM)
BB94 ssDNA	GzmA	122 (95–158)
	GzmB	35 (31–40)
	NE	272 (219–339)
	CATG	22 (17–29)
	H1	10 (8–12)
BB94 dsDNA	GzmA	120 (106–136)
	GzmB	161 (112–231)
	NE	607 (516–712)
	CATG	35 (24–52)
	H1	9 (7–13)
$dC_{(30)}$	GzmA	91 (65–127)
	GzmB	175 (140–219)
$dT_{(30)}$	GzmA	48 (42–55)
	GzmB	45 (26–78)

The apparent K_d with 95% CI in parentheses is given for each binding interaction.

Gzms bind DNA with nanomolar affinity

Because the Gzms bind to RNA and cleave many DNA binding proteins, we asked whether they could also bind DNA. We used FP to measure the binding of GzmA and GzmB to an ssDNA oligonucleotide of the same sequence as BB94 RNA (Fig. 3A). Both GzmA and GzmB bound ssDNA with nanomolar K_d (Table I). GzmB {K_d 35 nM [95% confidence interval (CI) 31–40]} bound ssDNA almost as strongly as H1 (K_d 10 nM [95% CI 8–12]), similar to reported values (27). GzmA binding was somewhat weaker (K_d 122 nM [95% CI 95–158]). Both Gzms also bound to a dsDNA oligonucleotide containing the same BB94 sequence with nanomolar affinities (Fig. 3B). To determine if Gzm binding might have a sequence preference, we performed FP assays with ssDNA homopolymers (dA_{30}, dT_{30}, and dC_{30}). Oligo(dG) was not tested because it tends to form higher order structures and aggregate. Both Gzms bound $dT_{30} > dC_{30}$ with nanomolar affinity, but only weakly bound to dA_{30} (Fig. 3C, 3D). This suggests that the Gzms bind preferentially to pyrimidines. These assays were performed in buffer containing 100 mM NaCl. Because many protein–DNA complexes are sensitive to salt concentration, we performed FP assays over a range of NaCl and KCl concentrations, while holding the GzmB and nucleic acid concentration constant. Although binding decreased at higher salt concentrations, binding of GzmB to DNA and RNA remained strong at physiological concentrations (150 mM NaCl or KCl) (Supplemental Fig. 1).

Myeloid granule serine proteases bind nucleic acids

Next we asked whether nucleic acid binding is a general property of serine proteases or limited to a subset. To visualize the evolutionary relationships between the Gzms and other serine proteases, we performed a phylogenetic analysis of all annotated human serine proteases. The Gzms form a monophyletic group with other leukocyte serine proteases (Fig. 4A). This group includes five neutrophil proteases (NE, CATG, NSP4, PRTN3, and AZU1) (28) and the mast cell protease CMA1. The Gzms are more distantly related to digestive enzymes, such as pancreatic elastase and trypsin. We

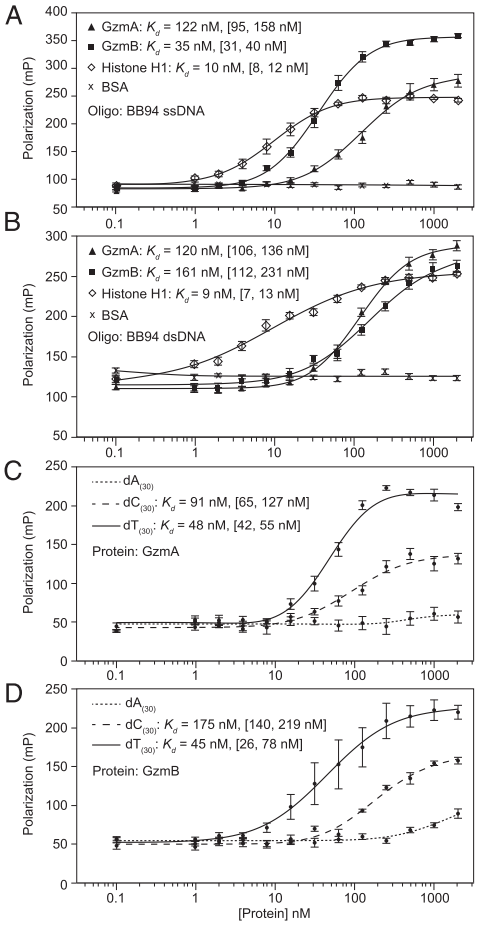

FIGURE 3. GzmA and GzmB bind DNA with nanomolar affinity. The binding of a FAM-labeled ssDNA (**A**) or dsDNA (**B**) oligonucleotide (BB94) to GzmA, GzmB, H1, and BSA was measured by FP. To determine whether binding was sequence dependent, interactions of GzmA (**C**) and GzmB (**D**) with 3′ FAM-labeled homo-oligomers [$dA_{(30)}$, $dC_{(30)}$, and $dT_{(30)}$] were measured by FP. Both Gzms bound pyrimidine tracts [$dT_{(30)}$ and $dC_{(30)}$] more strongly than the purine tract $dA_{(30)}$. The mean polarization values ± SEM are plotted, and the apparent K_d with 95% CI in brackets is shown. Results are representative of at least three independent experiments.

used FP to assess the affinity of native human CATG and NE, porcine pancreatic elastase, and bovine trypsinogen (the proenzyme of trypsin) for RNA, ssDNA, and dsDNA (Fig. 4B). Both neutrophil proteases bound these nucleic acids with nanomolar affinity like the Gzms, but neither digestive protease bound. This agrees with an earlier study showing that NE binds to DNA (29). To validate DNA binding with an independent assay, we used oligo(dT)-conjugated beads to pull down the Gzms, neutrophil proteases, and pancreatic elastase (Fig. 4C). Consistent with the FP results, the leukocyte proteases (GzmA, GzmB, NE, and CATG), but not the digestive protease, bound to oligo(dT) beads. Binding was specific to DNA because it was decreased by pretreating the beads with DNase. The proteases also did not bind to protein G–conjugated beads. We hypothesized that DNA binding

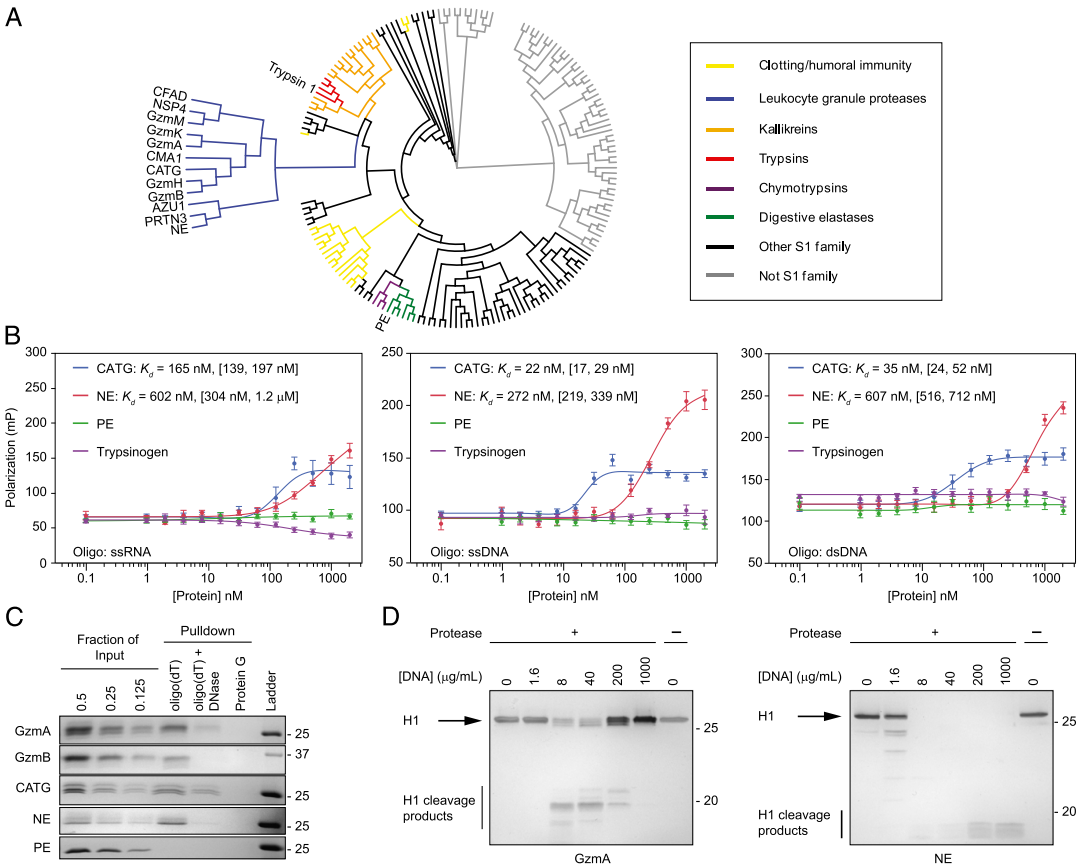

FIGURE 4. Leukocyte serine proteases bind to RNA and DNA with nanomolar affinity. (**A**) Phylogenetic analysis of all human serine proteases shows that leukocyte serine proteases form a monophyletic group. (**B**) Interactions of two neutrophil serine proteases (NE and CATG) and digestive serine proteases (trypsinogen and pancreatic elastase [PE]) with RNA, ssDNA, and dsDNA were measured by FP. NE and CATG bound with nanomolar affinity, but the digestive proteases did not. The mean polarization values ± SEM and the apparent K_d with 95% CI in brackets are shown. (**C**) Direct binding of GzmA, GzmB, NE, CATG, and PE to ssDNA was assessed by affinity pulldown with oligo(dT)$_{25}$-conjugated beads. The leukocyte proteases bound, but the digestive enzyme did not. Binding was reduced by DNase treatment. None of the proteases bound to protein G beads. (**D**) Purified H1 was not cleaved in the absence of added DNA. Cleavage of H1 by GzmA and NE was assessed in the presence of increasing amounts of salmon sperm DNA. Addition of small amounts of DNA enhanced cleavage by both GzmA and NE. At higher concentrations, DNA inhibited GzmA cleavage. Results are representative of at least three independent experiments.

would enhance leukocyte protease cleavage of DNA binding protein substrates, as shown above for RNA and previously shown for GzmA cleavage of H1 (5). We treated purified H1, a target of both GzmA and NE with each protease in the presence of increasing concentrations of salmon sperm DNA. H1 cleavage by NE was greatly increased by adding even a small amount of DNA (Fig. 4D). H1 cleavage by GzmA was first promoted, then inhibited, by increasing amounts of salmon sperm DNA. Inhibition by high concentrations of exogenous RNA was also seen when we analyzed GzmB cleavage of hnRNP C1 (Fig. 1E). These results suggest that an excess of nucleic acids interferes with formation of a substrate–nucleic acid–protease complex. Collectively, these results demonstrate that nucleic acid binding is a conserved and functionally important property of leukocyte serine proteases.

DNA binding mediates localization of Gzms to the nucleus

During killer cell attack, the Gzms rapidly concentrate in the nucleus of target cells by an unknown mechanism. A previous study suggested that nuclear localization is mediated by affinity of the Gzms to insoluble NFs (3). We hypothesized that the nuclear accumulation of Gzms is driven by direct binding to nuclear DNA. To test this idea, we incubated fixed and permeabilized HeLa cells with AF488-labeled serine proteases and visualized their localization with fluorescence microscopy (Fig. 5A). As expected, the Gzms stained the cytosol and nucleus, but concentrated in the nucleus. To test whether nuclear accumulation was mediated by DNA binding, we coincubated the Gzms with salmon sperm DNA before adding them to the fixed cells. Incubation with exogenous DNA abolished both cytosolic and nuclear staining of the Gzms (Fig. 5A). We treated fixed cells with DNase and RNase, which modestly reduced nuclear and cytosolic GzmB staining, respectively (Supplemental Fig. 2). DNase treatment did not remove all nuclear DNA, so it may be that GzmB binds to residual nucleic acids after nuclease treatment. Labeled NE also accumulated in the nuclei of fixed cells, in agreement with the known nuclear translocation of this enzyme during NETosis (12). Pancreatic

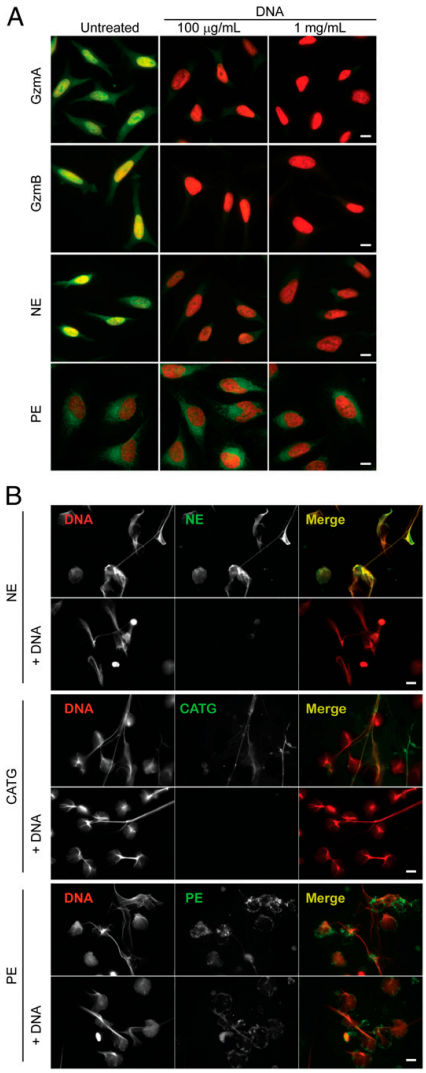

FIGURE 5. DNA binding regulates nuclear localization of leukocyte serine proteases and binding to NETs. The effect of DNA on localization of exogenously added serine proteases to permeabilized cells was assessed by fluorescence microscopy. (**A**) Permeabilized HeLa cells were incubated with AF488-labeled serine proteases (green) that had been preincubated with buffer or DNA and then stained with DAPI (red). GzmA, GzmB, and NE were visualized in the cytoplasm, but concentrated in the nucleus. Preincubation with salmon sperm DNA blocked cellular retention. Pancreatic elastase (PE) did not localize to the nucleus, and its staining pattern was not affected by preincubation with DNA. (**B**) AF488-labeled NE, CATG, and PE (green) were added with or without salmon sperm DNA to neutrophils during NET formation. Cells were fixed and stained for DAPI (red). NE and CATG localized to NETs, but pancreatic elastase did not. Salmon sperm DNA blocked binding of NE and CATG to NETs. Images are representative of three independent experiments. Scale bars, 10 μm.

elastase did not localize to fixed cell nuclei, and its staining intensity and pattern were not impacted by preincubation with salmon sperm DNA (Fig. 5A). Thus, DNA binding by the Gzms and NE likely mediates their nuclear trafficking during cytotoxic attack and NETosis, respectively.

Localization of NE and CATG to NETs is mediated by DNA binding

CATG and NE both concentrate on NETs (13). We asked whether DNA binding facilitates localization of these enzymes to NETs. Neutrophils isolated from human peripheral blood were treated with PMA for 3 h to induce NET formation in the presence of AF488-labeled NE, CATG, or pancreatic elastase. Competitor DNA was added to some samples during NET formation. Both neutrophil enzymes, but not pancreatic elastase, spontaneously concentrated on the NETs, and binding to the NETs was inhibited by adding salmon sperm DNA (Fig. 5B). Exogenous DNA added during NETosis also reduced the association of endogenous NE to NETs (Supplemental Fig. 3). Thus, CATG and NE specifically localize to NETs by binding to DNA.

Discussion

This work demonstrates that the Gzms and related leukocyte proteases are bona fide nucleic acid binding proteins with nanomolar affinities. The basis for substrate specificity of the Gzms, which are highly specific proteases, remains largely unknown. Although each Gzm has a strong preference for specific P1 residues in its substrates, primary amino acid sequence around the cleavage site does not predict Gzm cleavage. Structural features likely play a key role in Gzm substrate recognition. This study suggests that the high affinity of the Gzms for nucleic acids may be an important determinant of substrate specificity. Nucleic acid binding is a simple and elegant mechanism to direct leukocyte serine proteases to DNA and RNA binding protein targets and probably explains why nucleic acid binding proteins are highly overrepresented among Gzm substrates. Gzms and their substrates may be brought together by binding to nearby sites on the same nucleic acid strand. The Gzms form a monophyletic group with other leukocyte serine proteases, which also bind to nucleic acids with high affinity. Importantly, nucleic acid binding regulates the subcellular localization of Gzms and neutrophil proteases. Leukocyte protease concentration in cell nuclei was prevented by exogenous DNA. Our results support the affinity model for Gzm nuclear concentration posited over a decade ago and identify DNA as the unknown insoluble factor mediating this phenomenon (3). Similarly, the localization of NE and CATG to NETs and the antimicrobial activity of NETs likely depend in part upon the affinity of these proteases for DNA.

The leukocyte serine proteases rank among the most cationic proteins in the cell, with very high predicted isoelectric points (pIs): GzmA, 9.22; GzmB, 9.69; CATG, 11.37; and NE, 9.89 (20). The empirical pIs of NE and CATG are ∼11 and >11, respectively (30). This raises the question of whether nucleic acid binding is specific or simply a consequence of charge-balancing electrostatic interactions. For several reasons, we believe binding is specific and physiologically relevant. First, the digestive serine proteases, which do not bind nucleic acids, are also cationic with similar pIs as the Gzms. Porcine pancreatic elastase has a reported pI of 9.5 to >11, whereas the pI of trypsinogen is ∼9.3, but neither binds nucleic acids (31–33). Secondly, Gzm binding to DNA is sequence specific, favoring pyrimidine oligomers. Third, these proteases directly bind DNA under physiologic conditions. Finally, charge alone does not preclude specificity; RNA and DNA binding proteins are characterized by cationic patches that mediate binding to nucleic acids by electrostatic interactions (34). The Gzm structures predict positively charged surfaces that could be nucleic acid binding sites (35, 36). Further biochemical and structural studies

that look at the interactions of these leukocyte proteases with nucleic acids and specific protein substrates are needed.

Negatively charged sugars play a significant role in granule packaging and target cell uptake of cationic Gzms. In cytotoxic granules, the Gzms bind serglycin, a small negatively charged proteoglycan containing chondroitin 4-sulfate (37). Serglycin-null T cells are defective in packaging GzmB into granules. Upon degranulation, GzmB is released from serglycin and binds to cell membrane proteoglycans, most notably heparan sulfate. Purified GzmB has higher affinity for heparan sulfate than serglycin (38). Our results suggest that when Gzms enter target cells they bind to another class of negatively charged molecules, nucleic acids. Gzm binding to different anionic biomolecules as they move from the granules to the target cell nucleus may form a physical chain of custody to ensure proper Gzm trafficking and targeting.

Nucleic acid binding enhances the activity and function of leukocyte serine proteases, which may be critical to Gzm induction of cell death and neutrophil protease-mediated NET formation and function. Exogenous DNA transformed purified H1 from a very weak substrate to a robust target. However, excess DNA and RNA inhibited cleavage of H1 and hnRNP C1, respectively. A previous study also found that DNA inhibited NE and CATG proteolysis of the nonnucleic acid binding protein elastin (39). An excess of nucleic acid, which has high affinity for both the protease and its substrate, likely interferes with formation of the ternary protease–nucleic acid–substrate complex.

Preferential targeting of DNA and RNA binding proteins by Gzms is an underappreciated property critical for executing cell death. Nucleic acid binding is a simple mechanism to guide Gzms to targets that are essential for survival. Cleavage of nucleic acid binding substrates should enhance Gzm execution of death, independently of caspase activation. During Gzm-mediated cell death, targeting of RBPs disrupts pre-mRNA processing and nuclear export (4). In the extracellular environment, DNA binding may sequester leukocyte serine proteases to focus their activity on pathogens, which get caught in NETs, and minimize tissue injury.

Acknowledgments

We thank Farokh Dotiwala and Nishant Dwivedi for input and technical assistance and Brian Beliveau and Nancy Kedersha for advice and reagents.

Disclosures

The authors have no financial conflicts of interest.

References

1. Chowdhury, D., and J. Lieberman. 2008. Death by a thousand cuts: granzyme pathways of programmed cell death. *Annu. Rev. Immunol.* 26: 389–420.
2. Jans, D. A., P. Jans, L. J. Briggs, V. Sutton, and J. A. Trapani. 1996. Nuclear transport of granzyme B (fragmentin-2). Dependence of perforin in vivo and cytosolic factors in vitro. *J. Biol. Chem.* 271: 30781–30789.
3. Jans, D. A., L. J. Briggs, P. Jans, C. J. Froelich, G. Parasivam, S. Kumar, V. R. Sutton, and J. A. Trapani. 1998. Nuclear targeting of the serine protease granzyme A (fragmentin-1). *J. Cell Sci.* 111: 2645–2654.
4. Rajani, D. K., M. Walch, D. Martinvalet, M. P. Thomas, and J. Lieberman. 2012. Alterations in RNA processing during immune-mediated programmed cell death. *Proc. Natl. Acad. Sci. USA* 109: 8688–8693.
5. Zhang, D., M. S. Pasternack, P. J. Beresford, L. Wagner, A. H. Greenberg, and J. Lieberman. 2001. Induction of rapid histone degradation by the cytotoxic T lymphocyte protease Granzyme A. *J. Biol. Chem.* 276: 3683–3690.
6. Zhu, P., D. Martinvalet, D. Chowdhury, D. Zhang, A. Schlesinger, and J. Lieberman. 2009. The cytotoxic T lymphocyte protease granzyme A cleaves and inactivates poly(adenosine 5′-diphosphate-ribose) polymerase-1. *Blood* 114: 1205–1216.
7. van Domselaar, R., R. Quadir, A. M. van der Made, R. Broekhuizen, and N. Bovenschen. 2012. All human granzymes target hnRNP K that is essential for tumor cell viability. *J. Biol. Chem.* 287: 22854–22864.
8. Knickelbein, J. E., K. M. Khanna, M. B. Yee, C. J. Baty, P. R. Kinchington, and R. L. Hendricks. 2008. Noncytotoxic lytic granule-mediated CD8+ T cell inhibition of HSV-1 reactivation from neuronal latency. *Science* 322: 268–271.
9. Marcet-Palacios, M., B. L. Duggan, I. Shostak, M. Barry, T. Geskes, J. A. Wilkins, A. Yanagiya, N. Sonenberg, and R. C. Bleackley. 2011. Granzyme B inhibits vaccinia virus production through proteolytic cleavage of eukaryotic initiation factor 4 gamma 3. *PLoS Pathog.* 7: e1002447.
10. Krem, M. M., T. Rose, and E. Di Cera. 2000. Sequence determinants of function and evolution in serine proteases. *Trends Cardiovasc. Med.* 10: 171–176.
11. Brinkmann, V., and A. Zychlinsky. 2012. Neutrophil extracellular traps: is immunity the second function of chromatin? *J. Cell Biol.* 198: 773–783.
12. Papayannopoulos, V., K. D. Metzler, A. Hakkim, and A. Zychlinsky. 2010. Neutrophil elastase and myeloperoxidase regulate the formation of neutrophil extracellular traps. *J. Cell Biol.* 191: 677–691.
13. Urban, C. F., D. Ermert, M. Schmid, U. Abu-Abed, C. Goosmann, W. Nacken, V. Brinkmann, P. R. Jungblut, and A. Zychlinsky. 2009. Neutrophil extracellular traps contain calprotectin, a cytosolic protein complex involved in host defense against *Candida albicans*. *PLoS Pathog.* 5: e1000639.
14. Thiery, J., M. Walch, D. K. Jensen, D. Martinvalet, and J. Lieberman. 2010. Isolation of cytotoxic T cell and NK granules and purification of their effector proteins. In *Current Protocols in Cell Biology.* John Wiley & Sons, New York, p. 1-29.
15. Brinkmann, V., B. Laube, U. Abu Abed, C. Goosmann, and A. Zychlinsky. 2010. Neutrophil extracellular traps: how to generate and visualize them. *J. Vis. Exp.* 36: 1724.
16. Van Damme, P., S. Maurer-Stroh, H. Hao, N. Colaert, E. Timmerman, F. Eisenhaber, J. Vandekerckhove, and K. Gevaert. 2010. The substrate specificity profile of human granzyme A. *Biol. Chem.* 391: 983–997.
17. Van Damme, P., S. Maurer-Stroh, K. Plasman, J. Van Durme, N. Colaert, E. Timmerman, P.-J. De Bock, M. Goethals, F. Rousseau, J. Schymkowitz, et al. 2009. Analysis of protein processing by N-terminal proteomics reveals novel species-specific substrate determinants of granzyme B orthologs. *Mol. Cell. Proteomics* 8: 258–272.
18. Berriz, G. F., J. E. Beaver, C. Cenik, M. Tasan, and F. P. Roth. 2009. Next generation software for functional trend analysis. *Bioinformatics* 25: 3043–3044.
19. Carbon, S., A. Ireland, C. J. Mungall, S. Shu, B. Marshall, and S. Lewis; AmiGO Hub; Web Presence Working Group. 2009. AmiGO: online access to ontology and annotation data. *Bioinformatics* 25: 288–289.
20. UniProt Consortium. 2012. Reorganizing the protein space at the Universal Protein Resource (UniProt). *Nucleic Acids Res.* 40(Database issue): D71–D75.
21. Goujon, M., H. McWilliam, W. Li, F. Valentin, S. Squizzato, J. Paern, and R. Lopez. 2010. A new bioinformatics analysis tools framework at EMBL-EBI. *Nucleic Acids Res.* 38(Web Server issue): W695–W699.
22. Zhang, H., S. Gao, M. J. Lercher, S. Hu, and W.-H. Chen. 2012. EvolView, an online tool for visualizing, annotating and managing phylogenetic trees. *Nucleic Acids Res.* 40(Web Server issue): W569–W572.
23. Ryder, S. P., and J. R. Williamson. 2004. Specificity of the STAR/GSG domain protein Qk1: implications for the regulation of myelination. *RNA* 10: 1449–1458.
24. Jantz, D., and J. M. Berg. 2010. Probing the DNA-binding affinity and specificity of designed zinc finger proteins. *Biophys. J.* 98: 852–860.
25. Fialcowitz-White, E. J., B. Y. Brewer, J. D. Ballin, C. D. Willis, E. A. Toth, and G. M. Wilson. 2007. Specific protein domains mediate cooperative assembly of HuR oligomers on AU-rich mRNA-destabilizing sequences. *J. Biol. Chem.* 282: 20948–20959.
26. Park, S., D. G. Myszka, M. Yu, S. J. Littler, and I. A. Laird-Offringa. 2000. HuD RNA recognition motifs play distinct roles in the formation of a stable complex with AU-rich RNA. *Mol. Cell. Biol.* 20: 4765–4772.
27. Nightingale, K. P., D. Pruss, and A. P. Wolffe. 1996. A single high affinity binding site for histone H1 in a nucleosome containing the *Xenopus* borealis 5 S ribosomal RNA gene. *J. Biol. Chem.* 271: 7090–7094.
28. Perera, N. C., O. Schilling, H. Kittel, W. Back, E. Kremmer, and D. E. Jenne. 2012. NSP4, an elastase-related protease in human neutrophils with arginine specificity. *Proc. Natl. Acad. Sci. USA* 109: 6229–6234.
29. Belorgey, D., and J. G. Bieth. 1995. DNA binds neutrophil elastase and mucus proteinase inhibitor and impairs their functional activity. *FEBS Lett.* 361: 265–268.
30. Travis, J., P. J. Giles, L. Porcelli, C. F. Reilly, R. Baugh, and J. Powers. 1979. Human leucocyte elastase and cathepsin G: structural and functional characteristics. *Ciba Found. Symp.* 75: 51–68.
31. Brink, N. G., U. J. Lewis, and D. E. Williams. 1956. Pancreatic elastase: purification, properties, and function. *J. Biol. Chem.* 222: 705–720.
32. Ardelt, W. 1975. Physical parameters and chemical composition of porcine pancreatic elastase II. *Biochim. Biophys. Acta* 393: 267–273.
33. Higaki, J. N., and A. Light. 1985. The identification of neotrypsinogens in samples of bovine trypsinogen. *Anal. Biochem.* 148: 111–120.
34. Shazman, S., and Y. Mandel-Gutfreund. 2008. Classifying RNA-binding proteins based on electrostatic properties. *PLOS Comput. Biol.* 4: e1000146.
35. Estébanez-Perpiña, E., P. Fuentes-Prior, D. Belorgey, M. Braun, R. Kiefersauer, K. Maskos, R. Huber, H. Rubin, and W. Bode. 2000. Crystal structure of the caspase activator human granzyme B, a proteinase highly specific for an Asp-P1 residue. *Biol. Chem.* 381: 1203–1214.
36. Hink-Schauer, C., E. Estébanez-Perpiñá, F. C. Kurschus, W. Bode, and D. E. Jenne. 2003. Crystal structure of the apoptosis-inducing human granzyme A dimer. *Nat. Struct. Biol.* 10: 535–540.
37. Kolset, S. O., and H. Tveit. 2008. Serglycin—structure and biology. *Cell. Mol. Life Sci.* 65: 1073–1085.
38. Raja, S. M., S. S. Metkar, S. Höning, B. Wang, W. A. Russin, N. H. Pipalia, C. Menaa, M. Belting, X. Cao, R. Dressel, and C. J. Froelich. 2005. A novel mechanism for protein delivery: granzyme B undergoes electrostatic exchange from serglycin to target cells. *J. Biol. Chem.* 280: 20752–20761.
39. Duranton, J., D. Belorgey, J. Carrère, L. Donato, T. Moritz, and J. G. Bieth. 2000. Effect of DNase on the activity of neutrophil elastase, cathepsin G and proteinase 3 in the presence of DNA. *FEBS Lett.* 473: 154–156.

GO term	P-value (-log(10)) GzmB	GzmA	Sum of –log(10)P-values
mRNA metabolic process	50.1	67.6	117.7
nucleic acid metabolic process	58.8	54.9	113.7
gene expression	46.1	64.5	110.7
RNA metabolic process	49.6	57.4	107.0
nuclear part	61.9	44.5	106.4
nucleobase, nucleoside, nucleotide and nucleic acid metabolic process	54.6	46.9	101.5
RNA binding	36.9	61.4	98.3
intracellular organelle part	48.6	47.0	95.7
organelle part	49.2	46.1	95.3
ribonucleoprotein complex	39.0	51.9	90.9
cellular nitrogen compound metabolic process	47.7	41.4	89.1
nitrogen compound metabolic process	45.9	40.8	86.7
intracellular part	48.1	37.6	85.8
cellular macromolecule metabolic process	50.2	35.5	85.7
nucleus	45.5	34.4	79.8
intracellular organelle	40.8	38.5	79.3
organelle	40.6	38.4	79.0
viral transcription	21.8	53.6	75.4
macromolecular complex	43.8	30.7	74.4
translational elongation	24.7	49.7	74.4
viral infectious cycle	21.0	52.0	73.0
non-membrane-bounded organelle	24.9	48.1	73.0
intracellular non-membrane-bounded organelle	24.9	48.1	73.0
translational termination	20.8	51.4	72.2
cellular component disassembly at cellular level	23.0	48.7	71.7
cellular component disassembly	23.0	48.6	71.5
cellular macromolecular complex disassembly	21.2	48.2	69.4
macromolecular complex disassembly	21.1	48.1	69.2
cellular protein complex disassembly	19.7	49.2	68.9
protein complex disassembly	19.6	49.1	68.7
macromolecule metabolic process	40.1	27.5	67.6
RNA processing	30.3	35.5	65.8
cellular macromolecular complex subunit organization	20.3	44.6	64.9
endocrine pancreas development	18.1	46.0	64.2
protein binding	44.2	18.1	62.2
viral reproductive process	16.4	44.4	60.9
cellular macromolecule biosynthetic process	27.2	31.8	59.0
nucleic acid binding	24.4	34.0	58.4
intracellular membrane-bounded organelle	35.3	22.6	57.9
cellular metabolic process	35.8	22.1	57.9
membrane-bounded organelle	35.3	22.5	57.8
RNA biosynthetic process	20.8	37.0	57.8
macromolecule biosynthetic process	26.6	31.1	57.7
nucleoplasm	35.1	22.4	57.5
cellular component organization or biogenesis at cellular level	26.7	30.5	57.2
macromolecular complex subunit organization	18.7	36.5	55.2
cellular component organization at cellular level	26.4	27.6	54.0
cellular component organization or biogenesis	25.4	28.6	53.9
cytosol	28.6	23.4	52.0
cytoplasm	39.4	12.6	52.0
viral reproduction	14.8	36.5	51.3
primary metabolic process	31.8	19.4	51.2
mRNA processing	25.0	26.0	51.1
cellular component organization	25.0	25.8	50.9

Supplemental Table I: GO analysis of GzmA and GzmB targets from proteomics studies. GO terms with a summed $-\log_{10}(P)$ of 50 or greater are presented. Many of the top terms relate to nucleic acid binding and metabolic functions.

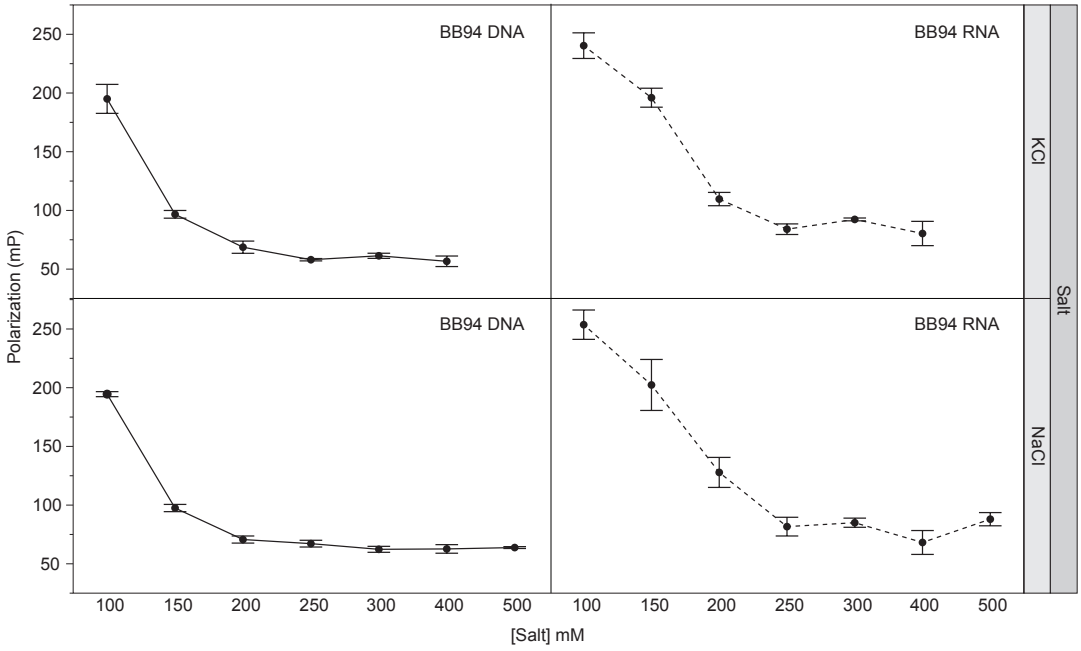

Supplemental Figure 1: Dependence on salt concentration of GzmB binding to nucleic acids.
Binding of GzmB to BB94 RNA and BB94 ssDNA was assayed by FP in the presence of varying concentrations of KCl and NaCl. Error bars represent the SEM of at least 6 independent wells from 2 experiments.

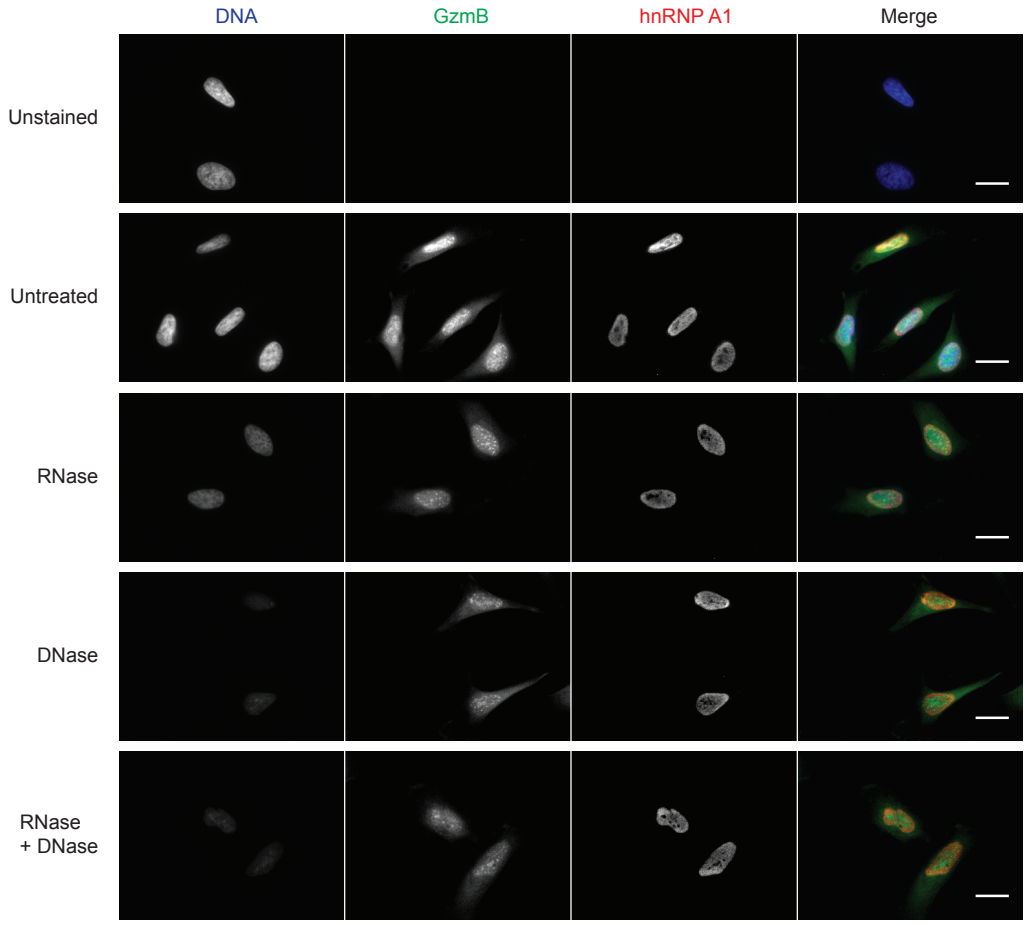

Supplemental Figure 2: DNase and RNase treatment of permeabilized HeLa cells alters GzmB subcellular localization. Permeabilized HeLa cells were pretreated with RNase, DNase, or both, then incubated with AF488-labeled GzmB (green) and stained for hnRNP A1 (red) to visualize cell nuclei and DAPI (blue) to visualize nuclear DNA. RNase and DNase modestly reduced cytosolic and nuclear GzmB staining, respectively. Treatment with both RNase and DNase reduced GzmB staining in both compartments. Nuclear localization of hnRNP A1 was independent of the presence of RNA or DNA. Images are representative of 3 independent experiments. Scale bar represents 10 μm.

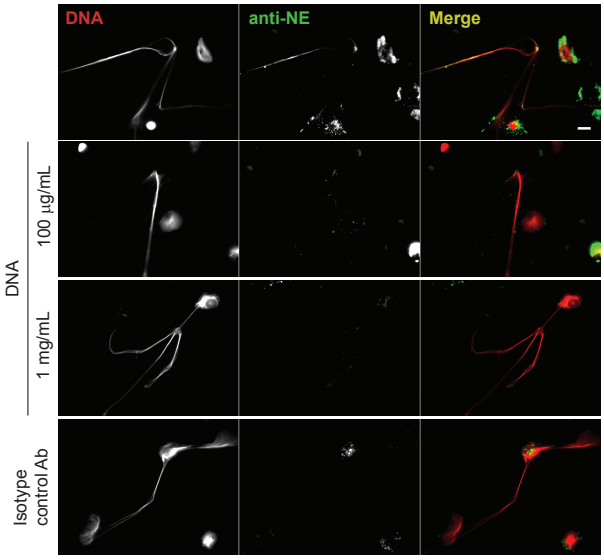

Supplemental Figure 3: Excess DNA blocks binding of endogenous neutrophil elastase to NETs.
Cells were stained with a neutrophil elastase antibody (green) and DAPI (red). Images are representative of three independent experiments. Scale bar represents 10 µm.

Immunological Reviews

Marshall P. Thomas
Judy Lieberman

Live or let die: posttranscriptional gene regulation in cell stress and cell death

Authors' address
Marshall P. Thomas[1], Judy Lieberman[1]
[1]Program in Cellular and Molecular Medicine, Boston Children's Hospital and Department of Pediatrics, Harvard Medical School, Boston, MA, USA.

Correspondence to:
Judy Lieberman
200 Longwood Avenue, WAB 255
Boston, MA 02115, USA
Tel.: +1 617 713 8600
Fax: +1 617 713 8620
e-mail: judy.lieberman@childrens.harvard.edu

Acknowledgements
The authors have no conflicts of interest to declare.

This article is part of a series of reviews covering RNA Regulation of the Immune System appearing in Volume 253 of *Immunological Reviews*.

Immunological Reviews 2013
Vol. 253: 237–252

Immunological Reviews
0105-2896

Summary: Studies of the regulation of gene expression historically focused on transcription. However, during stress and apoptosis, profound gene expression changes occur more rapidly and globally than is possible by regulating transcription. Posttranscriptional changes in mRNA processing and translation in response to diverse stresses shut down most protein translation to conserve energy and lead to rapid remodeling of the proteome to promote repair. Pre-mRNA splicing and mRNA stability are fundamentally altered under some stress conditions. Stress pathways coordinate a cytoprotective repair response, while simultaneously initiating signaling that can ultimately trigger cell death. How the cell mediates the decision between repair and apoptosis is largely not understood. In some stresses, microRNAs may tip the balance. Here, we review what is known about posttranscriptional gene regulation during stress, focusing on what is still unknown and how new technologies might be used to understand what changes are most physiologically important in different forms of stress and death.

Keywords: *stress, apoptosis, pre-mRNA splicing, translation, miRNA*

Introduction

The cell responds to stress rapidly by remodeling protein expression within minutes. Transcriptional changes are too slow to accomplish this task. Most mRNAs have half-lives on the scale of hours [on average 6.9 h in human cells, more than 50-fold longer than in *E. coli* (1, 2)]. Hence, posttranscriptional events play a pivotal role in regulating the initial rapid response to cell stress. A swift, almost global, shutoff of translation occurs in response to diverse cellular insults. This 'integrated stress response' is generally an adaptive program that helps a cell endure stress and renormalize when the stress abates. Concurrent with this rapid response, stresses trigger many slower-acting alterations in gene expression, including changes in transcription, many of which provide protection against potential future insults. However, persistent stresses favor changes in expression that will ultimately tip a cell toward apoptosis. The expression of proapoptotic effectors can be regulated at multiple checkpoints, with each checkpoint requiring continued stress.

One example of this is upregulation of the proapoptotic CHOP transcription factor during endoplasmic reticulum (ER) stress, as discussed later. How cells respond to stress ultimately depends on the type, severity, and duration of the stress. Although most research on the stress response has focused on inhibition of translation, strong and in some cases very rapid alterations in pre-mRNA splicing and mRNA stability occur in response to some stresses. These events need to be better characterized. Changes in posttranscriptional regulation occur both before and after cells that fail to repair become committed to apoptosis. The best-studied apoptotic change in gene expression is a global translational arrest, but the mechanistic underpinnings of this phenomenon remain poorly understood. Even less is known about changes in mRNA stability and splicing in apoptosis, although recent work from our laboratory suggests that dramatic changes in pre-mRNA splicing occur during programmed cell death that promote the cell's demise.

The basics of cell stress and apoptosis

Eukaryotes have evolved a comprehensive portfolio of mechanisms to cope with cell stress. In this review, we focus on the response to a few stresses in which posttranscriptional regulation has been best studied. The heat shock (HS) response is one of the best characterized. The master regulator of many aspects of the HS response is the transcription factor HSF1, which does not respond to HS *per se* but senses misfolded proteins in the cytoplasm that accumulate during HS and other stresses (3). When activated, HSF1 translocates to the nucleus and transactivates a repair program, most notably inducing the heat shock proteins (HSPs), molecular chaperones that promote proper protein folding. Genotoxic stress (4, 5), which is important in the etiology and treatment of cancer, activates expression of the tumor suppressor TP53, a key transcription factor that induces the expression of genes to promote cell cycle arrest and apoptosis. Unlike other stresses, genotoxic stress does not necessarily directly induce translational arrest, but can trigger profound TP53-dependent and -independent alterations in splicing. TP53 also enhances the transcription of microRNA primary transcripts that play a potentially important role in the genotoxic stress response. ER stress rapidly triggers a translation block through the unfolded protein response (UPR). Excessive protein load in the ER, malfunctioning ER protein-folding chaperones, or genetic protein-folding disorders can all induce the UPR. Three major ER sensors of unfolded proteins are ATF6, PERK, and IRE1 (6). The transcription factor ATF6 migrates from the ER to the Golgi during stress, where it is released by proteolytic cleavage and then traffics to the nucleus to transactivate genes that remediate ER stress. PERK and IRE1 are both kinases, which become activated by homo-oligomerization and autophosphorylation in response to ER stress to mediate profound alterations in translation and mRNA stability. Collectively, these proteins both reduce the protein load in the ER by reducing protein synthesis and activate a slower adaptive response that requires *de novo* transcription and translation to improve ER protein folding (7, 8). If ER stress is irremediable, a back-up program prepares the cell for apoptosis.

Apoptosis is a tightly controlled cell death program used to eliminate unwanted cells during development, infection, or malignant transformation and to eliminate cells experiencing irreparable stress-related damage. Apoptotic cells are rapidly recognized and cleared by macrophages and other scavenger cells without causing inflammation or harm to bystander cells. The best-studied cell death program (classical apoptosis) is mediated by the caspases, but alternate caspase-independent programs of cell death are also triggered by immune killer cells. In all these pathways, dying cells undergo membrane blebbing, mitochondrial damage, DNA degradation, chromatin condensation, and nuclear fragmentation. Executing programmed cell death requires that the cell membrane remain intact maintaining enough ATP to execute the program; apoptosis takes several hours to complete. The major effectors of classical apoptosis are the BCL-2 family proteins and the caspases, which form intertwined cell death pathways (9). The mitochondria are the site of action of the BCL-2 family and a key control point in cell death. The BCL-2 family is divided into three classes: multidomain anti-apoptotic proteins (BCL-2, BCL-X_L, MCL-1), the proapoptotic BH3-only proteins (such as BID and BAD), and the proapoptotic multidomain proteins (BAX and BAK) (10, 11). BAX and BAK form pores in the mitochondrial outer membrane to cause mitochondrial outer membrane permeabilization (MOMP) and the release of apoptogenic factors, including cytochrome c and SMAC/DIABLO, from the intermembrane space to the cytosol. The BH3-only proteins promote BAX and BAK multimerization, while the anti-apoptotic members inhibit it (11). The caspases are cysteine proteases that orchestrate cell death by cleaving a large number of substrates. The initiator caspases are activated by dimerization and autoproteolysis in response to death receptor ligation (caspases 8 and 10), MOMP (caspase 9), or stress signaling (caspase 2). Mitochondrial release of cytochrome c triggers formation of the apoptosome – a scaffold that binds and activates caspase 9. Once activated, caspase 9

and the other initiator caspases cleave and activate the downstream effector caspase zymogens (caspase 3, 6, and 7), which then cleave hundreds of cellular substrates in an accelerating cascade to complete the cell death program (9, 12). In the extrinsic pathway of cell death, death receptor signaling induces activation of caspase 8 or 10. In addition to activating the effector caspases by direct cleavage, the initiator caspases cleave the BH3-only protein BID to truncated BID (tBID), which activates BAX and BAK. Cell stresses can lead to apoptosis, generally through the intrinsic pathway of apoptosis by enhancing the activity or expression of BH3-only proteins (10). For example, in genotoxic stress, TP53 transactivates the BH3-only proteins NOXA and PUMA (4, 10). Some stresses activate caspase 2 by an unknown mechanism to cleave BID and initiate the mitochondrial pathway (13).

The granzymes (Gzms) are killer lymphocyte serine proteases, stored with other cytotoxic molecules (notably perforin, the pore-forming protein that delivers Gzms into cells targeted for immune elimination) in cytotoxic granules (14). The Gzms (5 distinct enzymes in humans, 10 in mice) activate diverse and redundant pathways of programmed cell death by cleaving many cellular proteins, to guarantee that it will be difficult for infected or transformed cells to evade immune attack. GzmB acts like an initiator caspase by directly cleaving BID and caspase 3. GzmA initiates a distinct pathway of caspase-independent apoptosis with mostly non-overlapping substrates that damages mitochondria without causing MOMP and causes single-stranded, rather than double-stranded, DNA damage (15, 16). The death mechanisms activated by the other Gzms are distinct from these two but not well characterized. The Gzms translocate into the target cell nucleus by an unknown mechanism (17, 18), where they have recently been shown to disrupt pre-mRNA splicing and nuclear export profoundly.

A very robust bistable switch controls the balance between life and apoptosis. A recent single-cell study of apoptotic cells indicates that initiator caspase activity can build slowly before triggering suicide through irreversible MOMP and effector caspase activation (19). Stress pathways simultaneously promote repair and activate molecules that can eventually trigger an irreversible commitment to apoptosis. The distinction between the preapoptotic and commitment phases is not trivial, and conflating the two can be misleading. For example, although it is clear that translation is strongly inhibited after the commitment to apoptosis, preapoptotic signaling events can inhibit translation even without cell death (20). In this review, we seek to draw a clear distinction between events that occur in response to preapoptotic stresses and those restricted to the commitment phase of cell death.

Effects of stress and death on splicing

Pre-mRNA splicing (hereafter referred to simply as splicing) occurs cotranscriptionally to excise introns and join exon ends to generate a mature mRNA (*Fig.* 1). Splicing is controlled by hundreds of constitutive and regulated splicing

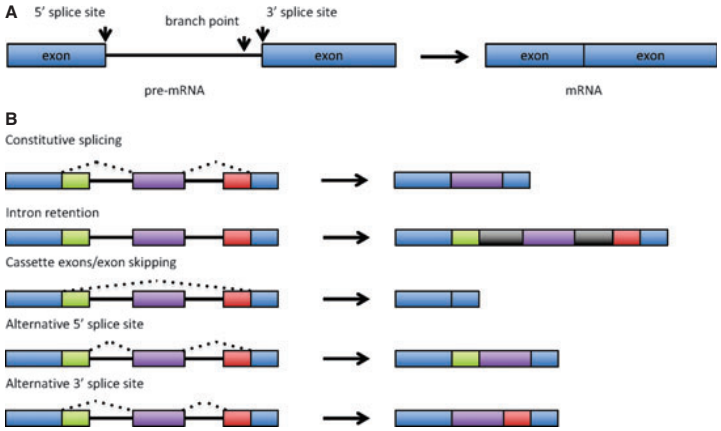

Fig. 1. pre-mRNA splicing and alternative splicing. (A) The *cis*-regulatory elements recognized by the spliceosome are the 5′ and 3′ splice sites and the branch point. Other elements in the mRNA are recognized by splicing regulators to ensure the fidelity of splicing. (B) Four major types of alternative splicing. First and last exons can also vary. Alternative transcription start sites and cleavage and polyadenylation sites also contribute to isoform diversity. Global splicing inhibition is manifested as intron retention, as occurs in apoptosis and HS. Other forms of alternative splicing are more common in genotoxic stress. Note that the 5′ and 3′ splice sites refer to the ends of the intron that is spliced out, not the retained exon.

factors (21). The basic splicing reaction is catalyzed by the spliceosome, a complex and well-studied RNA-protein machine (21, 22). The splicing reaction involves the recognition of three *cis*-regulatory elements on pre-mRNA – the 5′ splice site, the branch point, and the 3′ splice site (22) (*Fig. 1A*). Through an ordered assembly process, the spliceosome brings together the 5′ and 3′ splice sites and excises the intervening intron. However, the information contained in these three *cis*-regulatory elements is not sufficient to define exon boundaries; most transcripts contain many cryptic splice sites that are rarely or never used (23). The body of the transcript bears other *cis*-regulatory elements bound by splicing accessory factors that provide additional specificity to ensure the fidelity of splicing. In addition, chromatin signatures and nucleosome positioning affect exon recognition (24). The information conferred by these different factors is integrated by the spliceosome to generate mature mRNA. Two classes of abundant splicing regulators are the hnRNPs (heterogeneous nuclear ribonucleoproteins) and SR proteins, which are historically viewed as splicing repressors and enhancers, respectively (25, 26). In agreement with this view, *in vitro* assays on model templates have demonstrated that hnRNP A1 antagonizes exon inclusion promoted by the SR protein SRSF1 (SF2/ASF) (27, 28). These results are supported by recent genome-wide surveys showing that hnRNP C1/C2 binding is depleted around splice sites (29). However, other studies suggest that hnRNPs can either repress or activate splicing in a sequence-dependent manner (30, 31).

The complexity of the splicing code allows for variations in splicing, such that the same genomic locus can generate many different transcripts. Alternative splicing generates considerable transcriptome diversity. In fact, >95% of multiexon genes generate more than one splice isoform (25). Alternative splicing variants include exon skipping, intron retention, and the use of alternative 5′ and 3′ splice sites (*Fig. 1B*). Transcriptome-wide sequencing and microarray studies have focused on the large variation in alternative splicing found across tissues, and the corresponding variations in expression of splicing regulators, such as the hnRNP and SR proteins (25, 32, 33). In contrast with tissue-specific splicing, stress causes transient splicing alterations through rapid, often reversible, changes in *trans*-acting factors. Therefore, cell stress presents an opportunity to understand what factors regulate alternative and constitutive splicing in a physiological setting.

The best-characterized stress-induced alterations in splicing occur in heat shock. In HS, but not other stresses, there is potent, yet transient, global inhibition of splicing (26), leading to intron retention (*Fig. 1B*). Splicing of model templates treated with a nuclear extract from heat-shocked cells is completely inhibited (34). The SR protein SRSF10 (SRp38) is the master splicing inhibitor in HS (35). SRSF10 is normally abundantly phosphorylated, but, when hypophosphorylated during HS, strongly inhibits splicing *in vitro* (35). The HS-mediated block of splicing is independent of the HS master transcriptional regulator HSF1 (36). The SRSF10-mediated block on splicing is transient because SRSF10 is completely rephosphorylated within 1 h of recovery from HS (35). Although splicing inhibition by HS is well characterized in nuclear extracts, much less is known about what happens inside intact cells. As transcription is also strongly inhibited during HS (37), the relative importance of blocking transcription versus splicing is unknown. Furthermore, as most splicing occurs cotranscriptionally (38), *in vitro* studies using pretranscribed model splicing templates could lead to erroneous conclusions (35). One recent study utilized splicing-sensitive microarrays to analyze the transcriptome of HS-treated cells, and found an increase in the usage of downstream 'latent' 5′ splice sites (39) (*Fig. 1B*). However, this analysis filtered out cases of intron retention, which should be ubiquitous in HS. Many HS-induced isoforms contain premature termination codons, which mark transcripts for nonsense-mediated decay in the cytoplasm (40).

Not much is known about alterations in splicing during cell death. Our laboratory recently found that pre-mRNA nuclear export and splicing are profoundly disrupted in cell death mediated by GzmA and GzmB and likely during caspase-mediated apoptosis more generally. Because the Gzm serine proteases accumulate in the nucleus of target cells, we wished to identify their nuclear substrates. The proteomes of intact nuclei that were treated or not with GzmA were analyzed for proteins degraded by GzmA. Of 44 nuclear substrates, 33 were RNA-binding proteins, including 14 hnRNPs (41). Many hnRNPs were also degraded following caspase activation. As hnRNPs assemble on newly synthesized transcripts to orchestrate posttranscriptional processing, this prompted us to look at the fate of newly synthesized RNA in cells undergoing Gzm-mediated apoptosis. Newly synthesized RNA globally was retained in the nucleus and pre-mRNA splicing was severely compromised as assessed by measuring intron retention. Notably, GzmA cleaved hnRNP A1, causing it to mislocalize to the cytoplasm. A non-cleavable mutant of hnRNP A1 restored splicing and partially rescued cells from death, suggesting that the inhibition of pre-mRNA processing is an important component of the cell death program (*Fig. 2A*). Of note,

alterations in mRNA splicing and nuclear export were absent in cells undergoing oxidative stress, suggesting that global inhibition of splicing is not a general feature of non-apoptotic stress. The splicing defect was likely the reason for nuclear retention of newly synthesized mRNAs. Intronless transcripts of immediate early genes (such as Jun) transcriptionally activated in response to stress were rapidly exported and translated into protein, whereas stress-activated transcripts that contain introns (such as Fos) were not translated into new protein. On the basis of these findings, we hypothesize that disrupted splicing during apoptosis blunts an adaptive stress response and tips the cell toward death.

The great increase in intron retention observed during programmed cell death, which we interpreted as global inhibition of splicing, may seem surprising given that hnRNP proteins are generally considered splicing silencers (25, 27). However, a view of hnRNPs as only splicing silencers is an oversimplification. Most human introns are long, with a mean length of approximately 3.2 kb (42), and hnRNP A1 promotes the excision of long introns ($\geq$ 1 kb). When hnRNP A1-binding activity is inhibited *in vitro*, long introns are almost completely retained (31). In a recent genome-wide study of hnRNP function and targets, intron retention significantly increased when any of six hnRNPs were knocked down (30). Four of these hnRNPs are GzmA targets and several are validated caspase substrates as well (41). GzmA also potentially cleaves other splicing factors, which became undetectable after GzmA treatment. These included U5S1, a component of the spliceosome, and SRSF1, which aids the spliceosome in recognizing the 5′ splice site, and is required for the splicing of at least some transcripts *in vitro* (43). GzmA cleavage of some SR proteins could collaborate with hnRNP cleavage to enhance intron retention. Future studies should characterize what happens to the spliceosome and how splicing changes during different forms of stress and apoptosis. It is not clear whether the Gzms simply inhibit splicing (as evidenced by intron retention) or also activate alternative splicing (Fig. 1B).

Alternative splicing in stress and death

In contrast with the broad inhibition of splicing caused by HS and GzmA, other stresses appear to bring about more targeted alterations in splicing. Apoptotic genes in both the mitochondrial and caspase cell death pathways have pro- and anti-apoptotic splice isoforms, whose relative expression is modulated during stress. Genotoxic stress alters splicing by several distinct mechanisms. These include altering the rate of transcription, sequestration of splicing factors, and transactivation of certain splicing factors. Splice site selection is modulated by the transcription rate of RNA polymerase II (PolII), further supporting the idea that transcription and splicing are intimately coupled (44–46). The 'kinetic coupling' model posits that PolII pausing downstream of alternative exons with weak splice sites promotes their inclusion (47) (Fig. 2B). The putative mechanism is simple – when PolII is slowed, downstream constitutive splice sites are less available, providing more time for exons with weak splice sites to be included. Stresses that reduce the transcription rate of specific genes should disproportionately alter their splicing. Low-dose ultraviolet (UV) irradiation induces modest phosphorylation of PolII in the heptad repeats of its C-terminal domain (CTD), which reduces the rate of transcription and alters splicing of model transcripts and splicing reporter minigenes (48). Expression of PolII phosphomimetic mutants, which transcribe more slowly, recapitulates some of the UV-induced changes in splicing (48). A recent transcriptomic analysis supports the kinetic splicing model. In Jurkat cells treated with drugs to reduce the PolII elongation rate, downregulated transcripts have more alternative splicing, favoring inclusion of exons with weaker splice sites (49). However, PolII interacts during transcription with many pre-mRNA processing factors (50) in a manner that may also depend on CTD phosphorylation (45). Thus PolII phosphorylation may modulate splicing both by altering the rate of transcription and through changes in its interactions with splicing factors. However, altered cassette exon splicing in response to various genotoxic stresses is usually modest. The functional significance of altered splicing in response to altered PolII elongation rates remains unclear (47–49).

Stress also modulates the expression, localization, and activity of splicing factors. Osmotic shock and high doses of UV drive the phosphorylation and cytoplasmic relocalization of hnRNP A1 in a p38 MAPK-dependent manner (51). Other hnRNPs and SR proteins remain in the nucleus. Osmotic stress or constitutive p38 MAPK activation also alters splicing of a reporter minigene. However, it remains unclear whether altered splicing during these stresses is due to changes in hnRNP A1 localization.

Alternative splicing during cell stress can play a pivotal role in tuning the cellular response to stress. During genotoxic stress, TP53 is upregulated and transcriptionally activates many targets, including MDM2. MDM2 ubiquitinates TP53 and targets it for destruction, thus completing a negative feedback loop that limits TP53 activity. However, as long as the stress persists, despite the increase in MDM2 transcription, exon skipping during the processing of the

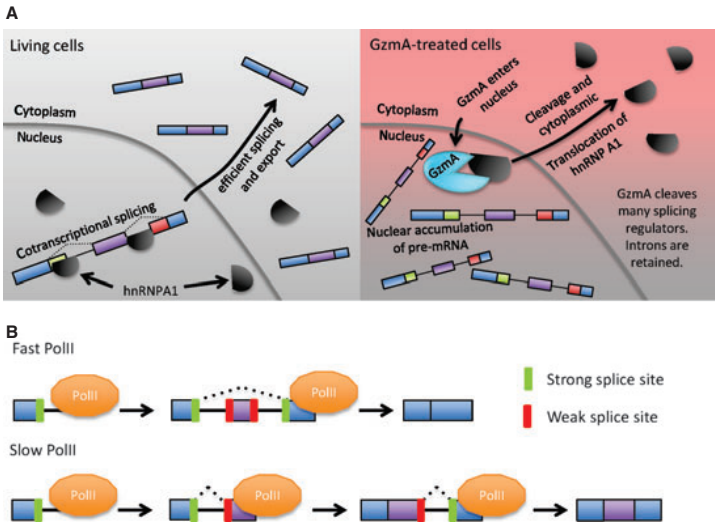

Fig. 2. Some mechanisms that regulate splicing in cell death and stress. (A) In living cells, the hnRNPs help to define intron boundaries. During killer cell attack, GzmA enters the nucleus, cleaving hnRNP A1, which relocalizes to the cytoplasm. A potent block on splicing leads to nuclear retention of nascent RNA and intron retention. Expression of a GzmA-uncleavable form of hnRNP A1 partially rescues both splicing and cell death. (B) The kinetic model of splicing posits that the rate of PolII transcription dictates exon choice. When PolII transcription is fast, strong splice sites are rapidly made available and those sites are preferred. Because splicing occurs cotranscriptionally, when transcription is slow, the spliceosome has time to utilize weak splice sites, permitting the inclusion of exons surrounded by weak sites. During some forms of stress PolII is phosphorylated in its C-terminal domain, which reduces the rate of transcription.

MDM2 pre-mRNA increases and consequently MDM2 mature mRNA and protein levels do not increase. At the same time, other mRNAs are normally processed (52). *MDM2* splicing is restored when the genotoxic stress is removed, producing MDM2 protein, which shuts down the stress response by degrading TP53. *MDM2* exon inclusion is promoted during transcription by an interaction between YB-1 and EWS proteins; this interaction declines during genotoxic damage. YB-1 and EWS also promote proper exon inclusion of other genes that undergo exon skipping in genotoxic stress (52). How stress signaling diminishes the EWS–YB-1 interaction remains unknown. As YB-1 promotes the recognition of weak 3′ splice signals and the inclusion of the associated exons (53), reduced YB-1 activity could explain how certain *MDM2* exons (those with weak splice signals) are skipped during genotoxic stress.

The transcriptional regulation of splicing factors can also affect cell fate in response to stress. E2F1, which is induced by genotoxic stress, transcriptionally activates SRSF2 (SC35), which promotes the expression of the proapoptotic splice variants of *CASP9*, *CASP8*, and *BCL2L1* (*BCL-xL/-xS*) (54). Knockdown of SRSF2 inhibits the upregulation of all proapoptotic splice variants and consequently inhibits apoptosis. The E2F-driven change in splice isoform ratios and the proapoptotic increase in the ratio of BCL-xS/BCL-xL appears to be much greater than that due to PolII phosphorylation (48) or TP53 signaling (55).

Unanswered questions concerning splicing in stress and cell death

There is no unified understanding of what happens to splicing during cellular stress. Although splicing is strongly inhibited by SRSF10 hypophosphorylation *in vitro*, some transcripts must still be correctly spliced to respond adequately to HS. While some heat shock proteins are encoded by intronless transcripts (*HSP70*), others are not (*HSP27*, *HSP90*). How are these still processed in the context of a potent block on splicing? Most studies in intact cells have assayed a mixture of stable prestress mRNAs and new mRNA produced after the stress (39, 49). This may miss many events because mature mRNAs are relatively stable and many stress-induced alterations to splicing are transient, such as the SRSF10-driven block to splicing in HS. Most studies of splicing and stress have relied on a handful of model transcripts or transfected splicing reporters to draw general conclusions about alternative splicing in stress and cell death

(41, 48, 52, 54, 55). However, splicing is sensitive to sequence context and is regulated by a complex milieu of *cis*- and *trans*-acting factors (23). New experimental techniques to metabolically label and capture nascent mRNAs (1, 56, 57), when combined with splicing-sensitive microarrays (30) or RNA-seq (32), can now be leveraged to assess the transcriptome-wide impact of HS on splicing and capture transient changes in pre-mRNA processing. These methodologies should be very powerful tools for understanding the global change in splicing that occurs in response to various stresses and apoptosis.

The alterations in alternative splicing observed during stress and cell death provide opportunities to improve our understanding of how splicing is regulated and to understand how changes in splicing contribute to a cell's survival or death. The same stress can manipulate splicing by multiple mechanisms. For example, genotoxic stresses alter the phosphorylation and localization of hnRNP A1 (51), slow PolII elongation (48), disrupt the interaction of YB-1 and EWS with the spliceosome (52), and transcriptionally upregulate splicing factors (54). The best studies have systematically addressed each of these possible mechanisms to assess their relative contributions to observed splicing defects (48, 52). As evidenced by vast differences in splicing driven by HS and genotoxic stress, the type, duration, and severity of the stress will determine the nature and extent of the splicing changes. Crucially, in almost every case, it remains unclear whether altered splicing in stress has functional consequences. Many apoptosis-associated genes undergo altered splicing in response to stress, generating transcript isoforms that produce proteins with significant functional differences (58). However, most stresses induce only modest changes in the ratio of the different splice isoforms (48, 55, 59). In limited cases, manipulating the *trans*-acting factors that control altered splicing after stress substantially alters cell survival (54). Very few studies have shown that a single alternative splicing event in the cell stress response is significant. Antisense oligonucleotides can be used to interfere with individual splice sites to modulate the expression of specific splice isoforms (60). This tool might be useful to manipulate specific splice isoforms during cell stress to assess their importance. Finally, altered splicing in stress cannot be viewed in a vacuum – virtually all stresses induce profound alterations to translation, and some factors (such as hnRNP A1 and SRSF1) regulate both splicing and translation initiation.

Regulation of translation in cell stress

Translational control has been extensively studied in stress and apoptosis (61, 62). Here, we focus on the interplay between stress and cell death, in particular how altered translation during stress protects cells from or predisposes them toward apoptosis. Most stresses cause a rapid and nearly global shutoff of protein synthesis through one of two mechanisms that interfere with translation initiation – phosphorylation of eIF2α and inhibition of the eIF4F complex (*Table* 1). Modifications of these factors are common in almost all stresses, and their effects can be assessed by global snapshots of translation, captured by ^{35}S labeling of newly synthesized proteins and separation of polyribosomes on density gradients. Inhibiting translation serves to conserve cell resources, as translation consumes >50% of cellular energy (61), and to remodel the proteome by selective translation of individual transcripts (63, 64). Recent work suggests that the balance between repair and cell death is regulated by translation.

***Table* 1. Effects of stress on translation**

Stress	eIF2α phosphorylation	Modifications to eIF4F complex	Stress granules	Notes
Apoptosis	Yes PKR is cleaved and activated	Hypophosphorylation of 4E-BPs Caspase cleavage of eIF4G	Unknown	PKR activation occurs after translation shutoff. Mechanism of 4E-BP phosphorylation unknown
Heat shock	Yes PKR and HRI, depending on cell type	HSP27 blocks eIF4G interaction with eIF4E	Yes	Unclear which mechanism(s) are most important for inhibiting translation
Osmotic shock	Yes Responsible kinase is unclear (probably HRI in erythroid cells)	Hypophosphorylation of 4E-BPs	Yes	Mild stress only alters 4E-BPs and eIF4F complex. eIF2a phosphorylation promotes apoptosis in more severe stress
ER stress	Yes PERK is activated	4E-BP1 expression induced by ATF4, which enhances translation inhibition	Yes	Some transcripts are translated to balance repair and stress, notably *ATF4* and *CHOP*

eIF2α phosphorylation occurs during all of these stresses and other stresses including nutrient starvation, UV irradiation, and oxidative stress. Cap-dependent translation is inhibited by disrupting the eIF4F complex, but this is achieved by diverse mechanisms.

Translation initiation requires a ternary complex composed of the translation initiation factor eIF2, GTP, and the methionine initiator tRNA (Met-tRNA$_i^{Met}$). During translation initiation, GTP is hydrolyzed to GDP, which must be recycled by eIF2B to form a new initiation-competent eIF2-GTP-Met-tRNA$_i^{Met}$ ternary complex. Stresses can activate one of four kinases that phosphorylate the eIF2 regulatory subunit (eIF2α) on serine 51. The kinases and their respective stress activators are PKR (viral infection), PERK (ER stress), GCN2 (nutrient starvation), and HRI (oxidative stress) (64). S51 phosphorylation of eIF2α leads to stable, inhibitory association of the eIF2-GDP complex with eIF2B, blocking recycling of the ternary complex. This results in a fast, potent, and reversible block of translation initiation. eIF2α phosphorylation is the main feature of the integrated stress response, a common protective program activated by most cellular stresses (65) (*Table* 1). A fraction of the proteome escapes translation inhibition through a unique mechanism, while some proteins are even upregulated in response to eIF2α phosphorylation (64). Transcripts that have one or more upstream open reading frames (uORFs) are able to escape eIF2α-dependent translation arrest. When the amount of eIF2-GTP-Met-tRNA$_i^{Met}$ ternary complexes is limited by eIF2α phosphorylation, ribosomes are more likely to scan through the uORFs and initiate translation at a downstream ORF to generate functional protein (61, 63, 64). In contrast, when eIF2-GTP-Met-tRNA$_i^{Met}$ ternary complexes are abundant, the ribosomes initiate first at uORFs and are subsequently less able to initiate at downstream ORFs encoding the relevant protein.

Inhibiting cap-dependent translation in stress

Another way to inhibit translation is to limit formation of the eIF4F complex, which is composed of the cap-binding protein eIF4E, the RNA helicase eIF4A, and the adapter protein eIF4G (66). eIF4F is required for initiating translation of cap-dependent transcripts, which are most mRNAs. The mechanisms of eIF4F inhibition have been reviewed elsewhere (61, 66, 67). Although eIF2α is a common target of almost every stress, only some stresses interfere with eIF4F, and they do so through a diversity of mechanisms (*Table* 1). For example, the heat shock protein HSP27 binds directly to eIF4G to inhibit eIF4F complex formation during HS, which profoundly limits translation to produce very few proteins (68). The best-studied regulators of eIF4F are the eIF4E-binding proteins (4E-BPs), which inhibit eIF4E binding to eIF4G. 4E-BP binding to eIF4E is regulated by phosphorylation: hypophosphorylated 4E-BP binds eIF4E with high affinity, but phosphorylated 4E-BP does not bind (67). The 4E-BPs are phosphorylated by mTORC1, a kinase complex that integrates signaling from multiple mitogenic pathways (67). In the absence of eIF4F, selected mRNAs can be translated through structured elements in their 5′UTRs termed internal ribosomal entry sites (IRES). Ribosome entry at IRESs requires IRES *trans*-acting factors (ITAFs). Numerous apoptosis-associated transcripts (with both pro- and anti-apoptotic functions) contain IRESs that allow them to be translated during cell stress.

Recently, a new mechanism for inhibiting cap-dependent translation has been described (69). tRNA fragments (tiRNAs) are generated during certain stresses by tRNA cleavage at a single site in the anticodon loop by the RNase A family member angiogenin, which is secreted by stressed cells and acts in an autocrine or paracrine fashion. The 5′ fragment tiRNA inhibits cap-dependent translation but not IRES-mediated translation, possibly by binding directly to eIF4G and eIF4E (69, 70).

Regulated translation and the commitment to apoptosis

Whether cells adapt to stress or commit to cell death depends on a delicate balance between the activation of different pathways during stress, which in turn depends on the intensity and duration of the stress. At levels of osmotic stress that induce apoptosis, translation is globally inhibited both through eIF2α phosphorylation and hypophosphorylation of 4E-BP1. Translation inhibition in response to osmotic stress is not rescued in MEFs expressing eIF2α lacking a phosphorylation site at serine 51 (S51 A/A), indicating that eIF2α phosphorylation is not required. Inhibition of the eIF4F complex is probably more important for blocking translation in this setting. In spite of this, S51 A/A MEFs are significantly protected from osmotic stress-induced apoptosis (71). Cytoplasmic relocalization of hnRNP A1 does not occur in S51 A/A MEFs during osmotic stress (51, 72). Cytosolic hnRNP A1 can act as an ITAF or an inhibitor of cap-dependent translation, depending on the transcript. For example, cytosolic hnRNP A1 activates cap-independent translation of the proapoptotic factor APAF-1, but inhibits expression of anti-apoptotic BCL-xL (71, 73). Overexpression of cytosolic hnRNP A1 in S51 A/A MEFs restores the same level of apoptosis during osmotic stress as observed in wildtype MEFs. This study and others suggest that some of the same factors that regulate altered splicing in response to

stress or cell death can also modulate translation inhibition (41, 51, 71).

Translation of individual mRNAs in the setting of global inhibition is important for balancing cell fate between repair and apoptosis. During hypoxic stress and hepatotoxic ER stress, phosphorylation of eIF2α by PERK protects against apoptosis (74, 75). In contrast, MEFs treated with ER stressors (such as tunicamycin and thapsigargin) undergo apoptosis that relies on eIF2α phosphorylation-dependent expression of the CHOP transcription factor, which upregulates expression of proapoptotic genes, such as *BIM* and *DR5* (76–79). CHOP commits cells to apoptosis during the stress response, as $Chop^{-/-}$ MEFs are resistant to death in response to ER stress (78). During ER stress, *CHOP* mRNA is transcriptionally upregulated by the stress transcription factors ATF6 and ATF4, but protein expression requires eIF2α phosphorylation. A single uORF in the *CHOP* 5′ UTR is used during ER stress (79). Prolonged stress leads to apoptosis (6, 7, 80). The proapoptotic upregulation of CHOP requires the coordinated action and sustained signaling of several ER stress pathways. During stress, translation of ATF4 is upregulated through uORFs in its 5′ UTR (81), and then ATF4 protein transactivates *CHOP* mRNA expression (82). In turn, continued eIF2α phosphorylation is required for *CHOP* mRNA translation, and then the protein transactivates target gene expression to exert its proapoptotic function. CHOP protein is therefore downstream in the ER stress response, and the events that lead to its expression require persistent ER stress at multiple points (6) (Fig. 3). This built-in delay could allow a cell time to execute a protective response before committing to apoptosis. A similar mechanism induces CHOP during oxidative stress or amino acid starvation (81), suggesting that it is a common means to push cells toward apoptosis in response to sustained insults.

Unanswered questions in cell stress

Although much is known about well-characterized stress response master regulators, such as ATF4, that are upregulated by eIF2α phosphorylation, for most stresses, the full complement of transcripts that escape translation inhibition or are induced by stress remains unknown. New methods of

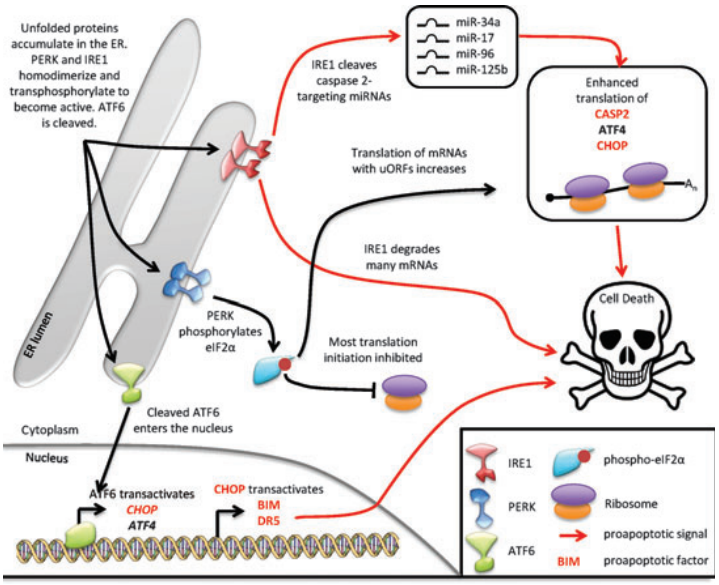

Fig. 3. Proapoptotic posttranscriptional events in the ER stress response. In response to ER stress, the three major ER-localized effectors (ATF6, IRE1, and PERK) all contribute to signaling that can ultimately lead to repair or apoptosis. The ATF6 transcription factor translocates to the Golgi apparatus and is cleaved. The released DNA binding domain enters the nucleus to transactivate expression of repair genes (such as *ATF4*) and proapoptotic genes (such as *CHOP*). PERK and IRE1 kinases become activated. PERK phosphorylates eIF2α, which blocks translation initiation. However, key transcripts, such as *ATF4* and *CHOP*, involved in the stress response escape this translation block through uORFs. The CHOP transcription factor activates expression of the BH3-only protein BIM, the death receptor DR5, and other proapoptotic targets. Latent RNase activity of IRE1 also becomes activated. IRE1 contributes to cell death by cleaving and inactivating multiple miRNAs that normally suppress translation of caspase 2. Caspase 2 translation then increases. IRE1 also cleaves many ER-resident mRNAs to reduce ER stress.

high-resolution comprehensive ribosome profiling (83) could be used to identify differentially translated proteins in stress. Although the translational responses to diverse stresses share many features, differences between types of stress and how changes in translation help a cell adapt to each type of insult could be better understood.

Inhibited translation in cell death

Translation is drastically inhibited early in cell death (84–86), and a number of mechanisms have been posited, mostly involving alterations to the same initiation factors that regulate the stress response. Although genotoxic stress occurs late during apoptosis, the generation of ROS is an early event that is likely to activate many of the same responses as non-lethal oxidative stress. During apoptosis, the eIF4F complex is disrupted by phosphorylation of 4E-BPs (87) and caspase cleavage of eIF4G (84), whereas eIF2α phosphorylation can be induced by caspase cleavage of the eIF2α kinase PKR, which activates it (85, 88). It remains still unclear which apoptotic alteration(s) are responsible for inhibited translation in cell death. They may vary with the apoptotic insult (62). For example, translation inhibition is caspase dependent in cells treated with death receptor ligands, but independent of the caspases in the same cells treated with the genotoxic agent etoposide (62, 89). Here, we discuss alterations that occur before and after 'commitment' to cell death, which we define as effector caspase activation.

Translation inhibition before the commitment to apoptosis

Stress signaling that occurs before the commitment to apoptosis could play a pivotal role in blocking translation. Jurkat T cells deficient in caspase 8 are almost completely resistant to death receptor-mediated apoptosis, whereas caspase 8-sufficient Jurkat cells activate the effector caspases and die under the same treatment conditions. eIF2α phosphorylation modestly increases shortly after adding anti-Fas, regardless of caspase 8 status (20). However, the impact of non-apoptotic eIF2α phosphorylation is modest because global translation inhibition only occurs in caspase 8-sufficient (dying) Jurkat cells. In MCF-7 cells treated for 4 h with the death receptor ligand TRAIL, global translation is reduced by approximately 50%, at a time when there is very little PARP1 cleavage and little phosphatidylserine externalization on the cell membrane (markers of apoptosis). However, at this early time 4E-BP1 hypophosphorylation and reduced binding of eIF4G to eIF4E inhibits the eIF4F complex to block cap-dependent translation (87). These alterations to 4E-BP1 are independent of caspase 3 but sensitive to the pan-caspase inhibitor zVAD-FMK, suggesting a role for the initiator caspase 8 (89). It remains unclear how 4E-BP1 becomes hypophosphorylated or whether this event is essential for translation inhibition. MCF-7 cells treated with etoposide demonstrate reduced translation even when caspase activity is inhibited. Wildtype MEFs treated with etoposide have increased eIF2α phosphorylation and association of 4E-BP1 with eIF4E concurrent with translation inhibition. However, MEFs deficient in the eIF2α kinase PKR have a comparable block to translation in response to etoposide without any increase in eIF2α phosphorylation or 4E-BP1–eIF4E interaction (89). These results suggest that other unknown events besides eIF2α phosphorylation and disruption of eIF4E binding to eIF4G may be important for inhibiting translation in cell death triggered by DNA damage.

Alterations to translation after commitment to cell death

Once activated, the effector caspases directly cleave many translation factors. Notably, caspase 3 cleaves eIF4G (84, 90, 91). It remains unclear, however, whether eIF4G cleavage products still support translation (62) or how much eIF4G cleavage contributes to translation inhibition, which is often already well underway by the time eIF4G is cleaved. In some studies, eIF4G cleavage correlates well with translation inhibition (84, 91), whereas in others, translation inhibition precedes eIF4G cleavage (85, 86). The relative impact of eIF4G cleavage on translation may depend on the cell type and death-inducing stimulus. eIF4G is not cleaved in caspase-3 null MCF-7 cells treated with TRAIL, but translation is still effectively inhibited (89). PKR is also cleaved by the caspases during death receptor-mediated apoptosis in Jurkat cells, but PKR cleavage and eIF2α phosphorylation are late events that occur well after translation inhibition and are probably not major contributors to translation inhibition in cell death (85).

Although large alterations in translation factors have been cataloged during initiation and execution of apoptosis, it remains still unclear which modifications are responsible for inhibiting translation. Alterations to translation factors have only been studied in bulk cell populations undergoing asynchronous cell death. Even genetically identical sister cells die asynchronously in response to apoptotic stimuli (92), making it difficult to dissect which alterations occur in the

preapoptotic versus commitment phases. For example, it has been argued that many IRES-containing mRNAs are upregulated in apoptotic cells (87), but markers of the commitment phase of apoptosis remain low at the time IRES-dependent translation was analyzed, raising the possibility that these translation alterations are actually preapoptotic. Synchronous and rapid means of inducing cell death or single-cell studies will be necessary for understanding which processes are truly responsible for blocking translation during apoptosis. New genetic models with key apoptosis effectors ablated may help dissect the contribution of different pathways. At a more fundamental level, although widely assumed, it has not been proven that translation inhibition is necessary for cell death.

MicroRNAs at the nexus of mRNA translation and stability in stress

MicroRNAs (miRNAs), approximately 22-nt RNAs that recognize target mRNAs by partial base-pairing, interfere with mRNA translation and stability when they are bound to the RNA-induced silencing complex (RISC) (93). miRNAs can affect the overall protein expression of many genes, sometimes only by a subtle amount. The regulated targets also vary with the particular cellular context. Recent studies suggest that miRNAs first inhibit translation initiation, then activate mRNA deadenylation and decay (94). Because miRNAs require only limited complementary sequence over a short sequence to recognize targets, target identification remains a major challenge (95). Knockouts of many miRNAs in mice exhibit no overt phenotypes under normal conditions, but phenotypes can emerge after stress. miRNAs can act as important mediators of the balance between repair and apoptosis (96). The miR-15 family is upregulated in the heart following ischemia/reperfusion (IR) injury and promotes apoptosis in response to this stress. In cardiomyocytes subjected to hypoxia and reoxygenation, antagonizing miR-15 increases expression of the antiapoptotic miR-15 target BCL-2 and reduces apoptosis (97, 98). miR-15 suppression *in vivo* significantly reduces the size of the infarct following IR injury. In contrast, miR-214, which is also upregulated in response to IR, protects against apoptosis. The hearts of miR-214 knockout mice resemble their wildtype counterparts under normal conditions, but these mice are much more susceptible to IR, with decreased survival and increased cardiac apoptosis (99).

miRNAs also play a role in the TP53-dependent response to genotoxic stress. miR-34a and other miRNAs are upregulated by diverse genotoxic stresses (100–104). The promoters of these miRNAs contain strong TP53 consensus sites transactivated by TP53. Ectopic expression of miR-34a induces potent cell cycle arrest and/or apoptosis *in vitro*. In one study, knockdown of miR-34a also significantly reduced apoptosis in response to etoposide (104). These and other early studies suggested a central role for the miR-34 family (and miR-34a especially) in promoting cell cycle arrest and cell death following genotoxic stress in a TP53-dependent manner. Multiple negative regulators of TP53 have also been identified as direct targets of miR-34a, suggesting that miR-34a and TP53 might form a positive feedback loop, with each promoting the expression or activity of the other (105) (Fig. 4). However, a recent study using miR-34 family knockout mice and mouse embryonic fibroblasts (MEFs) has called into question the importance of miR-34 in the response to genotoxic stress. Wildtype and miR-34 family knockouts tested under a variety of genotoxic stress conditions showed no difference in cell survival *in vitro* or *in vivo* (106). Indeed, the only differences observed were increased proliferation and transformation propensity of miR-34 knockout MEFs compared with wildtype MEFs. This finding agrees with work from our laboratory. We developed a novel biochemical approach to identify miRNA targets without bias by isolating mRNAs bound to a biotinylated miRNA mimic transfected into cultured cells. Although miR-34a pulldown significantly enriched both for genes in the TP53 network and genes involved in cell cycle progression, confirming earlier studies, the most significant enrichment was in genes whose products participate in all aspects of growth factor signaling (105). Cancer cell lines overexpressing miR-34a were less responsive to stimulation by serum growth factors, whereas miR-34a-deficient MEFs were less likely to die after serum starvation. As in the knockout study, we also found that knockdown of the miR-34 family did not affect cell survival after genotoxic stress (authors' unpublished results). In line with its role in regulating growth factor signaling, miR-34a transcription is also regulated by an alternate promoter that is activated by growth factor signaling (107). These new results suggest that the primary role of the miR-34 family may be to suppress growth-stimulating signaling and downstream cell cycle genes to temper the potentially oncogenic response to growth factors (Fig. 4). These studies also suggest that the integrated effect of modulating an individual miRNA during stress can be less straightforward than predicted by overexpression studies.

Although the above examples demonstrate the potential of miRNAs to play a central role in mediating cell fate in

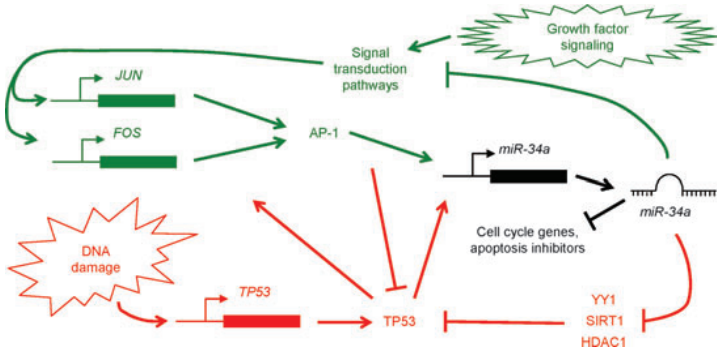

Fig. 4. miR-34a regulates growth factor signaling and the DNA damage response. The miR-34 family participates in the TP53-dependent response to DNA damage (indicated in red). The miR-34a promoter is strongly upregulated by TP53. miR-34a in turn downregulates many TP53 inhibitors, cell cycle genes, and apoptosis inhibitors. This positive feedback loop suppresses cell proliferation. miR-34a is also induced by growth factor signaling (indicated in green) and dampens responsiveness to mitogenic signals by suppressing many growth factor signaling pathways. Results from knockout mice suggest that regulating growth factor signaling is the major biological function of miR-34, as knockout mice have no detectable difference in their response to genotoxic stress.

response to stress, these regulatory events may be fairly slow because they require *de novo* transcription and processing of the miRNA before they can downregulate their targets. Intriguing new studies implicate a fast-acting role for miRNAs in IRE1-dependent cell death in response to ER stress (Fig. 3). IRE1 is an ER kinase composed of an N-terminal lumenal domain, and cytosolic kinase and RNase domains (6). During ER stress, IRE1 aggregation drives its *trans*-phosphorylation, unmasking its RNase activity. IRE1 cleaves a subset of miRNAs (miR-17, miR-34a, miR-96, and miR-125b) that blocks their target-suppressing functions. Normally, miRNAs are extremely stable (108), so the rapid decline in these miRNAs (by approximately 50% after 4 h of ER stress) is quite striking. Caspase 2 (CASP2) is a common target of these miRNAs. Caspase 2 upregulation is an important initiator of the mitochondrial pathway of cell death in response to ER stress (109). Knockdown of these miRNAs increases caspase 2 protein, while their overexpression prevents the accumulation of caspase 2 following ER stress. Although most miRNAs reduce the stability, and thus steady state levels, of their mRNA targets (110), *CASP2* mRNA levels are unchanged by ER stress, while its translation rate, as measured by polyribosomal occupancy, significantly increases. Unlike IRE1-driven mRNA decay, miRNA targeting is dependent on the IRE1 RNase domain but not its kinase domain. However, although kinase-inactive IRE1 induces CASP2 protein, it does not induce apoptosis. Thus, IRE1-dependent mRNA decay (discussed below) appears to be crucial for tripping the apoptotic switch in response to irreparable ER stress (111, 112).

miRNA alteration of mRNA stability in ER stress also can have an inflammatory effect. TXNIP (thioredoxin interacting protein) is a mediator of oxidative stress that may promote insulin resistance in type 2 diabetes induced by a high-fat diet (113). TXNIP protein is upregulated in response to diverse ER stresses in a PERK and IRE1-dependent manner. Signaling downstream of PERK enhances *TXNIP* transcription (114). Moreover, IRE1 cleavage of miR-17 also enhances the stability of its target *TXNIP*. The physiological impact of increased TXNIP following ER stress *in vitro* and *in vivo* is profound. Pancreatic islets activate the inflammasome to cleave the precursor of the proinflammatory cytokine IL-1β in response to ER stress, which is linked to the development of diabetes in this model (115). Inflammasome activation may be secondary to increased ROS generation when TXNIP increases, as pharmacological inhibition of IRE1 RNase activity or knockdown of *TXNIP* fully or partially inhibits, respectively, the increase in IL-1β in response to ER stress (114, 116). In response to pharmacological inducers of ER stress, fewer Txnip-null MEFs die than their wildtype counterparts, while Txnip deletion partially reduces development of diabetes in a model driven by ER stress (116). Together, these results suggest that miRNAs can play a central role in regulating inflammation and apoptosis under stress conditions.

Two consistent themes emerge in the study of miRNAs and stress. First, target identification is central to understanding a miRNA's true biological function, and second, that functions inferred from cell culture experiments must be validated *in vivo*. Many miRNA studies have relied on ectopic expression of miRNA mimics, which can suggest

functions that are not physiologically relevant. This is highlighted best by recent studies of miR-34a. miRNA levels may change rapidly in response to stress to alter protein levels that are critical to cell survival under stress. One mechanism for this has been described (miRNA cleavage by activated IRE1), but other unknown mechanisms may be at play.

Changes in mRNA stability during cell stress

Little is known about how cell stress affects mRNA stability. Most mRNAs are protected from decay by a 5′ $^{7\text{-meG}}$ cap and a 3′ poly(A) tail (117), and most basal mRNA turnover is mediated by deadenylation followed by decapping and exonucleolytic decay. However, mRNA decay can be initiated by a variety of other mechanisms, including endonucleolytic cleavage (118). Although many of the *trans*-acting factors that regulate mRNA turnover are well characterized (nucleases, RNA-binding proteins), little is known about what signals initiate basal mRNA decay and how individual mRNAs become tagged for decay. Recent work suggests an intimate coupling between mRNA translation and stability. However, although almost all stresses globally shut off translation, there is no evidence for a concomitant global decline in mRNA stability, suggesting that somehow, stability and translation are decoupled following cell stress.

Recent work suggests that altered mRNA stability could play a key role in the commitment to cell death following prolonged ER stress. IRE1 cleaves the *XBP1* mRNA to activate an unusual cytosolic splicing reaction, excising a 26-nt intron from *XBP1* to generate *XBP1-s* (7). This processed transcript encodes a functional XBP1 transcription factor that transactivates many genes that function to reduce the unfolded protein load in the ER and alleviate ER stress. Until recently, this was the only known stress-dependent function of IRE1 (7). However, it is now clear that IRE1 also directly degrades many mRNAs during stress (111, 119, 120). Gene expression profiling of *Drosophila* S2 cells depleted of *IRE1* or *XBP1* by RNAi demonstrated that a subset of transcripts is downregulated in ER stress in an IRE1-dependent, XBP1-independent fashion. Most of these degraded transcripts are normally found at the ER, leading to the hypothesis that IRE1 cleaves these mRNAs to reduce ER-localized translation. mRNA degradation would collaborate with the PERK/eIF2α-dependent inhibition of translation to reduce the protein load in the ER (119). Follow-up studies have confirmed that the IRE1 RNase directly targets some ER-localized mRNAs for decay (111, 120). This mRNA-targeted activity depends on both the kinase and the RNase domains of IRE1, whereas *XBP1* splicing does not require IRE1 kinase activity. As only cells expressing IRE1 protein with functional kinase and RNase domains undergo apoptosis in response to prolonged ER stress, the mRNA decay activities of IRE1 may be essential for committing to apoptosis (111). In support of this hypothesis, expressing an IRE1-binding peptide that enhances *XBP1* splicing activity, but reduces IRE1-dependent mRNA decay, protects cells from ER stress-induced apoptosis (121).

Stress granules: mysterious mRNA-protein reservoirs

No review of mRNA stability in stress would be complete without a discussion of stress granules (SGs) (122–125). SGs, microscopically defined cytoplasmic structures that aggregate in response to a diverse array of stresses, contain the 40S ribosomal subunit, several translation initiation factors and numerous RNA-binding proteins bound to large amounts of mRNA. G3BP1, TIA1, and TIAR proteins are important for SG formation, which is triggered by phosphorylation of eIF2α, a common feature of many stresses (125). Despite intensive research on SGs, it is still not completely clear what role they play in mRNA stability. Some transcripts translated during stress are excluded from SGs, while housekeeping genes are contained in them (122). This finding has led to the hypothesis that SGs 'store' mRNAs in a translationally inactive state during conditions of cell stress. When stress is relieved, SGs disappear and the stored mRNAs are available for translation. However, SGs localize close to P bodies, sites of miRNA-dependent and independent mRNA decay. Moreover, it is not possible to separate SGs from P bodies, and they contain some of the same proteins. SGs might protect mRNAs during transient stress but could hand them over to P bodies for degradation when stress persists. Moreover, the fate of individual mRNAs within SGs need not be uniform. Whether a SG-resident mRNA is stabilized may depend on the *cis*-regulatory sequences in the mRNA and the *trans*-acting factors that bind it. There is circumstantial evidence that localization to SGs can stabilize mRNAs. For example, IGF2BP1 (also known as zipcode binding protein) localizes to SGs in conditions of cell stress, and individual IGF2BP1 target mRNAs are stabilized by this protein during stress (126). Future work will be required to determine if mRNAs are indeed globally or partially stabilized by SGs under stress conditions.

mRNA stability during apoptosis

In contrast with the very well-characterized changes that occur to proteins, lipids, and DNA during cell death (9), the fate of mRNAs in apoptotic cells has not been extensively studied. In some cells, the 28S rRNA is cleaved by an unknown nuclease to generate distinct fragments (127). Because this occurs late in cell death and is not universally seen, it is unlikely to be important for cell death. Some intriguing studies that have assayed individual mRNA transcripts in apoptotic cells by Northern blotting suggest that mRNA decay may be an early feature of apoptosis (86, 128).

Postmortem: answering old questions with new techniques

Recently developed methods could be deployed to follow the effects of stress and apoptosis on the cellular transcriptome to better define the fate of newly transcribed RNAs. Recent methods to label and capture new transcripts could be paired with next-generation sequencing to track posttranscriptional changes in pre-mRNA processing and half-life (1, 56, 57). These experimental approaches could be coupled with genetic manipulation by knockout, knockdown, or overexpression of mutant or wildtype candidate factors to define the key pathways involved in controlling protein expression in stressed cells. Although global inhibition of translation in response to stress and cell death has been known for decades, other posttranscriptional events need further characterization. In particular, we lack an understanding of how the type, severity, and duration of stress impact mRNA splicing, translation, and stability. Although stress responses share some common features, the differences may prove important in determining how cells adapt to diverse insults. Ultimately, we need to understand how posttranscriptional changes during the stress response influence cell repair versus apoptosis.

Some of the basic mechanisms that regulate gene expression in the stress response remain unknown. Under normal conditions, mRNA translation and stability are intimately coupled, but generally mRNAs remain stable in stressed cells despite blocked translation. It remains to be seen whether the formation of SGs can explain this uncoupling. Similarly, there are major open questions in the study of apoptosis. The true cause(s) of translation inhibition during programmed cell death remain elusive. Is it secondary to the stresses that accompany apoptosis, or do activated caspases play a major role? Is blocking new protein expression necessary for carrying the apoptotic program to completion? More careful studies that separate preapoptotic cells from cells committed to apoptosis will be crucial to answer these questions.

References

1. Tani H, et al. Genome-wide determination of RNA stability reveals hundreds of short-lived noncoding transcripts in mammals. Genome Res 2012;**22**:947–956.
2. Selinger DW, Saxena RM, Cheung KJ, Church GM, Rosenow C. Global RNA Half-Life Analysis in Escherichia coli reveals positional patterns of transcript degradation. Genome Res 2003;**13**:216–223.
3. Richter K, Haslbeck M, Buchner J. The heat shock response: life on the verge of death. Mol Cell 2010;**40**:253–266.
4. Green DR, Kroemer G. Cytoplasmic functions of the tumour suppressor p53. Nature 2009;**458**:1127–1130.
5. Lord CJ, Ashworth A. The DNA damage response and cancer therapy. Nature 2012;**481**:287–294.
6. Merksamer PI, Papa FR. The UPR and cell fate at a glance. J Cell Sci 2010;**123**:1003–1006.
7. Rutkowski DT, Kaufman RJ. That which does not kill me makes me stronger: adapting to chronic ER stress. Trends Biochem Sci 2007;**32**:469–476.
8. Papa FR. Endoplasmic reticulum stress, pancreatic β-cell degeneration, and diabetes. Cold Spring Harb Perspect Med 2012;**2**:a007666.
9. Taylor RC, Cullen SP, Martin SJ. Apoptosis: controlled demolition at the cellular level. Nat Rev Mol Cell Biol 2008;**9**:231–241.
10. Danial NN, Korsmeyer SJ. Cell death: critical control points. Cell 2004;**116**:205–219.
11. Llambi F, et al. A unified model of mammalian BCL-2 protein family interactions at the mitochondria. Mol Cell 2011;**44**:517–531.
12. Riedl SJ, Shi Y. Molecular mechanisms of caspase regulation during apoptosis. Nat Rev Mol Cell Biol 2004;**5**:897–907.
13. Bouchier-Hayes L, Green DR. Caspase-2: the orphan caspase. Cell Death Differe 2012;**19**: 51–57.
14. Thiery J, et al. Perforin pores in the endosomal membrane trigger the release of endocytosed granzyme B into the cytosol of target cells. Nat Immunol 2011;**12**:770–777.
15. Chowdhury D, Lieberman J. Death by a thousand cuts: granzyme pathways of programmed cell death. Annu Rev Immunol 2008;**26**:389–420.
16. Bots M, Medema JP. Granzymes at a glance. J Cell Sci 2006;**119**:5011–5014.
17. Fan Z, et al. Cleaving the oxidative repair protein Ape1 enhances cell death mediated by granzyme A. Nat Immunol 2003;**4**:145–153.
18. Jans DA, Jans P, Briggs LJ, Sutton V, Trapani JA. Nuclear transport of granzyme B (Fragmentin-2). J Biol Chem 1996;**271**:30781–30789.
19. Albeck JG, Burke JM, Aldridge BB, Zhang M, Lauffenburger DA, Sorger PK. Quantitative Analysis of Pathways Controlling Extrinsic Apoptosis in Single Cells. Mol Cell 2008;**30**: 11–25.
20. Morley SJ, Jeffrey I, Bushell M, Pain VM, Clemens MJ. Differential requirements for caspase-8 activity in the mechanism of phosphorylation of eIF2α, cleavage of eIF4GI and signaling events associated with the inhibition of protein synthesis in apoptotic Jurkat T cells. FEBS Let 2000;**477**:229–236.
21. Jurica MS, Moore MJ. Pre-mRNA splicing: awash in a sea of proteins. Mol Cell 2003;**12**:5–14.
22. Hoskins AA, Moore MJ. The spliceosome: a flexible, reversible macromolecular machine. Trends Biochem Sci 2012;**37**:179–188.
23. Wang Z, Burge CB. Splicing regulation: from a parts list of regulatory elements to an integrated splicing code. RNA 2008;**14**:802–813.
24. Spies N, Nielsen CB, Padgett RA, Burge CB. Biased chromatin signatures around polyadenylation sites and exons. Mol Cell 2009;**36**:245–254.
25. Nilsen TW, Graveley BR. Expansion of the eukaryotic proteome by alternative splicing. Nature 2010;**463**:457–463.
26. Biamonti G, Caceres JF. Cellular stress and RNA splicing. Trends Biochem Sci 2009;**34**:146–153.

27. Zhu J, Mayeda A, Krainer AR. Exon identity established through differential antagonism between exonic splicing silencer-bound hnRNP A1 and enhancer-bound SR proteins. Mol Cell 2001;**8**:1351–1361.
28. Mayeda A, Krainer AR. Regulation of alternative pre-mRNA splicing by hnRNP A1 and splicing factor SF2. Cell 1992;**68**:365–375.
29. Konig J, et al. iCLIP reveals the function of hnRNP particles in splicing at individual nucleotide resolution. Nat Struct Mol Biol 2010;**17**:909–915.
30. Huelga SC, et al. Integrative genome-wide analysis reveals cooperative regulation of alternative splicing by hnRNP proteins. Cell Rep 2012;**1**:167–178.
31. Martinez-Contreras R, Fisette J-F, Nasim FH, Madden R, Cordeau M, Chabot B. Intronic binding sites for hnRNP A/B and hnRNP F/H proteins stimulate pre-mRNA splicing. PLoS Biol 2006;**4**:e21.
32. Wang ET, et al. Alternative isoform regulation in human tissue transcriptomes. Nature 2008;**456**:470–476.
33. Yeo G, Holste D, Kreiman G, Burge CB. Variation in alternative splicing across human tissues. Genome Biol 2004;**5**:R74.
34. Bond U. Heat shock but not other stress inducers leads to the disruption of a sub-set of snRNPs and inhibition of in vitro splicing in HeLa cells. EMBO J 1988;**7**:3509.
35. Shin C, Feng Y, Manley JL. Dephosphorylated SRp38 acts as a splicing repressor in response to heat shock. Nature 2004;**427**:553–558.
36. Shi Y, Nishida K, Giammartino DCD, Manley JL. Heat shock-induced SRSF10 dephosphorylation displays thermotolerance mediated by Hsp27. Mol Cell Biol 2011;**31**:458–465.
37. Mitchell JA, Fraser P. Transcription factories are nuclear subcompartments that remain in the absence of transcription. Genes Dev 2008;**22**:20–25.
38. Tilgner H, et al. Deep sequencing of subcellular RNA fractions shows splicing to be predominantly co-transcriptional in the human genome but inefficient for lncRNAs. Genome Res 2012;**22**:1616–1625.
39. Nevo Y, et al. Genome-wide activation of latent donor splice sites in stress and disease. Nucl Acids Res 2012;**40**:10980–10994.
40. Rebbapragada I, Lykke-Andersen J. Execution of nonsense-mediated mRNA decay: what defines a substrate? Curr Opin Cell Biol 2009;**21**:394–402.
41. Rajani DK, Walch M, Martinvalet D, Thomas MP, Lieberman J. Alterations in RNA processing during immune-mediated programmed cell death. Proc Natl Acad Sci USA 2012;**109**:8688–8693.
42. Gazave E, Marqués-Bonet T, Fernando O, Charlesworth B, Navarro A. Patterns and rates of intron divergence between humans and chimpanzees. Genome Biol 2007;**8**:R21.
43. Xiao SH, Manley JL. Phosphorylation of the ASF/SF2 RS domain affects both protein-protein and protein-RNA interactions and is necessary for splicing. Genes Dev 1997;**11**:334–344.
44. de la Mata M, et al. A slow RNA polymerase II affects alternative splicing in vivo. Mol Cell 2003;**12**:525–532.
45. Proudfoot NJ, Furger A, Dye MJ. Integrating mRNA processing with transcription. Cell 2002;**108**:501–512.
46. Buratowski S. Connections between mRNA 3′ end processing and transcription termination. Curr Opin Cell Biol 2005;**17**:257–261.
47. Kornblihtt AR, Mata MDL, Fededa JP, Muñoz MJ, Nogués G. Multiple links between transcription and splicing. RNA 2004;**10**:1489–1498.
48. Muñoz MJ, et al. DNA damage regulates alternative splicing through inhibition of RNA polymerase II elongation. Cell 2009;**137**:708–720.
49. Ip JY, et al. Global impact of RNA polymerase II elongation inhibition on alternative splicing regulation. Genome Res 2011;**21**:390–401.
50. Das R, et al. SR proteins function in coupling RNAP II transcription to pre-mRNA splicing. Mol Cell 2007;**26**:867–881.
51. van der Houven van Oordt W, et al. The Mkk3/6-p38–Signaling Cascade Alters the Subcellular Distribution of Hnrnp A1 and Modulates Alternative Splicing Regulation. J Cell Biol 2000;**149**:307–316.
52. Dutertre M, et al. Cotranscriptional exon skipping in the genotoxic stress response. Nat Struct Mol Biol 2010;**17**:1358–1366.
53. Wei W-J, et al. YB-1 binds to CAUC motifs and stimulates exon inclusion by enhancing the recruitment of U2AF to weak polypyrimidine tracts. Nucl Acids Res 2012;**40**:8622–8636.
54. Merdzhanova G, et al. E2F1 controls alternative splicing pattern of genes involved in apoptosis through upregulation of the splicing factor SC35. Cell Death Differ 2008;**15**:1815–1823.
55. Shkreta L, Michelle L, Toutant J, Tremblay ML, Chabot B. The DNA Damage Response Pathway Regulates the Alternative Splicing of the Apoptotic Mediator Bcl-x. J Biol Chem 2011;**286**:331–340.
56. Munchel SE, Shultzaberger RK, Takizawa N, Weis K. Dynamic profiling of mRNA turnover reveals gene-specific and system-wide regulation of mRNA decay. Mol Biol Cell 2011;**22**:2787–2795.
57. Rabani M, et al. Metabolic labeling of RNA uncovers principles of RNA production and degradation dynamics in mammalian cells. Nat Biotech 2011;**29**:436–442.
58. Schwerk C, Schulze-Osthoff K. Regulation of apoptosis by alternative pre-mRNA splicing. Mol Cell 2005;**19**:1–13.
59. Edmond V, et al. Acetylation and phosphorylation of SRSF2 control cell fate decision in response to cisplatin. EMBO J 2011;**30**:510–523.
60. Hua Y, Vickers TA, Okunola HL, Bennett CF, Krainer AR. Antisense masking of an hnRNP A1/A2 intronic splicing silencer corrects SMN2 splicing in transgenic mice. Am J Human Gen 2008;**82**:834–848.
61. Holcik M, Sonenberg N. Translational control in stress and apoptosis. Nat Rev Mol Cell Biol 2005;**6**:318–327.
62. Morley SJ, Coldwell MJ, Clemens MJ. Initiation factor modifications in the preapoptotic phase. Cell Death Differ 2005;**12**:571–584.
63. Wouters BG, van den Beucken T, Magagnin MG, Koritzinsky M, Fels D, Koumenis C. Control of the hypoxic response through regulation of mRNA translation. Sem Cell Dev Biol 2005;**16**:487–501.
64. Wek RC, Jiang H-Y, Anthony TG. Coping with stress: eIF2 kinases and translational control. Biochem Soc Trans 2006;**34**:7.
65. Harding HP, et al. An integrated stress response regulates amino acid metabolism and resistance to oxidative stress. Mol Cell 2003;**11**:619–633.
66. Gingras A-C, Raught B, Sonenberg N. Regulation of translation initiation by FRAP/mTOR. Genes Dev 2001;**15**:807–826.
67. Silvera D, Formenti SC, Schneider RJ. Translational control in cancer. Nature Rev Cancer 2010;**10**:254–266.
68. Cuesta R, Laroia G, Schneider RJ. Chaperone Hsp27 inhibits translation during heat shock by binding eIF4G and facilitating dissociation of cap-initiation complexes. Genes Dev 2000;**14**:1460–1470.
69. Yamasaki S, Ivanov P, Hu G, Anderson P. Angiogenin cleaves tRNA and promotes stress-induced translational repression. J Cell Biol 2009;**185**:35–42.
70. Ivanov P, Emara MM, Villen J, Gygi SP, Anderson P. Angiogenin-Induced tRNA Fragments Inhibit Translation Initiation. Mol Cell 2011;**43**:613–623.
71. Bevilacqua E, et al. eIF2alpha phosphorylation tips the balance to apoptosis during osmotic stress. J Biol Chem 2010;**285**:17098–17111.
72. Allemand E, Guil S, Myers M, Moscat J, Cáceres JF, Krainer AR. Regulation of heterogenous nuclear ribonucleoprotein A1 transport by phosphorylation in cells stressed by osmotic shock. Proc Natl Acad Sci USA 2005;**102**:3605–3610.
73. Cammas A, et al. Cytoplasmic relocalization of heterogeneous nuclear ribonucleoprotein A1 controls translation initiation of specific mRNAs. Mol Biol Cell 2007;**18**:5048–5059.
74. Teske BF, et al. The eIF2 kinase PERK and the integrated stress response facilitate activation of ATF6 during endoplasmic reticulum stress. Mol Biol Cell 2011;**22**:4390–4405.
75. Bi M, et al. ER stress-regulated translation increases tolerance to extreme hypoxia and promotes tumor growth. EMBO J 2005;**24**:3470–3481.
76. Yamaguchi H, Wang H-G. CHOP is involved in endoplasmic reticulum stress-induced apoptosis by enhancing DR5 expression in human carcinoma cells. J Biol Chem 2004;**279**:45495–45502.
77. Puthalakath H, et al. ER Stress Triggers Apoptosis by Activating BH3-Only Protein Bim. Cell 2007;**129**:1337–1349.
78. Zinszner H, et al. CHOP is implicated in programmed cell death in response to impaired function of the endoplasmic reticulum. Genes Dev 1998;**12**:982–995.

79. Palam LR, Baird TD, Wek RC. Phosphorylation of eIF2 facilitates ribosomal bypass of an inhibitory upstream ORF to enhance CHOP translation. J Biol Chem 2011;**286**:10939–10949.
80. Szegezdi E, Logue SE, Gorman AM, Samali A. Mediators of endoplasmic reticulum stress-induced apoptosis. EMBO Rep 2006;**7**:880–885.
81. Harding HP, et al. Regulated translation initiation controls stress-induced gene expression in mammalian cells. Mol Cell 2000;**6**:1099–1108.
82. Fawcett TW, Martindale JL, Guyton KZ, Hai T, Holbrook NJ. Complexes containing activating transcription factor (ATF)/cAMP-responsive-element-binding protein (CREB) interact with the CCAAT/enhancer-binding protein (C/EBP)-ATF composite site to regulate Gadd153 expression during the stress response. Biochem. J 1999;**339**:135–141.
83. Ingolia NT, Ghaemmaghami S, Newman JRS, Weissman JS. Genome-wide analysis in vivo of translation with nucleotide resolution using ribosome profiling. Science 2009;**324**:218–223.
84. Clemens MJ, Bushell M, Morley SJ. Degradation of eukaryotic polypeptide chain initiation factor (eIF) 4G in response to induction of apoptosis in human lymphoma cell lines. Oncogene 1998;**17**:2921–2931.
85. Saelens X, Kalai M, Vandenabeele P. Translation inhibition in apoptosis. J Biol Chem 2001;**276**:41620–41628.
86. Bushell M, Stoneley M, Sarnow P, Willis AE. Translation inhibition during the induction of apoptosis: RNA or protein degradation? Biochem Soc Trans 2004;**32**:606–610.
87. Bushell M, et al. Polypyrimidine Tract Binding Protein Regulates IRES-Mediated Gene Expression during Apoptosis. Mol Cell 2006;**23**:401–412.
88. Kalai M, et al. The caspase-generated fragments of PKR cooperate to activate full-length PKR and inhibit translation. Cell Death Differ 2007;**14**:1050–1059.
89. Jeffrey IW, Bushell M, Tilleray VJ, Morley S, Clemens MJ. Inhibition of protein synthesis in apoptosis differential requirements by the tumor necrosis factor α family and a DNA-damaging agent for caspases and the double-stranded RNA-dependent protein kinase. Cancer Res 2002;**62**:2272–2280.
90. Clemens MJ, Bushell M, Jeffrey IW, Pain VM, Morley SJ. Translation initiation factor modifications and the regulation of protein synthesis in apoptotic cells. Cell Death Differ 2000;**7**:603–615.
91. Marissen WE, Lloyd RE. Eukaryotic translation initiation factor 4G is targeted for proteolytic cleavage by caspase 3 during inhibition of translation in apoptotic cells. Mol Cell Biol 1998;**18**:7565–7574.
92. Spencer SL, Gaudet S, Albeck JG, Burke JM, Sorger PK. Non-genetic origins of cell-to-cell variability in TRAIL-induced apoptosis. Nature 2009;**459**:428–432.
93. Bartel DP. MicroRNAs: target recognition and regulatory functions. Cell 2009;**136**:215–233.
94. Fabian MR, Sonenberg N. The mechanics of miRNA-mediated gene silencing: a look under the hood of miRISC. Nat Struct Mol Biol 2012;**19**:586–593.
95. Thomas M, Lieberman J, Lal A. Desperately seeking microRNA targets. Nat Struct Mol Biol 2010;**17**:1169–1174.
96. Mendell JT, Olson EN. MicroRNAs in stress signaling and human disease. Cell 2012;**148**:1172–1187.
97. Cimmino A, et al. miR-15 and miR-16 induce apoptosis by targeting BCL2. Proc Natl Acad Sci USA 2005;**102**:13944–13949.
98. Hullinger TG, et al. Inhibition of miR-15 protects against cardiac ischemic injury. Circulation Res 2012;**110**:71–81.
99. Aurora AB, et al. MicroRNA-214 protects the mouse heart from ischemic injury by controlling Ca2 + overload and cell death. J Clin Invest 2012;**122**:1222–1232.
100. Chang T-C, et al. Transactivation of miR-34a by p53 broadly influences gene expression and promotes apoptosis. Mol Cell 2007;**26**:745–752.
101. He L, et al. A microRNA component of the p53 tumour suppressor network. Nature 2007;**447**:1130–1134.
102. Tarasov V, et al. Differential regulation of microRNAs by p53 revealed by massively parallel sequencing: miR-34a is a p53 target that induces apoptosis and G1-arrest. Cell Cycle 2007;**6**:1586–1593.
103. Bommer GT, et al. p53-mediated activation of miRNA34 candidate tumor-suppressor genes. Curr Biol 2007;**17**:1298–1307.
104. Raver-Shapira N, et al. Transcriptional activation of miR-34a contributes to p53-mediated apoptosis. Mol Cell 2007;**26**:731–743.
105. Lal A, et al. Capture of microRNA–bound mRNAs identifies the tumor suppressor miR-34a as a regulator of growth factor signaling. PLoS Genet 2011;**7**:e1002363.
106. Concepcion CP, et al. Intact p53-dependent responses in miR-34–deficient mice. PLoS Genet 2012;**8**:e1002797.
107. Navarro F, et al. miR-34a contributes to megakaryocytic differentiation of K562 cells independently of p53. Blood 2009;**114**:2181–2192.
108. Gantier MP, et al. Analysis of microRNA turnover in mammalian cells following Dicer1 ablation. Nucl Acids Res 2011;**39**:5692–5703.
109. Upton J-P, et al. Caspase-2 cleavage of BID is a critical apoptotic signal downstream of endoplasmic reticulum stress. Mol Cell Biol 2008;**28**:3943–3951.
110. Guo H, Ingolia NT, Weissman JS, Bartel DP. Mammalian microRNAs predominantly act to decrease target mRNA levels. Nature 2010;**466**:835–840.
111. Han D, et al. IRE1α kinase activation modes control alternate endoribonuclease outputs to determine divergent cell fates. Cell 2009;**138**:562–575.
112. Upton J-P, et al. IRE1α cleaves select microRNAs during ER stress to derepress translation of proapoptotic caspase-2. Science 2012;**338**:818–822.
113. Chutkow WA, et al. Deletion of the α-arrestin protein Txnip in mice promotes adiposity and adipogenesis while preserving insulin sensitivity. Diabetes 2010;**59**:1424–1434.
114. Oslowski CM, et al. Thioredoxin-interacting protein mediates ER stress-induced β cell death through initiation of the inflammasome. Cell Metab 2012;**16**:265–273.
115. Ehses JA, et al. IL-1 antagonism reduces hyperglycemia and tissue inflammation in the type 2 diabetic GK rat. Proc Natl Acad Sci USA 2009;**106**:13998–14003.
116. Lerner AG, et al. IRE1α induces thioredoxin-interacting protein to activate the NLRP3 inflammasome and promote programmed cell death under irremediable ER stress. Cell Metab 2012;**16**:250–264.
117. Fritz D, Bergman N, Kilpatrick W, Wilusz C, Wilusz J. Messenger RNA decay in mammalian cells. Cell Biochem Biophys 2004;**41**:265–277.
118. Schoenberg DR, Maquat LE. Regulation of cytoplasmic mRNA decay. Nat Rev Genetics 2012;**13**:246.
119. Hollien J, Weissman JS. Decay of endoplasmic reticulum-localized mRNAs during the unfolded protein response. Science 2006;**313**:104–107.
120. Hollien J, Lin JH, Li H, Stevens N, Walter P, Weissman JS. Regulated Ire1-dependent decay of messenger RNAs in mammalian cells. J Cell Biol 2009;**186**:323–331.
121. Bouchecareilh M, Higa A, Fribourg S, Moenner M, Chevet E. Peptides derived from the bifunctional kinase/RNase enzyme IRE1α modulate IRE1α activity and protect cells from endoplasmic reticulum stress. FASEB J 2011;**25**:3115–3129.
122. Anderson P, Kedersha N. RNA granules: post-transcriptional and epigenetic modulators of gene expression. Nat Rev Mol Cell Biol 2009;**10**:430–436.
123. Buchan JR, Parker R. Eukaryotic stress granules: the ins and outs of translation. Mol Cell 2009;**36**:932–941.
124. Balagopal V, Parker R. Polysomes, P bodies and stress granules: states and fates of eukaryotic mRNAs. Curr Opin Cell Biol 2009;**21**:403–408.
125. Kedersha N, Anderson P. Mammalian stress granules and processing bodies. Meth. Enzymol. 2007;**431**:61–81.
126. Stöhr N, et al. ZBP1 regulates mRNA stability during cellular stress. J Cell Biol 2006;**175**:527–534.
127. Degen WG, Pruijn GJ, Raats JM, van Venrooij WJ. Caspase-dependent cleavage of nucleic acids. Cell Death Differ 2000;**7**:616–627.
128. Prete MD, Robles MS, Guáo A, Martínez-A C, Izquierdo M, Garcia-Sanz JA. Degradation of cellular mRNA is a general early apoptosis-induced event. FASEB J. 2002;**16**:2003–2005.

Alterations in RNA processing during immune-mediated programmed cell death

Danielle K. Rajani[a,b,1], Michael Walch[a,b,1], Denis Martinvalet[a,b,2], Marshall P. Thomas[a,b], and Judy Lieberman[a,b,3]

[a]Immune Disease Institute and [b]Program in Molecular and Cellular Medicine, Children's Hospital Boston, Harvard Medical School, Boston MA 02115

Edited by Herman N. Eisen, Massachusetts Institute of Technology, Cambridge, MA, and approved April 18, 2012 (received for review January 25, 2012)

During immune-mediated death, death-inducing granzyme (Gzm) proteases concentrate in the nucleus of cells targeted for immune elimination, suggesting that nuclear processes are important targets. Here we used differential 2D proteomics of GzmA-treated nuclei to identify potential GzmA substrates. Of 44 candidates, 33 were RNA-binding proteins important in posttranscriptional RNA processing, including 14 heterogeneous nuclear ribonucleoproteins (hnRNP). Multiple hnRNPs were degraded in cells undergoing GzmA-, GzmB-, or caspase-mediated death. GzmA and caspase activation impaired nuclear export of newly synthesized RNA and disrupted pre-mRNA splicing. Expressing GzmA-resistant hnRNP A1 inhibited GzmA-mediated cell death and rescued pre-mRNA splicing, suggesting that hnRNP A1 is an important GzmA substrate. Cellular stresses are known to inhibit initiation of cap-dependent translation. Disrupting pre-mRNA processing should block further new protein synthesis and promote death by interfering with pathways induced to protect cells from death.

apoptosis | cytotoxic T lymphocyte

Killer lymphocytes deploy cytotoxic granule serine proteases to activate programmed cell death in cells targeted for immune elimination (1). Humans express five granzymes (Gzms), of which GzmA and GzmB are the most abundant and best characterized. GzmB activates the caspases and also directly cleaves some caspase substrates (2). GzmA induces caspase-independent programmed cell death, characterized by ssDNA damage and a unique pathway of mitochondrial damage without mitochondrial outer membrane permeabilization (3). GzmA and GzmB share few substrates. GzmA, a homodimer with tryptase activity, binds its substrates through an extended exosite and does not recognize a predictable cleavage site peptide (4). Thus, *in silico* methods cannot predict its substrates.

A key mitochondrial substrate was identified by proteomics of GzmA-treated mitochondria (5). This approach succeeded because a minimal Gzm concentration and incubation time were used to treat intact organelles in which potential substrates are in their native state. Although ~300 mitochondrial proteins were resolved, GzmA altered only a few. Thus, GzmA is a highly specific protease. Although hundreds of potential substrates have been identified by proteomics (6), only 14 GzmA substrates have been verified in GzmA-mediated cell death. Both Gzms concentrate in target-cell nuclei, suggesting that nuclear substrates are important. In fact, all but two validated intracellular GzmA substrates either are predominantly nuclear or move to the nucleus during oxidative stress [histones H1/H2B/H3, lamins A/B/C, PARP-1, Ku70, nucleolin (NUCL), SET, HMGB2, and APE1] (3).

To understand GzmA's nuclear function, we compared the proteome of isolated nuclei before and after GzmA treatment. Forty-four candidate substrates were identified, of which 33 are RNA-binding proteins that regulate mRNA processing. These RNA-binding proteins included 14 heterogeneous nuclear ribonucleoproteins (hnRNP) that assemble on nascent transcripts and participate in nearly all steps of mRNA maturation (7). Many hnRNPs are both GzmA and caspase substrates, cleaved during death by cytotoxic granules, death receptors, and cancer drugs. Thus, inactivating hnRNPs is a shared feature of programmed cell death. GzmA treatment or caspase activation, but not nonlethal oxidative stress, disrupted splicing and export of newly synthesized RNAs.

Results

Identification of Candidate Nuclear GzmA Substrates. We compared the proteome of isolated nuclei incubated with GzmA or buffer (Fig. 1 and Fig. S1). The GzmA concentration and incubation time used were the minimum needed to detect clearly cleavage of PARP-1 and lamins A/C, known substrates. Approximately 1,554 spots were resolved. Because the nuclear proteome comprises ~1,200–2,500 proteins, most nuclear proteins were resolved. Ninety-six spots were reduced by ≥10-fold in intensity by GzmA. Spots of similar apparent mass that might represent posttranslational modifications were grouped into 42 samples and analyzed by in gel digestion and mass spectrometry. Forty-four nuclear proteins, identified by at least three peptides, that had predicted molecular weight and isoelectric point (pI) similar to their migration were selected as candidates (Fig. 1, Table S1, and Dataset S1). The hits included previously described GzmA substrates, lamins A/B/C, and NUCL.

Thirty-three of 44 candidate proteins—a significant overrepresentation—participate in posttranscriptional regulation of RNA ($P = 1.8 \times 10^{-14}$; Ingenuity). These proteins included 14 of 24 hnRNP proteins (A0, A1, A2/B1, A3, C1/C2, C-like 1, D, G, L, M, Q, and U). hnRNPs assemble on nascent transcripts to regulate RNA processing and nuclear export. The list also included other RNA-binding proteins, including the mRNA-splicing and -processing protein SF2/ASF-1 (SFRS1), proteins involved in biogenesis of nucleoli and ribosomes, including nucleolin (NUCL) and nucleophosmin (NPM1), and mRNA export proteins. A protein interaction network of the candidate substrates was constructed, which confirmed the enrichment for RNA-processing proteins and suggested that GzmA may target multiple proteins within some complexes (Fig. 1). Besides hnRNP complexes, multiple hits were in the Drosha complex (DDX5, DDX17, hnRNP M, and hnRNP D) (8) and in NUCL complexes with hnRNP D or NPM1. Thus, GzmA may interfere with RNA processing.

GzmA Cleaves Multiple hnRNPs. We verified that GzmA cleaves multiple hnRNP family members. Nuclei treated with GzmA, catalytically inactive GzmA (S-AGzmA), or GzmB were analyzed by immunoblot for some hnRNP proteins (Fig. 2 *A* and *B*). hnRNP A1, A2/B1, C1/C2, and U were all cleaved by GzmA with kinetics similar to those of PARP-1 in a dose- and time-dependent

Author contributions: D.K.R., M.W., D.M., M.P.T., and J.L. designed research; D.K.R., M.W., D.M., and M.P.T. performed research; D.K.R., M.W., D.M., M.P.T., and J.L. analyzed data; and D.K.R., M.W., and J.L. wrote the paper.

The authors declare no conflict of interest.

This article is a PNAS Direct Submission.

[1]D.K.R. and M.W. contributed equally to this work.

[2]Present address: Department of Cell Physiology and Metabolism, Centre Medical Universitaire, University of Geneva, 1204 Geneva, Switzerland.

[3]To whom correspondence should be addressed. E-mail: lieberman@idi.harvard.edu.

This article contains supporting information online at www.pnas.org/lookup/suppl/doi:10.1073/pnas.1201327109/-/DCSupplemental.

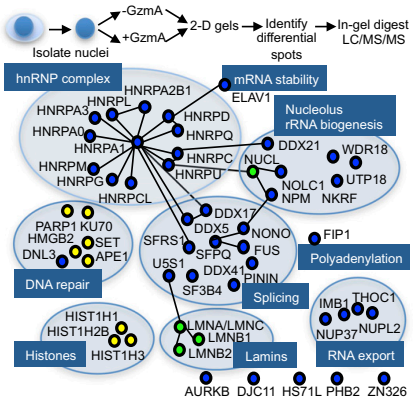

Fig. 1. Identification of candidate nuclear GzmA substrates. K562 nuclei were treated with 1 μM GzmA or buffer for 30 min at 37 °C, and nuclear proteins were resolved using 2D gel electrophoresis and visualized by silver staining. Spots that changed in intensity at least 10-fold after GzmA treatment were grouped into 42 spots that migrated with similar apparent molecular weight and were analyzed by mass spectrometry. Forty-four GzmA candidate nuclear substrates (Table S1 and Dataset S1) were analyzed by Ingenuity software for known protein–protein interactions. Proteins with similar functions that are not annotated as interacting were added. Previously unknown targets are in blue, previously validated substrates that scored as hits are indicated in green, and those not scored as hits are in yellow.

manner, as indicated by either a stable cleavage product or decreased intensity of the full-length protein. S-AGzmA had no effect. hnRNPs C1/C2, and U, but not A1 and A2/B1, also were cleaved by GzmB. Another proteomics hit, Nono/p54nrb, was not a clear GzmA substrate; a slight mobility shift suggested it might be cleaved near one end, but this possibility was not pursued. GzmA also cleaved all analyzed hnRNPs within hnRNP complexes immunopurified from HeLa nuclei using hnRNP C1/C2 or A1 antibodies (Fig. S2*A*).

To determine whether hnRNPs are physiologically relevant targets, we evaluated their cleavage in K562 cells treated with perforin (PFN) and Gzms (Fig. 2*C*). hnRNPs A1 and A2/B1 were cleaved by GzmA in intact cells with dose and time dependency similar to that of the known substrate SET. However, the cleavage fragments were labile and were not detected in whole cells. In contrast to treatment of isolated nuclei (Fig. 2*B*), GzmB and PFN treatment of intact cells led to hnRNP A1 and A2/B1 cleavage, confirming previous proteomics studies (9–16) suggesting that these hnRNPs might be caspase targets. When cells were treated with PFN and GzmB in the presence of the pan-caspase inhibitor zVAD-fmk, hnRNP A1 remained unchanged, confirming that hnRNP A1 is not a direct GzmB target but is a caspase target (Fig. S2*B*). hnRNP A1 also was cleaved when NK-92 natural killer (NK) cells attacked 721.221 B cells (Fig. S2*C*). hnRNP A1 cleavage occurred, but was reduced, in the presence of zVAD. Thus, hnRNP A1 is a shared substrate of GzmA and activated caspases. In fact, all six validated hnRNPs (A1, A2/B1, C1/C2, and U) were cleaved in GzmB-treated cells. However, hnRNP C1/C2 and U were cleaved directly by GzmB and the caspases, whereas hnRNP A1 and A2/B1 were cleaved efficiently only via caspase activation (Fig. 2 *B* and *C* and Fig. S2*B*).

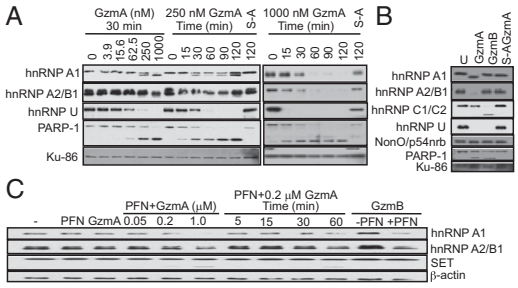

Fig. 2. GzmA cleaves multiple hnRNP proteins. (*A*) K562 nuclei were treated with increasing GzmA concentrations or with 250 or 1,000 nM GzmA for indicated times, and hnRNP cleavage was assessed by immunoblot. PARP-1 is a known GzmA substrate; Ku-86 was a loading control. S-A, inactive GzmA. (*B*) GzmA treatment of isolated K562 nuclei compared with GzmB. Treatment was with 1 μM Gzm for 1 h. U, untreated control. (*C*) K562 cells were treated with PFN and/or GzmA or GzmB at the indicated dose and time. hnRNP cleavage was assessed by immunoblot. Control samples were treated with buffer or with PFN only, GzmA only, or GzmB only for 1 h. SET is a known GzmA substrate (29); β-actin was a loading control. Blots are representative of at least three independent experiments.

hnRNPs Are Degraded During Caspase-Dependent Death. To investigate whether hnRNPs are degraded during caspase-mediated death, Jurkat cells were treated with anti-Fas or doxorubicin, and HeLa cells were treated with staurosporine (Fig. S3). A PARP-1 cleavage fragment was seen within 2 h after the addition of anti-Fas. hnRNP A1, C1/C2, and U levels also declined within 2–4 h of anti-Fas treatment. Cleavage was inhibited by zVAD-fmk. HMGB2, an abundant DNA-binding protein, was an uncleaved control. Doxorubicin, which induced apoptosis more slowly, based on PARP-1 cleavage and procaspase-3 disappearance, also led to caspase-dependent hnRNP A1 and C1/C2 cleavage and a decrease in hnRNP U. hnRNP A1, C1/C2, and U also were degraded in staurosporine-treated HeLa cells, roughly coincident with caspase activation. Thus, hnRNP degradation occurs in multiple apoptotic pathways.

GzmA Disrupts Export of Newly Synthesized RNA. Because cleavage of hnRNPs and other RNA-binding proteins might disrupt mRNA processing and nuclear export, we used immunofluorescence microscopy and a BrdU antibody that cross-reacts with BrU to assess the localization of newly synthesized BrU-labeled RNA in HeLa cells treated for 1 h with PFN and GzmA (Fig. 3).

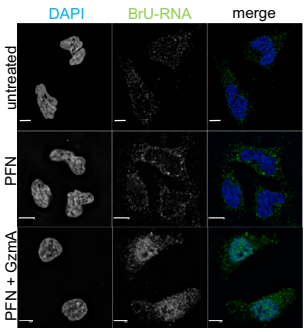

Fig. 3. GzmA causes nuclear retention of newly synthesized RNA. HeLa cells were labeled with BrU during treatment with PFN with or without 1 μM GzmA. Cells were fixed after 1 h and stained for BrdU, which also recognizes BrU (green), and DAPI (blue). Most newly synthesized RNA was retained in the nucleus after treatment with PFN and GzmA. Images are representative of three independent experiments. (Scale bars, 10 μm.)

IMMUNOLOGY

In untreated cells or in cells treated only with PFN, BrU-labeled RNA was mostly cytoplasmic, suggesting efficient processing and export. However, in cells treated with GzmA and PFN newly synthesized RNA was retained largely in the nucleus.

GzmA Disrupts Pre-mRNA Splicing. To investigate whether the RNA export defect was caused by deficient splicing and/or export, we designed primers to amplify spliced (primer pairs in adjacent exons), unspliced (primer pairs in adjacent exon and intron), and total (primer pairs within an exon) transcripts. We selected mRNAs (*MYC*, *FOS*, *DUSP5*, and *E2F1*) with short half-lives ($T_{1/2}$ ~10–90 min) to weight the analysis toward newly synthesized mRNAs. Nuclear and cytoplasmic RNA were isolated from untreated cells and from cells treated for 1 h with PFN and/or Gzms. Arsenite, which causes noncytotoxic oxidative stress, was a control noncytotoxic cellular stress that induced *FOS*, *DUSP5*, and *E2F1*. PFN- and GzmB-treated cells were analyzed with and without zVAD-fmk. Subcellular fractionation was verified by immunoblot for tubulin, which was not detected in the nuclear fractions. The ratio of spliced/unspliced RNA in each compartment was normalized to untreated cells. The ratios were not altered significantly by treatment with PFN alone or arsenite (Fig. 4*A*). However, splicing was sharply reduced (up to ~10-fold) for all four genes after treatment with PFN and either Gzm. The reduction in splicing after treatment with GzmA/PFN was significant for *MYC*, *FOS*, and *DUSP5*; a possible explanation for the lack of a significant reduction in *E2F1* may be that *E2F1* mRNA has the longest half-life. Caspase inhibition during GzmB treatment largely restored splicing to control levels. Thus, both GzmA and GzmB, the latter in a caspase-dependent manner, disrupted splicing of newly synthesized mRNAs.

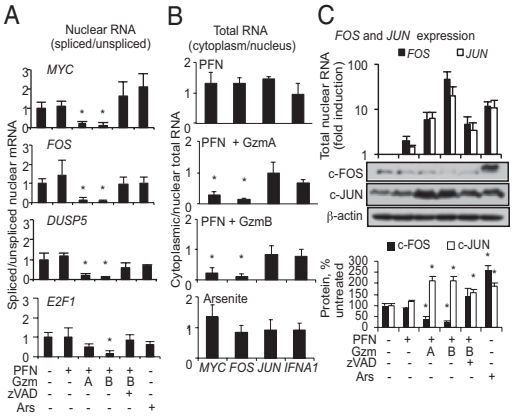

Fig. 4. GzmA interferes with mRNA splicing. (*A–C*) HeLa cells were untreated or treated with PFN and/or 0.5 μM GzmA or GzmB (± zVAD-fmk) or with arsenite (Ars) for 1 h before isolation of RNA from fractionated nuclei and cytoplasm. PCR primers were chosen to amplify unspliced, spliced, or total RNA. First, qRT-PCR results were normalized to *GAPDH*, and then the ratios were normalized to their value in untreated cells (ratio = 1). (*A*) Ratio of spliced:unspliced nuclear mRNA. (*B*) Ratio of cytoplasmic:nuclear total RNA for spliced genes (*MYC* and *FOS*) compared with intronless genes (*JUN* and *IFNA1*). Data are pooled from four independent experiments. Asterisks indicate a significant difference compared with untreated cells ($P < 0.05$). (*C*) *FOS* and *JUN* RNA was isolated from fractionated nuclei, and protein was extracted from whole-cell lysates. (*Top*) *FOS* and *JUN* transcripts (total RNA) were amplified by qRT-PCR normalized to *GAPDH* and then to expression in untreated cells. Both genes were significantly induced under all conditions. Data are mean ± SD of four independent experiments. (*Middle*) Protein expression was assessed by immunoblot with β-actin as loading control. (*Bottom*) Blots of four independent experiments were quantified by densitometry showing the intensity of the c-Fos or c-Jun band relative to the loading control (mean ± SEM percent of untreated cells; $*P < 0.05$).

Nuclear export of intron-containing transcripts requires splicing. The cytoplasm of untreated cells contained ~10–20 times more spliced mRNA for these genes than did the nuclear fractions. Thus, once splicing occurs, nuclear export is efficient. To assess whether defective RNA export was caused mostly by inefficient splicing and/or by inhibition of export, we next compared the ratio of cytoplasmic:nuclear total and spliced RNA, normalized to untreated cells, for *MYC* and *FOS* with the ratio for two intronless genes, *JUN* and *IFNA1*. As expected, *MYC* and *FOS* mRNA export was impaired severely in Gzm-treated cells, as compared with untreated cells or cells treated only with PFN or arsenite, but the export of *JUN* and *IFNA1* mRNA was not altered significantly (Fig. 4*B*). However, nuclear export of spliced *MYC*, *FOS*, *DUSP5*, and *E2F1* mRNAs, assessed by the cytoplasmic:nuclear spliced mRNA ratio, was unchanged (Fig. S4). Thus, spliced mRNAs were exported efficiently, and nuclear retention was caused by defective splicing.

FOS and *JUN* are induced by cellular stress. In fact, total *FOS* and *JUN* RNA increased ~eightfold within 1 h after the addition of GzmA and PFN and >30-fold with GzmB and PFN (Fig. 4*C*). *FOS* mRNA, which requires splicing, was not spliced or exported after treatment with PFN and either Gzm, whereas the export of intronless *JUN* mRNA was not impaired by the Gzms (Fig. 4*B*). Thus, we expected that c-FOS up-regulation would be blunted in cells undergoing programmed cell death but that c-JUN protein could be induced. Arsenite induced both c-JUN and c-FOS mRNA and protein (Fig. 4*C*). After treatment with Gzms and PFN, c-FOS protein declined in 1 h, as compared with levels in control cells, whereas c-JUN levels increased dramatically. Thus, induction of early-response proteins that orchestrate the cellular repair response probably is severely disrupted during programmed cell death only if their transcripts need splicing.

hnRNP A1 Cleavage Disrupts Its Nuclear Localization. We next focused on hnRNP A1, the best-studied hnRNP. An N-terminal GST-hnRNP A1 fusion protein was generated to identify GzmA cleavage sites. After purified GST-hnRNP A1 was treated with GzmA for 10 min, three N-terminal cleavage products were seen that increased with time as the full-length protein decreased (Fig. 5*A*). In-gel chymotryptic digestion and mass spectrometry identified R196, R232, and R284 as the cleavage sites. Site-directed mutagenesis of the three putative cleavage sites (R196/232/284A) protected mutant hnRNP from GzmA cleavage in vitro (Fig. S5*A*) and in transfected target cells treated with GzmA and PFN (Fig. 5*B*) or NK cells, provided zVAD-fmk was present (Fig. S2*C*). Thus, these three arginines are functional GzmA cleavage sites. hnRNP A1 has three RNA-binding domains, followed by a C-terminal noncanonical nuclear localization sequence (Fig. S5*B*). It shuttles between the nucleus and cytoplasm but is mostly nuclear. Cleavage at these sites would separate or disrupt the nuclear localization signal from the RNA-binding domains, likely disrupting hnRNP A1 nuclear localization. In fact, immunofluorescence microscopy (Fig. 5*C*) and immunoblot of cell fractions (Fig. 5*D*) showed that successive C-terminal truncations of N-terminal HA-tagged hnRNP A1 that would be produced by GzmA cleavage accumulated increasingly in the cytoplasm. Full-length HA-hnRNP A1, like endogenous hnRNP A1, was mostly nuclear (Fig. 5*E*). Moreover, endogenous hnRNP A1 redistributed toward the cytoplasm after GzmA and PFN treatment for 1 h (Fig. 5*E*). To verify that hnRNP A1 cleavage is responsible for its mislocalization, HeLa cells expressing WT or GzmA-uncleavable triple-mutant HA-hnRNP A1 were treated with PFN and GzmA and examined by immunofluorescence microscopy (Fig. S5*C*). In untreated cells, HA staining for both WT and mutant hnRNP A1 was exclusively nuclear. WT hnRNP A1 partly stained in the

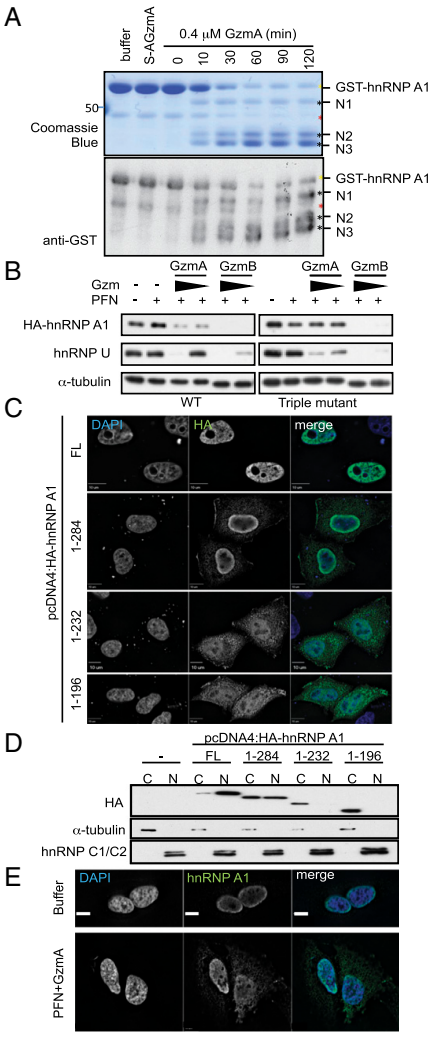

Fig. 5. GzmA cleaves hnRNP A1 after R196, R232, and R284, resulting in cytoplasmic mislocalization. (*A*) Recombinant purified GST-hnRNP A1 was treated with 0.4 μM GzmA or S-AGzmA and examined by Coomassie blue (*Upper*) or GST immunoblot (*Lower*). The GST tag was at the N terminus. Three N-terminal cleavage products (black asterisks) appear within 10 min. Yellow asterisk indicates full-length GST-hnRNP A1; red asterisk indicates a contaminating band. Mass spectrometry of excised bands indicated cleavage after R196, R232, and R284. (*B*) HeLa cells, expressing WT (*Left*) or GzmA-uncleavable mutant (*Right*) HA-hnRNP A1, were treated with PFN plus GzmA or GzmB (0.5 and 0.16 μM, respectively) for 1 h. HA-hnRNP A1 cleavage was assessed by immunoblot probed for HA. α–Tubulin was the loading control, and endogenous hnRNP U served as a cleavage control. WT HA-hnRNP A1 and endogenous hnRNP U were cleaved by both Gzms; mutant HA-hnRNP A1 was resistant to cleavage by GzmA but not by GzmB. (*C*) HeLa cells expressing full-length (FL) HA-hnRNP A1 or indicated truncations were stained with anti-HA (green) and DAPI (blue). (*D*) HeLa cells expressing GzmA-generated HA-hnRNP A1 truncations were separated into cytoplasmic (C) and nuclear (N) fractions, and HA-hnRNP A1 localization was assessed by anti-HA immunoblot. Tubulin and hnRNP C1/C2 are fractionation controls for the cytoplasm and nucleus, respectively. (*E*) Immunofluorescence localization of endogenous hnRNP A1. Untransfected HeLa cells were treated with buffer or PFN plus 1 μM GzmA for 1 h before staining for hnRNP A1 (green) and DAPI (blue). Blots and images are representative of at least three independent experiments.

cytoplasm after treatment with GzmA and PFN, but the GzmA-uncleavable mutant remained nuclear. Similar mislocalization of endogenous hnRNP A1 occurred within 2 h after the addition of staurosporine, increasing further after 3 h (Fig. S5*D*). Thus, both GzmA and caspases interfere with hnRNP A1 nuclear localization.

GzmA-Resistant hnRNP A1 Inhibits Death and Rescues Splicing. To determine whether hnRNP A1 cleavage is important during GzmA-mediated death, HeLa cells overexpressing WT or GzmA-resistant hnRNP A1 were treated with PFN and either Gzm and were evaluated by ^{51}Cr release assay (Fig. 6*A*) and annexin V/propidium iodide staining (Fig. 6*B*). Expression of triple-mutant hnRNP A1 rendered target cells more resistant to GzmA but equally sensitive to GzmB as cells expressing WT protein. Furthermore, GzmA-uncleavable hnRNP-A1 expression significantly restored *MYC*, *DUSP5*, and *FOS* splicing after GzmA treatment but did not affect their splicing after GzmB treatment (Fig. 6*C*). Thus, hnRNP A1 is an important GzmA substrate, because blocking its cleavage inhibits GzmA-mediated death and rescues splicing.

Discussion

The rapid concentration of Gzms in target cell nuclei motivated us to analyze changes in the proteome of GzmA-treated nuclei. Only 6% of protein spots changed after GzmA treatment, confirming GzmA's specificity. Notably, some abundant nuclear protein spots were unchanged. Treating proteins in intact nuclei likely reduced background that might occur in treating cell lysates. We identified 44 potential nuclear GzmA substrates, which included four previously known GzmA substrates (lamins and NUCL), but others (PARP-1, Ku70, Ape1, and histones) were missed. By setting a stringent criterion (10-fold less protein), we biased our hits toward key substrates at the price of reduced sensitivity. In fact, we were able to validate all the hits we examined experimentally (with the possible exception of Nono). Seventy-five percent of the candidate substrates, including 14 hnRNPs, are RNA-binding proteins that orchestrate posttranscriptional RNA processing. We verified that six of six hnRNPs examined were cleaved during GzmA-mediated death and also confirmed previous proteomics studies that suggested that these hnRNPs also are caspase targets (9–16).

Because RNA-binding proteins dominated our screen, we examined the effect of Gzms on RNA processing. A key common and unrecognized feature of caspase-independent and caspase-dependent programmed cell death is disruption of pre-mRNA splicing and nuclear export of newly synthesized RNA. At least 11 of the 44 candidate GzmA substrates, including hnRNP A1 and ASF1, have important roles in pre-mRNA splicing. Pre-mRNA levels of the early-response genes investigated in this study (*FOS*, *JUN*, *DUSP5*, *E2F1*, *MYC*, and *IFNA1*) increased by 7–50 fold within 1 h of treatment with either Gzm. Thus, transcription is unimpaired during the early stages of programmed cell death. However, because of impaired splicing, early-response proteins, whose mRNAs (like most mRNAs) require splicing, are not up-regulated. Inhibiting synthesis of cellular stress-response proteins, many of which have tightly regulated transcripts with short half-lives, likely interferes with cellular repair.

Disruption of pre-RNA splicing and RNA export is not a general feature of cellular stress, because, consistent with previous reports, it did not occur during nonapoptotic oxidative stress (17). Heat shock transiently interferes with pre-mRNA splicing of at least some genes (18). However, global changes in pre-RNA splicing and export of newly synthesized RNAs during

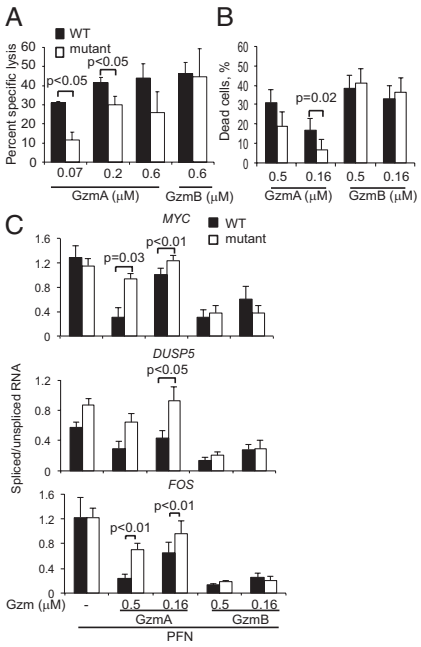

Fig. 6. Uncleavable hnRNP A1 rescues splicing and inhibits cell death. (*A–C*) HeLa cells stably expressing WT or GzmA-uncleavable mutant HA-hnRNP A1 were treated with PFN plus GzmA or GzmB. Death was monitored by a 4-h ^{51}Cr release assay (*A*) and annexin V/propidium iodide staining 1 h later for flow cytometry (*B*). Data in *A* show mean ± SD of three independent experiments of percent specific lysis after subtraction of percent specific lysis of control cells treated with PFN alone. Data in *B* show mean ± SEM of pooled data from six independent experiments. (*C*) RNA isolated from whole cells 1 h after treatment was analyzed by qRT-PCR to compare spliced/unspliced total cellular RNA. The ratio was normalized to untreated cells. Data are mean ± SEM of five independent experiments. In all panels, statistical differences between WT and mutant hnRNP A1-expressing cells were calculated using a paired Student's *t* test.

apoptosis have not been reported previously. Caspase activation, and cellular stress more generally, disrupts translation initiation. This disruption is accomplished by caspase cleavage of eIF4G, eIF2α, and other initiation factors only during apoptosis and by phosphorylation of eIF2α by a variety of stress-induced kinases during both stress and apoptosis (19). Because translation uses about half of the cell's energy consumption, global inhibition of translation husbands resources at times of stress. However, some mRNAs, especially cap-independent transcripts whose products may help the cell survive stress and apoptosis, overcome this block. During stress there are shifts from cap-dependent to internal ribosome entry site (IRES)-dependent translation and toward alternative splicing, especially of mRNAs for genes such as *bcl-X*$_L$, whose splice variants often play opposing roles in cell survival (20). Alternative splicing is regulated by SFRS1/ASF1 and hnRNP A1 binding to exonic sites to enhance or inhibit, respectively, binding of U2AF and the U2 small nucleotide ribonucleoprotein to the 3′ splice site (21). Both ASF1 and hnRNP A1 were hits in our screen for GzmA nuclear substrates, although we did not confirm that ASF1 is a bona fide target, and ASF1 is not a known caspase substrate. Alternative pre-mRNA splicing occurs early in caspase-mediated death (22). Future studies are needed to compare splice-site selection during caspase-independent and -dependent programmed cell death and to examine the role of hnRNP A1 and ASF1 cleavage in this process. The relative efficiency of cleavage of hnRNP A1 and/or ASF1 may influence the ratio of the splice variants that get made. Changes in alternative splicing might play a more important role in more protracted forms of apoptosis (such as following UV irradiation or chemotherapy) than in the relatively rapid Gzm-induced cell death.

Impaired RNA processing should synergize with the inhibition of translation to block de novo protein synthesis even of mRNAs that bypass the stress-induced block in cap-dependent translation initiation. If a target cell is unable to synthesize new proteins, it will be crippled in repairing cellular damage instigated by death stimuli. In previous studies we significantly reduced GzmA-mediated death by overexpressing noncleavable forms of key substrates, including Ape1, Ndufs3, PARP1, and Ku70 (3). These experiments work—perhaps surprisingly—because inducing cell death is not an all-or-none process: Programmed cell death disrupts multiple cellular pathways that together overcome cellular repair. Indeed, GzmA-noncleavable hnRNP A1, which rescued splicing, rendered cells significantly more resistant to GzmA-mediated death. hnRNP A1, one of the most abundant nuclear proteins, binds to nascent transcripts as soon as they are transcribed and remains bound during their nuclear export (23). It regulates both cap-dependent and IRES-mediated translation. It also is implicated in ribosomal RNA (rRNA) processing, which potentially could interfere with the translation of unspliced mRNAs and those intron-containing mRNAs that succeed in getting spliced and exported. Because of its central role in RNA processing, it is perhaps not surprising that hnRNP A1 on its own is a physiologically important GzmA target.

In some stresses, hnRNP A1 is phosphorylated by MAPK p38 and translocates to the cytoplasm (24). The cytoplasmic translocation of hnRNP A1 we observed following GzmA and staurosporine treatment could result from hnRNP A1 cleavage and/or stress-induced phosphorylation. However, cleavage is likely the dominant mechanism behind mislocalization, at least for GzmA, because the noncleavable mutant retained its nuclear localization. Expression of a phosphomimetic mutant of hnRNPA1 that localizes to the cytoplasm activates caspase 3. The proapoptotic effect of hnRNP A1 cleavage may have been partly the result of its cytoplasmic mislocalization.

Although multiple proteins involved in mRNA export are candidate GzmA targets (Fig. 1), mRNA export or protein expression of an unspliced immediate early gene product (c-JUN) was not inhibited in Gzm-treated cells. Further study is needed to assess if and when candidate proteins involved in RNA export are cleaved during programmed cell death and whether their cleavage affects export. Export may be impaired at times later than we analyzed. The list of candidate GzmA substrates also included RNA-binding proteins that affect synthesis and processing of rRNAs (which make up ~80% of cellular RNA) and microRNAs. Because newly synthesized RNA overall was retained globally in the nucleus after treatment with GzmA and PFN, the processing of other classes of RNAs, especially abundant rRNAs and tRNAs, is disturbed during apoptosis. Our identification of four proteins in the large Drosha complex as potential GzmA substrates suggests that microRNA processing is impaired also. High-throughput sequencing of nuclear and cytoplasmic RNAs or of newly synthesized RNAs in cells undergoing programmed cell death should help assess the effects of distinct programmed cell death pathways on all steps of RNA processing.

The SET complex, which contains three GzmA substrates (SET, HMGB2, and APE1) and is responsible for GzmA-mediated DNA damage, was the first recognized example of a programmed cell death protease targeting multiple substrates within the same complex (3). However, cleavage of multiple components of a multiprotein complex, as we found here for the hnRNPs, may be a more common phenomenon. Activated caspases also cleave

multiple proteins in the N-CoR/SMRT complex (13). GzmA and the caspases may cleave multiple components of a complex, such as the hnRNP complexes, because they are dimers: While one monomer is attacking one component in the complex, the other monomer may be well positioned to attack another.

Most previously identified GzmA substrates are unique to caspase-independent death. The two substrates shared with the caspases, PARP-1 and lamin B, illustrate processes that might need to be disrupted for programmed cell death and for avoiding necrosis. For example, failure to inactivate PARP-1 depletes cellular ATP, needed for programmed death (25, 26). Lamin cleavage may be needed to disrupt the nuclear envelope. In some cases the same pathways are disrupted but by targeting different proteins. For example, the repair of dsDNA breaks is inhibited by GzmA by targeting Ku70 and by the caspases by cleaving DNA-PK_{cs} (27, 28). The identification of multiple hnRNP proteins as shared targets of both GzmA and the caspases suggests that inhibiting mRNA processing is another critical feature of programmed cell death. It will be of interest to identify how many of the GzmA candidate targets are shared targets with GzmB and/or the caspases and whether other posttranscriptional RNA processing proteins are targeted during apoptosis.

Materials and Methods

Isolated nuclei were treated with GzmA or buffer and were analyzed by 2D SDS/PAGE isoelectric focusing gels, and candidate GzmA substrates were identified by mass spectrometry. Candidates were validated by immunoblot and shown to be cleaved during immune-mediated death. Changes in RNA splicing and cellular localization were followed by immunofluorescence microscopy and quantitative RT-PCR (qRT-PCR). Details are available in *SI Materials and Methods*.

ACKNOWLEDGMENTS. We thank Gideon Dreyfuss for hnRNP antibodies and Arlene Sharpe, Paul Anderson, Tom Kirchhausen, Melissa Moore and members of the J.L. laboratory for helpful discussions. This work was supported by National Science Foundation predoctoral fellowships (to D.K.R. and M.P.T.), a Kurt und Senta Herrmann-Foundation fellowship (to M.W.), and National Institutes of Health Grant AI45587 (to J.L.).

1. Chowdhury D, Lieberman J (2008) Death by a thousand cuts: Granzyme pathways of programmed cell death. *Annu Rev Immunol* 26:389–420.
2. Lord SJ, Rajotte RV, Korbutt GS, Bleackley RC (2003) Granzyme B: A natural born killer. *Immunol Rev* 193:31–38.
3. Lieberman J (2010) Granzyme A activates another way to die. *Immunol Rev* 235: 93–104.
4. Hink-Schauer C, Estébanez-Perpiñá E, Kurschus FC, Bode W, Jenne DE (2003) Crystal structure of the apoptosis-inducing human granzyme A dimer. *Nat Struct Biol* 10: 535–540.
5. Martinvalet D, Dykxhoorn DM, Ferrini R, Lieberman J (2008) Granzyme A cleaves a mitochondrial complex I protein to initiate caspase-independent cell death. *Cell* 133: 681–692.
6. Van Damme P, et al. (2010) The substrate specificity profile of human granzyme A. *Biol Chem* 391:983–997.
7. Dreyfuss G, Kim VN, Kataoka N (2002) Messenger-RNA-binding proteins and the messages they carry. *Nat Rev Mol Cell Biol* 3:195–205.
8. Fukuda T, et al. (2007) DEAD-box RNA helicase subunits of the Drosha complex are required for processing of rRNA and a subset of microRNAs. *Nat Cell Biol* 9:604–611.
9. Waterhouse N, et al. (1996) Heteronuclear ribonucleoproteins C1 and C2, components of the spliceosome, are specific targets of interleukin 1beta-converting enzyme-like proteases in apoptosis. *J Biol Chem* 271:29335–29341.
10. Brockstedt E, et al. (1998) Identification of apoptosis-associated proteins in a human Burkitt lymphoma cell line. Cleavage of heterogeneous nuclear ribonucleoprotein A1 by caspase 3. *J Biol Chem* 273:28057–28064.
11. Thiede B, Dimmler C, Siejak F, Rudel T (2001) Predominant identification of RNA-binding proteins in Fas-induced apoptosis by proteome analysis. *J Biol Chem* 276: 26044–26050.
12. Thiede B, Siejak F, Dimmler C, Rudel T (2002) Prediction of translocation and cleavage of heterogeneous ribonuclear proteins and Rho guanine nucleotide dissociation inhibitor 2 during apoptosis by subcellular proteome analysis. *Proteomics* 2:996–1006.
13. Mahrus S, et al. (2008) Global sequencing of proteolytic cleavage sites in apoptosis by specific labeling of protein N termini. *Cell* 134:866–876.
14. Dix MM, Simon GM, Cravatt BF (2008) Global mapping of the topography and magnitude of proteolytic events in apoptosis. *Cell* 134:679–691.
15. Van Damme P, et al. (2005) Caspase-specific and nonspecific in vivo protein processing during Fas-induced apoptosis. *Nat Methods* 2:771–777.
16. Van Damme P, et al. (2010) Complementary positional proteomics for screening substrates of endo- and exoproteases. *Nat Methods* 7:512–515.
17. Bond U (1988) Heat shock but not other stress inducers leads to the disruption of a sub-set of snRNPs and inhibition of in vitro splicing in HeLa cells. *EMBO J* 7: 3509–3518.
18. Yost HJ, Lindquist S (1986) RNA splicing is interrupted by heat shock and is rescued by heat shock protein synthesis. *Cell* 45:185–193.
19. Holcik M, Sonenberg N (2005) Translational control in stress and apoptosis. *Nat Rev Mol Cell Biol* 6:318–327.
20. Biamonti G, Caceres JF (2009) Cellular stress and RNA splicing. *Trends Biochem Sci* 34: 146–153.
21. Mayeda A, Krainer AR (1992) Regulation of alternative pre-mRNA splicing by hnRNP A1 and splicing factor SF2. *Cell* 68:365–375.
22. Schwerk C, Schulze-Osthoff K (2005) Regulation of apoptosis by alternative pre-mRNA splicing. *Mol Cell* 19:1–13.
23. Dreyfuss G, Matunis MJ, Piñol-Roma S, Burd CG (1993) hnRNP proteins and the biogenesis of mRNA. *Annu Rev Biochem* 62:289–321.
24. Lewis SM, et al. (2007) Subcellular relocalization of a trans-acting factor regulates XIAP IRES-dependent translation. *Mol Biol Cell* 18:1302–1311.
25. Zhu P, et al. (2009) The cytotoxic T lymphocyte protease granzyme A cleaves and inactivates poly(adenosine 5′-diphosphate-ribose) polymerase-1. *Blood* 114: 1205–1216.
26. Herceg Z, Wang ZQ (1999) Failure of poly(ADP-ribose) polymerase cleavage by caspases leads to induction of necrosis and enhanced apoptosis. *Mol Cell Biol* 19: 5124–5133.
27. Zhu P, et al. (2006) Granzyme A, which causes single-stranded DNA damage, targets the double-strand break repair protein Ku70. *EMBO Rep* 7:431–437.
28. Casciola-Rosen L, et al. (1996) Apopain/CPP32 cleaves proteins that are essential for cellular repair: A fundamental principle of apoptotic death. *J Exp Med* 183: 1957–1964.
29. Beresford PJ, Kam CM, Powers JC, Lieberman J (1997) Recombinant human granzyme A binds to two putative HLA-associated proteins and cleaves one of them. *Proc Natl Acad Sci USA* 94:9285–9290.

Supporting Information

Rajani et al. 10.1073/pnas.1201327109

SI Materials and Methods

Cell Culture. HeLa, Jurkat, K562, 721.221, and NK-92(MI) cells were obtained from ATCC. HeLa cells were maintained in DMEM plus 10% (vol/vol) heat-inactivated FCS plus supplement (100 U/mL penicillin G, 100 μg/mL streptomycin sulfate, 6 mM Hepes-free acid, 1.6 mM L-glutamine, 50 μM β-mercaptoethanol) (D10). Jurkat, 721.221, and K562 cells were maintained in RPMI-1640 plus 10% (vol/vol) heat-inactivated FCS with supplement (K10). NK-92(MI) cells were maintained in RPMI-1640 plus 10% (vol/vol) heat-inactivated human AB serum plus supplement.

Reagents/Antibodies. The following antibodies were used for immunoblotting and/or immunofluorescence: mouse antibodies to β-actin (JLA20; EMD Bioscience; 1/1,000), caspase 3 (3G2; Cell Signaling Technology; 1/1,000), heterogeneous nuclear ribonucleoprotein (hnRNP) A1 (4B10; Sigma; 1/5,000 for Western blotting; 1/2,000 for immunofluorescence), hnRNP A2/B1 (DP3B3; Sigma; 1/2,000), hnRNP C1/C2 (4F4; Sigma 1/5,000), hnRNP U (3G6; Santa Cruz Biotechnology; 1/1,000), lamin A/C (BD Biosciences; 1/1,000), tubulin-α (B5-1–2; Sigma; 1/5,000), and c-Fos (2G9C3; Abcam; 1/2,000); rat antisera to HA (3F10; Roche; 1/2,000) and BrdU (BU1/75; Abcam; 1/500); rabbit antisera to PARP-1/2 (H-250; Santa Cruz Biotechnology; 1/1,000), SET [Lieberman antibody (1); 1/1000], and c-Jun (Santa Cruz Biotechnology; 1/1,000); goat antisera to GST (GE; 1/2,000) and Ku80 (Santa Cruz Biotechnology; 1/1,000). Secondary antibodies were sheep anti–mouse-HRP (GE; 1/2,000), donkey anti-rabbit-HRP (GE, 1/2000), donkey anti-goat-HRP (Santa Cruz Biotechnology, 1/1,000), donkey anti–rat-HRP (Zymed; 1/2,000), donkey anti–mouse-488 (Invitrogen; 1/5,000), donkey anti-mouse-647 (Invitrogen; 1/2,000), donkey anti–rat-488 (Invitrogen; 1/5,000). Rabbit anti-mouse IgG (Jackson Immunoresearch), mouse IgG (Jackson Immunoresearch), and protein A-agarose beads (Roche) were used for immunoprecipitation. Mouse anti-Fas (CH11; Immunotech) was used at 1 μg/mL final concentration. Doxorubicin hydrochloride was from Fluka. zVAD-fmk was from Calbiochem. Recombinant granzyme A (GzmA) and catalytically inactive granzyme A (S-AGzmA) were purified from *Escherichia coli* as previously described (1, 2). Native granzyme B (GzmB) was purified from YT-Indy natural killer (NK) cells as previously described (3). Native rat PFN was purified from ascites fluid as previously described (1). Recombinant granzymes (Gzms) generated in a recently introduced mammalian expression system for high-yield protein (4) were used in experiments in Fig. 5 and Figs. S2*C* and S5. Briefly, GzmA or GzmB cDNA was cloned into pHLseq (kind gift of Yvonne Jones, University of Oxford, Oxford, UK) at the AgeI and KpnI sites using the forward primers 5′GAAACCGGTGACGACGACGACAAGATTATTGGAGGAAATGAA for GzmA and 5′GAAACCGGTGACGACGACGACAAGATCATCGGGGGACATGAG for GzmB (introducing enterokinase sites before the N terminus of the active proteases) and the reverse primers 5′GTGCTTGGTACCAACTGCTCCCTTGATAGTCATAAT for GzmA and 5′GTGCTTGGTACCGTAGCGTTTCATGGTTTTCTT for GzmB. The plasmid was transfected into 293T cells by calcium phosphate precipitation. The transfected cells were grown in serum-free medium (ExCell 293; Sigma) for 4 d. Recombinant protein in culture supernatants was purified by immobilized metal affinity chromatography using Nickel-NTA (Qiagen) following the manufacturer's instructions. Eluted granzymes were treated with enterokinase (0.05 IU/mL supernatant) (Sigma) for 16 h at room temperature. Active Gzms were purified on an S column, concentrated, and quality tested as previously described (5).

Cell Fractionation. K562 cells, maintained in exponential phase, were harvested by centrifugation at 400 × *g* for 10 min. The cell pellet was washed 3× in PBS, resuspended in 5× pellet volume of Buffer A [10 mM Tris (pH 7.9), 1.5 mM $MgCl_2$, 10 mM KCl, 0.2 mM EDTA], and incubated on ice for 30 min. Cells were disrupted (as monitored by trypan blue staining) by three strokes of a Dounce homogenizer on ice, and intact cells were pelleted by centrifugation (100 × *g*, 30 s, 4 °C). The supernatant then was centrifuged at 16,000 × *g* for 1 min at 4 °C. The nuclear pellet was washed 3× with 5 mL cold Buffer A, centrifuged at 16,000 × *g* for 30 s, and resuspended in 0.5–1 mL PBS plus 1 mM $MgCl_2$ (PBS+Mg). Cytosolic supernatant was clarified further by centrifugation at 16,000 × *g* for 10 min to remove organelles and insoluble material. Protein content was determined using the Pierce BCA Assay. HeLa cells, transfected 18 h earlier in six-well tissue-culture plates using 2 μg DNA and 5 μL Lipofectamine 2000 (Invitrogen), were washed three times in PBS before fractionation according to ref. 6. Two micrograms of total protein were resolved per lane by SDS/PAGE. After Gzm and PFN treatment, HeLa cells were harvested by centrifugation at 400 × *g* for 3 min at 4 °C. The cell pellet was resuspended gently in 150 μL RNase-free fractionation buffer (PARIS Kit; Ambion) and kept on ice for 5 min. Nuclei were pelleted by spinning at 500 × *g* for 3 min at 4 °C. The nuclear pellet was resuspended in 125 μL fractionation buffer and centrifuged immediately at 500 × *g* for 1 min at 4 °C. After 25 μL was saved for SDS/PAGE analysis to confirm the fractionation, the pooled supernatant was mixed with 750 μL TRIzol-LS (Invitrogen). The nuclear pellet was resuspended in 250 μL disruption buffer (PARIS Kit) and mixed with 750 μL TRIzol-LS after samples were saved for protein analysis.

Two-Dimensional Electrophoresis Sample Preparation. Whole K562 nuclei (1–3 mg protein equivalents), suspended in PBS+Mg to a final concentration of 0.5 mg/mL, were left untreated or treated with 1 μM GzmA for 30 min at 37 °C. Reactions were stopped by adding 1 mM PMSF. Nuclei then were treated with 300 U/mL Benzonase (Sigma) for 30 min at room temperature. Nuclease activity was quenched by adding 10 mM EDTA for 5 min at room temperature. Nuclei then were harvested by centrifugation at 16,000 × *g* for 30 s at 4 °C, solubilized in 200–400 μL of 2D solubilization buffer [4% (wt/vol) CHAPS, 7 M urea, 2 M thiourea], and incubated on ice for 30 min before pulse sonication for 3 s using a Misonix S-4000 sonicator set to 30% maximum. Insoluble material was pelleted by Eppendorf microfuge Model 5415D at top speed for 30 min at room temperature. The supernatant was harvested, and protein was precipitated using the 2D Clean-up Kit (GE). Pellets were air dried before resuspension in 100 μL 2D solubilization buffer followed by incubation at 37 °C overnight. Protein concentration was determined using the RcDc Assay (Bio-Rad).

Two-Dimensional Gel Electrophoresis. Two hundred fifty micrograms of protein were diluted in 300 μL solubilization buffer containing 40 mM DTT and 0.2% carrier ampholytes (pH 3–10) (Bio-Rad). Samples were actively loaded under 50-μA current onto pH 3–10 nonlinear 17-cm ReadyStrip immobilized pH gradient strips (Bio-Rad) at 20 °C for 24 h. After 1 h hydration, strips were overlaid with mineral oil. After hydration was complete, strips were blotted with distilled water and placed in

a clean focusing tray with water-wetted electrode wicks in place. After mineral oil was layered on top of the strip, the focusing program was initiated (step 1: 250 V, linear slope, 1 h; step 2: 500 V, rapid slope, 1 h; step 3: 8,000 V, rapid slope, 60,000 Vh; 50 μA limit/gel) using a Bio-Rad Protean isoelectric focusing cell. After isoelectric focusing, strips were reduced in 2D equilibration Buffer 1 [6 M urea, 375 mM Tris (pH 7.4), 2% (wt/vol) SDS, 2% (vol/vol) glycerol, 10 mg/mL DTT] for 10 min at room temperature. Buffer 1 was exchanged for Buffer 2 [6 M urea, 375 mM Tris (pH 7.4), 2% (wt/vol) SDS, 2% (vol/vol) glycerol, 25 mg/mL iodoacetamide] for 10 min at room temperature. Strips were cleaned in 1× TGS [25 mM Tris (pH 8.6), 192 mM glycine, 0.1% SDS] before casting on top of a 17-cm 10% (wt/vol) PAGE gel with a 5% (wt/vol) polyacrylamide stacking gel. Focusing strips and molecular-weight markers (Bio-Rad) were cast in low-melt agarose with bromophenol blue (Bio-Rad) and placed at 4 °C until set, about 5 min. Second-dimension electrophoresis was performed at 150 V until the dye front was less than 0.5 cm from gel bottom. Gels were uncast and were silver stained using the SilverQuest staining kit (Invitrogen) using 200 mL solution per gel per staining step.

Two-Dimensional Gel Image Analysis and Mass Spectrometry. Silver-stained gels were scanned, and images were analyzed using RedFin Image analysis software (Ludesi). Spots that decreased at least 10-fold after GzmA treatment were chosen as hits if they matched unambiguously, based on nearby spots, and had a minimal volume of 100 in the untreated sample. Additional negatively stained spots (negative volume by RedFin) were added manually based on visual analysis of decreased volume after GzmA treatment. Chosen spots were excised, trypsin-digested in gel, and then analyzed on a nanoscale reverse-phase HPLC by electrospray ionization and LTQ linear ion-trap mass spectrometry at the Taplin Biological Mass Spectrometry Facility, Harvard Medical School.

GzmA Treatment of Intact Nuclei. Small-scale treatments were performed as above using 0.5 mg/mL protein equivalents of nuclei in PBS+Mg with the indicated dose of GzmA for the indicated time at 37 °C. Reactions were stopped by adding 10 mM PMSF and 5× SDS loading buffer and boiling for 5 min.

Gzm and Perforin Treatment. K562 cells (5×10^4) or HeLa cells (2×10^5) in cell buffer (10 mM Hepes, 4 mM $CaCl_2$, 0.4% BSA in HBSS) were treated for the indicated time at 37 °C with a sublytic concentration of rat perforin (PFN) (defined as the concentration that causes 5–15% cell death by propidium iodide staining in the absence of Gzms) and the indicated GzmA or GzmB concentration [prediluted in PFN buffer (10 mM Hepes in HBSS)]. Reactions were stopped by boiling in 5× SDS loading buffer or by transfer to 4 °C before nuclear/cytoplasmic fractionation. Samples were resolved by SDS/PAGE and immunoblot. For caspase inhibition, cells were preincubated with 75 μM of zVAD-fmk in loading buffer before Gzms and PFN were added. To assess cell death, 2×10^4 cells were labeled with ^{51}Cr, and ^{51}Cr release was assessed after 4 h or were stained with annexin V and propidium iodide and analyzed 1 h after treatment by flow cytometry as previously described (5). Dead cells were defined as annexin V-positive and/or propidium iodide-positive.

Cytotoxicity Assay. 721.221 cells (5×10^4) were coincubated with NK-92 cells at an effector:target ratio of 5:1 for 4 h at 37 °C. At indicated times, cells were harvested by centrifugation (250 × g for 3 min) before lysis on ice in RIPA buffer [50 mM Tris-HCl (pH 7.4), 150 mM NaCl, 1% Triton X-100, 1% sodium deoxycholate, 0.1% SDS, 1 mM EDTA]. After 5× SDS loading buffer was added, samples were boiled for 1 min and analyzed by SDS/PAGE and immunoblot.

Immunopurification of hnRNP Complexes. hnRNP complexes were purified as described (7). Immunoprecipitates were resuspended in 40 μL of 2× SDS sample buffer and analyzed by immunoblot or silver staining.

Caspase Activation. Jurkat cells (0.5×10^6/mL in K10) were treated with 1 μg/mL anti-Fas (CH11 mAb) or 1 μM doxorubicin in the presence or absence of 75 μM zVAD-fmk for the indicated time. HeLa cells were treated with 1 mM staurosporine for the indicated time. Cell death and caspase inhibition were verified by annexin V/propidium iodide staining. Cells were harvested and resuspended in RIPA buffer plus 5× sample loading buffer containing β-mercaptoethanol.

Recombinant hnRNP. hnRNP genes were amplified from HeLa cDNA using primers that added 5′-EcoRI and 3′-NotI restriction sites for insertion into pGEX-4T1 (GE). Insertions were verified by sequencing. GST-hnRNP fusion proteins were purified from BL21(DE3) *E. coli* according to the supplier's instructions. Protein purity was assessed by Coomassie blue staining of SDS/PAGE gels.

Cleavage Site Determination. GST-hnRNP A1 was treated with increasing doses of GzmA and resolved on SDS/PAGE gels stained with Coomassie blue. Bands corresponding to cleavage fragments were excised, in-gel digested with chymotrypsin, and analyzed by mass spectrometry to identify GzmA cleavage sites.

Construction of hnRNP A1 mutants. Site-directed mutagenesis introduced point mutations of R196, R232, and R284 to alanine using the following primers:

R196A forward: 5′CATCCAGCCAAAGAGGTGCAAGTGGTTCTGGAAAC
R196A reverse: 5′GTTTCCAGAACCACTTGCACCTCTTTGGCTGGATG
R232A forward: 5′GGCTTTGGTGGCAGCGCTGGTGGTGGTGGATATG
R232A reverse: 5′CATATCCACCACCACCAGCGCTGCCACCAAAGCC
R284A forward: 5′GGAAATTTTGGAGGCGCAAGCTCTGGCCCCTATGG
R284A reverse: 5′CCATAGGGGCCAGAGCTTGCGCCTCCAAAATTTCC

Mutant sequences then were PCR amplified to substitute an N-terminal HA epitope tag for GST. HA-hnRNP genes were cloned into the EcoRI and XhoI sites of pcDNA4/V5-His (Invitrogen) and pBABEpuro to obtain pBABEpuro-HA-hnRNP A1 WT or mutant. Retrovirus-containing supernatant was obtained by harvesting 293T cells 48 h after transfection with pBABEpuro-HA-hnRNP A1 (WT or mutant), pgagpol, and pMG2D. Insertions and mutations were confirmed by sequencing. To construct hnRNP A1 truncations from the pGEX4T1:hnRNP A1 WT template, an N-terminal HA tag, 5′ EcoRI restriction site, and 3′ stop codon and XhoI restriction site were added using PCR and the following primers:

HA-A1 forward:
5′ATGGAATTCATGTACCCCTACGACGTGCCCGACTACGCCCTCTAAGTCAGAGTCTCC
A1 FL reverse: 5′ATGCTCGAGTCAAAATCTTCTGCCACTGCC
A1(1-196) reverse: 5′ATGCTCGAGTCATCGACCTCTTTGGCTGG
A1(1-232) reverse: 5′ATGCTCGAGTCAACGGCTGCCACCAAAGCC
A1(1-284) reverse: 5′ATGCTCGAGTCATCTGCCTCCAAAATTTCC

HA-hnRNP genes were cloned into the EcoRI and XhoI sites of pcDNA4/V5-His (Invitrogen). Truncations were confirmed by sequencing.

Fluorescence Microscopy. HeLa cells were transfected on collagen-coated coverslips with 1 μg DNA using 3 μL FuGene (Roche). Cells were fixed 18 h posttransfection with 2% paraformaldehyde for 20 min at room temperature. Fixative was removed and replaced with 50 mM ammonium chloride in PBS for 20 min at room temperature. Cells were washed 3× with wash buffer (0.05% Triton X-100 in PBS) and then were permeabilized for 15 min at room temperature with Perm buffer (0.2% Triton X-100 in PBS). After blocking with 10% FCS in wash buffer for 30 min, slides were stained with primary antibodies for 1 h at room temperature in wash buffer. Cells were washed 3× before incubation with fluorophore-conjugated secondary antibodies for 1 h at room temperature in wash buffer. Cells were washed 3× before being mounted on glass slides using VectaShield mounting medium (Vector Laboratories) with DAPI. Image acquisition by epifluorescence microscopy was performed using an Axiovert 200M microscope, equipped with a 63× lens (Pan Apochromat, 1.4 NA; Carl Zeiss). Images were analyzed with SlideBook 4.2 (Intelligent Imaging Innovations Inc.) to generate 3D stacks of optical sections acquired 0.2 μm apart before nearest-neighbor deconvolution.

BrU Incorporation. HeLa cells grown overnight in D10 on collagen-coated coverslips were washed 3× with HBSS and placed in 100 μL cell buffer containing 2 mM bromouridine (Sigma) with 100 μL PFN buffer containing PFN and GzmA (final concentration, 1 μM). Cells were incubated for 30 min at room temperature before 300 μL cell buffer was added and were incubated at room temperature for an additional 30 min. Medium was aspirated, and cells were fixed with 2% paraformaldehyde and stained as above.

Quantitative RT-PCR. Total RNA was reverse transcribed using random hexamers and superscript III reverse transcriptase (Invitrogen). Quantitative RT-PCR (qRT-PCR) was performed in duplicate samples using SYBR Green FastMix (Quanta) on a BioRad CFX96. mRNA levels were normalized to *GAPDH*. Primers to amplify spliced mRNAs were chosen at neighboring exons separated by a large intron that would not be amplified unless the intervening intron was removed by splicing. Primers to amplify unspliced transcripts were chosen in an adjacent exon and intron. Primers to amplify total RNA were chosen within a single exon. The following primers were used:

MYC (spliced and unspliced) forward 5′GGAGGCTATTCTGCCCATTT
MYC (spliced) reverse 5′CACCGAGTCGTAGTCGAGGT
MYC (unspliced) reverse 5′GCATTCGACTCATCTCAGCA
MYC (total) forward 5′TTGCCGCATCCACGAAACTT
MYC (total) reverse 5′TGCAAGGAGAGCCTTTCAGA
FOS (spliced and unspliced) forward 5′TTGTGAAGACCATGACAGGAGG
FOS (spliced) reverse 5′TCCTTTCCCTTCGGATTCTCCT
FOS (unspliced) reverse 5′TTCCCAGGAAGAGTACGCTAGA
FOS (total) forward 5′TCCAGTGCCAACTTCATTCCCA
FOS (total) reverse 5′TGTCATGGTCTTCACAACGCCA
DUSP5 (spliced and unspliced) forward 5′AATGTCAGCTACAGGCCAGCTT
DUSP5 (spliced) reverse 5′AACTCGCACTTGGATGCATGGT
DUSP5 (unspliced) reverse 5′AGCCCAGAATACCACTCAGGAT
DUSP5 (total) forward 5′ATCCTGAGTGTTGCGTGGATGT
DUSP5 (total) reverse 5′AGCTGGCCTGTAGCTGACATTT
E2F1 (spliced and unspliced) forward 5′AGCTGGACCACCTGATGAAT
E2F1 (spliced) reverse 5′TGCAATGCTACGAAGGTCCTGA
E2F1 (unspliced) reverse 5′AATCCAAGCCTCTCTAGTCCCA
E2F1 (total) forward 5′TTGACCCAGGACCTCCGACAG
E2F1 (total) reverse 5′TGTCAGTGTCCTCGGAGAGCAG
JUN forward 5′TGCGTGCGCTCTTAGAGAAACT
JUN reverse 5′TCACGTGAGGTTAGTTTGGGCT
IFNA1 forward 5′ACCTTGATGCTCCTGGCACAAA
IFNA1 reverse 5′TGGTTGCCATCAAACTCCTCCT

1. Beresford PJ, Xia Z, Greenberg AH, Lieberman J (1999) Granzyme A loading induces rapid cytolysis and a novel form of DNA damage independently of caspase activation. *Immunity* 10:585–594.
2. Beresford PJ, et al. (2001) Granzyme A activates an endoplasmic reticulum-associated caspase-independent nuclease to induce single-stranded DNA nicks. *J Biol Chem* 276: 43285–43293.
3. Shi L, Yang X, Froelich CJ, Greenberg AH (2000) Purification and use of granzyme B. *Methods Enzymol* 322:125–143.
4. Aricescu AR, Lu W, Jones EY (2006) A time- and cost-efficient system for high-level protein production in mammalian cells. *Acta Crystallogr D Biol Crystallogr* 62:1243–1250.
5. Thiery J, Walch M, Jensen DK, Martinvalet D, Lieberman J (2010) Isolation of cytotoxic T cell and NK granules and purification of their effector proteins. *Curr Protoc Cell Biol* Chapter 3:Unit 3.37.
6. Mili S, Shu HJ, Zhao Y, Piñol-Roma S (2001) Distinct RNP complexes of shuttling hnRNP proteins with pre-mRNA and mRNA: Candidate intermediates in formation and export of mRNA. *Mol Cell Biol* 21:7307–7319.
7. Swanson MS, Dreyfuss G (1999) Preparation of heterogeneous nuclear ribonucleoprotein complexes. *Methods Mol Biol* 118:299–308.

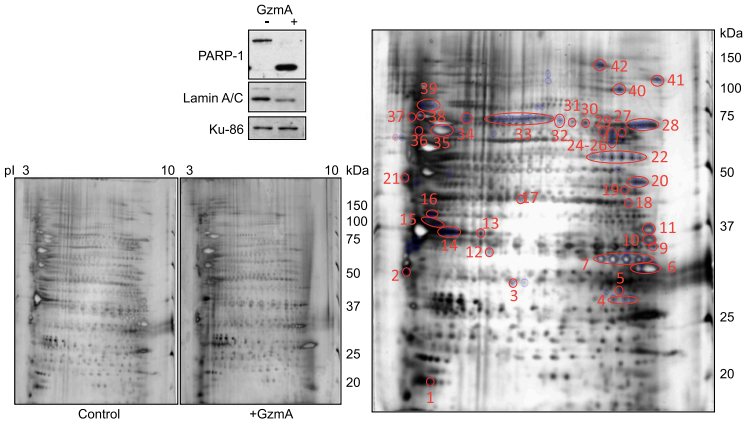

Fig. S1. Gels used to identify candidate nuclear GzmA substrates. K562 nuclei were treated with 1 μM GzmA or buffer for 30 min at 37 °C, and nuclear proteins were resolved using 2D gel electrophoresis and visualized by silver staining. GzmA nuclear activity was verified by assessing cleavage of known GzmA nuclear substrates, PARP-1, and lamin A/C, by immunoblot. Ku80, which is unaffected by GzmA, was used as a loading control. Most spots are unchanged by GzmA treatment. Spots that changed in intensity at least 10-fold after GzmA treatment were grouped into 42 spots that migrated with similar apparent molecular weight that were analyzed by mass spectrometry.

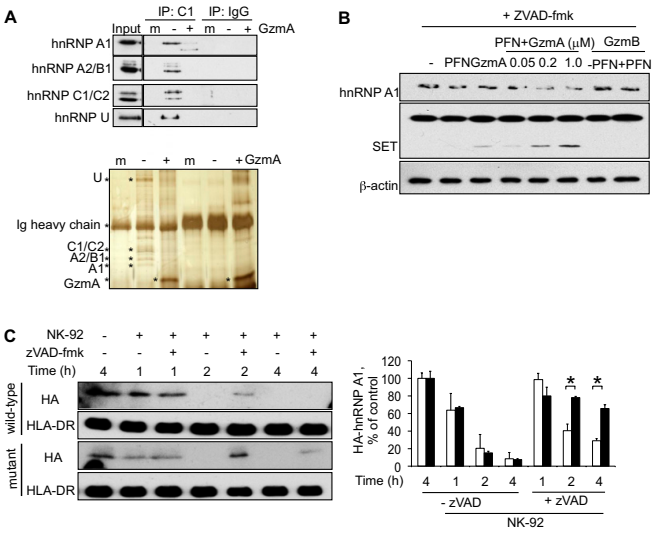

Fig. S2. GzmA cleaves multiple hnRNP proteins. (*A*) hnRNP complexes immunopurified from HeLa nuclei using anti-hnRNP C1/C2 monoclonal antibody or IgG control were mock treated or treated with 0.5 μM GzmA for 15 min at 37 °C, and protein degradation was monitored by immunoblot (*Upper*) or silver stain (*Lower*). The presumed identity of hnRNP species, Ig heavy chain, and GzmA are denoted with asterisks. m, immunoprecipitations performed without adding ("minus") nuclear lysates. Most hnRNP protein is degraded under these conditions. (*B*) K562 cells were treated with PFN and/or GzmA or GzmB at the indicated dose and time in the presence of zVAD-fmk to inhibit caspase activation. hnRNP A1 cleavage was assessed by immunoblot. Control samples were treated with buffer, PFN only, or GzmA only for 1 h. Caspase inhibition does not affect GzmA cleavage of hnRNP A1 but largely abrogates the effect of GzmB shown in Fig. 2C. SET is a known GzmA substrate (1); β-actin served as loading control. (*C*) (*Left*) 721.221B cells, transfected to express HA-tagged WT (*Upper*) or triple-mutant (*Lower*) hnRNP A1, were left untreated or treated with zVAD-fmk and coincubated with NK-92 cells at an effector cell:target cell (E:T) ratio of 5:1 for 1–4 h. hnRNP A1 cleavage was monitored by HA-immunoblot. HLA-DR served as a loading control. A representative blot is shown. (*Right*) Quantification by densitometry (mean± SEM, normalized to HLA-DR and then relative to untreated cells) of three independent experiments. Statistical differences between WT and mutant hnRNP A1-expressing cells were calculated using Student's *t* test (**P* < 0.05). In this experiment, which used an E:T ratio of 5:1, hnRNP A1 cleavage in the target cell was assessed by HA-tag immunoblot of exogenously expressed HA-tagged hnRNP A1. HA-tagged hnRNP A1 became undetectable within 2 h of natural killer cell incubation unless zVAD-fmk was added to inhibit caspase activation. HA-hnRNP A1 levels declined significantly even in the presence of caspase inhibition, suggesting that both caspase-dependent and -independent cleavage of hnRNP A1 occurred.

1. Beresford PJ, Kam CM, Powers JC, Lieberman J (1997) Recombinant human granzyme A binds to two putative HLA-associated proteins and cleaves one of them. *Proc Natl Acad Sci USA* 94:9285–9290.

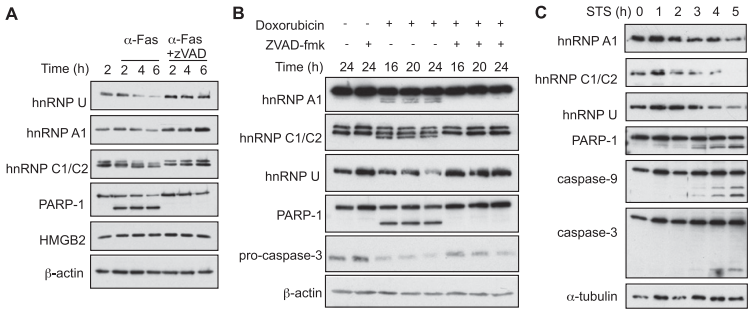

Fig. S3. Multiple hnRNPs are degraded during caspase-mediated apoptosis. Jurkat cells were treated with Fas antibody (*A*) or doxorubicin (*B*) for the indicated time in the absence or presence of zVAD-fmk. (*C*) HeLa cells were treated with staurosporine (STS) for the time indicated. hnRNP degradation was monitored by immunoblot. PARP-1 (a known caspase substrate) and procaspase-3/9 processing were monitored for caspase activation. β-Actin and tubulin served as loading controls.

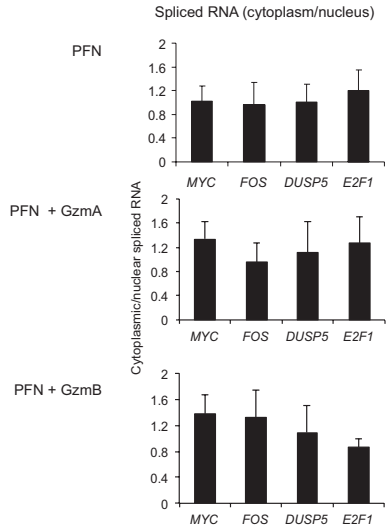

Fig. S4. Newly synthesized RNA that is spliced is exported from the nucleus efficiently during Gzm-mediated cell death. HeLa cells were left untreated or treated with PFN and/or 0.5 μM GzmA or GzmB for 1 h before RNA isolation from fractionated nuclei and cytoplasm. PCR primers were chosen to amplify unspliced, spliced, or total RNA. qRT-PCR results first were normalized to *GAPDH,* and then the ratios were normalized to their value in untreated cells. The ratio of cytoplasmic:nuclear spliced RNA is shown. The data shown are mean ± SD from four independent experiments. There was no significant difference in nuclear export of spliced RNA after Gzm treatment.

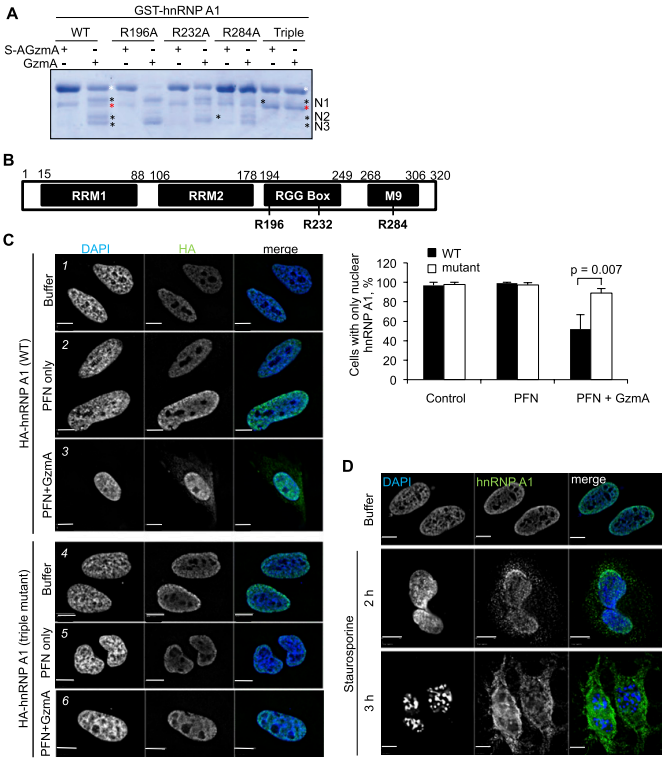

Fig. S5. GzmA cleaves hnRNP A1 after R196, R232, and R284, resulting in mislocalization to the cytoplasm. (*A*) Recombinant purified GST-hnRNP A1 (GST was added to the N terminus) was treated with 0.4 μM GzmA or S-AGzmA for 30 min at 37 °C and examined by Coomassie blue staining. Three N-terminal cleavage products (black asterisks) appear within 10 min. Yellow asterisk indicates full-length GST-hnRNP A1; red asterisk indicates a contaminating band. Peptide sequencing of these N-terminal fragments after in-gel chymotrypsin digestion identified cleavage after R196, R232, and R284. Single-point mutants (R196A, R232A, or R284A) and a triple-point mutant (R196/232/284A) of GST-hnRNP A1 also were treated with GzmA or S-AGzmA. The triple mutant was resistant to GzmA. (*B*) Domain structure of hnRNP A1 indicating GzmA cleavage sites. M9, nuclear localization signal; RGG, Arg-Gly-Gly–rich region; RRM, RNA recognition motif. (*C*) (*Left*) HeLa cells transfected with WT (panels 1–3) or uncleavable mutant (panels 4–6) of HA-hnRNP A1 were treated with buffer, PFN, and/or 1 μM GzmA for 1 h and stained for HA (green) and DAPI (blue). (Scale bars, 10 μm.) (*Right*) Quantitative analysis of proportion of cells without detectable cytoplasmic HA-hnRNP A1. Data shown are mean ± SD for three independent experiments. (*D*) Immunofluorescence localization of endogenous hnRNP A1 after staurosporine treatment. Untransfected HeLa cells were treated with 1 μM staurosporine for the indicated time and stained for hnRNP A1 (green) and DAPI (blue).

Table S1. GzmA candidate nuclear substrates identified by 2D differential proteomics

Name	Other names	MW	pI	Spot	Spot MW/pI	Peptides	% coverage
AURKB	Aurora/IPL1-related kinase 2	39.3	9.4	11	37.8/9	9	24.1
DCJ11	DNAJ homolog subfamily c member 11	63.3	8.5	25	69.2/7.5	3	6.4
DDX17	p72	72.4	8.8	23	68.7/8	10	13.2
DDX21	GU	87.3	9.3	29	72.5/7	3	3.8
DDX41		69.8	6.8	33	81/6	5	9.5
DDX5	p68	69.1	9.1	27	73.1/8	23	37
DNL3	DNA ligase 3, LIG3	102.7	9.0	40	97/8	4	4.4
ELAV1	HuR	36.1	9.2	6	28.5/9	11	31.3
FIP1	Pre-mRNA 3′-end-processing factor FIP1	66.5	5.4	37	80.7/3.5	3	6.7
FUS		53.4	9.4	23	68.7/8	5	8.6
HNRCL	hnRNP C-like 1	32.1	4.9	15	38.9/4.2	11	25.9
HNRPC	hnRNP C1/C2	33.7	5.0	16	41.1/4.2	8	27.1
HNRPD	hnRNP D0/hnRNP D	38.4	7.6	17	45.4/6	3	9
HNRPG	hnRNP G	42.3	10.1	18	44/8.5	8	19.9
HNRPL	hnRNP L	60.2	6.7	29	72.5/7	8	17.9
HNRPM	hnRNP M	77.4	8.9	31	77.7/6.2	39	36.9
HNRPQ	hnRNP Q	69.6	8.6	33	81/6	3	4.5
HNRPU	hnRNP U	90.5	6.0	41	104/9.5	7	12.6
HS71L	HSP70 like protein 1	70.4	6.0	35	74/4.8	3	5.1
IMB1	Importin beta-1 subunit (Importin 90)	97.2	4.7	38	82/3.5	4	7.5
LMNA	Lamin A/C	74.1	6.6	33	81/6	47	57.8
LMNB1	Lamin B1	66.4	5.2	35	74/4.8	67	66
LMNB2	Lamin B2	67.7	5.4	35	74/4.8	7	12.7
NKRF	NFκB-repressing factor	77.7	8.9	40	97/8	5	7
NOLC1	Nucleolar phosphoprotein p130, NOPP140	73.7	9.5	42	115/7	7	10
NONO	p54nrb	54.2	9.0	22	60/8	10	23.8
NPM	Nucleophosmin	32.6	4.6	13	33.2/5.5	6	24.5
NUCL	Nucleolin	76.5	4.6	31	77.7/6.2	3	4.7
NUP37	Nucleoporin NUP37	36.7	5.6	13	33.2/5.5	3	11
NUPL2	Nucleoporin-like 2, NLP-1, HCG1	44.9	9.3	18	44/8.5	4	11.1
PHB2	Prohibitin-2	33.3	9.8	7	30/8	10	33.1
PININ		81.5	6.8	42	115/7	5	6.1
ROA1	hnRNP A1	38.7	9.3	6	28.5/9	13	36.9
ROA2	hnRNP A2/B1	37.4	9.0	7	30/8	22	54.5
ROA3	hnRNP A3	40	9.1	11	37.8/9	9	21.4
ROA0	hnRNP A0	30.8	9.3	8	31.7/8	3	16.7
SF3B4	Splicing factor 3b subunit 4	44.4	8.6	19	48.2/8.2	3	12.7
SFPQ	H-splicing factor, PSF	76.1	9.5	40	97/8	17	17.3
SFRS1	SF2, ASF-1	27.6	10.4	5	23.7/8	5	20.2
THOC1	THO complex subunit 1, THO1	75.7	4.9	39	88.5/4	5	9.1
U5S1	116 kDa U5 small nuclear ribonucleoprotein component	109.5	4.8	39	88.5/4	3	3.4
UTP18	U3 small nucleolar RNA-associated protein 18	62	8.9	29	72.5/7	6	13.8
WDR18	WD repeat protein 18	47.4	6.2	17	45.4/6	8	21.8
ZN326	Zinc finger protein 326	65.7	5.1	34	80.7/5.2	6	11.2

The calculated molecular weight (MW) and isoelectric point (pI) are compared with their values from the GzmA-untreated 2D gel (Fig. S1). The number of peptides identified by mass spectrometry and their coverage of the protein are given. Hits were required to have at least three peptides, to be localized to the nucleus, and to be predicted to migrate roughly like the spot from which they were retrieved. MW, molecular weight.

Dataset S1. Summary of mass spectrometry results

Dataset S1

All proteins recovered by at least three peptides are shown.

OPEN ACCESS Freely available online PLoS GENETICS

Capture of MicroRNA–Bound mRNAs Identifies the Tumor Suppressor miR-34a as a Regulator of Growth Factor Signaling

Ashish Lal[1,2,3☯]*, Marshall P. Thomas[1,2☯], Gabriel Altschuler[4☯], Francisco Navarro[1,2☯], Elizabeth O'Day[1,2], Xiao Ling Li[3], Carla Concepcion[5], Yoon-Chi Han[5], Jerome Thiery[1,2], Danielle K. Rajani[1,2], Aaron Deutsch[1,2], Oliver Hofmann[4], Andrea Ventura[5], Winston Hide[4], Judy Lieberman[1,2]*

1 Immune Disease Institute, Program in Cellular and Molecular Medicine, Children's Hospital Boston, Boston, Massachusetts, United States of America, **2** Department of Pediatrics, Harvard Medical School, Boston, Massachusetts, United States of America, **3** Genetics Branch, National Cancer Institute, National Institutes of Health, Bethesda, Maryland, United States of America, **4** Department of Biostatistics, Harvard School of Public Health, Boston, Massachusetts, United States of America, **5** Department of Cancer Biology and Genetics, Memorial Sloan Kettering Cancer Center, New York, New York, United States of America

Abstract

A simple biochemical method to isolate mRNAs pulled down with a transfected, biotinylated microRNA was used to identify direct target genes of miR-34a, a tumor suppressor gene. The method reidentified most of the known miR-34a regulated genes expressed in K562 and HCT116 cancer cell lines. Transcripts for 982 genes were enriched in the pull-down with miR-34a in both cell lines. Despite this large number, validation experiments suggested that ~90% of the genes identified in both cell lines can be directly regulated by miR-34a. Thus miR-34a is capable of regulating hundreds of genes. The transcripts pulled down with miR-34a were highly enriched for their roles in growth factor signaling and cell cycle progression. These genes form a dense network of interacting gene products that regulate multiple signal transduction pathways that orchestrate the proliferative response to external growth stimuli. Multiple candidate miR-34a–regulated genes participate in RAS-RAF-MAPK signaling. Ectopic miR-34a expression reduced basal ERK and AKT phosphorylation and enhanced sensitivity to serum growth factor withdrawal, while cells genetically deficient in miR-34a were less sensitive. Fourteen new direct targets of miR-34a were experimentally validated, including genes that participate in growth factor signaling (*ARAF* and *PIK3R2*) as well as genes that regulate cell cycle progression at various phases of the cell cycle (cyclins D3 and G2, *MCM2* and *MCM5*, *PLK1* and *SMAD4*). Thus miR-34a tempers the proliferative and pro-survival effect of growth factor stimulation by interfering with growth factor signal transduction and downstream pathways required for cell division.

Citation: Lal A, Thomas MP, Altschuler G, Navarro F, O'Day E, et al. (2011) Capture of MicroRNA–Bound mRNAs Identifies the Tumor Suppressor miR-34a as a Regulator of Growth Factor Signaling. PLoS Genet 7(11): e1002363. doi:10.1371/journal.pgen.1002363

Editor: Michael T. McManus, University of California San Francisco, United States of America

Received July 18, 2011; **Accepted** September 13, 2011; **Published** November 10, 2011

Funding: This work was supported by a research grant (JL) and fellowship (FN) from the GSK-IDI Alliance and by NSF predoctoral fellowships (MPT, DKR). The funders had no role in study design, data collection and analysis, decision to publish, or preparation of the manuscript.

Competing Interests: The authors have declared that no competing interests exist.

* E-mail: lieberman@idi.harvard.edu (JL); lalas@mail.nih.gov (AL)

☯ These authors contributed equally to this work.

Introduction

microRNAs (miRNAs) that promote cell differentiation, inhibit cell proliferation, or enhance DNA damage or stress-induced cell cycle arrest or death, and whose expression is reduced in some cancers, are candidate tumor suppressor genes [1]. One of the most well studied tumor suppressor miRNAs is miR-34a. Depending on cellular context [2], ectopic over-expression of miR-34a induces cell cycle arrest [3], senescence [4] or apoptosis [5]. miR-34a is up-regulated by p53 in response to DNA damage [6–8], but can also be transcriptionally activated independently of p53 [9,10]. miR-34a is located on chromosome 1p36, a locus deleted in neuroblastoma, breast, thyroid, and cervical cancer [11,12]. In other cancers, miR-34a expression is epigenetically reduced by hypermethylation [13]. miR-34a administration can inhibit tumor outgrowth in mice [4]. Thus miR-34a satisfies the criteria for a tumor suppressor gene.

The best way to understand the function of a miRNA is to identify the genes it regulates. In this study we sought to understand how miR-34a acts as a tumor suppressor by identifying its direct target genes. However, target gene identification is not straightforward because of the partial complementarity of the short ~22 nt miRNA sequence with the miRNA recognition element (MRE) of the target gene [14]. MRE pairing to the miRNA seed region (nt 2–7) contributes significantly to target gene recognition and is the basis for the most successful target gene prediction algorithms [15,16]. However, a perfect seed match is not necessary [17,18] and does not guarantee targeting [19]. miRNA target prediction algorithms typically predict hundreds to thousands of putative miRNA target genes, but most predicted target genes are not bona fide targets and the best algorithms sometimes miss key targets [17,19–21]. It is unclear how many target genes are in fact regulated by a given miRNA in any physiological context. Analysis of genes whose mRNA or protein expression decreases when a miRNA is overexpressed or increases when it is antagonized identifies genes that may be either direct targets or indirectly regulated [22]. Biochemical methods to

Author Summary

microRNAs (miRNAs) are small RNAs that regulate gene expression by binding to mRNAs bearing a partially complementary sequence. miRNAs decrease the stability or translation of mRNA targets, leading to reduced protein expression. Understanding the biological function of a miRNA requires identifying its targets. Here we developed a sensitive and specific biochemical method to identify candidate microRNA targets that are enriched by pull-down with a tagged, transfected microRNA mimic. The method was applied to miR-34a, a miRNA that inhibits cell proliferation. We found that miR-34a can potentially regulate hundreds of genes. Computational analysis of these genes suggested a novel function for miR-34a—suppression of the pro-proliferative response to diverse growth factors. This function complements the previously known role of miR-34a in blocking cell cycle progression. Thus, by reducing the expression of an extensive network of genes, miR-34a dampens growth factor signaling as well as its downstream consequences, promotion of cell survival and proliferation.

capture RNA-induced silencing complex (RISC)-bound mRNAs potentially provide a more direct way to identify miRNA-regulated target genes [23–25]. However, immunoprecipitation has mostly been used to define the general features of miRNA-regulated mRNAs and their MREs, rather than to identify the targets of a particular miRNA.

Already 36 putative miR-34a targets have been validated by luciferase reporter assays. These targets strongly support miR-34a's role as a tumor suppressor. They include genes that promote cell cycle progression through the G_1/S transition (*CCND1*, *CCNE2*, *CDK4*, *CDK6*, *MYC*, *MYCN* and *E2F3*) [3,8,10,12,26], enhance transcription (*MYB*, *HNF4A* and *FOXP1*) [9,27,28] or growth factor signaling (*MET*, *MEK1*, *AXL* and *RRAS*) [8,29–32], inhibit apoptosis (*BCL2*) [33] or p53 activity (*YY1*, *MTA2*, *SIRT1* and *MAGE-A*) [5,32,34,35], and promote stem cell survival (*NOTCH1*, *NOTCH2*, *LEF1 WNT1*, *DLL1*, *JAG1* and *CD44*) [32,36–40]. The diversity of direct miR-34a targets suggests that miR-34a acts pleiotropically by regulating many genes.

To identify additional direct target genes of miR-34a without bias and understand better how miR-34a functions, we optimized a simple biochemical method to isolate mRNAs that bind to transfected biotinylated (Bi-)miR-34a [41,42]. mRNAs significantly enriched in the Bi-miRNA pull-down with streptavidin relative to their cellular expression were candidate targets. The pull-down was performed in two unrelated cancer cell lines, K562 erythroleukemia cells and HCT116 colon carcinoma cells. p53 activates transcription of miR-34a [8]. Under basal conditions, p53-sufficient HCT116 cells highly express miR-34a, while p53-null K562 cells do not express it above background (data not shown). We selected disparate cell lines to identify genes that may be regulated in multiple cell types or more specifically in a particular context. Several thousand genes were significantly enriched in the miR-34a pull-down in each cell line and 982 were significantly enriched in both cell lines. Most known miR-34a target mRNAs expressed in these cells were pulled down with miR-34a. Despite the large number of genes significantly enriched in the miR-34a pull-down, 91% of a random list of 11 genes enriched in both cell lines contained miR-34a-regulated 3′UTR sequences. These results suggest that the pull-down is quite specific and that miR-34a potentially directly regulates hundreds of genes. Bioinformatic analysis of the pulled down genes or of genes down-regulated after miR-34a transfection suggested that miR-34a regulates a dense network of genes that transduce proliferative signals arising from growth factor stimulation. Multiple candidate target genes participate in RAS-RAF-MAPK signaling. In fact miR-34a knockout reduced sensitivity to growth factor withdrawal by serum starvation, while miR-34a transfection led to increased vulnerability. Fourteen novel miR-34a targets identified by the pull-down in both cell lines were experimentally verified, including *ARAF* and *PIK3R2* in the RAS-RAF-MAPK pathway, and additional target genes required for cell cycle progression, including cyclins D3 and G2, *MAD2L2*, *MCM2*, *MCM5* and *PLK1*.

Results

Isolation of mRNAs bound to a transfected biotinylated–miRNA

We modified a method [5] for capturing miRNA-mRNA complexes using streptavidin-coated beads from cells transfected with miR-34a biotinylated at the 3′-end of the mature strand. Control samples were transfected with a biotinylated *C. elegans* miRNA (Bi-cel-miR-67) (Figure 1A). Biotinylation did not interfere with miRNA-mediated gene suppression as measured by luciferase reporter assay (Figure 1B). Over-expressing Bi-miR-34a or miR-34a in K562 cells also similarly suppressed expression of known miR-34a target genes (Figure 1C). Moreover, immunoprecipitation of HA-tagged Ago1 or Ago2 in K562 cells cotransfected with Bi-miR-34a specifically enriched for miR-34a by ~4-fold and ~6-fold, respectively (Figure 1D). Thus the Bi-miRNA is incorporated into the RISC and functions like the unbiotinylated miRNA.

We next optimized conditions to capture known target gene mRNAs. In the Bi-miR-34a pull-down of K562 cells, known miR-34a target transcripts *CDK4* and *CDK6*, but not UBC (a housekeeping gene), were enriched 12 hr after transfection, and their capture plateaued at 24–48 hr (Figure 1E). Therefore, 24 hr was chosen for subsequent experiments. The specificity of the pull-down and applicability to other cell types was verified since *CDK4*, *CDK6* and *MYB* mRNAs were consistently enriched by transfection of Bi-miR-34a, but not Bi-cel-miR-67, in K562 (Figure 1F) and HCT116 (Figure S1A) cells. Streptavidin beads did not enrich for non-target *SDHA* and *UBC* mRNAs, and the specific target mRNAs were not pulled down in cells transfected with unbiotinylated miR-34a (data not shown). miR-34a was specifically enriched >40-fold in the Bi-miR-34a pull-down compared to the input lysate (Figure S1B). Modifications of the pull-down to include formaldehyde cross-linking and/or pre-isolation of RNAs in high molecular weight cellular fractions reduced the amount of captured RNA, but did not improve the relative enrichment for known target gene mRNAs (data not shown). To confirm that association of Bi-miRNAs with target mRNAs was not a post-lysis artifact, we performed streptavidin pull-downs after adding Bi-miR-34a or Bi-cel-miR-67 to cytoplasmic extracts of untransfected K562 cells. *CDK4*, *CDK6* and *MYB* mRNAs were not enriched when Bi-miR-34a was added post-lysis (Figure S1C). The general applicability of the pull-downs to enrich for miRNA target genes was also verified for another miRNA, miR-24 in HepG2 cells. Bi-miR-24 capture enriched for 3 known miR-24 targets (*H2AFX*, *E2F2* and *MYC* [43]) by 2–5-fold (Figure 1G).

Sensitivity of the Bi-miR-34a pull-down

We next used gene expression microarrays to identify putative miR-34a targets captured by Bi-miR-34a in duplicate experiments from K562 (p53 deficient) and HCT116 cells (p53 proficient)

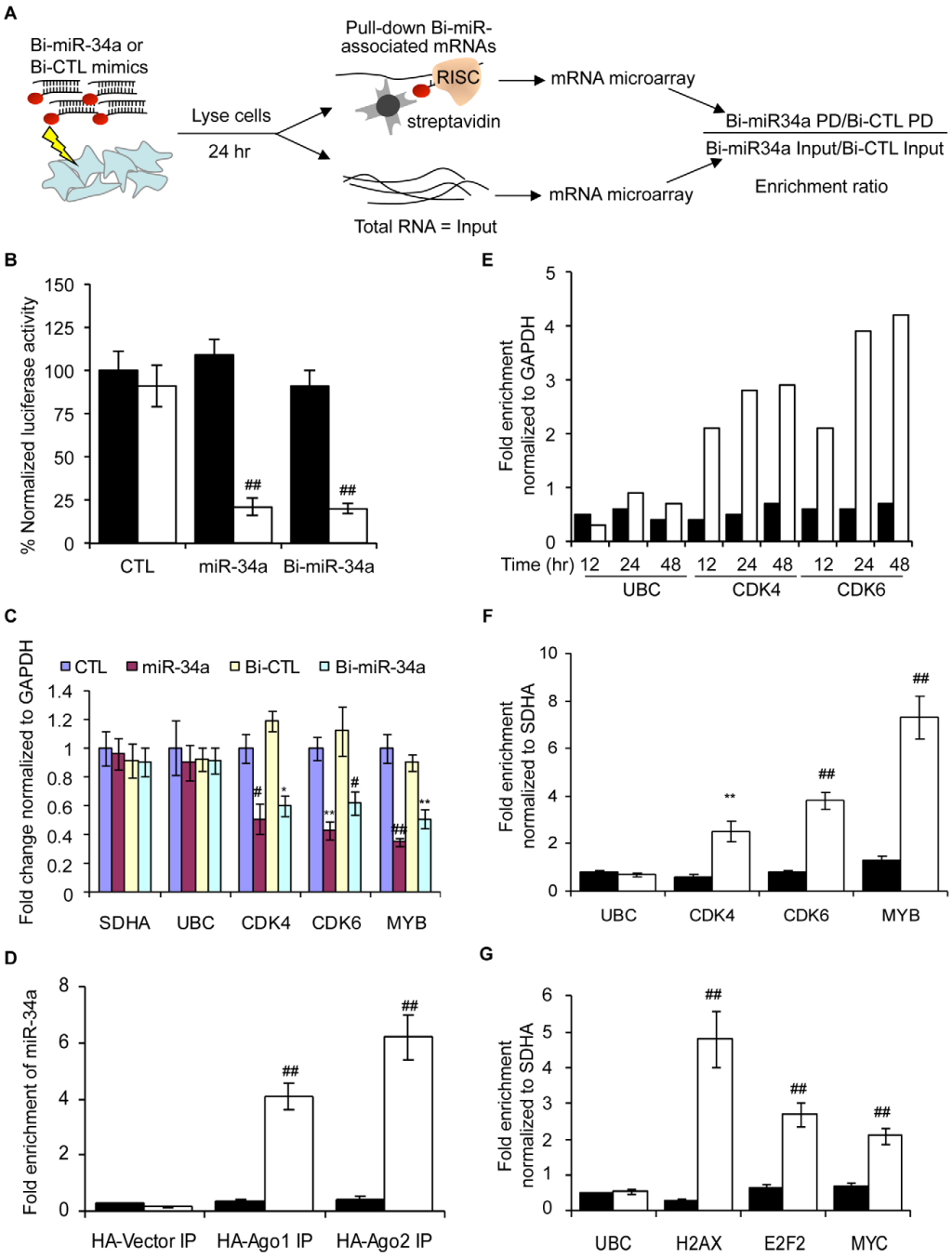

Figure 1. The Biotin-miRNA pulldown method. (A) Schematic of the Bi-miRNA pull-down (PD) assay. (B) Activity of 3′-biotinylated miR-34a (Bi-miR-34a) is similar to unbiotinylated miR-34a mimics by dual luciferase assay performed in HeLa cells cotransfected with psiCHECK-2 vector (black) or psi-CHECK-2 bearing a perfectly complementary sequence to miR-34a (psiCHECK-2-AS-miR-34a, white). Transfection with cel-miR-67 is the control (CTL). Luciferase expression was assayed after 24 hr; results are normalized to cells transfected with the luciferase vector and the CTL miRNA. (C) Bi-

miR-34a efficiently silences known miR-34a targets *CDK4, CDK6* and *MYB*. K562 cells were transfected with CTL miRNA, miR-34a, Bi-CTL or Bi-miR-34a mimics for 48 hr. Expression was measured by qRT-PCR normalized to *GAPDH*. The housekeeping genes *SDHA* and *UBC* are negative controls. (D) Cytoplasmic lysates from K562 cells were prepared 48 hr after cotransfection with Bi-CTL (black) miRNA or Bi-miR-34a (white) and a plasmid encoding HA-Ago1, HA-Ago2, or empty vector. Enrichment of miR-34a by HA immunoprecipitation was measured by qRT-PCR normalized to *U6*. Enrichment of Bi-miR-34a in the HA-immunoprecipitates suggests that Bi-miR-34a is incorporated into RISC. (E) Bi-miR-34a pull-downs optimally enrich targets 24 or 48 hr after transfection. K562 cells were transfected in duplicate with Bi-CTL (black) or Bi-miR-34a (white) mimics for the indicated times. Enrichment of known miR-34a targets (*CDK4* and *CDK6*) or control genes (*GAPDH* and *UBC*) was assessed by qRT-PCR relative to *GAPDH*. (F) The streptavidin pull-down enriches for miR-34a target genes in K562 cells transfected with Bi-CTL (black) or Bi-miR-34a (white) mimics. (G) Known miR-24 target mRNAs (*H2AX, E2F2* and *MYC*) are also pulled down with Bi-miR-24 in HepG2 cells reverse transfected 48 hr earlier with Bi-CTL (black) or Bi-miR-24 (white). Enrichment of target mRNAs in (F) and (G) was analyzed by qRT-PCR relative to *SDHA*. In all panels, data represent mean ± SD of 3 independent experiments. *, $p<0.05$, #, $p<0.01$, **, $p<0.005$, ##, $p<0.001$.
doi:10.1371/journal.pgen.1002363.g001

(Table S1). mRNA abundance in the streptavidin pull-down and input in Bi-miR-34a-transfected cells were separately normalized to their levels in Bi-cel-miR-67-transfected cells. For each biological replicate, the ratio of the abundance of the pull-down mRNA compared to the input mRNA for cells transfected with Bi-miR-34a versus Bi-cel-miR-67 was calculated, averaged and used to define the enrichment ratio {Bi-miR-34a PD/Bi-cel-miR-67 PD}/{Bi-miR-34a input/Bi-cel-miR-67 input}. Normalizing to the input improved identification of true targets in 2 ways – by reducing the background caused by highly abundant mRNAs that associate with streptavidin beads nonspecifically and by incorporating a measure of mRNA knockdown into the denominator of the ratio.

The miR-34a pull-downs enriched for 2416 genes in HCT116 cells (by ≥1 standard deviation (SD), enrichment ratio ≥2.5) and for 2816 genes in K562 cells (≥1 SD, enrichment ratio ≥3.3) (Figure 2A). The overlap of genes enriched ≥1 SD in both of these unrelated cell lines was 982 genes. To determine the sensitivity of the pull-down, we first looked at how many of the 36 published targets of miR-34a were captured in the K562 or HCT116 pull-downs (Figure 2B). Of the known expressed targets, 22 of 31 mRNAs (71%) were enriched in HCT116 cells and 14 of 29 (48%) were enriched in K562 cells. It should be noted that the choice of cut-off is somewhat arbitrary. Two additional known targets had enrichment ratios of 2.5–3.2 in K562 cells. The enrichment ratio ranged from 2.7–85. 12 genes were identified in both pull-downs. The enrichment ratio for the shared hits was not significantly different in K562 cells, which do not express miR-34a, compared to HCT116 cells, which do, suggesting that the pull-downs efficiently captured miR-34a targets even in cells that express endogenous miR-34a.

Analysis of genes down-regulated by miR-34a over-expression

To compare the mRNAs that associate with miR-34a to mRNAs that decrease with miR-34a over-expression, we measured mRNA abundance in cells transfected with miR-34a or cel-miR-67 by gene expression microarrays (Table S1). Genes whose mean mRNA level ratio decreased by at least 20% after miR-34a transfection were considered to be down-regulated either directly or indirectly by miR-34a. With this arbitrary cut-off (~1 SD), 2087 genes were down-regulated in HCT116 cells and 945 genes were down-regulated in K562 cells (Figure 2C). About a third of these transcripts in both cell lines were also pulled down with Bi-miR-34a (30% in HCT116, 36% in K562).

Down-regulated and pulled down mRNAs are enriched for miR-34a seed sequences

Many miRNA targets contain a perfect match to the miRNA seed region in their 3′UTR. We examined the frequency of 3′UTR matches to all hexamer sequences in miR-34a in the pull-down and down-regulated gene sets relative to all genes probed on the microarray (Figure S2A). Hexamer matches to nt 2–7 in the miR-34a seed region were significantly enriched in the pull-down (HCT116 p = 1.8E-95; K562 p = 2.4E-11) and down-regulated (HCT116 p = 1.7E-24; K562 p = 1.0E-11) datasets. There was also significant enrichment in the HCT116 pull-down genes for nt 13–19 exact matches, suggesting that base-pairing there enhances miRNA binding, as has previously been shown [44]. In both cell lines, seed enrichment was greater for the overlapping set of genes that was both pulled down and down-regulated by miR-34a. For genes in this overlap, exact matches to nt 2–7 were 1.8–2.0-fold more frequent per kb of 3′UTR than for all genes on the microarray. These data suggest that genes in the overlap may be more likely to be direct targets than genes identified by only one method or that a perfect seed match might enhance miRNA-mediated mRNA decay.

We next examined hexamer enrichment in the 982 genes enriched ≥1 SD in pull-downs from both HCT116 and K562 cells (Figure S2B). Seed matches were most enriched in the 3′UTRs of these genes, with the nt 2–7 match being the most abundant (1.7 fold more abundant than in all genes on the microarray (p = 8.4E-39). The coding region (CDS) of these genes also contained a highly significant enrichment for hexamer seed matches (p = 6.1E-13). These results are consistent with recent cross-linked RISC pull-downs that suggest that 25–50% of MREs may be in the CDS [23,25]. There was also a modest enrichment of hexamers matching the seed in the 5′UTR (p = 0.005). Thus the pull-down and down-regulated mRNAs were enriched for expected miRNA target sequence features.

We next analyzed whether mRNA expression of the enriched genes was reduced by miR-34a transfection in HCT116 cells (Figure 2D). The mRNAs of the 982 genes enriched in the miR-34a pull-down by ≥1 SD in both cell lines were significantly down-regulated after miR-34a transfection compared to the set of all genes expressed in the cell (p = 4.7E-80). The extent of down-regulation was comparable to the set of 469 TargetScan-predicted, evolutionarily conserved targets of miR-34a and significantly greater than in the larger list of 2904 poorly conserved, TargetScan-predicted genes (p = 1.6E-20). Increasing the cutoff for the enrichment ratio in the pull-down led to a greater proportion of highly down-regulated genes, indicating that a higher enrichment ratio correlates with more effective mRNA degradation and/or that highly enriched mRNAs are more likely to be miR-34a targets. Thus, the Bi-miR-34a pull-down enriches for known sequence and gene expression characteristics of *bona fide* miRNA targets.

Genes enriched in the miR-34a pull-down of both cell lines have a high probability of being direct miR-34a targets

To determine the specificity of the pull-down, we generated a random list (Table S2) of 11 genes enriched >2.5 fold in both pull-downs (median enrichment 3.5-fold, range 2.5–17.3). The random

A

B

Target	Fold enrichment HCT 116	Fold enrichment K562	Ref.	Target	Fold enrichment HCT 116	Fold enrichment K562	Ref.
ACSL1	0.24	2.39	32	MAGEA2	Abs.	Abs.	35
ACSL4	**8.42**	**84.90**	32	MAGEA3	1.20	0.99	35
AXL	**16.97**	**18.32**	31	MAGEA6	1.27	0.95	35
BCL2	1.78	1.05	33	MAGEA12	Abs.	1.29	35
BIRC5	1.77	2.14	32	MEK1	**2.71**	1.92	29
CCND1	**3.66**	**40.29**	3	MET	**6.77**	0.53	8
CCNE2	**3.65**	**6.69**	8	MTA2	**8.37**	**11.22**	32
CD44	1.39	2.37	40	MYB	**8.94**	2.47	9
CDK4	**3.45**	2.73	8	MYC	1.47	**4.80**	10
CDK6	**22.80**	**62.52**	3	MYCN	Abs.	Abs.	26
DLL1	**8.30**	Abs.	39	NOTCH1	**7.13**	3.22	38
E2F3	**2.71**	**5.20**	12	NOTCH2	**7.18**	Abs.	38
EFNB1	**5.33**	**3.88**	32	RRAS	**63.86**	**32.42**	32
FOXP1	**16.98**	**6.69**	27	SIRT1	**9.84**	**10.22**	5
HNF4A	**8.35**	Abs.	28	TPD52	**13.31**	1.01	32
JAG1	0.99	Abs.	37	VCL	**6.20**	1.81	32
LDHA	1.43	1.17	32	WNT1	Abs.	Abs.	36
LEF1	Abs.	**32.65**	32	YY1	**4.83**	**52.82**	34

C

D

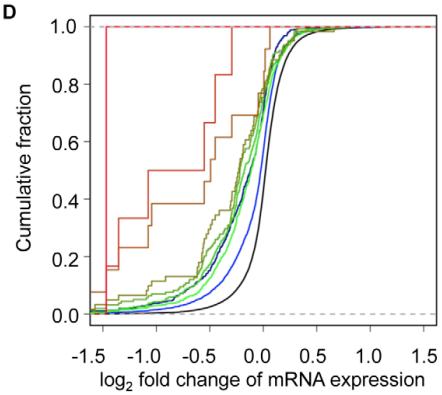

Genes		N	Genes		N
All genes	—	18,185	2.0 SD	—	167
TScan (all)	—	2904	2.5 SD	—	62
TScan (cons.)	—	469	3.0 SD	—	13
1.0 SD	—	982	3.5 SD	—	6
1.5 SD	—	408	4.0 SD	—	1

E

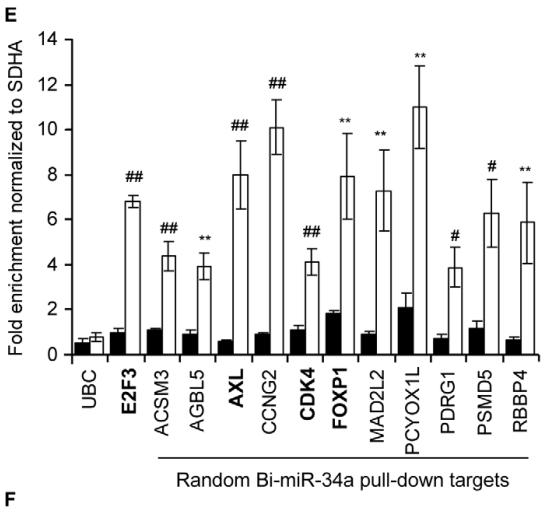

F

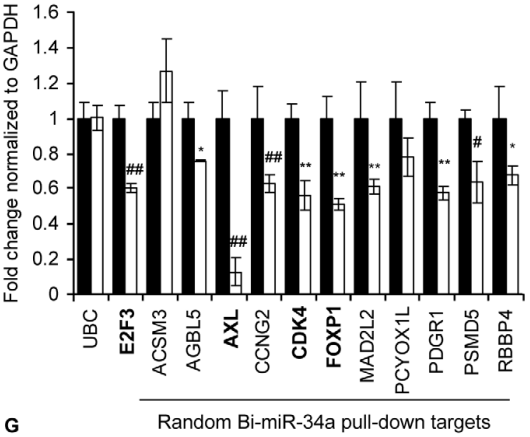

G

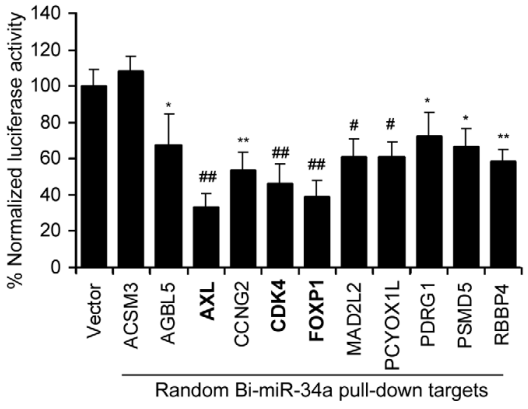

Figure 2. miR-34a pulls down transcripts of known and novel direct targets of miR-34a. (A) Overlap of genes enriched ≥1 SD in gene expression microarray analysis of Bi-miR-34a pull-downs from HCT116 and K562 cells. (B) Enrichment of previously described miR-34a target gene mRNAs in Bi-miR-34a pull-downs from HCT116 and K562 cells. Genes enriched ≥1 SD are indicated in bold. Abs = not expressed. (C) Genes down-regulated by ≥20% after miR-34a over-expression. (D) mRNA expression of candidate miR-34a targets identified by Bi-miR-34a pull-down in both HCT116 and K562 cells decreases after miR-34a over-expression. Cumulative distribution plots compare the extent of mRNA reduction of genes enriched to varying degrees in the Bi-miR-34a pull-down with conserved (cons) or all TargetScan (TScan)-predicted targets. Genes whose mRNAs are more highly enriched in the pull-down are progressively more likely to have reduced expression. (E) Pull-down of 11 mRNAs randomly selected from the set of genes enriched ≥2.5-fold by microarray in both HCT116 and K562 Bi-miR-34a pull-downs is confirmed by qRT-PCR relative to *SDHA* in K562 cells transfected for 24 hr with Bi-CTL (black) or Bi-miR-34a (white). *UBC* is a negative control and *E2F3* is a positive control. Three previously validated miR-34a targets (*AXL, CDK4* and *FOXP1*) in the random list of genes are indicated in bold. (F) miR-34a over-expression significantly decreases the expression of 9 of 11 of the randomly chosen candidate target genes. K562 cells were transfected with CTL miRNA (black) or miR-34a (white) mimics for 72 hr. Expression of random targets was measured by qRT-PCR normalized to *GAPDH*. Expression of 2 randomly selected genes (*ACSM3* and *PCYOX1L*) and the housekeeping mRNA *UBC* didn't change significantly. (G) miR-34a targets the 3′UTR of 10 of 11 randomly chosen targets. Luciferase activity was measured 48 hr after HeLa cells were cotransfected with the luciferase reporter psiCHECK2 bearing the 3′UTR of each gene and CTL miRNA or miR-34a mimics. Results obtained after miR-34a transfection were normalized to CTL miRNA. In (E–G), data represent mean ± SD of 3 independent experiments. *, $p<0.05$, #, $p<0.01$, **, $p<0.005$, ##, $p<0.001$.
doi:10.1371/journal.pgen.1002363.g002

list contained 3 known target genes (*AXL*, *CDK4* and *FOXP1*; *AXL* and *FOXP1* were not known when the list was generated). First, qRT-PCR analysis verified that the random gene mRNAs are pulled down by Bi-miR-34a and not Bi-cel-miR-67. All 11 mRNAs were enriched (~4–10 fold) by Bi-miR-34a pull-down in K562 cells, validating the microarray results (Figure 2E). miR-34a over-expression significantly down-regulated mRNA levels of 9 of 11 genes by 25–90% (Figure 2F). *PCYOX1L* expression declined by 20%, but the change was not significant. To test whether the 3′UTR of each gene could be regulated by miR-34a, the full 3′ UTR of each gene was cloned into a dual luciferase reporter plasmid. miR-34a repressed the 3′UTRs of 10 of 11 genes by ~20–80% (Figure 2G). Thus, miR-34a could regulate the 3′UTR of 91% of a random set of genes enriched in both miR-34a pull-downs. These results suggest that the Bi-miRNA pull-down is highly specific for identifying direct miRNA targets. An important implication of the large number of genes in the overlapping target list and the low false positive rate is that miR-34a is capable of regulating hundreds of genes.

miR-34a directly regulates growth factor signaling and cell cycle progression

To understand miR-34a's biological functions, we analyzed the cellular pathways whose genes were most enriched in the Bi-miR-34a pull-downs (Figure 3A). In both K562 and HCT116 cells, Bi-miR-34a pull-downs enriched for genes in pathways related to growth factor signaling and cell cycle control. Bi-miR-34a pull-downs enriched significantly for genes in the EGFR, TGF-β, interleukin, estrogen, and androgen receptor signaling pathways (Figure 3A). Many of these pathways utilize common downstream signaling molecules and have a well-established link to cancer. Genes in the MAPK pathway, activated by most growth factors, were highly enriched in the pull-downs for both cell lines. Growth factor signaling also activates cell proliferation. Genes involved in cell cycle regulation, especially the G_1/S transition, and the p53 response were enriched in both pull-downs, consistent with previously described targets and roles of miR-34a [3,4,7,8].

We performed a similar pathway enrichment analysis for genes down-regulated by miR-34a (Figure 3B), which includes both direct and indirect miR-34a targets. The downstream effects of growth factor signaling on cell proliferation and p53 activation were more prominent in the down-regulated genes than in the pulled-down gene set, especially in p53-sufficient HCT116 cells. Cell cycle and DNA repair pathways were enriched in genes down-regulated by miR-34a in both K562 and HCT116 cells. These results suggest that miR-34a directly inhibits growth factor signal transduction and cell cycle progression pathways, culminating in reduced expression of genes needed for cell proliferation.

A pathway enrichment analysis of the TargetScan-predicted targets of miR-34a (Figure S3) also highlighted the most significantly enriched pathways in the experimental pull-down and down-regulated gene sets, notably TGFβ and MAPK signaling and cell cycle and G_1/S transition. However, the significance of the enrichment was weaker and the strong role of miR-34a in growth factor signaling was less obvious.

miR-34a regulates a dense network of genes involved in signal transduction and cell cycle progression

To begin to understand regulation of growth factor signaling and cell proliferation at the gene level by miR-34a, an interactome of pulled down or down-regulated genes in HCT116 cells that participate in the significantly enriched pathways was generated (Figure 4). miR-34a potentially regulates the expression of critical genes involved in virtually every step and branch of growth factor signal transduction from ligand binding to downstream growth-promoting transcription factors. The putative direct targets included genes encoding multiple TGFβ and FGF isoforms, receptors for EGF, FGF, and insulin, and several oncogenic receptor tyrosine kinases, including *MET* and *AXL*. Several genes operating proximally in signal transduction, including *SRC*, *PLCG1* and *VAV2*, were selectively pulled down. miR-34a targets also included protein kinase subunits that activate downstream signaling, including subunits of protein kinase A and C. In the RAS-RAF-MAPK signal transduction pathway, putative directly regulated genes included *RRAS* and *RASA2*, *ARAF* and *BRAF*, *JAK2*, and 11 *MAPK* genes. Although knockdown of most of the targets would be expected to inhibit cellular activation by diverse growth factors, the genes also encode for some important inhibitors, including the ubiquitin ligase *CBLC*, *RASA2*, and 5 *DUSP* genes (MAPK phosphatases). The pull-down also captured 76 transcripts of transcription factors, including some that orchestrate the transcriptional response to signal transduction (including *STAT3*, *CREB1* and *CREB3*, *SP1*, *ELK1* and *SMAD4*).

A major downstream effect of growth factor signaling and its activated transcription factors is to stimulate cell proliferation. miR-34a is already known to suppress *E2F3* and some key cyclins and cyclin-dependent kinases that regulate the G_1/S transition. The miR-34a pull-down enriched for additional cyclins (*CCND3*, *CCNG2*), but also for transcripts of genes that inhibit the kinases that promote exit from G_1 (*CDKN1C* that encodes p57(KIP2), *CDKN2A* (p14(ARF)). Other enriched transcripts include *MCM5*, whose product is required to initiate DNA replication, and several genes required for mitosis (*PLK1*, *MAD2L2* and *CDC23*). Ectopic miR-34a expression led to down-regulation of mRNAs for many genes needed to replicate DNA, including 2 members of the initiating complex that assembles at origins of DNA replication, 7

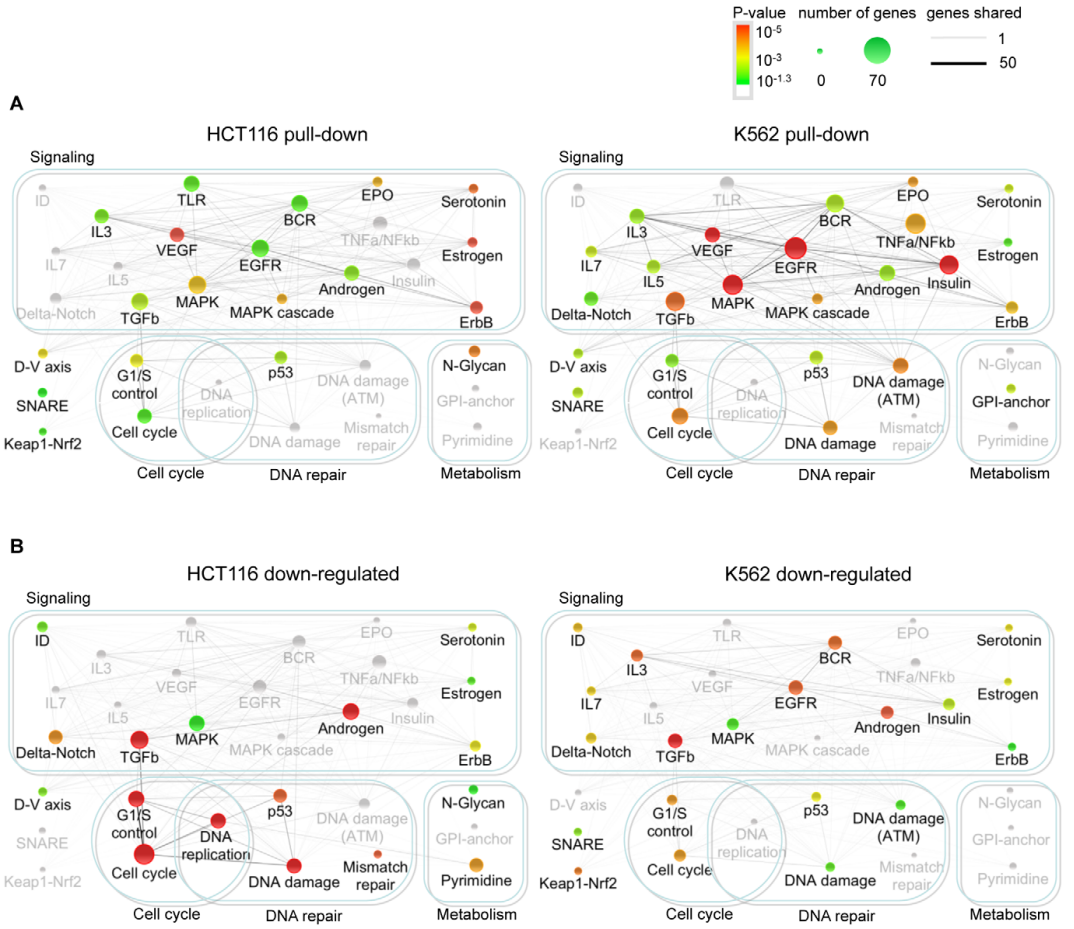

Figure 3. Genes in the Bi-miR-34a pull-down or down-regulated by miR-34a over-expression are enriched in growth factor signaling, cell cycle progression, and DNA repair pathways. Network of canonical pathways (Wikipathways and KEGG) significantly enriched for genes identified by Bi-miR-34a pull-down (A) or down-regulated following miR-34a over-expression (B) in HCT116 and K562 cells. Each pathway is represented by a node in the network. The node size increases with the number of identified genes in the pathway and the node color represents the p-value based on the hypergeometric distribution (see key). Pathways that are not significantly enriched in an experiment are still shown, but are in gray. The number of genes shared between two pathways is represented by an edge whose thickness increases with the number of shared genes. The pull-down enriched pathways (A) suggest that miR-34a extensively targets growth factor, signal transduction and cell cycle control pathways. The integrated outcome of both direct and indirect effects of miR-34a on gene expression in (B) is suppression of expression of genes participating in downstream signaling, cell cycle and DNA repair pathways.
doi:10.1371/journal.pgen.1002363.g003

components of the MCM complex, 4 DNA polymerases, and 5 components of the RFC complex, a cofactor for DNA polymerase. These results suggest that miR-34a not only interferes with the signaling that transduces the growth factor response, but also directly and indirectly suppresses the expression of numerous genes needed for cell proliferation.

miR-34a regulates cellular responses to growth factor signaling

The Ras–extracellular signal-regulated kinase (ERK) and phosphoinositide 3-kinase (PI3K)–AKT pathways are key transducers of the cellular response to growth factors. Since many candidate miR-34a target gene products act in pathways converging on ERK and AKT activation, we analyzed the effect of miR-34a over-expression on ERK and AKT phosphorylation. miR-34a transfection reduced basal phosphorylation of ERK and AKT in HCT116 and HeLa cells (Figure 5A, 5B), but not in A549 cells (Figure S4A). miR-34a over-expression both reduced basal proliferation in the absence of serum and blunted the ability of HCT116 (Figure 5C), HeLa (Figure 5D) and A549 (Figure S4B) cells to proliferate in response to serum growth factors. Conversely, immortalized mouse embryonic fibroblasts (MEFs) genetically deficient in miR-34a were more resistant to serum starvation than WT MEFs (Figure 5E). Apoptosis measured by annexin V and

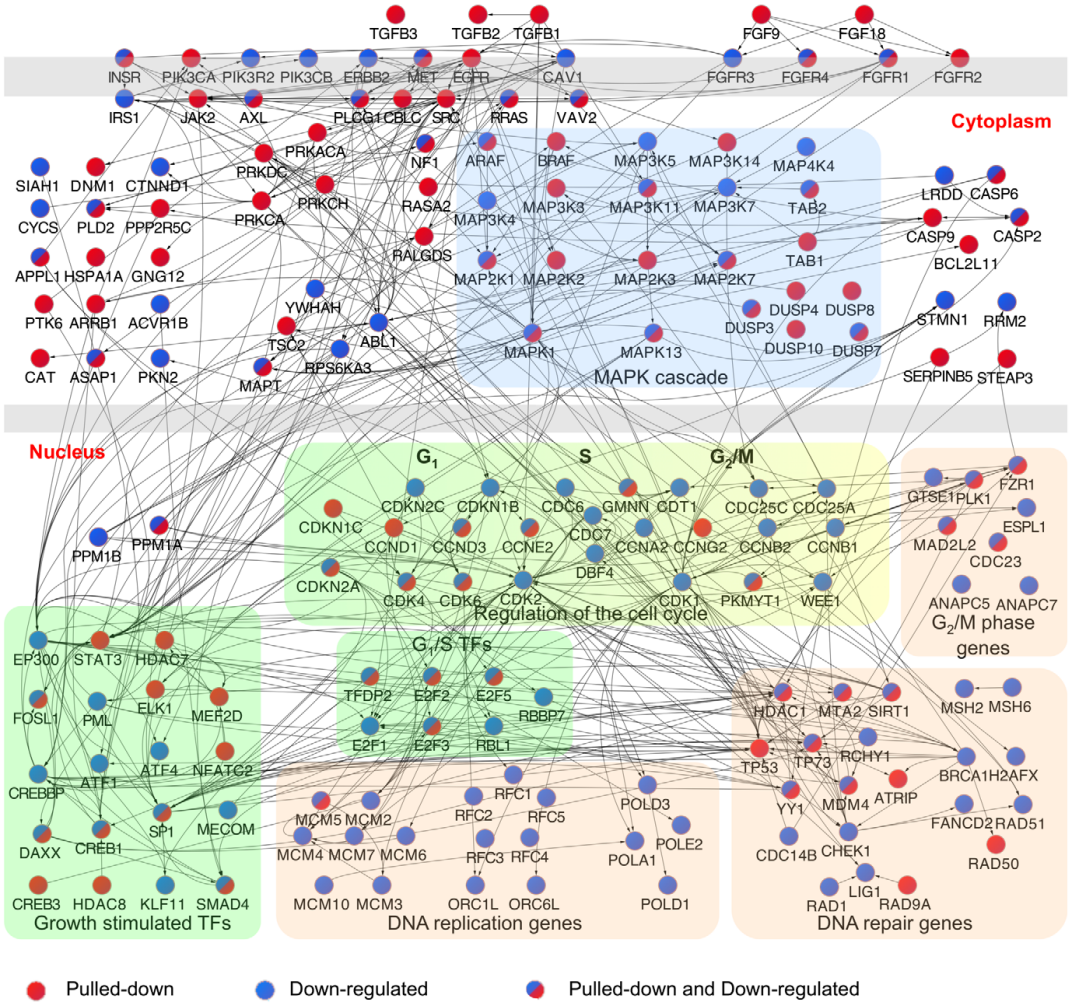

Figure 4. Interactome of genes in the enriched canonical pathways pulled down with Bi-miR-34a and/or down-regulated by miR-34a over-expression. Interactome of products of genes identified by Bi-miR-34a pull-down (red) or down-regulated by miR-34a over-expression (blue) in significantly enriched pathways (Figure 3) in HCT116 cells. Edges represent physical interactions. A dense network of genes involved in growth factor signaling and downstream effects on cell cycle progression and DNA repair is implicated.
doi:10.1371/journal.pgen.1002363.g004

propidium iodide staining was also significantly reduced in miR-34a$^{-/-}$ MEFs compared to wild-type MEFs after 24 hours of serum starvation (Figure 5F). Despite the strong difference in cell survival in cells deficient in miR-34a, expression of several known miR-34a targets did not differ significantly between wild-type and miR-34a$^{-/-}$ MEFs (data not shown). The lack of a notable difference may be due in part to compensatory up-regulation of miR-34b and miR-34c in miR-34a$^{-/-}$ MEFs (Figure 5G). These data suggest that miR-34a dampens the basal state of activation of proliferative and pro-survival pathways mediated by AKT and ERK by down-modulating multiple genes whose products contribute to their phosphorylation.

miR-34a directly targets genes that regulate ERK and AKT phosphorylation

To determine whether some of the candidate miR-34a target genes identified in the pull-down that participate in growth factor signaling are bona fide targets, we next tested miR-34a targeting of selected receptor-proximal (*AXL*, *MET* and *PIK3R2*) and more downstream (*ARAF* and *MEK1*) components of ERK and AKT signal transduction pathways. These 5 genes were both pulled down with Bi-miR-34a and down-regulated by miR-34a in HCT116 cells. ARAF is a serine/threonine protein kinase that phosphorylates and activates MEK1, which in turn phosphorylates ERK [45]. AXL is a receptor tyrosine kinase that stimulates cell

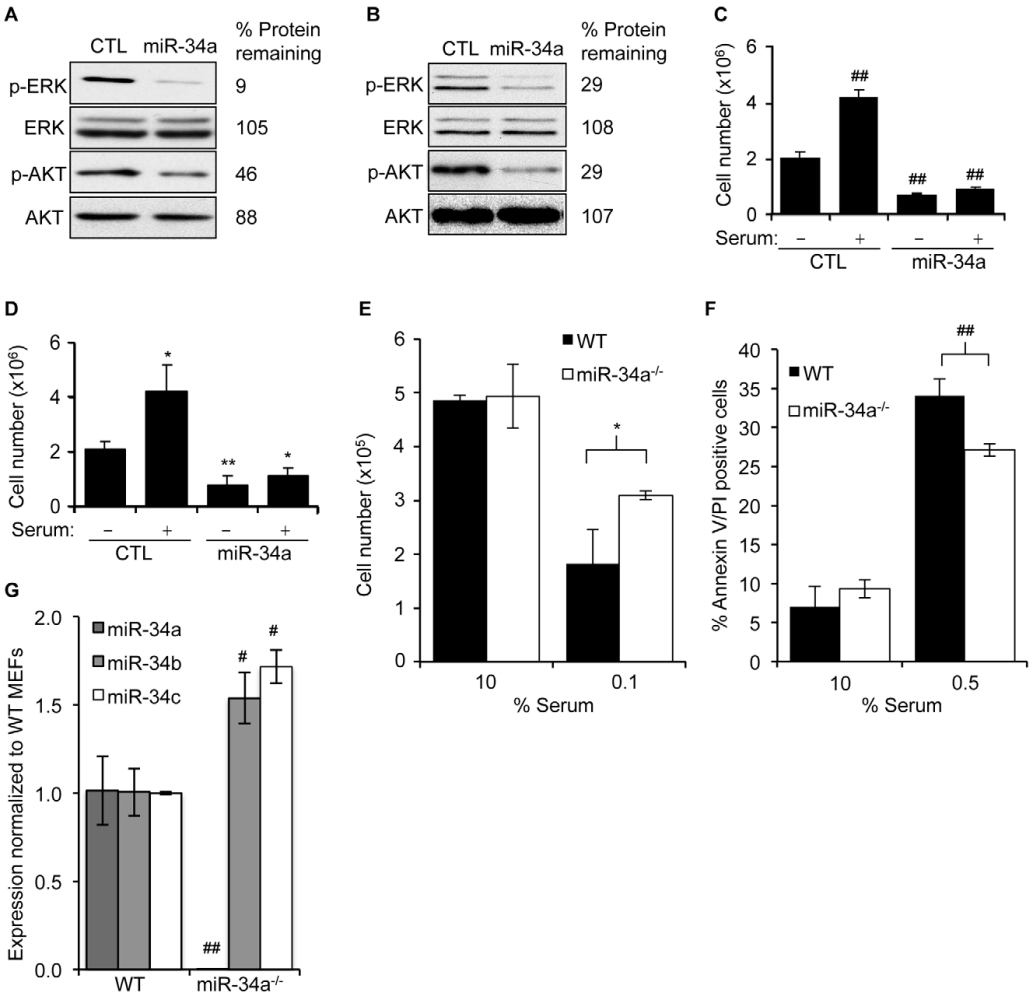

Figure 5. miR-34a expression suppresses cellular activation in response to serum growth factors. (A,B) miR-34a over-expression reduces basal phosphorylation of AKT and ERK as measured by immunoblot 48 hr after transfection of HCT116 (A) and HeLa (B) cells with control (CTL) miRNA or miR-34a mimics. Abundance of total ERK and AKT doesn't change. (C,D) miR-34a over-expression reduces cell proliferation in the absence of serum and suppresses the proliferative response of HCT116 (C) and HeLa (D) cells 24 hr after adding serum. (E) Total numbers of miR-34a$^{+/+}$ or miR-34a$^{-/-}$ MEFs after 24 hr of culture in 10% serum (10%) or 24 hr in 10% serum followed by 24 hr in 0.1% serum (0.1%). MEFs sufficient for miR-34a were more sensitive to serum starvation. (F) miR-34a$^{+/+}$ MEFs were more prone to apoptosis than miR-34a$^{-/-}$ MEFs after 24 hr of culture in reduced serum. (G) Expression of miR-34 family members in miR-34$^{+/+}$ (WT) and miR-34$^{-/-}$ MEFs assessed by qRT-PCR. miR-34a$^{-/-}$ MEFs expressed higher levels of miR-34b and miR-34c. In C,D,F, and G, data represent mean ± SD of 3 independent experiments. *, p<0.05, #, p<0.01, **, p<0.005, ##, p<0.001.
doi:10.1371/journal.pgen.1002363.g005

proliferation and also promotes metastasis [46,47]. PIK3R2 is a regulatory subunit of PI3K [48] and MET is a tyrosine kinase receptor that activates both PI3K and RAS [49]. *AXL*, *MET* and *MEK1* are described miR-34a targets [8,29,31], although *AXL* and *MEK1* were not known when these studies were performed.

The transcripts of all 5 genes were enriched 3–15-fold in the Bi-miR-34a pull-down by qRT-PCR, validating the microarray results (Figure 6A). Furthermore, over-expression of miR-34a down-regulated both the mRNA and protein levels of all 5 genes (Figure 6B, 6C). All but *ARAF* are also predicted miR-34a targets by TargetScan. To determine whether these genes are direct miR-34a targets, we tested the 3′UTRs for 4 of the genes (*ARAF*, *AXL*, *MEK1* and *MET*) by luciferase assay. miR-34a reduced reporter activity of these 3′UTRs by ~40–75% (Figure 6D). Using the PITA algorithm [50] to identify potential MREs in their 3′UTRs, we found 1 potential MRE in *AXL*, 2 in ARAF, 3 in *MEK1*, 4 in *PIK3R2* and 5 in *MET* (Figure S4). We tested repression of these MREs by miR-34a using luciferase assays. All 5 genes contained at least one miR-34a-responsive MRE (Figure 6E). Point mutations that disrupt the MRE-miR-34a interaction restored luciferase

activity, validating their regulation by miR-34a. Therefore, these 5 important genes in PI3K and MAPK signaling are all directly regulated by miR-34a.

miR-34a pull-downs identify new miR-34a targets that regulate cell cycle progression

Ectopic expression of miR-34a reduces expression of multiple direct target genes whose products facilitate the G_1/S transition (*CDK4*, *CDK6*, *CCND1*, *CCNE2* and *E2F3*). The pull-down identified novel genes acting at the G_1/S transition and genes involved in DNA replication and mitosis. Two cell cycle-regulating genes enriched in the miR-34a pull-down are in the random gene list and were already shown (Figure 2C–2E) to be miR-34a-regulated - *CCNG2*, which is most highly expressed in late S phase, and *MAD2L2*, a component of the mitotic spindle assembly checkpoint complex. To examine whether some of the other putative targets that participate in cell cycle progression are direct miR-34a targets, we focused on genes that were both pulled down and down-regulated by miR-34a in HCT116 cells (Table S2). Fourteen cell cycle-regulating genes (*CDK4*, *CDK6*, *CCNE2*, *E2F2*, *E2F3*, *E2F5*, *HDAC1*, *CDKN2A*, *MCM5*, *PKMYT1*, *PLK1*, *SMAD4*, *MAD2L2* and *CCND3*) met these criteria. Four of these (*CDK4*, *CDK6*, *CCNE2* and *E2F3*) are known miR-34a targets. We experimentally tested 5 of the 9 putative novel targets. These genes were *CCND3*, a cyclin that binds to CDK4 or CDK6 and regulates Rb phosphorylation; *MCM5*, a mini-chromosome maintenance (MCM) protein involved in initiating DNA replication, *MYT1*, a serine/threonine protein kinase that phosphorylates and inactivates CDC2, thereby negatively regulating cell cycle progression at the G_2/M transition; *PLK1*, a serine/threonine protein kinase required for mitotic spindle maturation; and *SMAD4*, a TGFβ-activated transcription factor that induces G_1 arrest and apoptosis. To determine whether these miR-34a pull-down genes are *bona fide* miR-34a target genes, we first verified that their transcripts associate with Bi-miR-34a (Figure 7A). After miR-34a over-expression, 3 of the 5 genes (*MCM5*, *PLK1* and *MYT1*) had reduced mRNA by at least 2-fold (Figure 7B) and all 5 had significantly reduced protein (Figure 7C). Two other MCM genes, *MCM2* and *MCM4*, also demonstrated a significant miR-34a-dependent reduction in mRNA, and their protein levels became undetectable in miR-34a-transfected cells.

To investigate whether these 5 genes are directly regulated, we measured changes in luciferase activity in HeLa cells after miR-34a co-transfection with reporters containing their 3′UTRs. The 3′UTRs of 4 of 5 of these genes (*CCND3*, *MCM5*, *PLK1* and *SMAD4*) were significantly repressed 30–60% by miR-34a (Figure 7D). The 3′UTR of *MYT1*, which bound to Bi-miR-34a and was down-regulated by miR-34a over-expression (Figure 7A, 7B), was not regulated by miR-34a. *MYT1* expression could be regulated by MREs outside the 3′UTR or indirectly. PITA and TargetScan were used to identify miR-34a MREs in the 3′UTRs of *CCND3*, *SMAD4*, *MCM5*, and *PLK1* (Figure 7E, Figure S5). *CCND3* MRE1, *SMAD4* MRE1 and *MCM5* MRE5 were significantly suppressed by miR-34a (Figure 7E, Figure S5). The *CCND3* and *SMAD4* MREs were predicted by TargetScan, while *MCM5* MRE5 contains a miR-34a hexamer seed match. Mutations that disrupt base pairing with miR-34a rescued luciferase expression, further confirming that these genes are direct miR-34a targets. Because the enrichment ratios for *MCM2* and *MCM4* in the pull-down (~2.3) were close to our cut-off, we also evaluated whether *MCM2* and *MCM4* might be direct targets. *MCM2* is a direct target as verified by mRNA enrichment in the pull-down, decrease in mRNA and protein following miR-34 over-expression, miR-34a regulation of its 3′UTR by luciferase activity and MRE identification (Figure 7A–7E). However, the *MCM4* 3′UTR was not active in luciferase assays. Collectively, these findings suggest that miR-34a acts as a master regulator of cell proliferation, directly suppressing many key genes that control cell cycle progression.

Discussion

Despite improvements in bioinformatic and experimental tools, distinguishing the direct targets of a miRNA from indirectly regulated genes remains challenging [14]. Here we describe a simple biochemical method to isolate candidate miRNA targets by streptavidin pull-down of mRNAs that associate with a transfected Bi-miRNA, and apply it to study miR-34a. Comparison of the set of mRNAs that directly associate with the Bi-miRNA with mRNAs down-regulated by miRNA over-expression makes it possible to distinguish the direct and indirect effects of a miRNA. Candidates identified by Bi-miR-34a pull-down have properties of validated miRNA targets: they are enriched for sequences complementary to the miR-34a seed and tend to decrease in expression with miR-34a over-expression. Genes that both decrease in mRNA abundance after over-expression and are isolated by Bi-miR-34a pull-down are further enriched for seed matches, indicating that either they are more likely true miR-34a targets or that a perfect seed match might enhance target mRNA degradation.

In our analysis we defined candidate direct targets using an arbitrary enrichment ratio cut-off of 1 SD, which corresponded to an enrichment of ≥2.5-fold for HCT116 cells and ≥3.3-fold for K562 cells. As the enrichment ratio cut-off was increased, mRNA suppression after ectopic miR-34a expression increased in tandem (Figure 2D). A more stringent cut-off would reduce the already low false positive rate, but also reduce the sensitivity to detect direct targets (Figure 2B). With this cut-off, we identify 71% of the known miR-34a targets expressed in HCT116 cells as "hits", but only 48% of the known expressed targets in K562 cells. If we had also chosen a 2.5-fold cut-off for K562 cells, our sensitivity for picking targets would have increased to 55%, while a 2-fold cut-off would have increased it to 69%. Since 10 of 11 genes in the random list of genes enriched by ≥2.5 fold by Bi-miR-34a pull-downs in both cells have 3′UTRs regulated directly by miR-34a by luciferase assay, a lower cut-off for the enrichment ratio might have increased sensitivity without an unacceptable false discovery rate. Some bona fide target genes are only enriched in the pull-down by ~2-fold; one of the novel genes we validated by identifying its MRE (*MCM2*) was only enriched by 2.3-fold in the pull-down of both cell lines. The low false positive rate of target identification demonstrated with the random gene list was also supported by the high degree of experimental validation of the growth factor signaling and cell cycle regulatory genes we chose to examine experimentally (Table S2). In all, we provided experimental evidence for 14 novel direct targets of miR-34a and identified 14 miR-34a MREs, of which 11 had a perfect hexamer seed match and the 3 others had perfect matches if G:U wobbles were allowed. Thus, the majority of genes we identified as regulated by miR-34a contain canonical 3′UTR MREs with good seed pairing. In the setting of over-expression by transfection, protein levels of all 11 genes we analyzed by immunoblot declined substantially. The few target genes that we tested for which we did not find miR-34a regulation of the 3′UTR might be false positives or might be direct targets, regulated by sequences in the 5′UTR or CDS. In fact we found enrichment for hexamer seed matches in these regions in the mRNAs pulled down with miR-34a, consistent with MRE

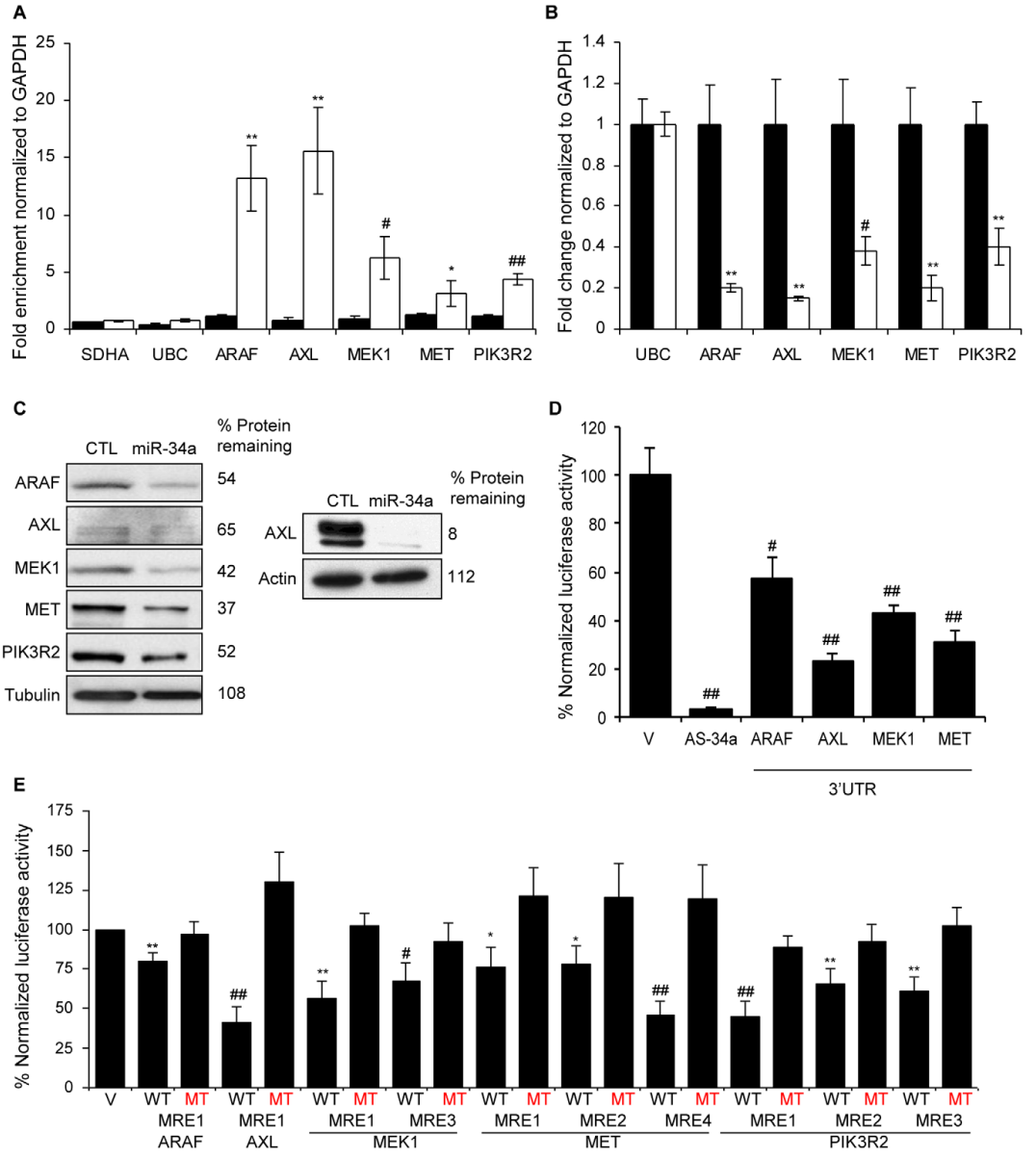

Figure 6. miR-34a directly inhibits growth factor signaling and signal transduction pathways by regulating novel genes. (A) Five genes involved in growth factor signaling or signal transduction are pulled down by Bi-miR-34a. HCT116 cells were transfected with Bi-cel-miR67 (CTL miRNA, black) or Bi-miR-34a (white) mimics for 24 hr and mRNA capture was measured by qRT-PCR normalized to *GAPDH*. Five of 5 (*ARAF*, *AXL*, *MEK1*, *MET* and *PIK3R2*) genes identified by microarrays, but not housekeeping mRNAs *SDHA* and *UBC*, are significantly enriched in the Bi-miR-34a pull-down. (B) miR-34a decreases *ARAF*, *AXL*, *MEK1*, *MET* and *PIK3R2* mRNAs, measured by qRT-PCR relative to *GAPDH*, in HCT116 cells transfected with CTL (black) or miR-34a (white) for 48 hr. *UBC* is a negative control gene. Relative mRNA levels were normalized to levels in CTL miRNA-transfected cells. (C) ARAF, AXL, MEK1, MET and PIK3R2 protein levels decline by immunoblot after miR-34a over-expression in HCT116 cells harvested 48 hrs after transfection with CTL miRNA or miR-34a mimic. Because of the low signal for AXL, an additional experiment probed for AXL with a longer exposure is shown at right. (D) miR-34a significantly regulates the 3′UTR of *ARAF*, *AXL*, *MEK1* and *MET* in HeLa cells co-transfected with a dual luciferase reporter bearing the 3′UTR of each gene and CTL miRNA or miR-34a for 48 hr. Insertion of a sequence fully complementary to miR-34a into the *Renilla luciferase* 3′UTR (AS-34a) is the positive control. Luciferase activity was normalized to results obtained with the empty vector (V). (E) Luciferase

reporters bearing PITA-predicted wild-type (WT) MREs from each target gene are significantly repressed in HeLa cells cotransfected with miR-34a. Point mutations (MT) that disrupt base pairing with miR-34a rescue reporter expression. MRE sequences are provided in Figure S4.
doi:10.1371/journal.pgen.1002363.g006

properties in recent cross-linking-RISC immunoprecipitation experiments [23,25].

Known targets may not have been identified by the pull-down for a variety of reasons. First, not all of the targets in the literature may be correctly assigned. Second, some known targets, such as CD44, are only modestly regulated by miR-34a [40]. The ratio that defines a "hit" is arbitrary. We set a relatively high threshold for identifying "hits" to maximize the specificity of the method (especially given the large numbers of enriched mRNAs in the pull-down), which came at the cost of sensitivity. Some known targets, which we did not designate hits with our 1 S.D. threshold of the enrichment ratio (which corresponded to >3.3 in K562 cells) had enrichment ratios of 2.5–3.2 in K562 cells. Other bona fide targets may have low, but detectable expression levels, and could have been missed due to the low sensitivity and inter-assay variability of microarray experiments. In addition to cellular variation in endogenous miRNA expression and RISC abundance, other context-dependent biological factors, such as target site accessibility, might vary due to the expression of RNA binding proteins, which could influence the efficiency of miRNA target site binding and the mechanism of targeting [51,52]. Cell-type specific expression of other MRE-containing genes that compete for miRNA binding could also influence the pull-down enrichment ratio [53]. Finally, some missed targets are likely to be false negatives.

Normalizing the pulled down mRNAs to their abundance in the input cellular mRNA was critical to eliminate from consideration highly abundant housekeeping mRNAs. Our pull-down method modified a previously developed protocol [41,42], which did not normalize the pull-down mRNAs to the input RNA. Many of the "hits" pulled down with Bi-miR-10a included ribosomal mRNAs, which may represent background binding of very abundant transcripts. Moreover, the miR-10a "hits" were not enriched for mRNAs containing miR-10a 3′UTR seed matches and were not down-regulated by miR-10a over-expression. In other work to be presented elsewhere, the pull-down method was used to identify genome-wide targets of miR-200c and miR-21. Importantly, the miR-200c and miR-21 pulled down mRNAs are also enriched for known targets and for 3′UTR seed sequences.

An advantage to the Bi-miRNA pull-down method described here is its simplicity. In contrast to mRNA expression-based target identification methods, Bi-miRNA pull-downs should identify only direct targets, excluding genes whose expression is indirectly modulated by changes in miRNA expression. Because the degree of mRNA suppression mediated by miRNAs is often small relative to changes in protein, methods that rely on changes in mRNA expression in response to manipulation of miRNA levels will necessarily miss some direct targets. Although the enrichment ratio takes into account a reduction in target gene mRNA in its denominator, the pull-down should not only identify target genes whose mRNA levels decline, but also those that are regulated primarily by inhibiting translation. Unlike approaches based on Ago pull-downs, the Bi-miRNA pull-down identifies the mRNAs directly associated with a specific miRNA, simplifying analysis of biological processes regulated by the miRNA.

The method described here without cross-linking does not directly identify MREs. The streptavidin pull-down method might, however, readily be modified to include cross-linking, RNase digestion of unbound mRNA segments and sequencing, similar to the HITS-CLIP protocol [23,24], to capture not only direct targets, but also identify MREs of an individual Bi-miRNA. Isolating RNAs associated with an individual miRNA rather than all RISC-associated RNAs in cells over-expressing the miRNA of interest might be a more direct way to define specific target sequences. Future bioinformatic studies of Bi-miRNA pull-down datasets could be used to better define in an unbiased manner the sequence features that dictate miRNA targeting, and could reveal non-canonical modes of targeting, such as those that contain only partial seed complementarity [17] or pairing to the central region of the miRNA [18] or that lie outside the 3′UTR. Indeed, in this work, we enriched for mRNAs with 5′UTR and CDS seed matches, indicating that some direct miR-34a targets may be regulated outside of their 3′UTR.

Only 29% of the 2416 enriched genes in the HCT116 pull-down had down-regulated mRNA levels by mRNA microarray analysis after over-expressing miR-34a for one day, while 10 of 11 randomly chosen genes in the pull-down had significantly decreased mRNA by qRT-PCR analyzed 72 hr after transfection. Thus although miRNAs may commonly lead to mRNA degradation, the degree of mRNA down-regulation of most genes is slight if cells are harvested within a day of transfection. mRNA microarrays may be too noisy to detect subtle changes in expression, unless the analysis is performed on many replicates. Our data also suggest that the kinetics of mRNA degradation may be slow. The early 24 hr time point used for the assay may have fortuitously enhanced our ability to capture miRNA-bound transcripts before too many had been degraded. Indirect effects of the miRNA are also likely to increase over time. The set of genes enriched in the miR-34a pull-down of both HCT116 and K562 cells contains 76 transcription factors or co-factors, whose suppression would reduce many mRNAs.

One important corollary of our results is that miR-34a likely directly regulates hundreds of genes. However, further experimental work is needed to assess how many of the hundreds to thousands of genes whose mRNAs associated with ectopic miR-34a are actually directly regulated by endogenous miR-34a. Possibly only a minority of potential targets is indeed directly regulated in an individual cell at any time. Based on our analysis (Figure 2D), the genes whose transcripts are most enriched in the pull-down may be the most significant targets in a given context. Additional experiments are needed to probe the functional consequences of miR-34a regulation of the genes we identified as targets. The directly regulated genes might vary considerably from cell type to cell type or even in the same cell lineage depending on differentiation state or environmental conditions. For this study we focused on the shared targets identified in two very different types of cells, rather than the ones that were unique to each cell-type. The pull-down method could be used in the future to compare miRNA target genes in different cellular contexts. Notably, the effect of miR-34a on cell signaling differed in the cancer cells we examined. Basal phosphorylation of AKT and ERK was reduced by miR-34a over-expression in HCT116 and HeLa cells (Figure 5), but not in A549 cells (Figure S4). Constitutively active RAS in A549 cells may override the effect of miR-34a in that context. Our results suggest that a dense network of genes that participate in common pathways, sometimes with opposing functions, is capable of being regulated by one miRNA. Although we observed a clear effect of genetic loss of miR-34a on the ability to cells to survive growth factor withdrawal, we did not see reduced expression in miR-34a$^{-/-}$ compared to wild-type

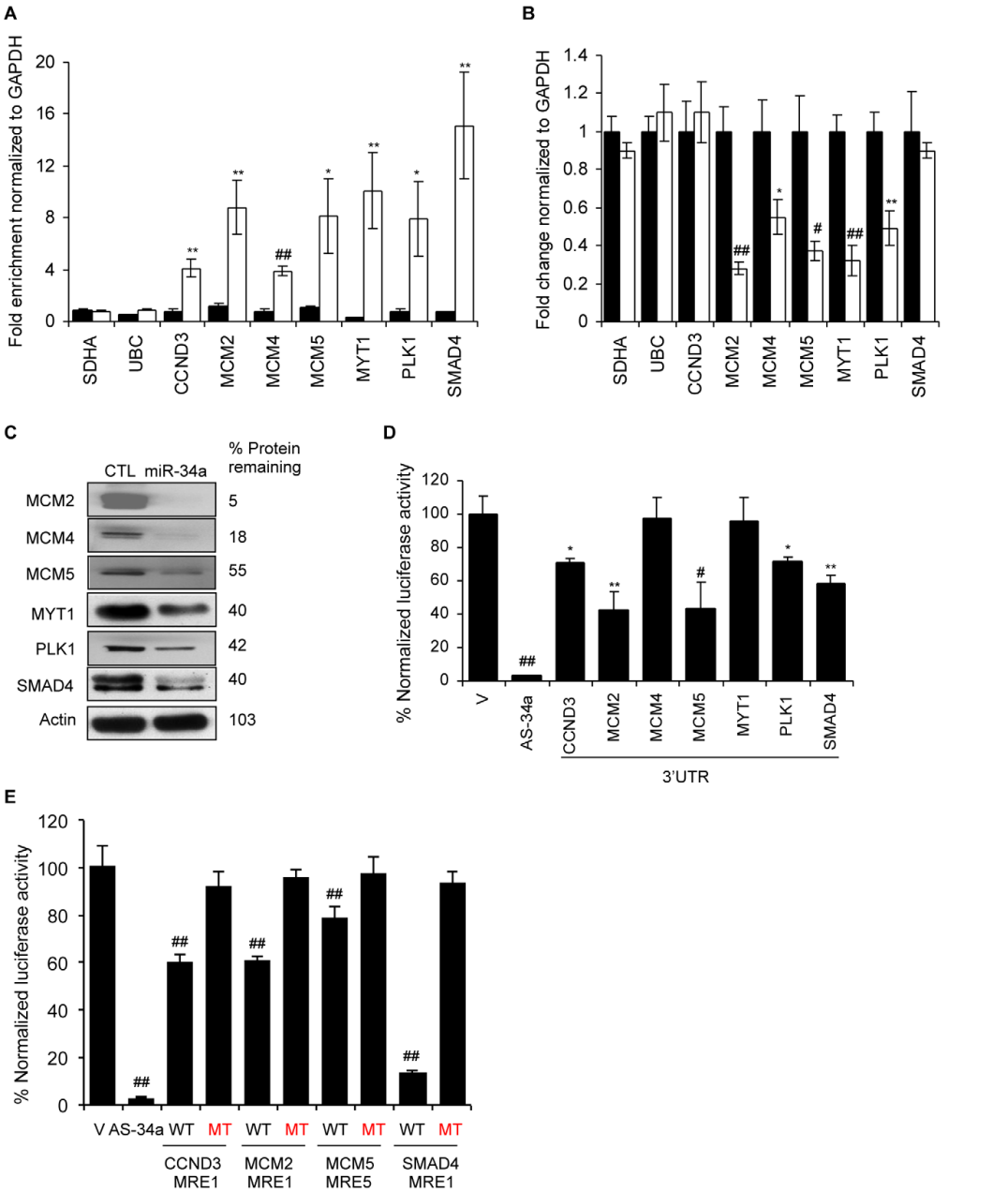

Figure 7. miR-34a pull-downs identify novel miR-34a targets involved in cell cycle progression. (A) Bi-miR-34a pull-down captures transcripts of cell cycle genes. Enrichment of candidate mRNAs in HCT116 cells transfected with Bi-cel-miR-67 miRNA (CTL, black) or Bi-miR-34a (white) for 24 hr was assessed by qRT-PCR analysis normalized to *GAPDH*. *SDHA* and *UBC* mRNAs are housekeeping genes not enriched in the pull-downs. (B) miR-34a over-expression significantly suppresses mRNA levels of 5 of 7 cell cycle genes tested. mRNA expression was analyzed by qRT-PCR relative to *GAPDH* performed on total RNA harvested from HCT116 cells transfected with CTL miRNA (black) or miR-34a (white) mimics for 48 hr. Two candidate target genes (*CCND3* and *SMAD4*) and the housekeeping genes *SDHA* and *UBC* are not significantly altered. (C) Protein levels of 6 of 6 cell cycle genes examined decrease with miR-34a over-expression. HCT116 cells were transfected with CTL miRNA or miR-34a mimics for 48 hr before immunoblot. β-Actin is a loading control. (D) miR-34a represses the 3′UTR of *CCND3*, *MCM2*, *MCM5*, *PLK1* and *SMAD4*, but not *MCM4* and *MYT1*. HeLa

cells were cotransfected for 48 hr with CTL miRNA or miR-34a mimics and psiCHECK-2 empty vector (V) or psiCHECK-2 containing the 3′UTR of each gene in the *Renilla luciferase* 3′UTR. The positive control reporter contained a perfectly complementary sequence to miR-34a (AS-34a). Relative luciferase activity in miR-34a-transfected cells is normalized to CTL miRNA-transfected cells. (E) Dual luciferase reporter plasmids bearing wild-type (WT) MREs from *CCND3*, *MCM2*, *MCM5* and *SMAD4* are significantly repressed by co-transfection with miR-34a in HeLa cells. Mutation of the seed region of each MRE (MT) rescues reporter expression. MRE sequences are provided in Figure S5. *, $p<0.05$, #, $p<0.01$, **, $p<0.005$, ##, $p<0.001$.
doi:10.1371/journal.pgen.1002363.g007

cells of some of the key miR-34a target genes we identified. Since growth factor signaling is so central to cell survival and proliferation, the permanent loss of miR-34a expression likely led to myriad compensatory changes. This seeming paradox supports the conclusions of our study – namely that a single miRNA may exert its biological effect by regulating expression of hundreds of genes. The capacity of miR-34a to potentially regulate so many genes that affect growth factor signaling may enable it to exert an effect in diverse contexts.

The numbers of genes that are actually regulated by miR-34a in any setting will likely depend on how strongly miR-34a is expressed. In our pull-down, we greatly over-expressed miR-34a. However, the level of over-expression throughout this study was not greater than endogenous miR-34a expression in some physiological settings, i.e. in K562 cells stimulated with phorbol ester where miR-34a increases 1000-fold [9]. There may be a target gene hierarchy – some genes regulated by low levels of miR-34a, others regulated only by high levels.

The dense network of cell signaling genes captured in the pull-downs suggests that an important function of miR-34a is to regulate the proliferative and activation responses to extracellular growth factors. Despite its function in regulating growth factor signaling and cell proliferation, we did not find a significant variation in miR-34a expression after serum starvation or when cells were synchronized in different phases of the cell cycle (data not shown). In this study we experimentally verified as direct miR-34a targets 5 growth factor signaling genes (*ARAF*, *AXL*, *MEK1*, *MET* and *PIK3R2*). miR-34a was previously shown to inhibit the G_1/S transition [3,8]. Here we identified 7 novel cell cycle-regulating direct targets that included genes also required for DNA replication and mitosis. The ultimate anti-proliferative effect of miR-34a integrates both direct consequences of suppressing expression of genes required for progression through the G1/S transition and at other steps of the cell cycle as well as indirect anti-proliferative effects from repressing the growth factor signaling pathways that activate cell cycle progression. Consistent with our genome-wide target gene analysis, miR-34a expression resets the basal state of ERK and AKT phosphorylation in several cell lines, rendering cells less responsive to growth factor signaling (Figure 5). This was shown both by miR-34a overexpression as well as by genetic deletion. miR-34a may reduce cellular sensitivity to growth factor signaling by suppressing many genes in multiple signal transduction pathways. miR-34a candidate targets include genes that are universally involved in transmitting growth factor activation signals as well as some that participate in specific pathways. The particular signaling genes that are suppressed in a given cell line will likely vary from cell to cell, depending on the growth factors to which the cell responds. These types of differences likely contribute to the incomplete overlap between the enriched pathways captured in the two hematopoietic and colon cancer cell lines examined here.

Materials and Methods

Cell lines

HCT116, K562, A549 and HeLa cells were from ATCC. miR-34a$^{+/+}$ and miR-34a$^{-/-}$ MEFs were generated from E14.5 littermate embryos. A full description of the mice will be published elsewhere. MEFs were transformed by infecting the cells with retroviruses encoding H-RAS-V12 and E1A and by selection with puromycin (1 μg/ml) and hygromycin (50 μg/ml). The plasmids for expression of H-RAS-V12 (plasmid 9051) and E1A (plasmid 18748) were obtained from Addgene. The VSV-G pseudotyped viruses were produced in 293T cells using the standard protocol. MEFs, HCT116, A549 and HeLa cells were grown in DMEM with 10% fetal bovine serum and supplemented with penicillin, streptomycin, HEPES, L-glutamine and β-mercaptoethanol, K562 cells were grown in RPMI containing 10% fetal bovine serum and the same supplements.

Transfection of miRNA mimics and plasmid DNA

For most experiments, 2×10^6 HCT116 or K562 cells were transfected with 200 pmol hsa-miR-34a or cel-miR-67 miRNA mimics (Dharmacon), using Amaxa nucleofection according to the manufacturer's protocol. Biotin was attached to the 3′-end of the active strand. HeLa and A549 cells were transfected with Lipofectamine 2000 and miRNA mimics at a final concentration of 50 nM (Invitrogen). To study the association of Bi-miRNAs with HA-Ago1 or HA-Ago2, pIRESNeo (Clontech) or pIRESNeo-HA-Ago1 or pIRESNeo-HA-Ago2 (Addgene) plasmids were co-transfected in six-well plates (2 μg/well, 1×10^6 cells/well) with 200 pmol Bi-miR-34a or Bi-cel-miR-67 using Amaxa as per the manufacturer's instructions.

RNA isolation and quantitative RT–PCR

Total RNA was isolated using Trizol reagent (Invitrogen), treated with DNase I (Ambion) and reverse transcribed using random hexamers and superscript III reverse transcriptase (Invitrogen). qRT-PCR was performed in triplicate samples using SYBR Green FastMix (Quanta) on a BioRad CFX96. mRNA levels were normalized to housekeeping genes *GAPDH*, *UBC* or *SDHA*. miRNA was quantified in triplicate using the TaqMan MicroRNA Assay (Applied Biosystems) as per the manufacturer's instructions and normalized to U6. Primer sequences are listed in Table S3.

Immunoblot

Whole cell lysates from transfected K562 or HCT116 cells were prepared using RIPA buffer. Proteins were analyzed by SDS-PAGE, transferred to nitrocellulose membranes and probed with the following antibodies: AXL [4566], ARAF [4432], MEK1 [9124], CDK4 [2906], MCM2 [3619], PKMYT1 [4282], PLK1 [4513], SMAD4 [9515], FOXP1 [2005], RBBP4 [4633], AKT [9272], pAKT ser-473 [4051], ERK [4370], pERK [9107] from Cell Signaling; MET [sc-161], MCM5 [sc-165995], E2F1 [sc-251], E2F3 [sc-879], CHEK1 [sc-8408] from Santa Cruz; ACSM3 [SAB1400253], MAD2L2 [SAB1400387], AGBL5 [AV53752], CCNG2 [AV03032], PSMD5 [WH0005711M1] from Sigma; MCM4 [06-1296] from Millipore; and PI3KR [610045], BD Biosciences. Western Blots were quantified by densitometry.

Biotin pull-down

HCT116 or K562 cells (1×10^6) were transfected in triplicate with Bi-miR-34a or Bi-cel-miR-67 (Dharmacon) as described

above and then cultured in six-well plates. Twenty-four hours later, the cells from 3 wells were pelleted at 500×g. After washing twice with PBS, cell pellets were resuspended in 0.7 ml lysis buffer (20 mM Tris (pH 7.5), 100 mM KCl, 5 mM $MgCl_2$, 0.3% NP-40, 50 U of RNase OUT (Invitrogen), complete mini-protease inhibitor cocktail (Roche Applied Science)), and incubated on ice for 5 min. The cytoplasmic lysate was isolated by centrifugation at 10,000×g for 10 min. Streptavidin-coated magnetic beads (Invitrogen) were blocked for 2 hr at 4°C in lysis buffer containing 1 mg/ml yeast tRNA and 1 mg/ml BSA (Ambion) and washed twice with 1 ml lysis buffer. Cytoplasmic lysate was added to the beads and incubated for 4 h at 4°C before the beads were washed five times with 1 ml lysis buffer. RNA bound to the beads (pull-down RNA) or from 10% of the extract (input RNA), was isolated using Trizol LS reagent (Invitrogen). The level of mRNA in the Bi-miR-34a or Bi-cel-miR-67 control pull-down was quantified by qRT-PCR or mRNA microarray. For qRT-PCR, mRNA levels were normalized to a housekeeping gene (*GAPDH*, *SDHA* or *UBC*). The enrichment ratio of the control-normalized pull-down RNA to the control-normalized input levels was then calculated.

Microarray analysis

Total RNA (independently in two experiments) was amplified, labeled and hybridized to Affymetrix U133 plus 2.0 mRNA microarrays. The quality of the RNA was assessed before performing the microarray and the quality of the microarray data was assessed using affyPLM and Affy software. The replicate data sets for the 4 sets of samples (pull-down and input for miR-34a and cel-miR-67) were compared using an unsupervised hierarchical clustering algorithm, which verified the similarity of the duplicates. The microarray data were normalized using RMA [7] to reduce interarray variation. The enrichment ratio {Bi-miR-34a PD/Bi-cel-miR-67 PD}/{Bi-miR-34a input/Bi-cel-miR-67 input} was calculated for each probe. For genes represented by multiple probes, the mean ratio for all the probes was calculated. Genes for which none of the probe hybridization signals exceeded the background were considered not expressed and were disregarded in the analysis. For informatic analysis of the PD data, genes whose enrichment ratio were ≥1 SD above background based on a log-normal distribution were considered "hits".

Gene down-regulation after miR-34a over-expression

HCT116 or K562 cells were transfected in independent duplicate experiments as above with unbiotinylated miR-34a or cel-miR-67 (Dharmacon) and total RNA was harvested 24 hr later and analyzed as above by gene expression microarrays. After normalization, fold changes for each probe were calculated as the ratio of input RNA from miR-34a-transfected cells to the ratio of input RNA from cel-miR-67-transfected cells. Genes were considered down-regulated if the ratio decreased by at least 20%, which corresponded to ~1 SD. To test the expression levels of putative target sets, each gene list was plotted in a cumulative distribution function (CDF) plot, and the Kolmogorov-Smirnov [KS] test was used for statistical comparisons between gene sets.

Analysis of miR-34a target genes by target prediction algorithms

To determine whether a gene was also a predicted target of miR-34a, the presence of miR-34a binding sites was analyzed using TargetScan 4.2 (http://www.targetscan.org/) [39,54,55] or PITA (http://132.77.150.113/pubs/mir07/mir07_prediction.html) [50].

Hexamer analysis

The mature hsa-miR-34a sequence was obtained from miRBase (http://mirbase.org/). All RefSeq human mRNA sequences were downloaded from NCBI in July 2009 (http://ftp.ncbi.nih.gov/). mRNAs were indexed by Entrez Gene ID; in cases where multiple sequences matched a gene ID, the sequence with the longest 3′UTR was selected. For each test gene list and miR-34a hexamer, the miR-34a hexamer frequency (hexamer matches per kb of sequence) was calculated. The frequency of hexamer matches for all genes on the microarray (the background set) was also determined. Gene IDs with no corresponding sequence in the database were excluded from analysis. Monte Carlo simulations of equally sized random gene sets (without replacement) were used to generate an empirical 2-tailed p-value for each gene set/hexamer combination. When $p<1E-4$, the p-value was calculated from curve fitting relative to the random background distribution.

Pathway enrichment analysis and network visualization

For each of the lists of down-regulated and pull-down-enriched genes, the p-value of over-representation in a suite of canonical pathways (KEGG [56] and Wikipathways [57]) was determined using the hypergeometric distribution. A visualization of the relationship between the enriched pathways ($p<0.001$) based on the number of overlapping genes was rendered using Cytoscape [58]. The network of gene-gene interactions underlying these relationships was constructed based on interactions supplied by MetaCore (GeneGo Inc). Physical, predicted and genetic interactions were used to connect the down-regulated and pull-down enriched genes within the significant signaling, cell cycle or DNA repair pathways. Signaling pathway genes with no connection to any other node were removed and the network was arranged according to predicted sub-cellular localization.

Luciferase assay

HeLa cells were cotransfected in 24 well plates using Lipofectamine 2000 (Invitrogen) with 50 nM miR-34a mimic or control miRNA mimic and 50 ng of psiCHECK2 (Promega) vector containing the MRE or 3′UTR of indicated genes cloned into the multiple cloning site of *Renilla* luciferase. After 48 hr of transfection (unless otherwise indicated) luciferase activities were measured using the Dual Luciferase Assay System (Promega) and Top count NXT microplate reader (Perkin Elmer) per manufacturer's instructions. All experiments were performed at least in triplicate. Results were normalized to those obtained in cells transfected with an empty vector. For some experiments, a perfectly complementary antisense sequence to the active strand of miR-34a was inserted into the multiple cloning site for use as a positive control. Data were normalized to *Firefly* luciferase and results from 3 independent experiments were compared. Sequence of primers used for cloning 3′UTRs for miR-34a target genes are listed in Table S4. MREs sequences were cloned into psiCHECK-2 by annealing complementary oligomers matching each MRE sequence (Figures S4, S5) with overhanging ends complementary to the XhoI and NotI sites of psiCHECK-2.

Cell growth experiments

HCT116, HeLa and A549 cells were transfected as described above. One day after transfection, cells were placed in serum-free medium or medium containing 10% fetal calf serum. 48 hours after the medium was changed, total cell numbers were counted. MEFs were plated at a density of 2.5×10^5 or 5×10^5 cells per well of a 6-well plate. The medium was changed to vary serum concentration 24 hr after plating. The MEFs were harvested 24 hr

later and counted using Trypan blue staining or stained in PBS+0.4% BSA with annexinV-APC (Invitrogen) at a 1:30 dilution, then washed once and stained with propidium iodide (4 μg/ml) (Sigma-Aldrich).

Supporting Information

Figure S1 (A) HCT116 cells were transfected with Bi-miR-34a or Bi-cel-miR-67 (CTL) and after 24 hr, abundance of known miR-34a target mRNAs (*CDK4*, *CDK6* and *MYB*) was measured by qRT-PCR analysis of pull-down RNA. *CDK4*, *CDK6* and *MYB* and not *UBC* (a housekeeping mRNA) were significantly enriched in the Bi-miR-34a pull-downs (white) and not the control pull-down (black). (B) K562 cells were transfected with Bi-miR-34a (white) or Bi-CTL (black), and RNA isolated from the streptavidin pull-down was analyzed by qRT-PCR for miR-34a and miR-24 (a control miRNA) after normalization to *U6*. miR-34a was ~50-fold higher in miR-34a pull-down as compared to control pull-down. miR-24 was not enriched and its levels were similar in each pull-down. (C) Addition of Bi-miR-34a (white) or Bi-CTL (black) to cytoplasmic extracts prepared from untransfected K562 cells does not enrich for known miR-34a target mRNAs, suggesting that the specific association of these mRNAs with Bi-miR-34a occurs in live cells and not post-lysis. Data in (B) are from 3 independent experiments and in (A) and (C) are from duplicate experiments.
(TIF)

Figure S2 Sequence characteristics of Bi-miR-34a pull-down targets. (A) Enrichment of hexamers matching each position of the mature miR-34a sequence in the HCT116 and K562 pull-down (red), down-regulated genes (blue), and genes down-regulated by miR-34a and pulled-down (yellow). Genes both enriched by Bi-miR-34a pull-down and down-regulated by miR-34a are the most enriched for miR-34a seed matches (B) Hexamer enrichment analysis for genes enriched in both HCT116 and K562 Bi-miR-34a pull-downs. Bi-miR-34a pull-down enriched for sequences matching two miRNA regions: the seed (positions 1–8) and a possible 3′ compensatory region (positions 13–19). Bi-miR-34a pull-down mRNAs are also enriched for CDS and 5′UTR matches to these sequences (*$p \leq 0.0001$).
(TIF)

Figure S3 Pathway networks representing the significant canonical pathways enriched for TargetScan conserved (A) and TargetScan non-conserved (B) target predictions.
(TIF)

Figure S4 miR-34a regulation of growth factor signaling. (A) Western blots of A549 cells transfected with miR-34a or CTL mimics. No reproducible change in pERK or pAKT was observed in these cells. (B) A549 cells were transfected with miR-34a or cel-miR-67 (CTL) mimics, and placed in normal growth medium with 10% serum (+) or growth medium lacking serum (−). Cells transfected with miR-34a did not proliferate in response to serum. Candidate miR-34a microRNA recognition elements (MRE) in the 3′UTR of *AXL*, *ARAF*, *MEK1*, *MET* and *PIK3R2* mRNAs predicted by PITA (see Materials and Methods). Numbers in parenthesis represent the location of the MRE in the 3′UTR. Wild-type MREs in (C) were repressed by miR-34a (see Figure 5F) whereas MREs that were not responsive to miR-34a are shown in (D). Point mutations that disrupt the base-pairing with miR-34a are shown in red in the mutant MREs.
(TIF)

Figure S5 Candidate miR-34a microRNA recognition elements (MRE) in the 3′UTR of *CCND3*, *MCM2*, *MCM5*, *PLK1* and *SMAD4* mRNAs predicted by PITA or TargetScan (see Materials and Methods). Numbers in parenthesis represent the location of the MRE in the 3′UTR (*PLK1* MRE2 spans the stop codon of *PLK1*). Wild-type MREs in (A) were repressed by miR-34a (see Figure 6E), whereas MREs that were not responsive to miR-34a are shown in (B). Point mutations that disrupt the base-pairing with miR-34a are shown in red in the mutant MREs.
(TIF)

Table S1 Genes enriched in Bi-miR-34a pull-downs or down-regulated by miR-34a over-expression in HCT116 and K562 cells.
(XLS)

Table S2 Experimental validation of miR-34a target genes.
(XLS)

Table S3 Sequence of primers used for qRT-PCR.
(XLS)

Table S4 Sequence of primers used for cloning 3′UTR of miR-34a target genes.
(XLS)

Acknowledgments

We thank Alex Amiet and Devin Leake (Dharmacon) for providing the Bi-miRNAs and A. Regev (Broad Institute), D. Chowdhury (DFCI), N. Caplen (NCI), P. Aplan (NCI) and Lieberman laboratory members for useful discussions.

Author Contributions

Conceived and designed the experiments: AL MPT GA FN AV WH JL. Performed the experiments: AL MPT FN EO XLL CC Y-CH JT DKR AD. Analyzed the data: AL MPT GA OH. Contributed reagents/materials/analysis tools: AV WH. Wrote the paper: AL MPT JL.

References

1. Garzon R, Calin GA, Croce CM (2009) MicroRNAs in Cancer. Annu Rev Med 60: 167–179. doi:10.1146/annurev.med.59.053006.104707.
2. He L, He X, Lowe SW, Hannon GJ (2007) microRNAs join the p53 network [mdash] another piece in the tumour-suppression puzzle. Nat Rev Cancer 7: 819–822. doi:10.1038/nrc2232.
3. Sun F, Fu H, Liu Q, Tie Y, Zhu J, et al. (2008) Downregulation of CCND1 and CDK6 by miR-34a induces cell cycle arrest. FEBS Letters 582: 1564–1568. doi:10.1016/j.febslet.2008.03.057.
4. Tazawa H, Tsuchiya N, Izumiya M, Nakagama H (2007) Tumor-suppressive miR-34a induces senescence-like growth arrest through modulation of the E2F pathway in human colon cancer cells. Proceedings of the National Academy of Sciences 104: 15472–15477. doi:10.1073/pnas.0707351104.
5. Yamakuchi M, Ferlito M, Lowenstein CJ (2008) miR-34a repression of SIRT1 regulates apoptosis. Proceedings of the National Academy of Sciences 105: 13421–13426. doi:10.1073/pnas.0801613105.
6. Raver-Shapira N, Marciano E, Meiri E, Spector Y, Rosenfeld N, et al. (2007) Transcriptional Activation of miR-34a Contributes to p53-Mediated Apoptosis. Molecular Cell 26: 731–743. doi:10.1016/j.molcel.2007.05.017.
7. Chang T-C, Wentzel EA, Kent OA, Ramachandran K, Mullendore M, et al. (2007) Transactivation of miR-34a by p53 Broadly Influences Gene Expression and Promotes Apoptosis. Molecular Cell 26: 745–752. doi:10.1016/j.molcel.2007.05.010.
8. He L, He X, Lim LP, de Stanchina E, Xuan Z, et al. (2007) A microRNA component of the p53 tumour suppressor network. Nature 447: 1130–1134. doi:10.1038/nature05939.
9. Navarro F, Gutman D, Meire E, Caceres M, Rigoutsos I, et al. (2009) miR-34a contributes to megakaryocytic differentiation of K562 cells independently of p53. Blood 114: 2181–2192. doi:10.1182/blood-2009-02-205062.
10. Christoffersen NR, Shalgi R, Frankel LB, Leucci E, Lees M, et al. (2009) p53-independent upregulation of miR-34a during oncogene-induced senescence represses MYC. Cell Death Differ 17: 236–245.
11. Bagchi A, Mills AA (2008) The Quest for the 1p36 Tumor Suppressor. Cancer Research 68: 2551–2556. doi:10.1158/0008-5472.CAN-07-2095.
12. Welch C, Chen Y, Stallings RL (2007) MicroRNA-34a functions as a potential tumor suppressor by inducing apoptosis in neuroblastoma cells. Oncogene 26: 5017–5022.

13. Vogt M, Munding J, Grüner M, Liffers S-T, Verdoodt B, et al. (2011) Frequent concomitant inactivation of miR-34a and miR-34b/c by CpG methylation in colorectal, pancreatic, mammary, ovarian, urothelial, and renal cell carcinomas and soft tissue sarcomas. Virchows Arch 458: 313–322. doi:10.1007/s00428-010-1030-5.
14. Thomas M, Lieberman J, Lal A (2010) Desperately seeking microRNA targets. Nat Struct Mol Biol 17: 1169–1174. doi:10.1038/nsmb.1921.
15. Bartel DP (2009) MicroRNAs: Target Recognition and Regulatory Functions. Cell 136: 215–233. doi:10.1016/j.cell.2009.01.002.
16. Rajewsky N (2006) microRNA target predictions in animals. Nat Genet 38 Suppl: S8–13. doi:10.1038/ng1798.
17. Lal A, Navarro F, Maher CA, Maliszewski LE, Yan N, et al. (2009) miR-24 Inhibits Cell Proliferation by Targeting E2F2, MYC, and Other Cell-Cycle Genes via Binding to "Seedless" 3′UTR MicroRNA Recognition Elements. Molecular Cell 35: 610–625. doi:10.1016/j.molcel.2009.08.020.
18. Shin C, Nam J-W, Farh KK-H, Chiang HR, Shkumatava A, et al. (2010) Expanding the MicroRNA Targeting Code: Functional Sites with Centered Pairing. Molecular Cell 38: 789–802. doi:10.1016/j.molcel.2010.06.005.
19. Baek D, Villén J, Shin C, Camargo FD, Gygi SP, et al. (2008) The impact of microRNAs on protein output. Nature 455: 64–71. doi:10.1038/nature07242.
20. Alexiou P, Maragkakis M, Papadopoulos GL, Reczko M, Hatzigeorgiou AG (2009) Lost in translation: an assessment and perspective for computational microRNA target identification. Bioinformatics 25: 3049–3055. doi:10.1093/bioinformatics/btp565.
21. Tay Y, Zhang J, Thomson AM, Lim B, Rigoutsos I (2008) MicroRNAs to Nanog, Oct4 and Sox2 coding regions modulate embryonic stem cell differentiation. Nature 455: 1124–1128. doi:10.1038/nature07299.
22. Johnson CD, Esquela-Kerscher A, Stefani G, Byrom M, Kelnar K, et al. (2007) The let-7 MicroRNA Represses Cell Proliferation Pathways in Human Cells. Cancer Res 67: 7713–7722. doi:10.1158/0008-5472.CAN-07-1083.
23. Chi SW, Zang JB, Mele A, Darnell RB (2009) Argonaute HITS-CLIP decodes microRNA-mRNA interaction maps. Nature 460: 479–486. doi:10.1038/nature08170.
24. Zisoulis DG, Lovci MT, Wilbert ML, Hutt KR, Liang TY, et al. (2010) Comprehensive discovery of endogenous Argonaute binding sites in Caenorhabditis elegans. Nat Struct Mol Biol 17: 173–179. doi:10.1038/nsmb.1745.
25. Hafner M, Landthaler M, Burger L, Khorshid M, Hausser J, et al. (2010) Transcriptome-wide Identification of RNA-Binding Protein and MicroRNA Target Sites by PAR-CLIP. Cell 141: 129–141. doi:10.1016/j.cell.2010.03.009.
26. Wei JS, Song YK, Durinck S, Chen Q-R, Cheuk ATC, et al. (2008) The MYCN oncogene is a direct target of miR-34a. Oncogene 27: 5204–5213. doi:10.1038/onc.2008.154.
27. Rao DS, O'Connell RM, Chaudhuri AA, Garcia-Flores Y, Geiger TL, et al. (2010) MicroRNA-34a Perturbs B Lymphocyte Development by Repressing the Forkhead Box Transcription Factor Foxp1. Immunity 33: 48–59. doi:10.1016/j.immuni.2010.06.013.
28. Takagi S, Nakajima M, Kida K, Yamaura Y, Fukami T, et al. (2010) MicroRNAs Regulate Human Hepatocyte Nuclear Factor 4α, Modulating the Expression of Metabolic Enzymes and Cell Cycle. Journal of Biological Chemistry 285: 4415–4422. doi:10.1074/jbc.M109.085431.
29. Ichimura A, Ruike Y, Terasawa K, Shimizu K, Tsujimoto G (2010) MicroRNA-34a Inhibits Cell Proliferation by Repressing Mitogen-Activated Protein Kinase Kinase 1 during Megakaryocytic Differentiation of K562 Cells. Molecular Pharmacology 77: 1016–1024. doi:10.1124/mol.109.063321.
30. Li N, Fu H, Tie Y, Hu Z, Kong W, et al. (2009) miR-34a inhibits migration and invasion by down-regulation of c-Met expression in human hepatocellular carcinoma cells. Cancer Letters 275: 44–53. doi:10.1016/j.canlet.2008.09.035.
31. Mudduluru G, Ceppi P, Kumarswamy R, Scagliotti GV, Papotti M, et al. (2011) Regulation of Axl receptor tyrosine kinase expression by miR-34a and miR-199a/b in solid cancer. Oncogene 30: 2888–2899.
32. Kaller M, Liffers S-T, Oeljeklaus S, Kuhlmann K, Röh S, et al. (2011) Genome-wide characterization of miR-34a induced changes in protein and mRNA expression by a combined pulsed SILAC and micro-array analysis. Molecular & Cellular Proteomics. Available: http://www.mcponline.org/content/early/2011/05/12/mcp.M111.010462.abstract. Accessed 1 Jul 2011.
33. Bommer GT, Gerin I, Feng Y, Kaczorowski AJ, Kuick R, et al. (2007) p53-mediated activation of miRNA34 candidate tumor-suppressor genes. Curr Biol 17: 1298–1307. doi:10.1016/j.cub.2007.06.068.
34. Chen Q-R, Yu L-R, Tsang P, Wei JS, Song YK, et al. (2011) Systematic Proteome Analysis Identifies Transcription Factor YY1 as a Direct Target of miR-34a. Journal of Proteome Research 10: 479–487. doi:10.1021/pr1006697.
35. Weeraratne SD, Amani V, Neiss A, Teider N, Scott DK, et al. (2011) miR-34a confers chemosensitivity through modulation of MAGE-A and p53 in medulloblastoma. Neuro-Oncology 13: 165–175. doi:10.1093/neuonc/noq179.
36. Hashimi ST, Fulcher JA, Chang MH, Gov L, Wang S, et al. (2009) MicroRNA profiling identifies miR-34a and miR-21 and their target genes JAG1 and WNT1 in the coordinate regulation of dendritic cell differentiation. Blood 114: 404–414. doi:10.1182/blood-2008-09-179150.
37. Pang RTK, Leung CON, Ye T-M, Liu W, Chiu PCN, et al. (2010) MicroRNA-34a suppresses invasion through downregulation of Notch1 and Jagged1 in cervical carcinoma and choriocarcinoma cells. Carcinogenesis 31: 1037–1044. doi:10.1093/carcin/bgq066.
38. Li Y, Guessous F, Zhang Y, DiPierro C, Kefas B, et al. (2009) MicroRNA-34a Inhibits Glioblastoma Growth by Targeting Multiple Oncogenes. Cancer Research 69: 7569–7576. doi:10.1158/0008-5472.CAN-09-0529.
39. Lewis BP, Shih I-hung, Jones-Rhoades MW, Bartel DP, Burge CB (2003) Prediction of Mammalian MicroRNA Targets. Cell 115: 787–798. doi:10.1016/S0092-8674(03)01018-3.
40. Liu C, Kelnar K, Liu B, Chen X, Calhoun-Davis T, et al. (2011) The microRNA miR-34a inhibits prostate cancer stem cells and metastasis by directly repressing CD44. Nat Med 17: 211–215. doi:10.1038/nm.2284.
41. Ørom UA, Lund AH (2007) Isolation of microRNA targets using biotinylated synthetic microRNAs. Methods 43: 162–165. doi:10.1016/j.ymeth.2007.04.007.
42. Ørom UA, Nielsen FC, Lund AH (2008) MicroRNA-10a Binds the 5′UTR of Ribosomal Protein mRNAs and Enhances Their Translation. Molecular Cell 30: 460–471. doi:10.1016/j.molcel.2008.05.001.
43. Lal A, Pan Y, Navarro F, Dykxhoorn DM, Moreau L, et al. (2009) miR-24-mediated downregulation of H2AX suppresses DNA repair in terminally differentiated blood cells. Nat Struct Mol Biol 16: 492–498. doi:10.1038/nsmb.1589.
44. Grimson A, Farh KK-H, Johnston WK, Garrett-Engele P, Lim LP, et al. (2007) MicroRNA Targeting Specificity in Mammals: Determinants beyond Seed Pairing. Molecular Cell 27: 91–105. doi:10.1016/j.molcel.2007.06.017.
45. Roberts PJ, Der CJ (2007) Targeting the Raf-MEK-ERK mitogen-activated protein kinase cascade for the treatment of cancer. Oncogene 26: 3291–3310. doi:10.1038/sj.onc.1210422.
46. Linger RMA, Keating AK, Earp HS, Graham DK (2008) TAM receptor tyrosine kinases: biologic functions, signaling, and potential therapeutic targeting in human cancer. Adv. Cancer Res 100: 35–83. doi:10.1016/S0065-230X(08)00002-X.
47. Gjerdrum C, Tiron C, Høiby T, Stefansson I, Haugen H, et al. (2010) Axl is an essential epithelial-to-mesenchymal transition-induced regulator of breast cancer metastasis and patient survival. Proceedings of the National Academy of Sciences 107: 1124–1129. doi:10.1073/pnas.0909333107.
48. Vanhaesebroeck B, Ali K, Bilancio A, Geering B, Foukas LC (2005) Signalling by PI3K isoforms: insights from gene-targeted mice. Trends in Biochemical Sciences 30: 194–204. doi:10.1016/j.tibs.2005.02.008.
49. Whittaker S, Marais R, Zhu AX (2010) The role of signaling pathways in the development and treatment of hepatocellular carcinoma. Oncogene 29: 4989–5005.
50. Kertesz M, Iovino N, Unnerstall U, Gaul U, Segal E (2007) The role of site accessibility in microRNA target recognition. Nat Genet 39: 1278–1284. doi:10.1038/ng2135.
51. Elcheva I, Goswami S, Noubissi FK, Spiegelman VS (2009) CRD-BP Protects the Coding Region of [beta]TrCP1 mRNA from miR-183-Mediated Degradation. Molecular Cell 35: 240–246. doi:10.1016/j.molcel.2009.06.007.
52. Vasudevan S, Tong Y, Steitz JA (2007) Switching from Repression to Activation: MicroRNAs Can Up-Regulate Translation. Science 318: 1931–1934. doi:10.1126/science.1149460.
53. Salmena L, Poliseno L, Tay Y, Kats L, Pandolfi PP (2011) A ceRNA Hypothesis: The Rosetta Stone of a Hidden RNA Language? Cell 146: 353–358. doi:16/j.cell.2011.07.014.
54. Lewis BP, Burge CB, Bartel DP (2005) Conserved Seed Pairing, Often Flanked by Adenosines, Indicates that Thousands of Human Genes are MicroRNA Targets. Cell 120: 15–20. doi:10.1016/j.cell.2004.12.035.
55. Friedman RC, Farh KK-H, Burge CB, Bartel DP (2009) Most mammalian mRNAs are conserved targets of microRNAs. Genome Research 19: 92–105. doi:10.1101/gr.082701.108.
56. Kanehisa M, Goto S (2000) KEGG: Kyoto Encyclopedia of Genes and Genomes. Nucleic Acids Research 28: 27–30. doi:10.1093/nar/28.1.27.
57. Pico AR, Kelder T, van Iersel MP, Hanspers K, Conklin BR, et al. (2008) WikiPathways: Pathway Editing for the People. PLoS Biol 6: e184. doi:10.1371/journal.pbio.0060184.
58. Shannon P, Markiel A, Ozier O, Baliga NS, Wang JT, et al. (2003) Cytoscape: A Software Environment for Integrated Models of Biomolecular Interaction Networks. Genome Research 13: 2498–2504. doi:10.1101/gr.1239303.

PERSPECTIVE

nature structural & molecular biology

Desperately seeking microRNA targets

Marshall Thomas[1], Judy Lieberman[1] & Ashish Lal[1,2]

MicroRNAs (miRNAs) suppress gene expression by inhibiting translation, promoting mRNA decay or both. Each miRNA may regulate hundreds of genes to control the cell's response to developmental and other environmental cues. The best way to understand the function of a miRNA is to identify the genes that it regulates. Target gene identification is challenging because miRNAs bind to their target mRNAs by partial complementarity over a short sequence, suppression of an individual target gene is often small, and the rules of targeting are not completely understood. Here we review computational and experimental approaches to the identification of miRNA-regulated genes. The examination of changes in gene expression that occur when miRNA expression is altered and biochemical isolation of miRNA-associated transcripts complement target prediction algorithms. Bioinformatic analysis of over-represented pathways and nodes in protein-DNA interactomes formed from experimental candidate miRNA gene target lists can focus attention on biologically significant target genes.

MicroRNAs regulate virtually every aspect of biology, including developmental timing, differentiation, proliferation, antiviral defense and metabolism. MicroRNAs are ~22-nucleotide-long RNAs that are generated by sequential processing from longer transcripts that contain a stem-loop[1–4]. One strand is loaded into the miRNA-induced silencing complex (miRISC), which contains the proteins argonaute (Ago) and Tnrc6 (trinucleotide repeat–containing 6; GW182). The other strand is usually degraded. The mature miRNA guides the miRISC to partially complementary sequences, termed miRNA recognition elements (MREs), in target mRNAs to repress mRNA translation, promote transcript decay or both[1,5–7]. MicroRNAs probably regulate the expression of most coding genes[8].

Most metazoan miRNAs pair imperfectly with their cognate mRNAs, and it is difficult to identify their biologically important targets. Bioinformatic analysis of the first known miRNA-regulated genes showed that pairing of miRNA nucleotides 2–8, called the seed region, to the 3′ untranslated region (UTR) of the target mRNA is often important[5]. Algorithms based on seed pairing and evolutionary conservation became a powerful tool for identifying miRNA-regulated genes[5,8–14]. However, these algorithms typically predict hundreds to thousands of target genes for each miRNA, and most predicted genes are not *bona fide* targets[15]. Moreover, the algorithms sometimes fail to predict the most biologically important miRNA targets, such as the oncogenes *KRAS* and *HRAS* for the miRNA let-7 (ref. 16) or the transcription factor *E2F2* and the oncogene *MYC* for miR-24 (ref. 17). Recent studies provide examples of MREs located outside of the 3′ UTR (especially in the coding sequence (CDS)) or that lack exact seed pairing, but compensate by downstream complementarity[17–20].

Experimental methods for identifying miRNA targets identify mRNAs or proteins that are downregulated when a miRNA is overexpressed or that are upregulated when a miRNA is antagonized[17,21–25], or mRNAs that precipitate with miRISC-associated proteins[26–31]. High-throughput sequencing of Ago-immunoprecipitated RNAs after crosslinking now provides a way to identify miRNA-MRE pairings[32–34]. These methods confirm that current target prediction algorithms miss many genes. Both prediction algorithms and experimental methods generate large lists of candidate miRNA targets. However, choosing the important targets from these long lists is daunting. Gene ontology and interactome analyses of candidate target gene lists can be useful tools for this task[17]. Here, we review methods for identifying biologically relevant miRNA targets.

Computational prediction of miRNA targets

Bioinformatics captures the sequence and location characteristics of MREs to predict miRNA targets[5,14,35]. Commonly used algorithms place variable weight on: (i) complementarity to the miRNA seed region; (ii) evolutionary conservation of the MRE; (iii) free energy of the miRNA-mRNA heteroduplex; and (iv) mRNA sequence features outside the target site[17,36–38] (**Table 1**). Early algorithms, such as TargetScan and PicTar[8,9], focus on the seed region in miRNA targeting (**Table 1**). TargetScan[8,10,11] requires an exact match to ≥7 bases of the seed sequence, but PicTar[9] doesn't, instead imposing a stringent free energy cutoff for imperfect matches. (TargetScan includes a special class of seed matches with a hexamer match in positions 2–7, plus an adenosine at position 1). Both TargetScan and PicTar improve their predictions by taking into account evolutionary conservation. TargetScan also adds a 'context score', which considers features in the surrounding mRNA, including local A-U content and location (near either end of the 3′ UTR is preferred) and improves predictions for nonconserved sequences[39]. Messenger RNAs that have a high context score or multiple predicted MREs are more likely to be true targets.

The miRanda algorithm[12] aligns a miRNA to the target mRNA to identify highly complementary sequences. Seed pairing is weighed more strongly than pairing elsewhere[40], but seed G•U wobbles and mismatches (**Table 1**) are allowed. High-scoring targets are then filtered on a secondary criterion of heteroduplex free energy (ΔG). Finally, only conserved predictions are considered. Because miRanda does not

[1]Immune Disease Institute and Program in Cellular and Molecular Medicine, Children's Hospital Boston, Harvard Medical School, Boston, Massachusetts, USA. [2]Present address: Genetics Branch, National Cancer Institute, National Institutes of Health, Bethesda, Maryland, USA. Correspondence should be addressed to J.L. (lieberman@idi.harvard.edu) or A.L. (lalas@mail.nih.gov).

Published online 6 October 2010; doi:10.1038/nsmb.1921

Table 1 miRNA target prediction algorithms differ in their ability to identify unconventional miRNA recognition elements (MREs)

MRE feature	Example			Target prediction algorithm[a]				
				TargetScan	PicTar	miRanda	PITA	rna22
Perfect seed	HMGA2 5′ CCGACAUUCAAUUUCUACCUCA 3′ let-7a 3′ UUGAUAUGUUGGAUGAUGGAGU 5′		Ref. 36					
G:U wobble seed	NF2 5′ UACAAGAGAUUCUCCUGCCUCA 3′ let-7a 3′ UUGAUAUGUUGGAUGAUGGAGU 5′		Ref. 37	–				
Imperfect seed/seedless	E2F2 5′ GUGGGUGCU-CUGGGCUGAACCA 3′ miR-24 3′ GACA-AGGACGACUUGACUCGGU 5′		Ref. 17	–				
Outside the 3′ UTR	DNMT3B 5′ UGGCAAAGAAGAUGUUUUGUGGUGCACUGAG 3′ miR-148 3′ -UGUUU.....CAAGACAUCACGUGACU- 5′		Ref. 38	–	–	–	+	+

[a]The algorithms are listed in the rough order by which they weigh perfect seed pairing and location within the 3′ UTR. The algorithms that allow identification of noncanonical recognition sites generally are more inclusive, but have much higher false prediction rates. +, algorithm predicts targets of this class; –, algorithm does not predict targets of this class.

require exact seed pairing, it predicts sites such as the two *let-7* sites in the *Caenorhabditis elegans* gene *lin-41,* which contain either a bulge or a G•U wobble in the seed region[40,41].

Other algorithms account for target site accessibility[42,43]. Instead of considering only the Δ*G* of the miRNA-mRNA duplex[12,13], these algorithms estimate the free energy cost to unfold the mRNA secondary structure that surrounds the target site. The PITA algorithm[42] combines this free energy cost with the Δ*G* of miRNA-target pairing to measure ΔΔ*G*. The algorithm finds seed matches (allowing a user-specified number of mismatches), and calculates ΔΔ*G* for each match, irrespective of conservation. Although designed and tested for 3′ UTRs, PITA can predict MREs outside the 3′ UTR. The algorithm mirWIP[43] is based on sequence features of mRNAs isolated by immunoprecipitation of the *C. elegans* miRISC[26]. The mirWIP program scores targets on the basis of: (i) perfect and imperfect seed matches; (ii) site accessibility from predicted mRNA secondary structure; and (iii) ΔG_{total}, an analog of ΔΔ*G*. The sensitivity and specificity of mirWIP are high relative to those of other algorithms for the miRISC dataset that was used to develop it. However, it was not tested against other high-throughput datasets.

The rna22 algorithm differs radically from other algorithms[13]. It relies on recognition of shared miRNA sequence patterns. Briefly, the training dataset considered all known mature miRNA sequences to identify statistically over-represented sequence patterns. Potential MREs were identified as complementary patterns. Predictions are made by 'folding' each known miRNA *in silico* into a heteroduplex with the predicted target sequence and identifying miRNAs with the lowest Δ*G*. The rna22 algorithm does not consider conservation, its predictions are not restricted to the 3′ UTR, and the user can allow seed mismatches. This algorithm has been used to locate 'seedless' and CDS MREs (**Table 1**). The developers of rna22 reported a low false-positive rate[13]. However, rna22 did not perform as well as seed-biased algorithms on high-throughput proteomic data[21,22], and only some rna22-predicted MREs were validated in low-throughput studies[17,44].

Robust comparisons of prediction algorithms are lacking. However, a few reviews have compared predictions against a 'benchmark' of experimentally validated or refuted miRNA targets[14,45]. In these comparisons seed-based predictions that require stringent pairing have the highest specificity and sensitivity[45]. Proteomics studies by the developers of TargetScan and PicTar suggest that their seed-based algorithms have superior predictive power[15,21,22]. Many experimental studies have found that miRNA targets are enriched for exact miRNA seed matches. Moreover, many experimentally validated targets were chosen on the basis of seed-based algorithms. However, recent high-throughput experimental analyses of Ago-bound miRNA-mRNA pairings suggest that around 25%–45% of MREs lack a perfect seed match to expressed miRNAs[32,33]. An increasing list of validated MREs lack a canonical seed[17,18,24,41]. Therefore, filtering gene lists by requiring an exact seed match will eliminate true targets.

All bioinformatic analyses need to consider variations in the annotated sequence databases used to generate predictions. The same algorithm run on two databases (UCSC and Ensembl) generated target predictions that overlapped by less than 50%[46]. Current databases do not take into account cell type–specific mRNA isoforms. Some mRNAs are alternatively polyadenylated in cellular proliferation[47], cancer[48] and differentiation[49], generating transcripts with unique 3′ UTRs. It is important to know whether the expressed isoforms in a cell under study contain the predicted MREs. High-throughput mRNA sequencing of tissue-, development- or disease-specific gene expression[50] can be combined with miRNA profiling to identify candidate miRNA targets[32].

Genetic approaches to miRNA target identification

Forward genetics involves screening for mutants with interesting phenotypes, whereas reverse genetics is used to examine the functional effect of manipulating a specific gene[51]. The founding miRNA lin-4 and its target *lin-14*, which were identified in forward genetic screens for larval defects in *C. elegans,* led to the discovery of miRNAs[51–53]. Other miRNAs and a few of their targets were identified by screens for mutant phenotypes in *C. elegans* and *Drosophila melanogaster*[51]. These targets were generally deduced from epistatic relationships and the complementary phenotypes that sometimes occur when a miRNA and a key target are mutated[51,53].

Reverse genetics has been especially useful for identifying the biological function of miRNAs, and a few examples are described here. Conditional overexpression of each of the six miRNAs in the oncogenic miR-17–92 cluster pinpointed a prominent role for miR-19, which largely recapitulated the oncogenic properties of the cluster, in hematological cancers *in vitro* and *in vivo*[54–56]. Furthermore, when combined with computational, expression or functional analyses, these studies all identified the tumor suppressor *Pten* as an important target of miR-19. The function of the miR-143–145 cluster, which is highly expressed in smooth muscle cells, was elucidated by knocking it out in mice. Knockout mice lacked gross developmental defects, indicating that the cluster is not essential for development[57,58]. However, smooth muscle cells from the knockout mice were less differentiated than those from wild-type animals, and were impaired in responding to vascular injury. Targets of the cluster were then identified by manually selecting interesting candidate genes from computational predictions[57]. Combining reverse genetics with computational and other molecular methods is a powerful method for dissecting miRNA function[21,27,32].

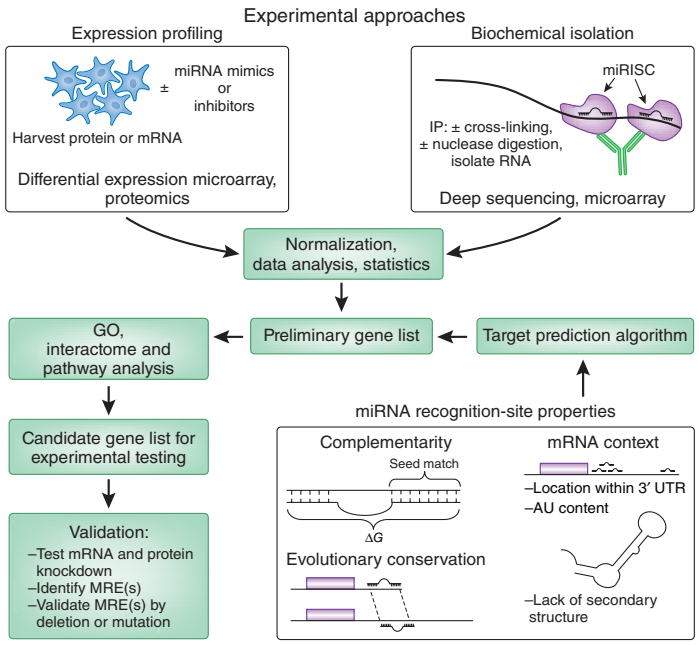

Figure 1 Methods for identifying miRNA targets. Putative target genes can be identified by expression profiling of cells in which the miRNA is overexpressed or antagonized, by biochemical isolation of the miRISC or by target prediction algorithms. These methods generally identify hundreds of candidate genes or more. Bioinformatic analysis of these large candidate gene lists for over-represented Gene Ontology (GO) terms, enriched biological pathways or gene interaction networks can then help researchers to select candidate genes to evaluate experimentally.

Forward genetics can also be used to identify miRNA targets without bias. In one study, candidate miR-19 targets were identified by a genome-wide short hairpin RNA screen to discover genes whose knockdown 'phenocopied' overexpression of miR-19 (ref. 54). The screen identified eight candidate miR-19–regulated genes, of which four were validated. An important benefit of forward genetic methods is that they might identify the most biologically meaningful targets.

Microarray analysis after miRNA overexpression or knockdown

Because miRNAs reduce the steady-state transcript levels of most target genes[6,21–23], identifying mRNAs that are downregulated after ectopic miRNA expression or upregulated after miRNA antagonism provides a useful way to identify putative miRNA-regulated genes (**Fig. 1**). Although this method cannot distinguish direct from indirect targets, harvesting cells soon after transfection might enhance the proportion of direct targets[24,59]. This strategy can also pinpoint miRNA function by bioinformatic analysis of the effect of miRNA manipulation on global gene expression[17,23,59] (**Fig. 1**). This approach was first used to investigate changes in mRNA after overexpression of muscle-specific miR-1 and brain-specific miR-124 (ref. 23). Remarkably, transfection of miR-1 into HeLa cells shifted their gene expression profile toward that of muscle cells, whereas transfection of miR-124 shifted the profile toward that of brain cells. For miR-1, 88% of downregulated genes contained a 3′ UTR hexamer seed match, and 76% of genes that were downregulated by miR-124 had a similar match. CDS seed matches were also somewhat enriched. When miR-124 with mutations in seed region bases 5 and 6 was transfected into cells, the downregulated genes no longer overlapped with genes downregulated by wild-type miR-124. However, when bases 9 and 10 were altered, 89% of downregulated genes overlapped. Recently, similar transcriptome analysis identified a class of functional 'seedless' targets that pair with 11 central bases of the miRNA[18].

Overexpression of miRNAs has also been used to study the biological effects and targets of cancer-related miRNAs. Overexpression of let-7 decreased the proliferation of liver and lung cancer cells, and more than 200 transcripts were downregulated in both cell types[24]. Gene ontology analysis of the downregulated genes indicated that they were enriched in genes for DNA replication and cell cycle pathways. Similarly, transfection of miR-15a and miR-16 into colon cancer cell lines increased the proportion of cells in cell cycle phase G0/G1 and genes that were downregulated were enriched in cell cycle–related genes[59]. Paradoxically, these downregulated cell cycle genes were not enriched in miR-15a or miR-16 seed matches, suggesting that much of the effect of these miRNAs might be indirect.

Loss of function has also been used to identify miRNA targets (**Fig. 1**). *In vivo* knockdown of the liver-specific miR-122 modestly upregulated hundreds of mRNAs[60]. The most enriched 3′ UTR hexamer motif of these genes matched the miR-122 seed and the upregulated genes were enriched in genes for cholesterol biosynthesis pathways. An analysis of changes in gene expression after knockdown of miR-15 and -16 was performed at the same time as the overexpression study described above[59]. The increase in mRNA expression after knockdown was small compared to the downregulation that occurred after ectopic overexpression, suggesting that ectopic miRNA expression might be more useful than miRNA antagonism for identifying targets. However, the relative benefits of overexpression and knockdown depend on biological context. Overexpression may result in supraphysiological miRNA levels, leading to artifacts. In particular, transfection of miRNA mimics can increase the expression of endogenous miRNA targets, probably because it limits the available miRISC[61]. Conversely, repression of an underexpressed miRNA is unlikely to have a substantial effect on target genes. It can also be difficult to suppress a highly expressed endogenous miRNA.

Proteomics

Proteomic analysis can also identify miRNA targets. Stable isotope labeling with amino acids in cell culture (SILAC) followed by mass spectrometry can assess the effect of the loss or overexpression of miRNAs on global protein expression[21,22] (**Fig. 1**). In one study, the nuclear proteome was analyzed after overexpression of miR-124, miR-1 and miR-181 in HeLa cells[21]. The results support the importance of the seed region. For miR-124 and miR-1, the most enriched heptanucleotide motif in the transcripts of the most downregulated proteins matched the miRNA seed sequence, and for miR-181, the second most enriched motif matched the seed. SILAC was also used to compare the expression of cytoplasmic and nuclear proteins in neutrophils from wild-type and miR-223 knockout mice. The mRNAs of proteins that were overexpressed in miR-223 knockout neutrophils were most highly enriched for miR-223 seed matches. Although algorithms that

require stringent seed pairing had the greatest power to predict changes in protein levels, only 33% of the targets predicted by such algorithms showed a change in protein expression, suggesting that the algorithms have a high false-positive rate[21].

SILAC was also used to analyze the proteome of HeLa cells that overexpressed one of five different miRNAs[22]. The 3′ UTR hexamer motifs that most correlated with changes in protein expression were complementary to the miRNA seed for each miRNA. To assess whether depletion and overexpression of miRNAs influenced the expression of the same proteins, the authors knocked down let-7b. The protein changes in cells that overexpressed let-7b and cells in which it was knocked down were negatively correlated. However, the effect of knockdown was only about one-third as great as that of overexpression. Therefore, miRNA overexpression has more of an effect than miRNA antagonism on both protein and mRNA expression.

Changes in mRNA expression correlated well with protein changes in both studies. Proteomics, like mRNA expression studies, cannot distinguish between direct and indirect miRNA targets. SILAC experiments are time-consuming, expensive and not accessible to most laboratories. Moreover, current methods can resolve only a fraction of the proteome at a time. Given these practical challenges, and because mRNA and protein expression changes are highly correlated, microarray analysis might be preferred for its simplicity.

Identification of miRISC-associated miRNA targets

The mammalian miRISC contains a mature miRNA and several proteins, including an Ago protein and Tnrc6 (refs. 62,63). Several studies have identified miRNA targets by their association with miRISC proteins, using immunoprecipitation of epitope-tagged miRISC components[27–30] or native miRISC[31], often while manipulating a specific miRNA to identify its targets[27,29,30] (**Fig. 1**). The Cohen laboratory used microarrays to identify mRNAs that immunoprecipitated with hemagglutinin (HA)-tagged Ago1 in *D. melanogaster* S2 cells[27]. The 89 reproducibly isolated mRNAs were enriched for 3′ UTR seed matches, and some contained CDS seed matches. When introduced into the luciferase open reading frame, CDS MREs were moderately active in reporter assays. The HA-Ago1 immunoprecipitation was performed in transgenic flies with mutant or wild-type miR-1, and 108 transcripts were selectively depleted in embryos with mutated miR-1. The 11 transcripts that contained miR-1 heptamer seed matches all had some activity by luciferase assay. This study highlighted the potential utility of biochemical pulldown to identify miRNA targets. However, it captured only 10% of the expected number of miR-1 target genes[28]. A more sensitive protocol was later developed by optimizing immunoprecipitation conditions and increasing amplification of the mRNAs that were pulled down[28].

Several other studies immunoprecipitated tagged miRISC components to identify targets. The Hannon laboratory identified 294 mRNAs that bound specifically to myc-tagged Ago2 in cells that overexpressed miR-124a (ref. 29). Of these mRNAs, 67% contained 3′ UTR heptamer miR-124a seed matches. Notably, many mRNAs that were enriched in the immunoprecipitation were not downregulated in the cells that overexpressed miR-124a. However, when their 3′ UTRs were tested by luciferase assay, 21 out of 30 were suppressed. A similar Ago2 pulldown to identify miR-124a and miR-1 targets[30] isolated 49% of the putative miR-124a targets identified by the Hannon laboratory. Many putative targets had seed matches in the CDS, but not the 3′ UTR. Expression of mRNAs with CDS seed matches decreased after transfection with miRNA, but genes with 3′ UTR matches were more strongly suppressed, consistent with earlier studies[27,30]. Immunoprecipitation with Tnrc6 has also been used to isolate targets in mammalian cells[62] and *C. elegans*[26]. Another approach to target identification has been to clone and sequence mRNAs that immunoprecipitated with endogenous Ago1 and Ago2 (ref. 31). Five out of six randomly chosen genes that were sequenced more than once were experimentally validated as miRNA targets. However, most of the clones were recovered only once, suggesting that the depth of sequencing may have been a limiting factor.

The biochemical approach to target identification has mostly been used to describe the general features of MREs, rather than to identify specific targets. Pulldown of Ago-associated mRNAs usually enriches transcripts containing seed matches. Experimental validation of putative miRNA targets identified by immunoprecipitation is high, supporting the usefulness of the method[29,30]. Immunoprecipitation studies have identified targets whose mRNAs do not decrease after overexpression of miRNAs[29] as well as unanticipated CDS MREs[27,30]. However, some questions remain about the utility of Ago immunoprecipitation for identifying miRNA targets. The miRNAs and mRNAs that are pulled down with Ago1 or Ago2 might not be identical to those found in miRISCs that contain other Agos[64]. Moreover, epitope-tagged Ago has some drawbacks. Epitope-tagged Ago proteins can associate with transfer RNAs[65], potentially introducing experimental artifacts[27]. Overexpression of Ago globally increases endogenous miRNA production[66,67], which could skew the profile of endogenous miRNA-mRNA interactions. As Ago proteins in cell extracts can associate with cognate mRNAs after lysis[29] some Ago-immunoprecipitated mRNAs might not be true targets. Finally, the Ago pulldowns have the limitation that they identify mRNAs rather than specific MREs and are usually not specific for an individual miRNA.

Pulldowns using miRISC components enrich for all miRNA targets, but don't directly identify mRNAs associated with a specific miRNA. To circumvent this problem, a recent study sought to identify mRNAs directly bound to transfected biotinylated miR-10a (refs. 68,69). However, the results are controversial because the pulled down mRNAs were not enriched for known targets or for miR-10a seed matches. Moreover, they were mostly abundant ribosomal mRNAs, suggesting they might have associated with biotinylated miR-10a nonspecifically. Most identified genes were translationally upregulated, rather than being downregulated, by miR-10a. The authors attributed this unexpected result to the presence of weak miR-10a binding sites in the 5′ UTR.

Identifying miRISC-bound MREs

An important recent development, called Ago HITS-CLIP (high throughput sequencing by crosslinking and immunoprecipitation), directly identifies miRNA-bound MREs[32–34]. Nucleic acids are crosslinked by ultraviolet radiation to miRISC proteins and then immunoprecipitated with an antibody to a miRISC component. Unbound RNA is digested to leave miRISC-protected RNA fragments, which are then analyzed by high-throughput RNA sequencing to identify both Ago-associated miRNAs and their target MREs. In the first study, protected transcript fragments associated with native Ago complexes in mouse brain or HeLa cells were most enriched for motifs that matched the seeds of the most abundant miRNAs. Fragments of mRNAs were also enriched for sequences just after the stop codon or before the polyadenylation site, consistent with studies indicating that MREs in the middle of 3′ UTRs contribute less to silencing than those at the ends[39]. Both the false-positive and false-negative rates of the MRE predictions were low in this study. Notably, detection of previously validated miRNA targets correlated with their expression; highly expressed targets were more readily identified. Of the enriched sequences, 25% mapped to the CDS and 27% lacked a perfect seed match to the 20 most highly expressed miRNAs. These results support recent findings that miRNAs regulate many genes by 'seedless' or CDS interactions[17,18,20,38,41,70,71].

A HITS-CLIP study in *C. elegans*[32] also found enrichment for 3′ UTR seed matches to isolated miRNAs. However, 37% of sequences lacked

a conserved seed match, even after allowing one G•U wobble. CDS sequences were significantly enriched for matches to the central region of the miRNA, but not for seed matches. The identified MREs were found in more accessible regions (lacking secondary structure).

An improved method for isolating protein-associated RNAs, termed PAR-CLIP (photoactivatable-ribonucleoside-enhanced crosslinking and immunoprecipitation), has also been used to identify miRNA targets[34]. Cells are cultured with photoreactive 4-thiouridine, which can substitute for uridine during transcription, before cross-linking and immunoprecipitation. Protein-bound miRNAs and mRNAs are then analyzed by high-throughput sequencing. The incorporation of 4-thiouridine substantially improves RNA yields. Because reverse transcription of 4-thiouridine leads to T-C transitions, the MRE-miRISC interaction site can be accurately mapped. PAR-CLIP of Flag- or HA-tagged AGO1–4 identified almost 20,000 enriched sequences. Nine out of ten of the most enriched heptamers matched the seed sequence of highly expressed miRNAs. Fifty percent of the crosslinked candidate MREs mapped to the CDS, whereas 46% matched a 3′ UTR. Target site identification was tested by antisense inhibition of the 25 most highly expressed miRNAs followed by expression profiling. Targets with seed matches were more frequently upregulated than targets without seed matches. Similarly, mRNAs that were sequenced exclusively in the 3′ UTR were more frequently upregulated after the miRNA was antagonized than those with CDS-only sequence clusters.

Although these methods provide an elegant way to identify miRNA targets, they involve a technically challenging, multistep protocol. The challenges of the procedure need to be weighed against the benefit of genome-wide direct identification of miRNA target sites.

Gene network analysis of miRNA targets

Given the potential of a miRNA to regulate a large number of genes, it can be challenging to identify key miRNA targets and functions from the long lists of putative target genes generated by the methods described above. Gene ontology and interactome analysis can be used to probe the features of lists of candidate genes[17] (**Fig. 1**). We applied this approach to investigating the biological function of miR-24, a miRNA that is consistently upregulated during cellular differentiation[72,73]. Candidate miR-24 targets were identified by their downregulation after overexpression of miR-24. We found that 248 mRNAs had significantly reduced expression, of which 40% were predicted by TargetScan and 51% had a 3′ UTR miR-24 hexamer seed, suggesting that a significant proportion of the downregulated mRNAs were direct targets of miR-24. The cellular pathways that were enriched in the downregulated genes suggested that miR-24 regulates cell cycle progression and DNA repair. Consistent with this hypothesis, overexpression of miR-24 inhibits cellular proliferation and sensitizes cells to DNA damage[17,72].

We used the Ingenuity Pathways software to examine the interactome formed by the downregulated genes. The network of genes that were downregulated by miR-24 was enriched for proteins that have key roles in cell cycle progression. E2F2 and MYC formed highly connected nodes of this interactome, and the effects of miR-24 on cell cycle progression could be reproduced by manipulating E2F2 (a direct target that was not predicted by any algorithm and that lacks a 3′ UTR miR-24 seed match). We suggested, on the basis of these results, that the genes at nodes of a miRNA target interactome might be biologically important targets. This idea needs to be tested in other experimental systems. Many of the genes in the interactome that are downregulated by miR-24 are key elements of cell cycle regulation, including genes that are transcriptionally regulated by E2F2 and MYC. These were also validated as direct targets. Most of those also lacked a seed match, which is consistent with the Ago HITS-CLIP findings noted above. The importance of seed pairing for target mRNA selection could vary amongst miRNAs. This example of a miRNA that suppresses key transcription factors and also directly suppresses their transcriptional target genes suggests that some miRNAs function as master regulators by downregulating a dense network of genes in the same pathway. Applying unbiased systems biology approaches to experimental datasets may help to define miRNA function and pinpoint important target genes.

Validation of putative target genes

The identification of putative miRNA targets is only the first step. To validate candidate genes, the effect of manipulating the miRNA (by overexpression, knockdown or genetic ablation) on protein and mRNA levels of the candidate gene needs to be assessed. An inverse relationship between the gene product (at least the protein) and the miRNA is expected. Direct regulation of gene expression by an miRNA is then tested by reporter assays that use expression plasmids incorporating the entire 3′ UTR or CDS in cells that have been transfected to overexpress the miRNA mimic. Showing that the entire 3′ UTR of a gene is regulated by a miRNA adds confidence that the transcript is recognized in its native context. Further confirmation is provided by identifying the MRE. Candidate MREs can be identified using seed-based algorithms or algorithms that do not require an exact seed match, such as rna22 or PITA[13,42]. Direct regulation by the miRNA is then confirmed by mutating or deleting binding residues in the reporter and testing for restored expression. Most studies test direct regulation by miRNA overexpression using reporters driven by a strong promoter. Showing that a gene can be regulated by physiologically relevant levels of the miRNA provides additional evidence that regulation of the gene by the miRNA is biologically important.

Some genes that have been identified by experimental approaches have candidate CDS MREs. As CDS MREs have a weaker effect on gene expression than 3′ UTR MREs, it is important to determine whether these potential CDS MREs are functional. To do this, CDS MREs and (potentially) their surrounding sequences should be cloned in-frame into the CDS of an appropriate reporter[27,71]. The presence of rare codons upstream of a CDS MRE may slow down translation, permitting miRNAs to bind to CDS MREs and effectively to repress gene expression[74]. This fact needs to be considered in designing CDS MRE reporters.

Concluding remarks

Genome-wide miRNA target identification methods are constantly improving. Ectopic miRNA expression followed by microarray analysis may be the simplest way to identify the biological function and candidate targets of a miRNA. This approach is supported by proteomics studies, which have provided evidence that changes in the expression of mRNA and proteins correlate well[21,22]. However, this strategy has limitations. First, targets that are translationally repressed will be missed. Second, overexpression of a miRNA does not distinguish direct from indirect targets and supraphysiological overexpression can introduce artifacts. Knockdown of a miRNA may therefore be better than overexpression for identifying miRNA targets in a physiological context, although it is less sensitive. Biochemical pulldown methods are continuing to improve and will ultimately provide a more specific and sensitive method for identifying miRNA targets.

Although the importance of the miRNA seed region in miRNA target recognition is clear, a subset of biologically relevant MREs lack a canonical seed or are located in the CDS. Filtering miRNA overexpression or pulldown gene lists by requiring an exact 3′ UTR seed match will eliminate potentially important target genes from consideration. Therefore, we favor an unbiased selection of candidate targets. Gene ontology and interactome analysis or forward genetics can help to pinpoint biologically interesting targets from the hundreds of genes identified by any method. The identification of biologically important targets will be crucial for understanding miRNA function.

COMPETING FINANCIAL INTERESTS
The authors declare no competing financial interests.

Published online at http://www.nature.com/nsmb/.
Reprints and permissions information is available online at http://npg.nature.com/reprintsandpermissions/.

1. Ghildiyal, M. & Zamore, P.D. Small silencing RNAs: an expanding universe. *Nat. Rev. Genet.* **10**, 94–108 (2009).
2. Davis, B. & Hata, A. Regulation of microRNA biogenesis: a miRiad of mechanisms. *Cell Commun. Signal.* **7**, 18 (2009).
3. Winter, J., Jung, S., Keller, S., Gregory, R.I. & Diederichs, S. Many roads to maturity: microRNA biogenesis pathways and their regulation. *Nat. Cell Biol.* **11**, 228–234 (2009).
4. Kim, V.N., Han, J. & Siomi, M.C. Biogenesis of small RNAs in animals. *Nat. Rev. Mol. Cell Biol.* **10**, 126–139 (2009).
5. Bartel, D.P. MicroRNAs: target recognition and regulatory functions. *Cell* **136**, 215–233 (2009).
6. Hendrickson, D.G. *et al.* Concordant regulation of translation and mRNA abundance for hundreds of targets of a human microRNA. *PLoS Biol.* **7**, e1000238 (2009).
7. Brodersen, P. & Voinnet, O. Revisiting the principles of microRNA target recognition and mode of action. *Nat. Rev. Mol. Cell Biol.* **10**, 141–148 (2009).
8. Friedman, R.C., Farh, K.K., Burge, C.B. & Bartel, D.P. Most mammalian mRNAs are conserved targets of microRNAs. *Genome Res.* **19**, 92–105 (2009).
9. Krek, A. *et al.* Combinatorial microRNA target predictions. *Nat. Genet.* **37**, 495–500 (2005).
10. Lewis, B.P., Burge, C.B. & Bartel, D.P. Conserved seed pairing, often flanked by adenosines, indicates that thousands of human genes are microRNA targets. *Cell* **120**, 15–20 (2005).
11. Lewis, B.P., Shih, I., Jones-Rhoades, M.W., Bartel, D.P. & Burge, C.B. Prediction of mammalian microRNA targets. *Cell* **115**, 787–798 (2003).
12. John, B. *et al.* Human microRNA targets. *PLoS Biol.* **2**, e363 (2004).
13. Miranda, K.C. *et al.* A pattern-based method for the identification of microRNA binding sites and their corresponding heteroduplexes. *Cell* **126**, 1203–1217 (2006).
14. Rajewsky, N. microRNA target predictions in animals. *Nat. Genet.* **38** (suppl.), S8–S13 (2006).
15. Alexiou, P., Maragkakis, M., Papadopoulos, G.L., Reczko, M. & Hatzigeorgiou, A.G. Lost in translation: an assessment and perspective for computational microRNA target identification. *Bioinformatics* **25**, 3049–3055 (2009).
16. Johnson, S.M. *et al.* RAS is regulated by the let-7 microRNA family. *Cell* **120**, 635–647 (2005).
17. Lal, A. *et al.* miR-24 inhibits cell proliferation by targeting E2F2, MYC, and other cell-cycle genes via binding to "seedless" 3′UTR microRNA recognition elements. *Mol. Cell* **35**, 610–625 (2009).
18. Shin, C. *et al.* Expanding the microRNA targeting code: functional sites with centered pairing. *Mol. Cell* **38**, 789–802 (2010).
19. Tay, Y.M. *et al.* MicroRNA-134 modulates the differentiation of mouse embryonic stem cells, where it causes post-transcriptional attenuation of Nanog and LRH1. *Stem Cells* **26**, 17–29 (2008).
20. Tay, Y., Zhang, J., Thomson, A.M., Lim, B. & Rigoutsos, I. MicroRNAs to Nanog, Oct4 and Sox2 coding regions modulate embryonic stem cell differentiation. *Nature* **455**, 1124–1128 (2008).
21. Baek, D. *et al.* The impact of microRNAs on protein output. *Nature* **455**, 64–71 (2008).
22. Selbach, M. *et al.* Widespread changes in protein synthesis induced by microRNAs. *Nature* **455**, 58–63 (2008).
23. Lim, L.P. *et al.* Microarray analysis shows that some microRNAs downregulate large numbers of target mRNAs. *Nature* **433**, 769–773 (2005).
24. Johnson, C.D. *et al.* The let-7 MicroRNA represses cell proliferation pathways in human cells. *Cancer Res.* **67**, 7713–7722 (2007).
25. Chang, T. *et al.* Transactivation of miR-34a by p53 broadly influences gene expression and promotes apoptosis. *Mol. Cell* **26**, 745–752 (2007).
26. Zhang, L. *et al.* Systematic identification of *C. elegans* miRISC proteins, miRNAs, and mRNA targets by their interactions with GW182 proteins AIN-1 and AIN-2. *Mol. Cell* **28**, 598–613 (2007).
27. Easow, G., Teleman, A.A. & Cohen, S.M. Isolation of microRNA targets by miRNP immunopurification. *RNA* **13**, 1198–1204 (2007).
28. Hong, X., Hammell, M., Ambros, V. & Cohen, S.M. Immunopurification of Ago1 miRNPs selects for a distinct class of microRNA targets. *Proc. Natl. Acad. Sci. USA* **106**, 15085–15090 (2009).
29. Karginov, F.V. *et al.* A biochemical approach to identifying microRNA targets. *Proc. Natl. Acad. Sci. USA* **104**, 19291–19296 (2007).
30. Hendrickson, D.G., Hogan, D.J., Herschlag, D., Ferrell, J.E. & Brown, P.O. Systematic identification of mRNAs recruited to argonaute 2 by specific microRNAs and corresponding changes in transcript abundance. *PLoS ONE* **3**, e2126 (2008).
31. Beitzinger, M., Peters, L., Zhu, J.Y., Kremmer, E. & Meister, G. Identification of human microRNA targets from isolated argonaute protein complexes. *RNA Biol.* **4**, 76–84 (2007).
32. Zisoulis, D.G. *et al.* Comprehensive discovery of endogenous Argonaute binding sites in *Caenorhabditis elegans*. *Nat. Struct. Mol. Biol.* **17**, 173–179 (2010).
33. Chi, S.W., Zang, J.B., Mele, A. & Darnell, R.B. Argonaute HITS-CLIP decodes microRNA-mRNA interaction maps. *Nature* **460**, 479–486 (2009).
34. Hafner, M. *et al.* Transcriptome-wide identification of RNA-binding protein and microRNA target sites by PAR-CLIP. *Cell* **141**, 129–141 (2010).
35. Hammell, M. Computational methods to identify miRNA targets. *Semin. Cell Dev. Biol.* **21**, 738–744 (2010).
36. Mayr, C., Hemann, M.T. & Bartel, D.P. Disrupting the pairing between let-7 and Hmga2 enhances oncogenic transformation. *Science* **315**, 1576–1579 (2007).
37. Meng, F. *et al.* The microRNA let-7a modulates interleukin-6-dependent STAT-3 survival signaling in malignant human cholangiocytes. *J. Biol. Chem.* **282**, 8256–8264 (2007).
38. Duursma, A.M., Kedde, M., Schrier, M., le Sage, C. & Agami, R. miR-148 targets human DNMT3b protein coding region. *RNA* **14**, 872–877 (2008).
39. Grimson, A. *et al.* MicroRNA targeting specificity in mammals: determinants beyond seed pairing. *Mol. Cell* **27**, 91–105 (2007).
40. Betel, D., Wilson, M., Gabow, A., Marks, D.S. & Sander, C. The microRNA.org resource: targets and expression. *Nucleic Acids Res.* **36**, D149–D153 (2008).
41. Vella, M.C., Choi, E., Lin, S., Reinert, K. & Slack, F.J. The *C. elegans* microRNA let-7 binds to imperfect let-7 complementary sites from the lin-41 3′UTR. *Genes Dev.* **18**, 132–137 (2004).
42. Kertesz, M., Iovino, N., Unnerstall, U., Gaul, U. & Segal, E. The role of site accessibility in microRNA target recognition. *Nat. Genet.* **39**, 1278–1284 (2007).
43. Hammell, M. *et al.* mirWIP: microRNA target prediction based on microRNA-containing ribonucleoprotein-enriched transcripts. *Nat. Methods* **5**, 813–819 (2008).
44. Navarro, F. *et al.* miR-34a contributes to megakaryocytic differentiation of K562 cells independently of p53. *Blood* **114**, 2181–2192 (2009).
45. Sethupathy, P., Megraw, M. & Hatzigeorgiou, A.G. A guide through present computational approaches for the identification of mammalian microRNA targets. *Nat. Methods* **3**, 881–886 (2006).
46. Ritchie, W., Flamant, S. & Rasko, J.E.J. Predicting microRNA targets and functions: traps for the unwary. *Nat. Methods* **6**, 397–398 (2009).
47. Sandberg, R., Neilson, J.R., Sarma, A., Sharp, P.A. & Burge, C.B. Proliferating cells express mRNAs with shortened 3′ untranslated regions and fewer microRNA target sites. *Science* **320**, 1643–1647 (2008).
48. Mayr, C. & Bartel, D.P. Widespread shortening of 3′UTRs by alternative cleavage and polyadenylation activates oncogenes in cancer cells. *Cell* **138**, 673–684 (2009).
49. Ji, Z., Lee, J.Y., Pan, Z., Jiang, B. & Tian, B. Progressive lengthening of 3′ untranslated regions of mRNAs by alternative polyadenylation during mouse embryonic development. *Proc. Natl. Acad. Sci. USA* **106**, 7028–7033 (2009).
50. Wang, E.T. *et al.* Alternative isoform regulation in human tissue transcriptomes. *Nature* **456**, 470–476 (2008).
51. Ambros, V. The functions of animal microRNAs. *Nature* **431**, 350–355 (2004).
52. Wightman, B., Ha, I. & Ruvkun, G. Posttranscriptional regulation of the heterochronic gene lin-14 by lin-4 mediates temporal pattern formation in *C. elegans*. *Cell* **75**, 855–862 (1993).
53. Lee, R.C., Feinbaum, R.L. & Ambros, V. The *C. elegans* heterochronic gene lin-4 encodes small RNAs with antisense complementarity to lin-14. *Cell* **75**, 843–854 (1993).
54. Mavrakis, K.J. *et al.* Genome-wide RNA-mediated interference screen identifies miR-19 targets in Notch-induced T-cell acute lymphoblastic leukaemia. *Nat. Cell Biol.* **12**, 372–379 (2010).
55. Mu, P. *et al.* Genetic dissection of the miR-17:92 cluster of microRNAs in Myc-induced B-cell lymphomas. *Genes Dev.* **23**, 2806–2811 (2009).
56. Olive, V. *et al.* miR-19 is a key oncogenic component of mir-17–92. *Genes Dev.* **23**, 2839–2849 (2009).
57. Xin, M. *et al.* MicroRNAs miR-143 and miR-145 modulate cytoskeletal dynamics and responsiveness of smooth muscle cells to injury. *Genes Dev.* **23**, 2166–2178 (2009).
58. Elia, L. *et al.* The knockout of miR-143 and -145 alters smooth muscle cell maintenance and vascular homeostasis in mice: correlates with human disease. *Cell Death Differ.* **16**, 1590–1598 (2009).
59. Linsley, P.S. *et al.* Transcripts targeted by the microRNA-16 family cooperatively regulate cell cycle progression. *Mol. Cell. Biol.* **27**, 2240–2252 (2007).
60. Krützfeldt, J. *et al.* Silencing of microRNAs *in vivo* with 'antagomirs'. *Nature* **438**, 685–689 (2005).
61. Khan, A.A. *et al.* Transfection of small RNAs globally perturbs gene regulation by endogenous microRNAs. *Nat. Biotechnol.* **27**, 549–555 (2009).
62. Landthaler, M. *et al.* Molecular characterization of human Argonaute-containing ribonucleoprotein complexes and their bound target mRNAs. *RNA* **14**, 2580–2596 (2008).
63. Ding, L. & Han, M. GW182 family proteins are crucial for microRNA-mediated gene silencing. *Trends Cell Biol.* **17**, 411–416 (2007).
64. Su, H., Trombly, M.I., Chen, J. & Wang, X. Essential and overlapping functions for mammalian Argonautes in microRNA silencing. *Genes Dev.* **23**, 304–317 (2009).
65. Maniataki, E. & Mourelatos, Z. Human mitochondrial tRNAMet is exported to the cytoplasm and associates with the Argonaute 2 protein. *RNA* **11**, 849–852 (2005).
66. Zhang, X., Graves, P.R. & Zeng, Y. Stable Argonaute2 overexpression differentially regulates microRNA production. *Biochim. Biophys. Acta* **1789**, 153–159 (2009).
67. Diederichs, S. & Haber, D.A. Dual role for Argonautes in microRNA processing and post-transcriptional regulation of microRNA expression. *Cell* **131**, 1097–1108 (2007).
68. Ørom, U.A. & Lund, A.H. Isolation of microRNA targets using biotinylated synthetic microRNAs. *Methods* **43**, 162–165 (2007).
69. Ørom, U.A., Nielsen, F.C. & Lund, A.H. MicroRNA-10a binds the 5′UTR of ribosomal protein mRNAs and enhances their translation. *Mol. Cell* **30**, 460–471 (2008).
70. Didiano, D. & Hobert, O. Perfect seed pairing is not a generally reliable predictor for miRNA-target interactions. *Nat. Struct. Mol. Biol.* **13**, 849–851 (2006).
71. Lal, A. *et al.* p16INK4a translation suppressed by miR-24. *PLoS ONE* **3**, e1864 (2008).
72. Lal, A. *et al.* miR-24-mediated downregulation of H2AX suppresses DNA repair in terminally differentiated blood cells. *Nat. Struct. Mol. Biol.* **16**, 492–498 (2009).
73. Neilson, J.R., Zheng, G.X., Burge, C.B. & Sharp, P.A. Dynamic regulation of miRNA expression in ordered stages of cellular development. *Genes Dev.* **21**, 578–589 (2007).
74. Gu, S., Jin, L., Zhang, F., Sarnow, P. & Kay, M.A. Biological basis for restriction of microRNA targets to the 3′ untranslated region in mammalian mRNAs. *Nat. Struct. Mol. Biol.* **16**, 144–150 (2009).